



Aalborg Universitet

AALBORG UNIVERSITY
DENMARK

Characterizing human breathing and its interactions with room ventilation

Xu, Chunwen

DOI (link to publication from Publisher):
[10.5278/VBN.PHD.ENG.00044](https://doi.org/10.5278/VBN.PHD.ENG.00044)

Publication date:
2018

Document Version
Publisher's PDF, also known as Version of record

[Link to publication from Aalborg University](#)

Citation for published version (APA):

Xu, C. (2018). *Characterizing human breathing and its interactions with room ventilation*. Aalborg Universitetsforlag. Ph.d.-serien for Det Ingeniør- og Naturvidenskabelige Fakultet, Aalborg Universitet
<https://doi.org/10.5278/VBN.PHD.ENG.00044>

General rights

Copyright and moral rights for the publications made accessible in the public portal are retained by the authors and/or other copyright owners and it is a condition of accessing publications that users recognise and abide by the legal requirements associated with these rights.

- ? Users may download and print one copy of any publication from the public portal for the purpose of private study or research.
- ? You may not further distribute the material or use it for any profit-making activity or commercial gain
- ? You may freely distribute the URL identifying the publication in the public portal ?

Take down policy

If you believe that this document breaches copyright please contact us at vbn@aub.aau.dk providing details, and we will remove access to the work immediately and investigate your claim.

**CHARACTERIZING HUMAN
BREATHING AND ITS INTERACTIONS
WITH ROOM VENTILATION**

**BY
CHUNWEN XU**

DISSERTATION SUBMITTED 2018



AALBORG UNIVERSITY
DENMARK

CHARACTERIZING HUMAN BREATHING AND ITS INTERACTIONS WITH ROOM VENTILATION

by

Chunwen Xu



AALBORG UNIVERSITY
DENMARK

Dissertation submitted 2017

Dissertation submitted: January 2018

PhD supervisor: Associate Prof. Li Liu
Aalborg University

Assistant PhD supervisors: Prof. Peter V. Nielsen
Aalborg University
Prof. Guangcai Gong
Hunan University

PhD committee: Professor Per Heiselberg (chairman)
Aalborg University
Professor Mats Sandberg
Högskolan i Gävle
Professor Catherine Noakes
University of Leeds

PhD Series: Faculty of Engineering and Science, Aalborg University

Department: Department of Civil Engineering

ISSN (online): 2446-1636
ISBN (online): 978-87-7210-129-3

Published by:
Aalborg University Press
Langagervej 2
DK – 9220 Aalborg Ø
Phone: +45 99407140
aauf@forlag.aau.dk
forlag.aau.dk

© Copyright: Chunwen Xu

Printed in Denmark by Rosendahls, 2018

CURRICULUM VITAE

CHUNWEN XU

DATE OF BIRTH:

March 06th, 1986

E-MAIL:

cxu@upc.edu.cn



WORK ADDRESS:

College of Pipeline and Civil Engineering, China University of Petroleum No. 66,
Changjiang West Road , Huangdao District , Qingdao , China , 266580

WORK EXPERIENCE:

2014 to present Lecturer, Gas Engineering, College of Pipeline and
Civil Engineering, China University of Petroleum,
Qingdao, China

EDUCATION:

2012 to present Ph.D. in Indoor Environment Engineering Aalborg
University
2014 Ph.D. in HVAC, Hunan University
2011 M. E. in HVAC, Hunan University
2008 B. E. in Building Environment and Equipment
Engineering, Hunan University

RESEARCH INTERESTS:

Environmental Health and engineering, indoor environmental quality, CFD, Natural Ventilation, Displacement Ventilation, HVAC system, heating, humidity and condensation, thermal engineering, Hygrothermal control, personal exposure, respiratory aerosol and disease transmission modelling, infection risk control, indoor airflow dynamics, gas transportation and storage, gas leak control

Thesis details

Title:

Characterizing human breathing and its interactions with room ventilation

PhD student:

Chunwen Xu

Supervisors:

Associate Professor Li Liu

Professor Peter V. Nielsen

The main body of this thesis consist of the following papers:

[a] Chunwen Xu, Peter V. Nielsen, Guangcai Gong, Rasmus L. Jensen, Li Liu, Influence of air stability and metabolic rates on exhaled flow, *Indoor Air*, 2015, 25(2):198-209

[b] Chunwen Xu, Guangcai Gong, Peter V. Nielsen, Li Liu, Rasmus L.Jensen, Hangxin Li, Effect of air stability on the dispersal of exhaled contaminant in rooms, 12th International Conference on Sustainable Energy technologies Proceedings, 2013.8.27-2013.8.29.

[c] Chunwen Xu, Peter V. Nielsen, Guangcai Gong, Li Liu, Rasmus L. Jensen, Measuring the exhaled breath of a manikin and human subjects, *Indoor Air*, 2015, 25(2):188-197

[d] Chunwen Xu, Peter V. Nielsen, Li Liu, Rasmus L. Jensen, Guangcai Gong, Human exhalation characterization with the aid of schlieren imaging technique, *Building and Environment*, 2017, 112:190-199

[e] Chunwen Xu, Peter V. Nielsen, Li Liu, Rasmus L. Jensen, Guangcai Gong. Impacts of airflow interactions with thermal boundary layer on performance of personalized ventilation, *Energy Conversion and Management*, 2017. (*submitted*)

Copyright:

This thesis has been submitted for assessment in partial fulfilment of the PhD degree. The thesis is based on the submitted or published scientific papers which are listed above. Parts of the papers are used directly or indirectly in the extended summary of the thesis. As part of the assessment, co-author statements have been made available to the assessment committee and are also available at the Faculty. The thesis is not in its present form acceptable for open publication but only in limited and closed circulation as copyright may not be ensured.

ENGLISH SUMMARY

Human breathing can become potential sources for airborne disease transmission. Accurate prediction of the infection prone zones and spreading routes of the expelled contaminants can aid in identifying and implementing the control strategies. This thesis focuses on characterizing human breathing and its interactions with room ventilation.

Room ventilation, body plume and human breathing interacts between each other, causing possible complex dispersion characteristics of exhaled flow and affecting the inhaled air quality for occupants. This thesis compares the different characteristics of the dispersion of exhaled flow under two ventilation principles, namely mixing ventilation (MV) and displacement ventilation (DV). Analogizing the steady free jet, the centerline velocity and centerline concentration in the pulsating exhaled flow are devised and are further used to explore the influences of the two ventilation principles. In addition to assessing the exhaled flow with MV and DV, the inhaled air quality is also evaluated considering the interactions of human thermal boundary layer with personalized airflow.

Three different tools that are commonly used for human breathing assessment are applied and compared here:

- the computer simulated person (CSP)
- breathing thermal manikin (BTM)
- human subjects

The simulations with the CSP are compared with the measurements with the BTM, and the breathing from the BTM is then assessed with that from human subjects. This is done to examine to what extent the tools, such as the CSP and the BTM, can mimic real human breathing. The deviations and reasons are analyzed, which is important for accuracy improvement by simulations.

To better understand real human breathing process, characterizations are further performed on human subjects with the aid of schlieren imaging technique.

Two different velocities for breathing assessment are applied in this thesis, which are the centerline velocity u_m and the propagation velocity u_p . The differences between these two velocities are discussed at the end of this thesis.

DANSK RESUME

Menneskelig vejrtrækning kan være en potentiel kilde til luftbåren spredning af sygdomme. En præcis beregning af infektionszoner og spredningsruter for udåndet luftbåren smitte kan hjælpe til at identificere og udføre kontrolstrategier. Afhandlingen fokuserer på bestemmelsen af menneskelig vejrtrækning og dennes interaktion med ventilationen i lokalet.

Ventilationen i et lokale, termisk strømning omkring kroppen og menneskelig vejrtrækning interagerer med hinanden og skaber mulige komplekse spredningsmønstre og påvirker indåndingens luftkvalitet for personer i lokalet. Afhandlingen sammenligner de forskellige strømningsmønstre for udånding ved de to luftfordelingsprincipper, nemlig opblandingsventilation (MV) og fortrængningsventilation (DV). Strømningsforholdene er analyseret ved at sammenligne med jet-strømning og ved at fokusere på lufthastigheden og koncentrationen i centerlinjen i den pulserende udåndingsstrømning. Resultaterne er endvidere brugt til at undersøge indflydelsen fra de to ventilationsprincipper. Ud over at analysere udåndingsstrømningen ved MV og DV er der også set på den indåndede luftkvalitets påvirkning af det menneskelige termiske grænselag med et personligt ventilationssystem.

Tre forskellige værktøjer er ofte brugt til at studere og sammenligne human vejrtrækning, nemlig:

- En computersimuleret person (CSP)
- En termisk manikin med vejrtrækningsfunktion (BTM)
- Forsøgspersoner

Simuleringer med CSP er sammenlignet med målinger med BTMs åndingsmønsteret og de er derefter sammenlignet med personers åndingsmønstre. Dette er udført for at vurdere i hvor høj grad værktøjer som CSP og BTM kan gengive reelle vejrtrækningsmønstre. Afvigelser og årsager til afvigelser analyseres, hvilket er vigtigt for at opnå gode simuleringer af vejrtrækningsprocessen.

For at opnå en endnu bedre forståelse af vejrtrækningsprocessen er der ydermere udført forsøg med personer ved hjælp af Schlieren-teknologien.

Der er anvendt to forskellige indfaldsvinkler til forståelse af vejrtrækningsprocessen i denne afhandling, nemlig: den maksimale centerlinjehastighed u_m og udbredeshastigheden u_p . De to hastigheder beskrives i slutningen af afhandlingen.

ACKNOWLEDGEMENTS

This thesis “Characterizing human breathing and its interactions with room ventilation” is submitted for acquiring the Danish PhD degree. It presents my PhD work at Aalborg University supervised by Associate Prof. Li Liu and Prof. Peter V. Nielsen.

Department of Civil Engineering and the laboratory of Indoor Climate gave me great host and support during my stay at Aalborg in 2012 and 2015. I wish to express my gratitude to them.

Special thanks should be given to Li Liu and Prof. Peter V. Nielsen for their patient and valuable instructions on my work and giving me this opportunity to fulfill this PhD study. Prof. Guangcai Gong also deserves my gratitude for his support and encouragement.

Many thanks to Rasmus L. Jensen for his help at the laboratory and technical explanations. I would also like to thank all the colleagues and friends in both the Danish and Chinese universities.

Finally, I want to thank my family for their sincere love and support.

Chunwen Xu

June 2017

TABLE OF CONTENTS

Chapter 1. Introduction.....	15
1.1. Research background	15
1.2. Respiration	15
1.2.1. Human respiratory system.....	15
1.2.2. Composition of exhaled breath	17
1.2.3. Breathing patterns in humans	18
1.2.4. Influencing factors	20
1.3. Tools for evaluating human breathing.....	22
1.4. Aims and scope	24
Chapter 2. Method and materials.....	26
2.1. Tools for breathing assessments.....	26
2.1.1. Breathing thermal manikin.....	26
2.1.2. Computer simulated person.....	28
2.1.3. Human volunteers	29
2.1.4. Comparisons among the three tools	31
2.2. Ventilation setups.....	34
2.2.1. Mixing ventilation and displacement ventilation	34
2.2.2. Personalized ventilation	37
2.3. Measuring facilities and methods.....	38
Chapter 3. Interactions among room ventilation, body plume and human breathing.....	41
3.1. Mixing ventilation and displacement ventilation	41
3.1.1. Interaction between body plume and inhaled air.....	42
3.1.2. Interaction between body plume and exhaled air	43
3.1.3. Interaction between ventilation and exhaled flow dispersion	44
3.1.4. Conclusions in this section.....	52
3.2. Personalized ventilation	52
3.2.1. Introduction.....	52
3.2.2. Interaction between manikin body and PV flow	56

3.2.3. Interaction between TBL and PV flow.....	59
3.2.4. Discussion and conclusions in this section.....	61
Chapter 4. Comparisons of exhaled breath among the three tools.....	64
4.1. CSP vs. BTM	64
4.1.1. Flow field validation	65
4.1.2. Exhaled flow validation	67
4.1.3. Discussion	71
4.2. BTM vs. Human subjects	72
4.2.1. Pulsating velocity and velocity profile	72
4.2.2. Velocity decay.....	75
4.2.3. Concentration decay.....	76
4.2.4. Conclusions in this section.....	77
4.3. Schlieren imaging study on exhaled flow	78
4.3.1. Introduction.....	78
4.3.2. Flow shape and direction	80
4.3.3. Velocity characterization	82
4.3.4. Conclusions in this section.....	86
Chapter 5. Conclusions and future work	88
Literature list.....	91
Appendices.....	97

NOMENCLATURE

a	Characteristic coefficient
a_0	Mouth area (m^2)
Ar	Archimedes number
b	characteristic coefficient
c_0	Mean concentration of tracer gas at the mouth (ppm)
c_a	Mean concentration of tracer gas in the ambient air in the room (ppm)
c_{bz}	Mean concentration of tracer gas in inhalation or at a point in the breathing zone (ppm)
c_{pv}	Mean concentration of tracer gas at the nozzle exit (ppm)
c_R	Mean concentration of tracer gas in the exhaust of the room (ppm)
c_x	Mean concentration of tracer gas at centerline with a horizontal distance of x (ppm)
d	Propagation distance or relative distance between the nozzle and the nose (m)
g	Gravitational acceleration (m/s^2)
k	Slope for the linear fitting
K_c	Characteristic constants for concentration decay
K_v	Characteristic constants for velocity decay
L	Feature length (m)
n	Characteristic coefficient
n_1	Characteristic velocity exponent
n_2	Characteristic concentration exponent
Pr	Prandtl number
Ra	Rayleigh number
t	Time step size (s)
T_a	Ambient air temperature ($^{\circ}\text{C}$)
T_{exh}	Exhaled air temperature ($^{\circ}\text{C}$)
$u(x,y)$	Mean peak velocity at certain point (x,y) (m/s)
$\dot{u}(x,y,t)$	Instantaneous velocity measured at point (x,y) (m/s)
u_0	Initial velocity of exhalation (m/s)
u_b	Mean resultant velocity (m/s)
u_m	Maximum velocity at the centerline (m/s)
u_m'	Standard deviation of peak velocities (m/s)

u_p	Propagation velocity (m/s)
u_x	Mean velocity along the x axis
u_y	Mean velocity along the y axis
x	Horizontal distance (m)
y	Vertical height (m)
ε_p	Air quality index
α	Thermal diffusivity (m ² /s)
β	Expansivity (K ⁻¹)
δ	Half width of the exhaled flow to the location of $u_m/2$ (m)
Δd	Propagation distance over Δt (m)
ΔT	Temperature difference (K)
Δt	Time interval (s)
η	Dimensionless height y/δ
η_c	Dimensionless concentration

Abbreviations

ACR	Air change rate (h ⁻¹)
BF	Breathing frequency (min ⁻¹)
BMV	Breathing minute volume (l/min)
BSA	Body surface area (m ²)
BTM	Breathing thermal manikin
BZ	Breathing zone
CSP	Computer simulated person
DV	Displacement ventilation
MV	Mixing ventilation
PV	Personalized ventilation

CHAPTER 1. INTRODUCTION

This chapter provides a brief overview of the breathing related issues in indoor environment. The goals are to highlight the importance of this research, summarize the existing tools to mimic and evaluate human breathing, and point out the remaining work to be accomplished.

1.1. RESEARCH BACKGROUND

Exposure of human beings to different airborne pathogens has resulted in the emergence of epidemics of respiratory infections (Shrivastava et al., 2013). The airborne infection diseases have resulted in heavy burden to the world. Dye et al. (1999) evaluated 1.87 million deaths caused by tuberculosis infection in about 22 countries. The outbreak of H1N1 in April 2009 in Mexico quickly spread countries worldwide, causing over 18,000 deaths (WHO, 2010). The social and economic losses because of the epidemics of airborne infections are inestimable and endless. It is very important to find ways to control the disease transmission to rim down the deaths. Accurate prediction of the infection prone zones and spreading routes of the diseases can aid in identifying and implementing the control strategies.

1.2. RESPIRATION

The goal of the present work is to characterize the dynamic process of human breathing and its interaction with room ventilation. In this section, a brief introduction of human respiratory system, droplets in exhaled air and the breathing patterns among humans will be presented. Then the major influencing factors on the transport and dispersion of exhaled air will be summarized and discussed.

1.2.1. HUMAN RESPIRATORY SYSTEM

Human respiratory system is a complex biological system, consisting of specific organs and structures, as shown in Figure 1.1. The anatomical features of human respiratory system include trachea, bronchi, bronchioles, lungs, and diaphragm.

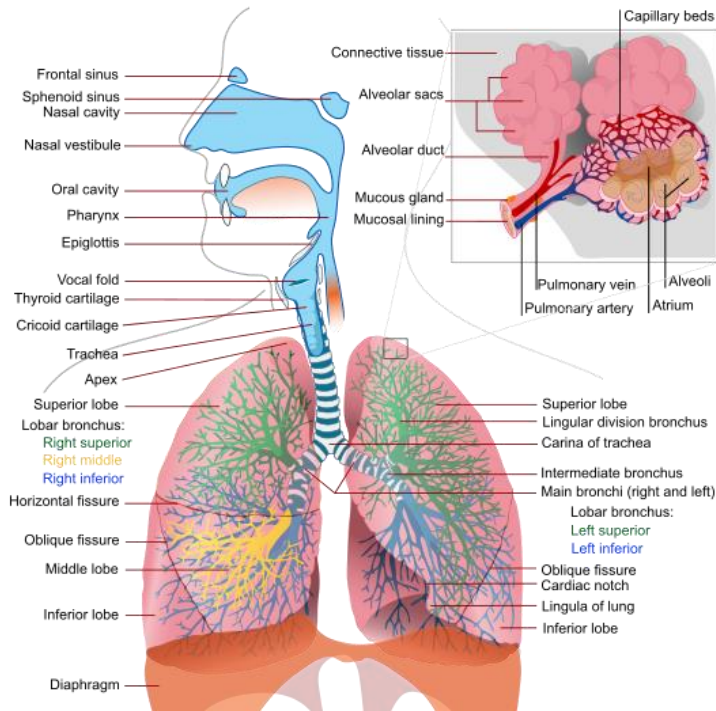


Figure 1.1 Schematic view of human respiratory system (from Wikipedia, the free encyclopedia).

Although the respiratory system contains many defending mechanisms to prevent pathogens from entering the body, if the respiratory tract is constantly exposed to microbes, infection may occur. Evidences have demonstrated associations between disease transmission and pathogen contact through human respiratory routes (Badeau et al., 2002).

Human respiratory behaviors are the physiological pulmonary functions, including breathing, talking, coughing, sneezing and so on. In present work, special attention is given to one of these important respiratory behaviors – *breathing*. However, the exhalation airflow from breathing is a common but poorly-understood phenomenon. One research respective of this study is to investigate the exhalation airflow as one featuring characteristic of the infected source.

The transport of pathogen from one to another have many routes. The routes dictates the control methods, i.e. the long-range airborne route is controlled by the dilution by the room ventilation. However, when the mutual distance between people is small, the short-range airborne route exists (Liu et al., 2016). The efficiency of the room

ventilation to minimize the direct exposure of the expiratory droplet nuclei is in question, since the transport can happen fast. Therefore, it is crucial to investigate the expiratory airflow that carries the pathogens from the infected. Among all respiratory activities, human breathing releases the least droplets per exhalation, but the most during a long and continuous exposure period (Fairchild and Stamper, 1987; Papineni and Rosenthal, 1997).

1.2.2. COMPOSITION OF EXHALED BREATH

Our current understanding of human breathing will be treated in more details in this section. The air we inspired and expired respectively is typically composed by the gases listed in Table 1.1.

Table 1.1 Volume composition of inhaled air and exhaled air (West, 1994).

Inhaled air		Exhaled air	
nitrogen	78.04%	nitrogen	78.04%
oxygen	21%	oxygen	13.6%~16%
argon	0.96%	carbon dioxide	4%~5.3%
		argon and other gases	1%

Except for the gases, the expiratory droplets are released during breathing, talking, coughing and sneezing. The droplets from contagious individuals may contain infectious microorganisms. Droplet infection is an important pathway of disease transmission.

Larger droplets may rapidly settle out of the air due to gravity force, contributing to short distance infection (Gold and Nankervis, 1989) and the critical size causing droplet deposition is still in discussion (Xie et al. 2007, Liu et al. 2016 and Wei et al. 2016). Smaller droplets normally referring to droplets smaller than 5 μm , may remain suspended in the air and transport for meters (McCluskey et al., 1996). Evidences have shown that respirable particles carrying infectious virus are not only produced by coughing or sneezing, but may also be found in breathing alone (Fabian et al., 2008; Huynh et al., 2008; Stelzer-Braid et al., 2009).

There are numerous studies covering the issues of droplet particle sizes, evaporation time of the moist coatings, transmission distances, potential infectious doses, and the influence of environmental factors on droplet transport (Papineni and Rosenthal, 1997; Qian et al., 2006; Lai and Cheng, 2007; Xie et al., 2007; Chao et al., 2008; Chao et al., 2009; Mui et al., 2009; Morawska et al., 2009; Chen and Zhao, et al. 2010). Although the exact underlying mechanism of respiratory droplet infection is still not fully understood, it is vital to know exactly how the expiratory aerosols disperse indoors because the close relevance to human health.

The measurement and monitoring of airflow patterns is commonly considered as one indicator of the potential for aerosol and airborne transmission of infection. This PhD project is aimed to investigate the methods of measuring, visualizing and quantify exhalation airflow patterns, which can aid in infection control and biosafety guideline setups.

1.2.3. BREATHING PATTERNS IN HUMANS

Human breathing is a kind of rhythmic activity. Generally speaking, the breathing of a simulated person (manikin, computer-simulated person) is often treated as a fixed pattern with one breathing frequency and constant amplitude of each respiratory cycle. One measured example in Figure 1.2 shows the variation of respiratory airflow has an approximate sinusoidal shape (Gupta et al., 2010).

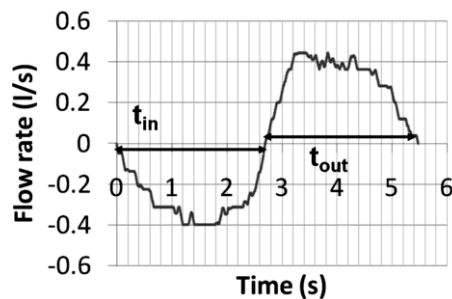


Figure 1.2 Pulmonary ventilation of a human volunteer (Gupta et al., 2010).

However, it should be noted that simplified pattern for simulation purpose is not the real condition for humans. Human breathing is observed with significant diversity between individuals. On the other hand, some literatures (Bachy et al., 1986; Eisele et al., 1992) have reported that the similarity of the flow shape in terms of individual. Then a questions is proposed here: can the simplified model simulate human breathing to a satisfying degree? To answer this question, data obtained from real persons is needed. Meanwhile the characteristics of human breathing should be exactly known.

Breathing frequency and volume

Hutchinson (1850) obtained the breathing frequency of 1714 adult subjects, by means of observation rather than any measuring devices. This study appears to be the most extensive one so far. It shows that the breathing frequency varies over a wide range, from 6 to 31 min^{-1} at rest. Adams (1993) measured the volume rate of air inhaled in different types of activities both in laboratory and in field protocols (160 subjects). It was aimed to simply the task of predicting the average value of inhaled volume rate. Values of both the breathing frequency and the volume rate of inhaled air show significant dependency on activities, genders, ages and other variables (Adams, 1993).

For engineering application convenience, ASHRAE (2009) estimates the typical metabolic heat generation rate for various specific activities. Combined the results obtained by Adams (1993) and ASHRAE (2009), a linear relationship between the breathing frequency and the metabolic rate or between the minute volume and the metabolic rate can be found, as shown in Figure 1.3.

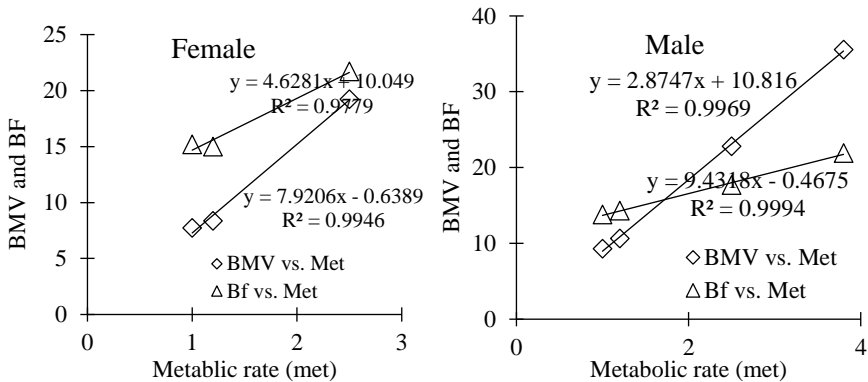


Figure 1.3 Linear fitting of breathing minute volume (BMV) and breathing frequency (BF) with metabolic rate.

Flow profiles

The flow profiles show relative stable characteristics for an individual. Bachy et al. (1986) measured the breathing airflow of human subjects at rest, analyzed the respiratory signals obtained from the pneumotachogram and reported that there was similarity of breath cycle shape in one subject and dissimilarity between different subjects. Some works tried to assume an identical flow shape as an optimal pattern of breathing in non-dimensional form. But Eisele et al. (1992) suggested that “the individuality of breathing patterns is a concept rather than a fixed pattern: each individual has his own way of breathing in any one condition...”. Results show that individuality of flow shape changed between at rest and during exercise and a diversity of breathing patterns can be observed in both activities (Eisele et al., 1992).

Breath-to-breath variations

Priban (1963) demonstrated that the breath-to-breath fluctuations of the variables in respiratory cycles were not purely random. This non random nature of respiratory fluctuations was further confirmed by subsequent studies with time-series and statistic analyses. One of the autocorrelation models (Benchetrit, 2000) is presented here:

$$X_n - X = a(X_{n-1} - X) + \varepsilon_n \quad (1.1)$$

where, X is the mean value of a respiratory variable, e.g. inspiratory or expiratory time, tidal volume; a is a constant; and ε_n is the disturbance. It means the breathing cycle is adjusted according to the former one, producing a certain pattern of breathing. The auto-adaptive characteristics in breathing sequence might be a self-optimizing behavior to keep the performance of respiratory system at its minimum (Pribean and Fincham, 1965).

To summarize, there exists diversity in the breathing pattern of humans, in terms of breathing frequency, volume rate and flow shapes. Simultaneously, the breathing of one individual appears to be relatively stable in several conditions and has his own pattern of breathing. Hence, it is difficult to reproduce the breathing of every individual for experiment or simulation purpose with respect to the diversity and individuality, and one possible way to fulfill the purpose is to use one particular breathing pattern with the average characteristics of overall people.

1.2.4. INFLUENCING FACTORS

The complexity of the dispersion of the airflow from human breathing indoors is not only due to the diversity among individuals, but also due to multiple factors affecting it. These influencing factors can be summarized in two broad terms: human factors (e.g. metabolic levels) and room conditions (e.g. ventilation, ambient temperature, humidity, turbulence and so on). Table 1.2 gives some relevant findings of these influencing factors. It can be expected that the interactions among these factors add complexity to the dispersion of exhaled air.

Two of these factors: ventilation strategies and metabolic levels are emphasized in this thesis. Some literatures have reported that airflow pattern is the most significant parameter influencing contaminant transport in indoor environment (He et al., 2005; Lai et al., 2007; Chao et al., 2008). Two ventilation schemes being widely used in public buildings are chosen and investigated in this thesis, which are mixing ventilation and displacement ventilation. Personalized ventilation is also considered in this thesis in terms of its interaction with body plume and its impact on inhaled air quality. The metabolic levels are closely related to the breathing volume rate and heat release from bodies, which should also be of concern in terms of simulations.

Table 1.2 Findings of relevant influencing factors.

Factors	Tools	Studies and findings
Metabolic levels	\	<p>The metabolic levels may indirectly affect the transport of exhaled contaminant by means of influencing:</p> <ul style="list-style-type: none"> ✓ breathing frequency ✓ the initial velocity of exhalation ✓ the temperature of human body ✓ the intensity of thermal plume around a person
Ventilation strategies	<p>CSP^a</p> <p>Manikin</p> <p>CSP & Manikin & Panel</p> <p>Manikin & CSP</p>	<p>Different ventilation patterns may influence:</p> <ul style="list-style-type: none"> ✓ The dispersion and mixing of exhaled droplets with ambient air and overall contaminant distribution indoors (Mui et al., 2009;). ✓ The trajectories of exhaled air and droplets with different diameters (Qian et al., 2006; Olmedo et al., 2012). ✓ The intake exposure level for a receive person when facing to an infected person or a contaminant source (He et al., 2011; Olmedo et al., 2012; Brohus, 1997). ✓ Velocity of thermal plume above a person's head (Liu et al., 2009b)
Temperature	<p>Panel</p> <p>CSP</p>	<ul style="list-style-type: none"> ✓ Ambient air temperature affects the exhaled temperature from mouth or nose (Hoppe, 1981). ✓ Temperature affects droplet evaporating but the influence on dispersion trajectory can be neglected (Chen and Zhao, 2010).
Relative humidity	CSP	<ul style="list-style-type: none"> ✓ Relative humidity affects the evaporation of droplets directly, but the influence can be neglected when the initial diameter of droplets is < 200 μm (Chen and Zhao, 2010).
Turbulence	<p>Manikin</p> <p>Manikin & CSP</p>	<ul style="list-style-type: none"> ✓ The turbulence intensity in the breathing zone is expected to be larger than other parts of the room: Cermak et al. (2002) – 35%; Xia et al. (2000) – 40%; Marr et al. (2005) – 130%. ✓ Physical movement increases the turbulence mixing in a room and decreases the protective effect of boundary layer around a person. (Bjørn and Nielsen, 2002)
Other factors	\	<p>Other possible factors:</p> <ul style="list-style-type: none"> ✓ Droplet size ✓ Scales of breathing organs ✓ Dimension of the room ✓ Obstacles in rooms ✓ ...

^a CSP=computer-simulated person.

1.3. TOOLS FOR EVALUATING HUMAN BREATHING

From Table 1.2, it can also be seen that there are mainly three tools commonly used for breathing assessment. They are:

- ✓ computer simulated persons (CSPs)
- ✓ breathing thermal manikins (BTMs)
- ✓ human subjects

This section will present some former applications of the three tools. In the following chapters, a CSP, a BTM and human subjects will be considered for breathing assessment.

For comparison, advantages and disadvantages of these three tools in practical application are listed in Table 1.3.

Table 1.3 Overview of the advantages and disadvantages of the three tools for human breathing studies.

Tools	Advantages	Disadvantages
CSPs	<ul style="list-style-type: none"> ✓ Fast and cost-efficient. ✓ It can provide detailed information on flow field or heat transfer that might be difficult to measure through experiments. 	<ul style="list-style-type: none"> • It may induce false or inaccurate results due to improper handling with the problem (Nielsen, 2004). • Limited by computer power.
BTMs	<ul style="list-style-type: none"> ✓ Quick, accurate and repeatable (Holmér, 2004). ✓ Provide valuable results for CFD comparison. ✓ It can act as a substitute of human to perform toxic or hazardous test. 	<ul style="list-style-type: none"> • Expensive instrument with delicate design. • It can be standard person but ignores the diversity of people.
Human volunteers	<ul style="list-style-type: none"> ✓ Realistic subjects and situations 	<ul style="list-style-type: none"> • Safety is all-important. Techniques in connection with high intensity lasers, irritant or toxic gases or particulates are not applicable (Tang et al. 2011). • Highly variable results, depending on physical and psychological factors.

CSPs

With the development of computer resources, numerical models are developed to simulate thermal manikins and their interaction with indoor environment. A CSP may be a three-dimensional model, with simple or lifelike geometry with human, and used in different occasions, i.e., offices, homes, public buildings or vehicles etc.

Due to the complex interaction of human exhaled flow with ventilation, thermal plume around the body and physical activities, the application of CSPs can potentially provide some insight of the interaction mechanism. The advantage of using a CSP to predict the influence of a person indoors is evident, which is low cost and fast, but the accuracy of the simulated results should be validated with experimental data obtained from BTM or human subjects.

BTMs

A BTM is constructed with breathing and heating functions to simulate the breathing process and thermal properties of a person. Manikins were originally developed to provide accurate information on clothing insulation properties and heat transfer between human body and the environment (Tanabe et al., 1994 and Madsen, 1999). The increasing use of manikins in indoor climate research has led to the development of a manikin with breathing functions (Björn, 1999).

To evaluate the roles of a person as well as the breathing in indoor climate, various types of manikins have been manufactured. The human-shaped manikin is a kind of expensive and delicate instrument, and at the same time a powerful tool with useful features for indoor climate evaluation. The typical fields that apply the BTMs are listed below. These manikins are generally employed to predict or evaluate:

- ✓ indoor air quality
- ✓ cross-infection risk
- ✓ thermal comfort
- ✓ heat transfer properties of the body through convection, radiation or sweating
- ✓ flow characteristics around the body
- ✓ clothing insulation coefficients
- ✓ etc.

In addition, some otherwise hazardous methods to humans can be applied to these BTMs, including:

- ✓ gas or particle tracing approaches
- ✓ smoke visualization
- ✓ Particle Image Velocimetry (PIV)
- ✓ Laser Doppler Anemometry (LDA) or Phase Doppler Anemometry (PDA)

Holmér (2004) expected two directions of the advancement of the manikins. One is towards more delicate and complex construction, to be as realistic as a real person. The improvements include realistic movement, sweating and respiratory system, or auto thermal regulation setup. Another trend is towards simple, yet accurate and reliable manikins that are inexpensive. No matter how complex or how simple a thermal manikin model is, there is one goal both directions should reach, which is to

simulate human behavior more accurately and reliably. To realize this goal, accurate information obtained from human subjects is necessary.

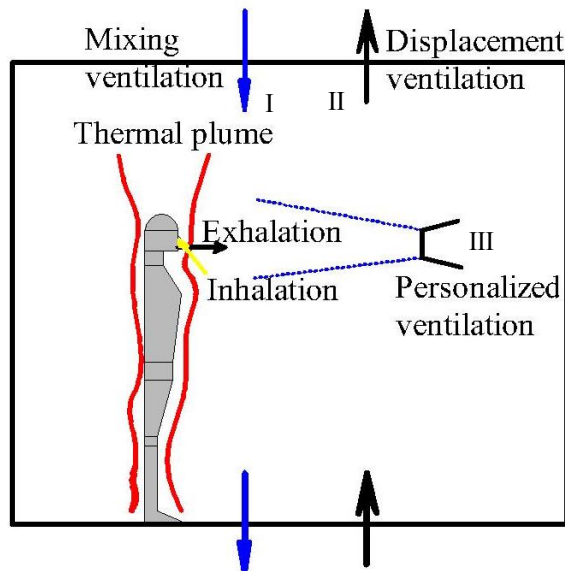
Human volunteers

Compared with substantial information on human breathing provided by using CSPs or BTMs, there exists only a few published papers (Gupta et al., 2010; Tang et al., 2011; Tang et al., 2013; Kwon et al., 2012) about actual human breathing. Main difficulties for human experimentation can be drawn from Table 1.3.

One difficulty is the diversity among individuals and not very stable characteristics of human breathing (Chapter 1.2.3), resulting in variable results and sometimes difficult generalization. What is more, the strict safety requirements for human experimentation limit the use of instruments or approaches that are hazardous to human beings. Hence, most researchers prefer the human-like models (BTMs or CSPs) to provide valuable information on human breathing.

However, differences between the simulated results and the reality remain a question. Accurate data obtained from human subjects is needed. The use of human volunteers adds an additional realism to the results and is possible to enhance our understanding of the behavior of human exhaled airflow.

1.4. AIMS AND SCOPE



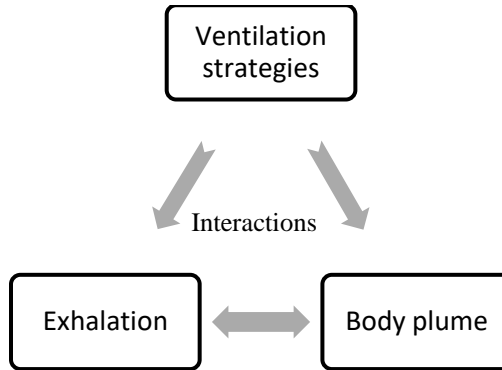


Figure 1.4 Overview of the research scope and aspects of this thesis.

The aim of the present work is to characterize human breathing and its interactions with room ventilation. Figure 1.4 shows the research scope of this thesis. The pairwise correlations and interactions among the three factors: ventilation strategies, breathing and human body plume, will be investigated. It is aimed to gain more knowledge of the influences of ventilation principles and body plume on human breathing. Three conventional ventilation strategies: mixing ventilation (MV), displacement ventilation (DV) and personalized ventilation (PV), are introduced and applied to study their direct impacts on human exhalation or their indirect impact by influencing the development of thermal plume around body which then interacts with human breathing.

Three kinds of tools: a BTM, a CSP and human subjects, are considered in this study. Special focus is given to human experiments regarding its importance and the relatively less information on real human breathing.

CHAPTER 2. METHOD AND MATERIALS

This chapter briefly introduces the tools and ventilation principles applied in this thesis. The methodologies and facilities used during experiments and numerical simulations will also be illustrated.

2.1. TOOLS FOR BREATHING ASSESSMENTS

2.1.1. BREATHING THERMAL MANIKIN

The breathing thermal manikin (BTM) was constructed to mimic an averaged female subject for full-scale experiments. Figure 2.1 shows the geometry of the BTM, which has a simplified body shape and is designed as close as possible to a real woman (Bjørn, 1999). The BTM has a body surface area (BSA) of 1.44 m² and a height of 1.68 m. The facial part is also composed of simple geometrical shapes, with a semi-ellipsoid mouth opening (120 mm²) and two cylindrical nostrils (diameter 12 mm).

The manikin's hollow aluminum shell can be heated by heating wires uniformly distributed inside it. Two fans, forcing the internal air to circulate, aids in creating an even temperature distribution. For this study, two metabolic rates are considered: 1.2 met and 2 met, which can be translated to 70 W/m² and 115 W/m² heat output according to ASHRAE (2009). As the aluminum-shelled manikin has no sweating function, only sensitive heat through convection and radiation is applied. Table 2.1 gives the percentage of the two kinds of heat occupied in total metabolic heat (Stampe, 1982).

Breathing frequency and pulmonary ventilation of the manikin can be regulated by connecting it to a mechanical lung. Figure 2.1(b) simply shows the connection. Two cylinder rubber tubes, responsible for exhalation and inhalation respectively, are connected to the mouth/nose by one side and to the artificial lung by the other side to create respiration from mouth/nose. One heating pipe mounted on the tube for exhalation can regulate the exhaled air temperature. Table 2.2 summarized the setup for breathing with the three different ventilation strategies.

Nitrogen oxide (N₂O) is used as tracer gas, representing the component of CO₂ in exhaled air. The density of the dry exhaled air from the BTM with 4 vol.% N₂O is corrected to simulate the same density as ideal saturated air with water vapor in exhalation (Bjørn, 1999).

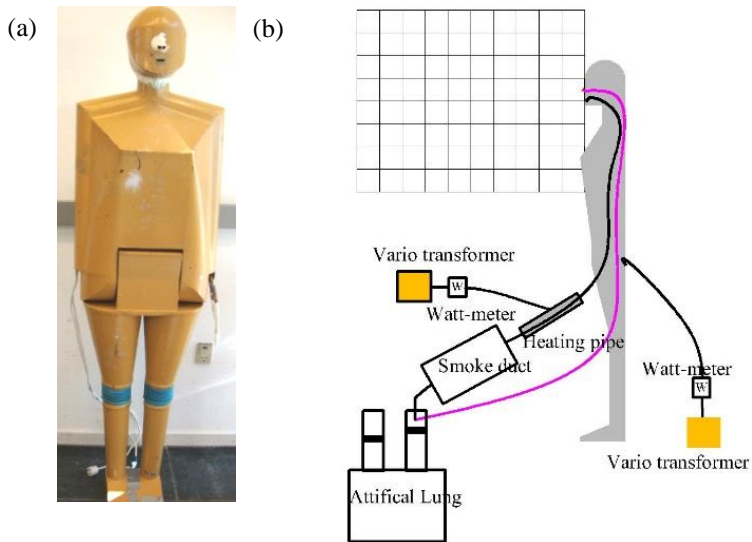


Figure 2.1 (a) Picture of the manikin. (b) Connection to the artificial lung, heating pipe and heating control devices.

Table 2.1 Percentage of convective and radiative heat released from the manikin's body (Stampe, 1982).

Metabolic level	Convection	Radiation	Evaporation (by sweating and respiration)
1.2 met	35%	34%	31%
2 met	31%	30%	39%

Table 2.2 Respiration of the BTM with MV, DV and PV.

	MV & DV	PV
Breathing frequency (Admas 1993)	16 min ⁻¹ (1.2 met, standing) 19 min ⁻¹ (2 met, standing)	10 min ⁻¹ (1.2 met, sedentary)
Minute volume (Admas 1993)	8.8 l/min (1.2 met, standing) 15.2 l/min (2 met, standing)	6 l/min (1.2 met, sedentary)
Exhaled air temperature	33.0 °C	Not considered.
N ₂ O	4 % (by volume)	

2.1.2. COMPUTER SIMULATED PERSON

Geometry

The geometry of the computer simulated person (CSP) is shown in Figure 2.2. This model is built mostly in accordance with the BTM shown in Figure 2.2. Slight changes are made at the head, shoulder and feet for the convenience of modelling. The BSA of the CSP is 1.63 m². The mouth is simplified as a circular shape with an area of 113 mm². Only mouth breathing is considered for the CSP. The mesh is refined at the mouth opening and on the body surface. Refined tetrahedral cells are used around the CSP and hexahedral cells are used in the rest of the room. The minimum size of the mouth cells is 1.2 mm. The y^+ in the wall-adjacent cells is approximately 30. Standard wall function is generally applicable when the y^+ of the first cell center adjacent to the wall is larger than 30 (ANSYS FLUENT User's guide, 2010) and it is therefore adopted in this thesis. Grid independence is achieved at 0.85 million mesh elements as a further increase to 10.2 million mesh elements causes negligible changes in exhaled air velocity and concentration profiles.

Equations

The purpose of this model is to create a tool for evaluating the accuracy of simulation of human breathing by means of CFD. To solve the unsteady and non-isothermal problem, combined with the consideration of species component of CO₂ in exhaled air, four conservation equations should be solved, which are continuity, momentum, energy and species transport equations. All the equations are discretized with second order upwind. The effect of radiation is included by using the S2S radiation model. The RNG k - ϵ is chosen for RANS turbulence modelling due to its good performance of airflow and contaminant distributions indoor (Srebrica, et al. 2008). SIMPLEC scheme is used to solve the velocity-pressure coupling.

Software

A commercial CFD code Fluent (Ansys 2010) is used to compute the flow dynamics around the CSP and exhalation and inhalation characteristics with MV and DV.

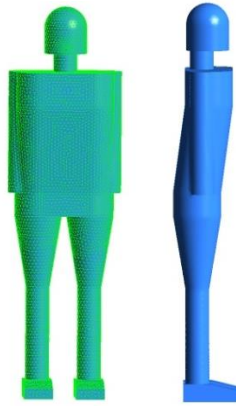


Figure 2.2 The CSP used to simulate the BTM. Left: front view of the CSP and grid layout on the surface. Right: side view of the CSP.

2.1.3. HUMAN VOLUNTEERS

Two groups of young adults are instructed to participate in different experiments. All experiments on human subjects are performed in case of fully mixed ventilation. Table 2.3 presents the basic information of two group subjects as well as the corresponding experiments conducted on them.

Table 2.3 Basic information and experiments performed on the two groups of human subjects.

	Group 1		Group 2	
Gender	Male	Female	Male	Female
Subject no.	15	8	8	10
Age	26.1(23.0-35.0)	27.4(21.0-33.0)	29(22-33)	28(26-29)
Weight (kg)	71.8(52.9-95.0)	53.3(46.0-70.4)	69.7(62.0-75.1)	52.9(47.2-64.1)
Height (m)	1.76(1.60-1.86)	1.65(1.58-1.71)	1.74(1.64-1.81)	1.63(1.55-1.72)
BSA (m ²) (Du Bois 1989)	1.87(1.57-2.20)	1.56(1.44-1.82)	1.83(1.73-1.92)	1.55(1.49-1.71)
Experiment types	<ul style="list-style-type: none"> ✓ Velocity profile description (shown in Figure 2.3) ✓ Velocity decay assessment (shown in Figure 2.3) ✓ Concentration decay 		<ul style="list-style-type: none"> ✓ Schlieren imaging test (shown in Figure 2.4) ✓ Velocity decay assessment (shown in Figure 2.3) 	
Postures	<ul style="list-style-type: none"> ✓ Standing 		<ul style="list-style-type: none"> ✓ Standing ✓ Lying 	

Breathing pattern	✓	Mouth only (with nose chip)	✓	Mouth only (with nose clip)
	✓	Nose in and mouth out	✓	Nose in and mouth out
			✓	Nose only

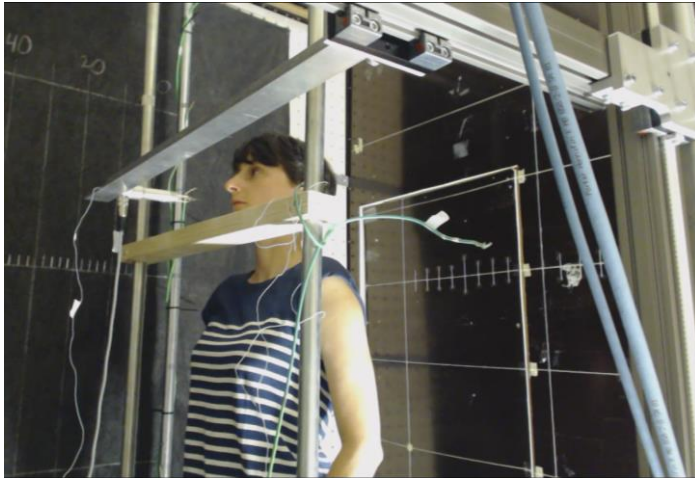


Figure 2.3 Photo of one female subject taking velocity measurement. Probes for testing temperature, velocity and gas concentration can be installed on the robot arm and be carried along horizontal and vertical directions. This female subject is selected from Group 1 in Table 2.3.

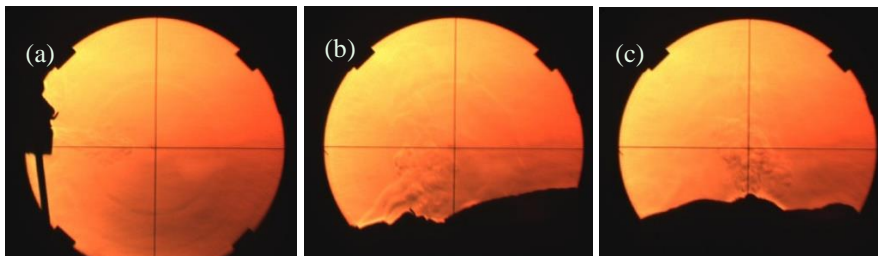
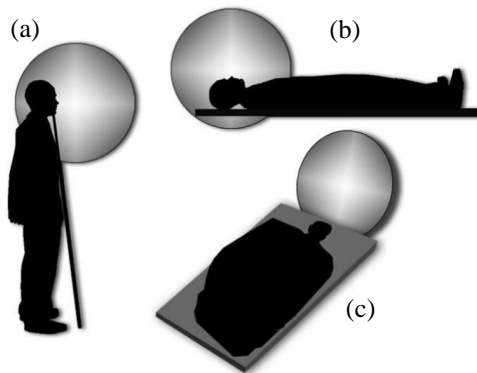


Figure 2.4 Schlieren images of one male subject included in Group 2 (Table 2.3) with mouth breathing. (a) standing- side view, (b) lying- side view and (c) lying-front view.

Experiments conducted on subjects of Group 1 are used to validate the simulated breathing by the BTM and CSP. Thereby, all the setups of the human experiment keep in consistent with those of the BTM (Figure 2.3). Experiments for Group 2 are aimed to provide further information on human breathing characterization, which are realized by means of schlieren imaging technique (Figure 2.4).

2.1.4. COMPARISONS AMONG THE THREE TOOLS

A direct comparison of the physiological parameters among the three tools is given in Table 2.4. The CSP model is built according to the BTM and the BTM is constructed in accordance with a life-size women (Bjørn, 1999). To exactly mimic the breathing behavior of human, the physiological parameters of the BTM are set with great likeness to those of real persons.

In this section, comparisons in terms of geometry, breathing function and metabolism are conducted among the three tools, which are summarized in Table 2.4. Comparisons are made on the basis of merely standing posture with a metabolic rate of about 1.2 met under MV or/and DV.

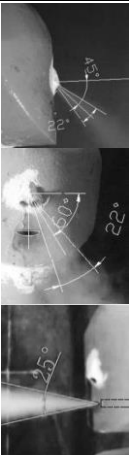
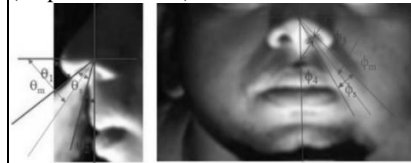
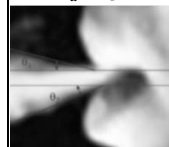
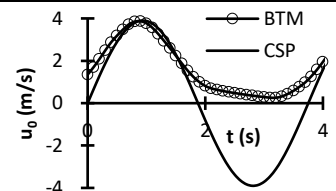
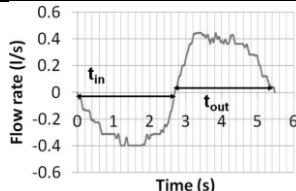
It can be seen from Table 2.4 that all the parameters of the manikin and the CSP are set with approximate likeness to a real person to create lifelike conditions as far as possible. Accurate configuration of the manikin or the CSP is the first step to simulate human breathing behavior accurately. Chapter 4 will further discuss the results obtained with the three tools.

Table 2.4 Comparison of physiological parameters among the BTM, the CSP and human subjects (Group 1).

Parameter	BTM	CSP	Male subjects	Female subjects
Posture	Standing	Standing	Standing. All subjects are instructed to stand with their heads supported by a fixed bar to avoid movement during experiments.	
Ventilation principle	MV&DV	MV&DV	MV	MV
Height (m)	1.72	1.72	1.75(1.60-1.86)	1.65(1.58-1.71)
Weight (kg)	\	\	71.8(52.9-95.0)	53.3(46.0-70.4)
Age (years)	\	\	26(23-35)	27(21-33)
BSA (m ²)	1.47	1.63	1.87(1.57-2.20)	1.56(1.44-1.82)
BF (min ⁻¹)	16	16	14.6(7-20)	16.3(10-22)

BMV (l/min)	8.8	8.8	9.87(8.21-11.48)	7.22(6.67-8.45)
----------------	-----	-----	------------------	-----------------

Table 2.4 continued .

Parameter	BTM	CSP	Male subjects	Female subjects
Mouth area(cm ²)	1.23	1.13	1.2±0.52	1.16±0.67
Nose area (cm ²)	0.56	\	0.71±0.23	0.56±0.10
Breathing direction		Circular mouth opening with horizontal direction	Angles obtained from human subjects (Gupta et al. 2010) :  $\theta_m = 60^\circ \pm 6^\circ$ $\Phi_m = 69^\circ \pm 8^\circ$ $\theta_a = 23^\circ \pm 14^\circ$ $\Phi_s = 21^\circ \pm 10^\circ$  $\theta_1 + \theta_2 = 30^\circ$	
Waveform	 The velocity from the manikin's mouth is always positive due to the use of a hot sphere anemometer that cannot measure the direction of velocity.		 (Gupta et al. 2010)	
Metabolic rate	1.2 met (see Table 2.1)	1.2 met (in line with the BTM)	Not measured. Standing relaxed for more than 10 minutes before experiments.	
Breathing patterns	✓ Mouth only ✓ Nose in and mouth out.	✓ Mouth breathing only	See Table 2.3 Group 1.	
Exhaled air temperature	34 °C	32.5 °C	Mean 33.8 °C Range 32-36 °C	
Exhaled air component	Air + 4 vol.% N ₂ O,	Air + 4 vol. % CO ₂	Saturated moist air.	

2.2. VENTILATION SETUPS

2.2.1. MIXING VENTILATION AND DISPLACEMENT VENTILATION

Experiment

Experiments with MV and DV are performed in a full-scaled test chamber shown in Figure 2.5. The chamber consists of plenums to the ceiling and to the floor. Cold and fresh air (about 17 °C) enters the plenum, passes through hundreds of small holes (diameter of 10 mm) uniformly distributed in the ceiling (MV) or the floor (DV) and circulates in the room. The small holes are used to distribute air uniformly. Ventilation patterns can be altered between flow typical for MV to flow typical for DV by switching the combinations of the inlet and outlet shown in Figure 2.5.

The temperature gradient along vertical height can be expected to be basically uniform with MV and to increase with the height with DV. To create a relatively uniform temperature gradient, dT/dy , two radiators (R1 of 350 W and R2 of 40 W) are mounted on the wall for DV. The air change rate (ACR) is 7.5 h^{-1} with MV. For DV, as the heat loads in the chamber are increased by applying the two radiators, the ACR is increased to 10 h^{-1} . The reason for the application of a large ACR in present study is to create a relatively large temperature gradient for DV. The temperature differences between the exhaled air and the ambient room air will also be raised by increasing ACR, yielding a larger Archimedes number as given in the following equation (Olmedo et al., 2012). The trajectory of the non-isothermal exhaled flow will be more significantly affected by both higher temperature gradient and larger Ar (Liu, et al., 2009b).

$$Ar = \frac{\beta g (T_{exh} - T_a) \sqrt{a_0}}{u_0^2} \quad (2.1)$$

where β , g , T_{exh} , T_a , a_0 and u_0 are volume expansivity (K^{-1}), gravity acceleration (m/s^2), exhaled temperature ($^{\circ}\text{C}$), ambient air temperature ($^{\circ}\text{C}$), mouth area (m^2), and maximum velocity of exhalation (m/s).

Simulation

In order to validate the simulated results with the CSP (shown Figure 2.2), the same layout and geometry of the simulated chamber (see Figure 2.6) as the test one (see Figure 2.5) is used. Ventilation is simulated by considering the floor/ceiling as a whole opening for supplied or exhausted air. Boundary conditions are set in accordance with experiments. Details about the boundary conditions are reported in Table 2.5.

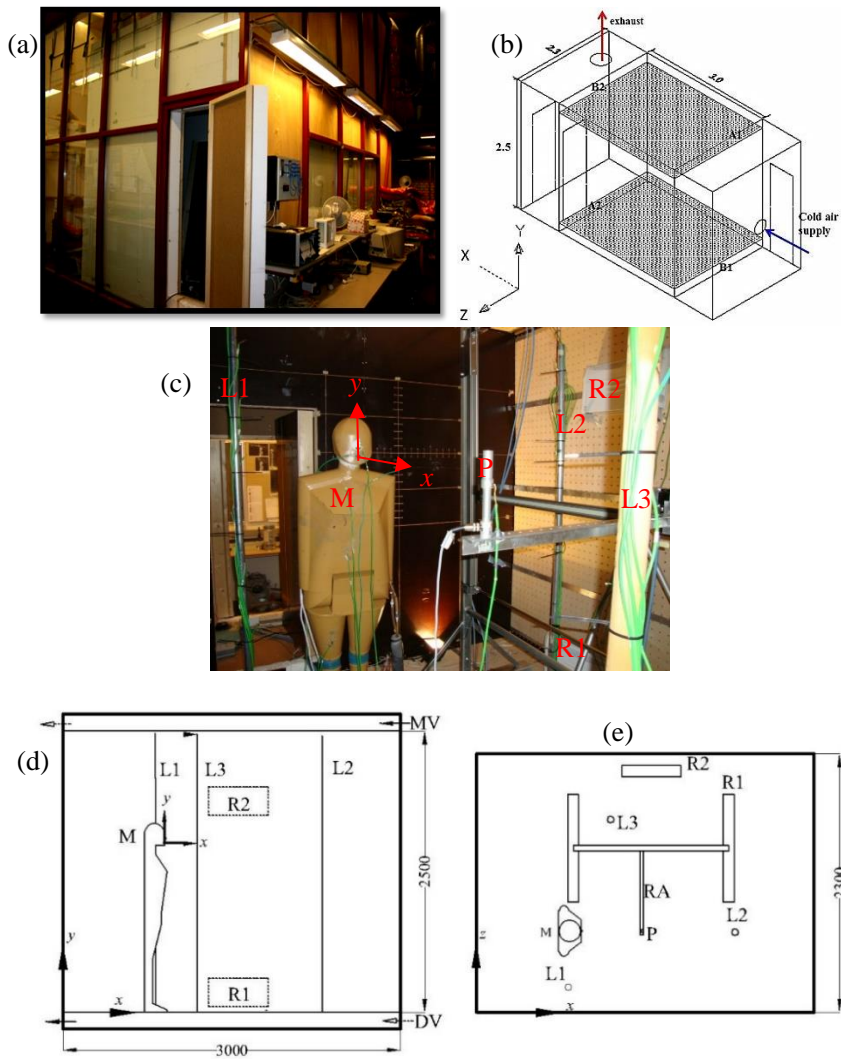


Figure 2.5 (a) Picture of the test chamber insulated by plastic foam board with a thickness of 10 cm. (b) Sketch of the test chamber. (c) Picture of the inner layout of the test chamber. (d) and (e) Sketches of the inner layout from side and top view, respectively. The ventilation patterns can be switched between MV case and DV case. R1 and R2 are two radiators, M is the manikin, L1, L2 and L3 are three poles with thermocouples, RA is the robot arm, and P is the testing probe that is calibrated before experiments. A coordinate with x and y axis is built from the manikin's mouth.

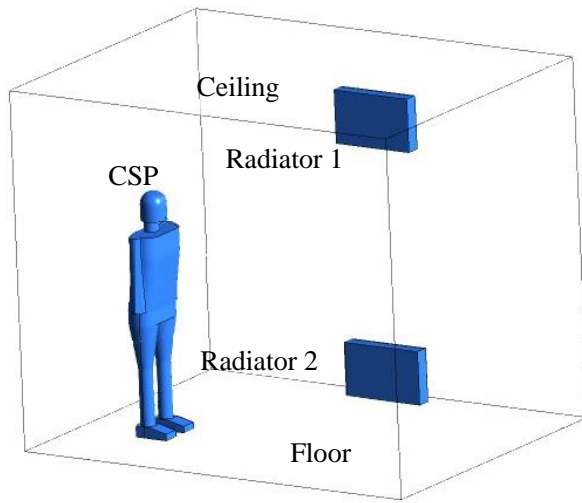


Figure 2.6 Setup of the test room with the CSP.

Table 2.5 Boundary settings of the simulated room with the CSP.

	MV	DV
Ventilation	Whole floor in and whole ceiling out Ceiling: mass flow inlet Flow rate=4.88 kg/s air=7.5 h ⁻¹ ACR Floor: pressure outlet Supplied air temp. 21.5 °C Turbulence intensity of supplied air I=2%	Whole floor in and whole ceiling out Floor: mass flow inlet Flow rate=6.51 kg/s air=10 h ⁻¹ ACR Ceiling: pressure outlet Supplied air temp. 19 °C Turbulence intensity of supplied air I=2%
Radiator	Radiator 1 -0 W Radiator 2 -0 W	Radiator 1 - 623.7 W/m ² (350 W) Radiator 2 -71 W/m ² (40 W)
CSP	Exhaled air flow rate=4.7×10 ⁻⁴ kg/s=8.8 l/min Mass fraction of CO ₂ =7.9 g/kg air Exhaled air temp.=32.5 °C Breathing frequency=16 min ⁻¹ Turbulence intensity of exhaled air I=5% Body surface temp.=27.6 °C	
Chamber	Side wall –adiabatic	

CO₂ is used as the tracer gas for the CSP with a volume fraction of 4%. The heat release from the CSP is converted into constant body surface temperature of about 27.6 °C that is in line with the measured average body temperature. For transient breathing, a UDF program is imported to describe the pulsating velocity at the mouth opening with a sinus waveform. The time-step size for transient solution is set as 0.01 s. Full Buoyancy Effects is enabled in Fluent regarding the buoyancy effect on ϵ (RNG

$k-\varepsilon$ model). Gas density is set up as a function of temperature using the Boussinesq model.

2.2.2. PERSONALIZED VENTILATION

Measurements on PV are performed in a full-scale chamber equipped with diffuse ceiling ventilation, as shown in Figures 2.7 and 2.8. More introductions of the test chamber can be found in Zhang et al. (2015).

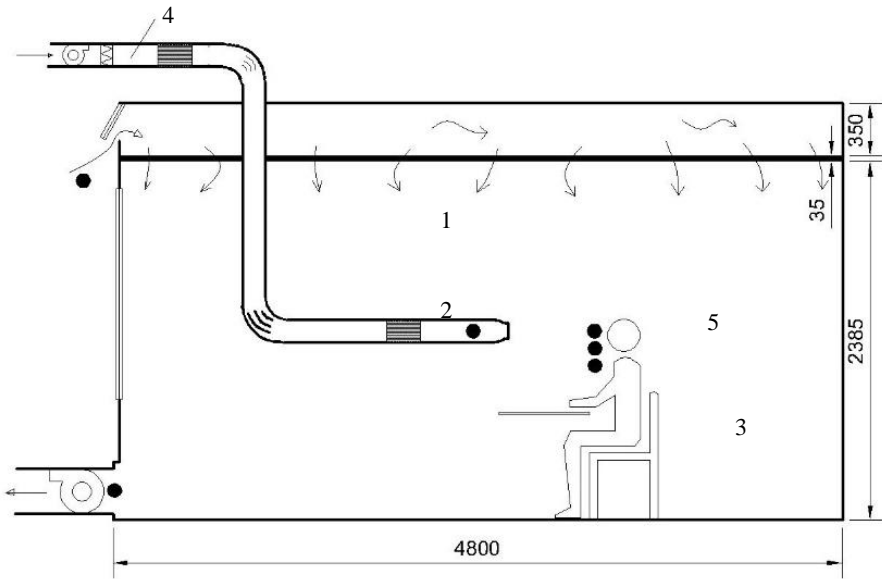


Figure 2.7 Experimental set-up of the test chamber equipped with 1-diffuse ceiling and 2-personalized ventilation. The 3-BTM is placed 0.12 m away from the front table edge, facing to the nozzle. N_2O is dosed with a constant volume fraction of 4% at 4 and sampled at six points 5 (solid dots). Units in mm.

The diffuse ceiling ventilation supplied 60.2 l/s of laboratory air to the chamber, corresponding to an air change rate of 5.4. The velocity generated by mixing ventilation, namely the diffuse ceiling ventilation, is below 0.06 m/s, except for local velocity of around 0.13 m/s close to the ceiling. The temperature gradients along the vertical height can be negligible. The averaged room air temperature is about 24 °C during all experiments.

The PV system supplies outdoor air with a varying flow rate (1.5~4 l/s). The air temperature from the nozzle opening varies from 22.6 °C to 23.2 °C.

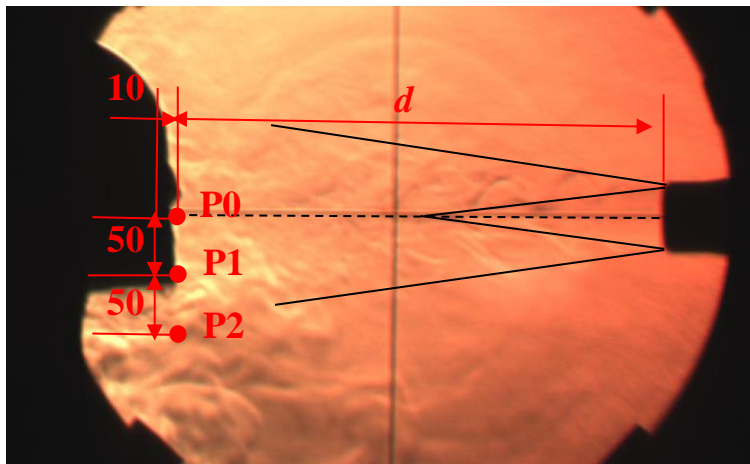


Figure 2.8 Relative position between the nozzle and the manikin. The centerline of the nozzle (a diameter of 50.8 mm and a tube diameter of 83.0 mm) is pointing to the nose point P_0 which is 10 mm away from the face. Velocities at P_0 , P_1 and P_2 were measured by the LDA. N_2O in inhaled air were measured in the tube connected to the artificial lung rather than at P_0 .

2.3. MEASURING FACILITIES AND METHODS

Table 2.6 summarizes the main measuring facilities applied in this thesis. Table 2.7 represents the application methods of the measurement facilities under MV/DV and PV, respectively.

Table 2.6 Measurement instruments and uncertainty.

Testing items	Type	Uncertainty
Temperature	Type K thermocouples (connected to Hellos data logger)	± 0.1 °C
Velocity	Dantec 54R50 Omni- directional hot sphere anemometer	± 0.025 m/s
	Laser Doppler Anemometry (LDA)	± 0.001 m/s
Tracer gas concentration	Multipoint sampler and doser (INNOVA 1303) Photoacoustic field gas monitor (INNOVA 1412)	$\pm 2\%$
Flow visualization method	SAFEX fog generator (for BTM)	\
	Schlieren imaging technique (for persons and personalized air)	\

Table 2.7 Application of the measurement instruments with MV/DV and PV.

Testing items	MV and DV	PV
Temperature	Position: <ul style="list-style-type: none"> ✓ Three poles: L1, L2 and L3, equally mounted with eleven thermocouples for each (shown in Figure 2.5). ✓ Six thin thermocouples respectively placed in the mouth, the nostril, on the robot arm and on the body surface. ✓ Supplied air and exhaust. 	Position: <ul style="list-style-type: none"> ✓ Four poles equally distributed in the room to measure the vertical temperature distribution (shown in Figure 2.8). ✓ Manikin's body surface. ✓ Supplied air from general ventilation and PV respectively.
Velocity	Dantec 54R50: <ul style="list-style-type: none"> ✓ Carried by a robot arm to different horizontal and vertical distances within the exhaled flow. ✓ Acquisition frequency: 10 Hz. 	LDA: <ul style="list-style-type: none"> ✓ 2 Dimensional ✓ Placed in the BZ at 10 mm away from the nose tip along a vertical transverse line near the manikin's face (shown in Figure 2.8). ✓ The mean resultant velocity, u_b, is obtained by composition of u_x and u_y (mean velocity along the x and y axis), which can be expressed by: $u_b = \sqrt{u_x^2 + u_y^2}$
Tracer gas concentration	N ₂ O (manikin): <ul style="list-style-type: none"> ✓ Dosing position: added in manikin's exhalation with a volume fraction of 4% ✓ Sampling positions: exhaled air from the manikin along the centerline (c_x) and in the exhaust (c_R). CO ₂ (human subjects): <ul style="list-style-type: none"> ✓ Sampling positions: exhaled air from human subjects along the centerline and probe carried by the robot arm (c_x) and in the exhaust (c_R). 	N ₂ O (manikin): <ul style="list-style-type: none"> ✓ Dosing position: added in front of the nozzle with a constant volume fraction of 4% and fully mixed with fresh air from outdoor. ✓ Sampling positions: the N₂O concentration at the nozzle exit (c_{pv}), in the exhaust (c_e), and in inhalation or at a point in the BZ (c_{bz}).
Flow visualization method	Manikin: <ul style="list-style-type: none"> ✓ Oil-based smoke added in exhalation. Human subjects: <ul style="list-style-type: none"> ✓ Schlieren imaging technique used for visualizing body plume and exhaled air. 	Manikin: <ul style="list-style-type: none"> ✓ Schlieren imaging technique used to visualize the nozzle jet and its interactions with thermal plume around body.

CHAPTER 3. INTERACTIONS AMONG ROOM VENTILATION, BODY PLUME AND HUMAN BREATHING

This chapter will serve as an illustration on the interactions among the three factors introduced in Figure 1.4, i.e. room ventilation, thermal plume around the body and human breathing. For the displacement ventilation and the mixing ventilation, the influences of ventilation principles and body plume on exhaled air dispersion will be highlighted in order to examine the potential of human exhalation as contaminant source. For personalized ventilation, the inhaled air quality will be focused in order to evaluate the protection effect of personalized ventilation by considering its interaction with thermal boundary layer around the body.

The main findings of this chapter are based on Papers [a], [b] and [e].

3.1. MIXING VENTILATION AND DISPLACEMENT VENTILATION

Mixing ventilation (MV) and displacement ventilation (DV) are conventionally used ventilation principles in buildings. The dispersion of exhaled flow has been observed with different characteristics under these two ventilation principles (Brohus and Nielsen, 1996; Bjøn and Nielsen, 2002; Qian et al., 2006 and Olmedo et al., 2012).

Four cases by combining the two metabolic levels (1.2 met and 2 met) with the two ventilation patterns (MV and DV), are studied. Attempts will be made in this section to reveal the dependence of dispersion of exhaled air on both MV and DV. As no significant temperature differences are found at the three different locations of L1, L2 and L3 in Figure 2.5, the measured temperature at L1 is extracted and used to indicate vertical temperature distribution in the test room, as shown in Figure 3.1. The vertical temperature gradient, defined as dT/dy , is approximately $0\text{ }^{\circ}\text{C/m}$ for MV due to its fully mixing feature, and it is about $1.5\text{ }^{\circ}\text{C/m}$ and $1.8\text{ }^{\circ}\text{C/m}$ for DV 1.2 met case and DV 2 met case, respectively. The larger gradient for the 2 met case is caused by higher heat release from the manikin's body.

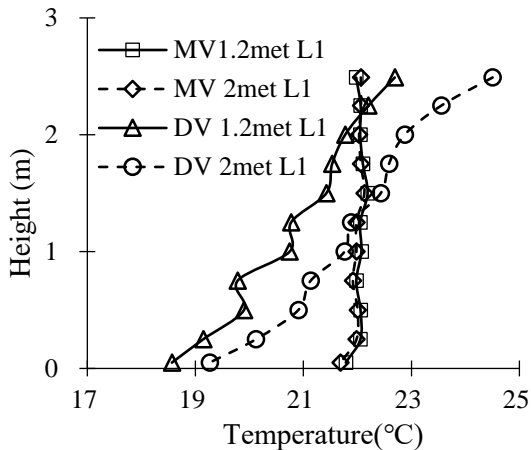


Figure 3.1 Temperature gradients along L1, L2 and L3 with MV and DV [a].

3.1.1. INTERACTION BETWEEN BODY PLUME AND INHALED AIR

The tracer gas (N_2O) is expired through exhalation. When examining the inhaled air, we find a portion of exhaled pollutants is re-inhaled from the front and lower part of the manikin’s body. Hayashi (2002) also reported that the inhalation region is mainly around human body and the highest percentage of inhaled air is from the front part of the body.

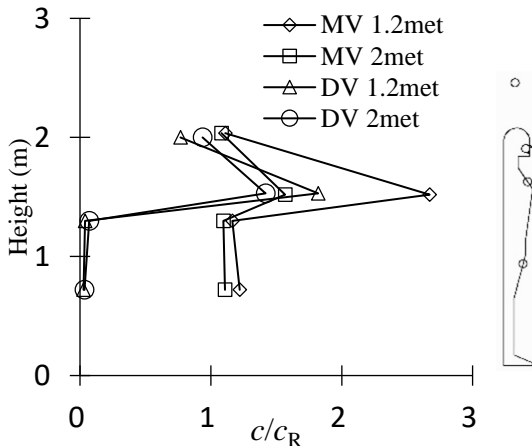


Figure 3.2 Measured N_2O concentration, c , at the four different heights (thigh, chest, nose and above head) around the manikin, divided by c_R . N_2O concentration at the exhaust. The c and c_R are averaged concentration of tracer gas [a].

Figure 3.2 shows that the c/c_R in inhalation is enhanced for MV case compared to DV case with the same metabolic rate. That is because the DV creates a clean zone at the lower part of the room with c/c_R approximate to zero and the inhaled air is partly drawn from this zone by the rising thermal plume. When the metabolic rate increases, the effect of thermal plume on inhaled air becomes more significant. It can be seen from Figure 3.2 that c/c_R is decreased with growing metabolic level. This can serve as another proof that the majority of inhaled air is from the thermal plume around body.

3.1.2. INTERACTION BETWEEN BODY PLUME AND EXHALED AIR

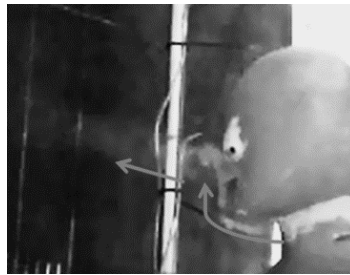


Figure 3.3 Visualization of the smoke plume entering the exhaled flow. The smoke released at the floor level is carried up to the facial part by the thermal convective flow around the manikin and is expelled when the manikin exhales. No extra smoke is added to exhalation.

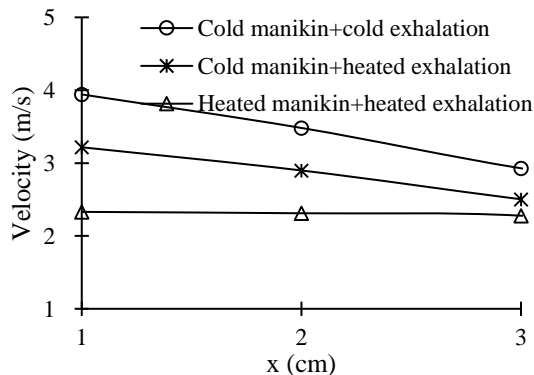


Figure 3.4 Maximum velocity measured close to the mouth. Three conditions are considered: both exhalation and manikin body are heated, corresponding to 1.2 met; only the exhalation is heated; and no heat input for the manikin. Other factors of the manikin and its breathing keep consistent with the settings for the manikin with MV 1.2 met case shown in Table 2.2.

The thermal stream around the body will not only enters inhaled air but can also be entrained by exhaled flow. Smoke is released at the floor level and no extra smoke is added to the exhalation, but it can be observed that the smoke stream appears in exhalation flow as shown in Figure 3.3. This is caused by the collision of upward

thermal plume layer with exhaled flow. The collision also causes velocity decrement when the exhaled air penetrates the thermal boundary layer, see Figure 3.4. In Figure 3.4, the exhaled velocity decreases due to the presence of thermal plume around the manikin and further decreases with heat added to exhalation.

3.1.3. INTERACTION BETWEEN VENTILATION AND EXHALED FLOW DISPERSION

3.1.3.1 Stratification

Figure 3.5 shows the trajectory of exhaled flow for the four cases. As expected, the exhaled flow at higher metabolic rate (2 met) with higher breathing frequency and pulmonary ventilation rate can penetrate longer distance than that at lower metabolic rate (1.2 met).

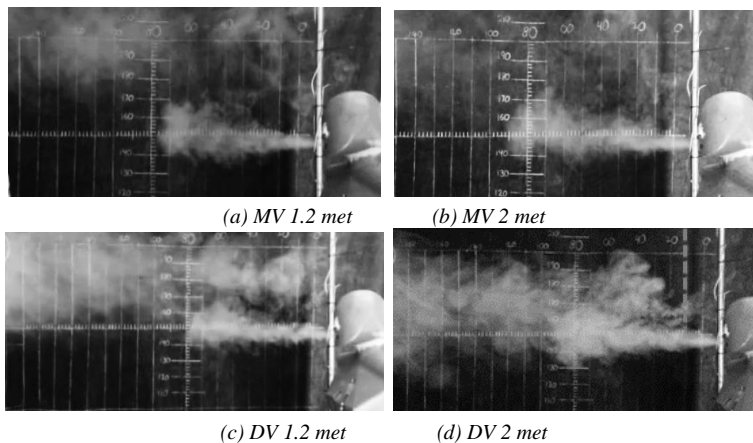


Figure 3.5 Smoke visualization of the exhaled flow from the manikin's mouth with two metabolic rates and corresponding heat release under MV and DV [a].

The exhaled air moves up and is diluted rapidly by room ventilation with MV. While clear stratification of the exhaled smoke can be observed under DV. The presence of the temperature gradient with DV is shown to have significant effect on the mixing of exhaled flow with ambient air as well as the upward movement.

Figure 3.5 (c) illustrates that the stratification height is above the manikin's head and it is lowered to the chest height in Figure 3.5 (d). This can be explained by higher dT/dy for the DV 2 met case. The dependence of stratification height on the magnitude of temperature gradients has also been observed by Bjørn and Nielsen (2002) and Gao et al. (2012). Higher temperature gradients have larger tendency to resist vertical movement of exhaled air make room air more stable. *This phenomenon indoor shares the same principle with atmospheric stability. Reserved temperature gradient resists*

vertical movement of air mass and reduces its turbulence intensity, implying a stable atmosphere environment [b].

To further illustrate the distribution characteristics of exhaled contaminant around the manikin's body, tracer gas measurements are performed.

Earlier measurements of the mean concentration of N_2O in the vicinity of the manikin's body in Figure 3.2 has revealed similar phenomena observed in Figure 3.5. For DV, c/c_R is approximate zero at the thigh and chest height and $c/c_R \approx 1$ above the head, indicating a very clean zone at the lower part of the room and a polluted upper zone. This corresponds well with the smoke test result shown in Figure 3.5 (c) and (d). However, $c/c_R \approx 1$ with MV both at the lower part and at the upper part of the room because of the fully mixing of exhaled contaminant with room air under MV.

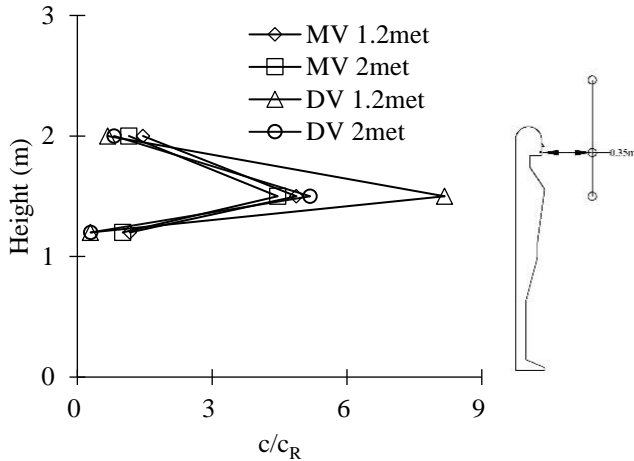


Figure 3.6 Dimensionless concentration at a distance of 0.35 m in front of the manikin's face at three different heights (chest, mouth and above head). c/c_R is the ratio of the mean N_2O concentration at certain measuring point to that in exhaust opening [a].

Figure 3.6 shows c/c_R along a vertical line with a distance of 0.35 m away from the manikin. It can be found that $c/c_R \approx 1$ at the chest height and above the head under fully mixed condition. For DV, c/c_R shows similar trend with that in Figure 3.2 at the chest height and above the head. At the mouth height, c/c_R is about 8.0 for DV 1.2 met, which is significantly higher than that for MV 1.2 met of about 4.7. The increased concentration of exhaled contaminant indicates potential higher exposure level to a receptor person standing in front of the source person. However, for the manikin with a higher metabolic rate of 2 met, the concentrations of N_2O are comparable for DV and MV. This indicates that the influence of the temperature gradient on the contaminant block-up is more significant for lower metabolic level due to a lower momentum of the exhaled flow [a].

3.1.3.2 Exhaled velocity profiles

The manikin connected to the artificial lung can produce a pulsating sinusoidal breathing (Bjørn,1999). Figure 3.6 illustrates the method used in this thesis to describe the pulsating velocity.

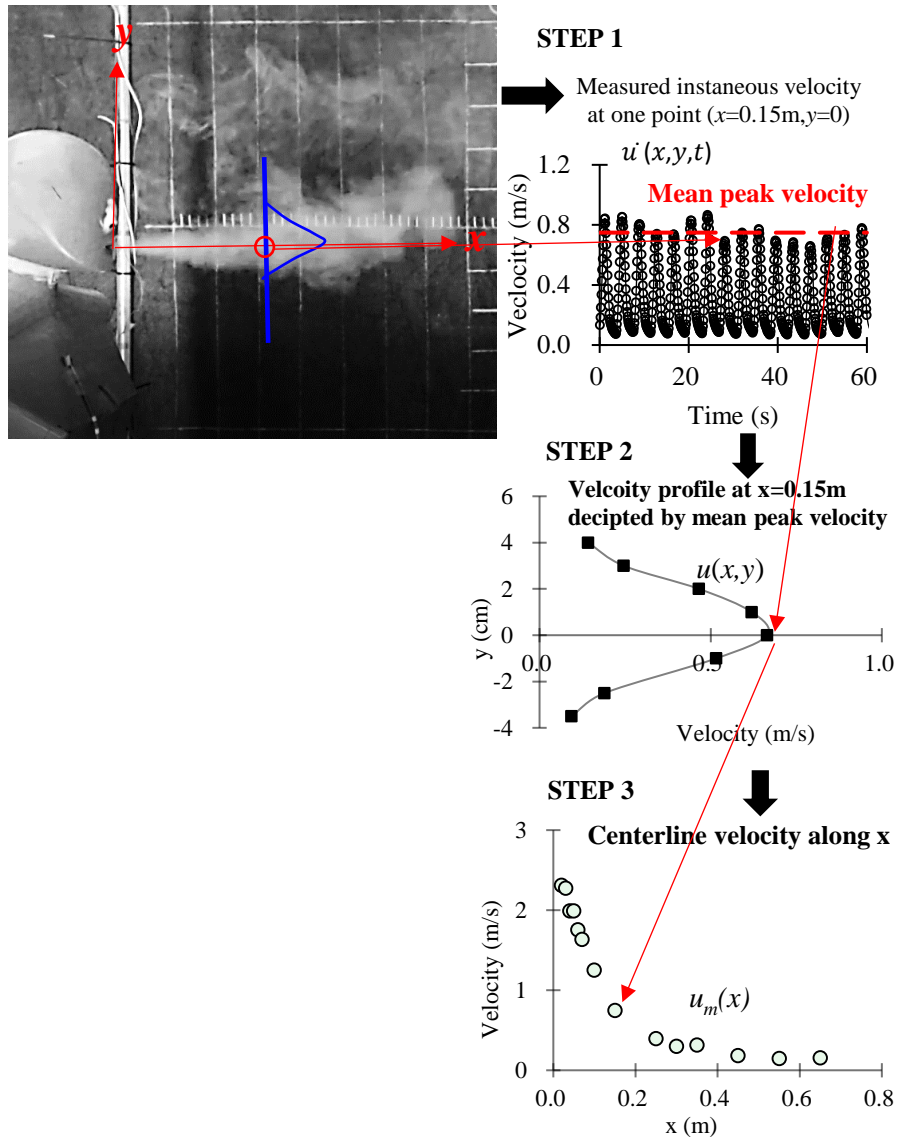


Figure 3.7 Steps to describe the exhaled velocity. The curves are based MV 1.2 met case.

Table 3.1 defines the velocities used to describe the exhaled flow from Step 1 to Step 3 shown in Figure 3.7. Then follows detailed discussions of these defined velocities.

Table 3.1 Definition of exhaled velocity by different means.

Velocity	Definition
$\dot{u}(x, y, t)$	Instantaneous velocity measured at point (x, y)
$u(x, y)$	Mean peak velocity, the average value of velocity peaks, at certain point (x, y) in the two-dimensional plane.
$u_m(x)$	Centerline velocity, $u_m(x)$, is the maximum $u(x, y)$ along y in x plane

STEP 1

Figure 3.8 shows that pulsating velocity, $\dot{u}(x, y, t)$, measured by the hot-sphere anemometer. As the anemometer cannot measure the direction of the velocity, it is always positive as depicted in Figure 3.8. The exhaled velocity shows a sine shape, which is similar to real human breathing (Gupta et al., 2010). Nielsen et al. (2009, 2012) has reported that the pulsating exhalation of the manikin described by mean peak velocity has a similar behavior to a steady jet. The peaks are hereby extracted and averaged. The mean peak velocity $u(x, y)$, is plotted in a certain x plane to depict the velocity profile, as illustrated in Figure 3.9.

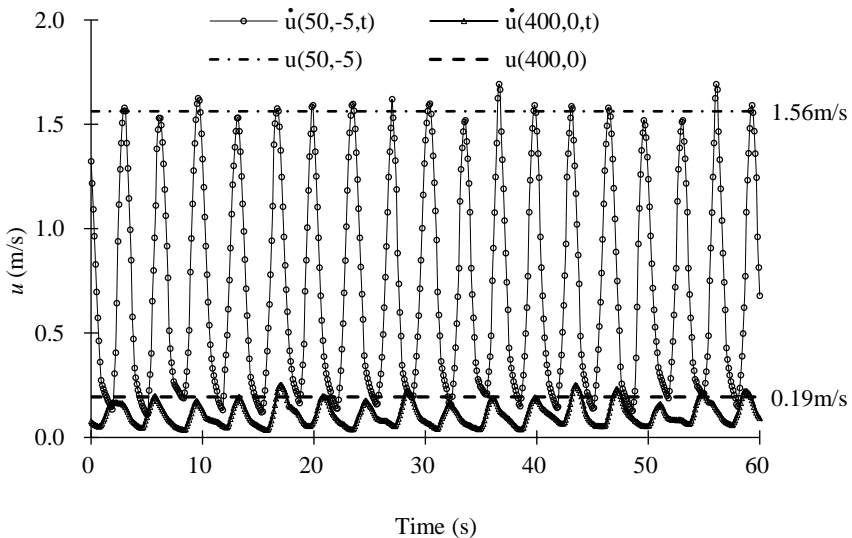


Figure 3.8 Pulsating velocity measured by the hot sphere anemometer. The coordinate scale is in units of mm [a].

STEP 2

Velocity profiles along y direction in different x planes are shown in Figure 3.8. The ventilation patterns show no significant impacts on the velocity profiles. The velocity profiles described by the mean peak velocity shows similar trend with a steady jet. To further validate the similarities to a steady jet, universal profiles are depicted.

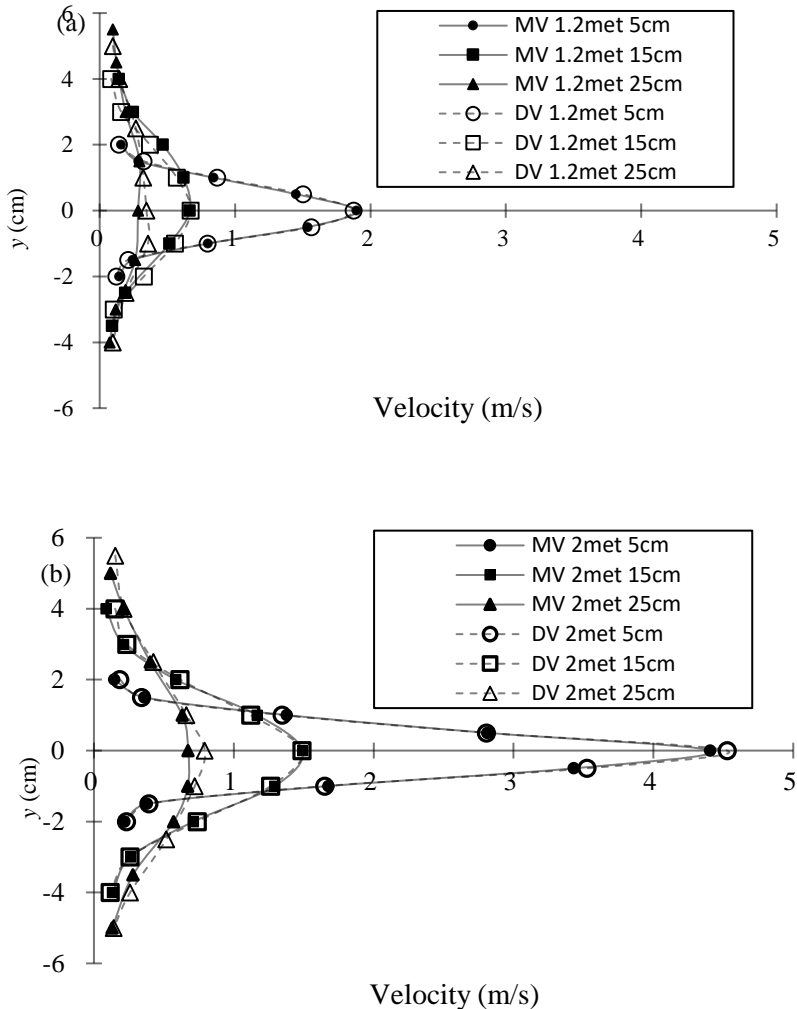


Figure 3.9 Velocity profiles of exhalation from the mouth for (a) 1.2 met and (b) 2met [a].

Similar expression of the universal profile as a steady jet (Abramovich, 1963) is given by equation 2.1.

$$u/u_m = \exp(n\eta^2) \quad (3.1)$$

where, u_m is the maximum velocity at the centerline; $\eta = y/\delta$; δ is the half width of the exhaled flow to the location of $u_m/2$; n is the coefficient.

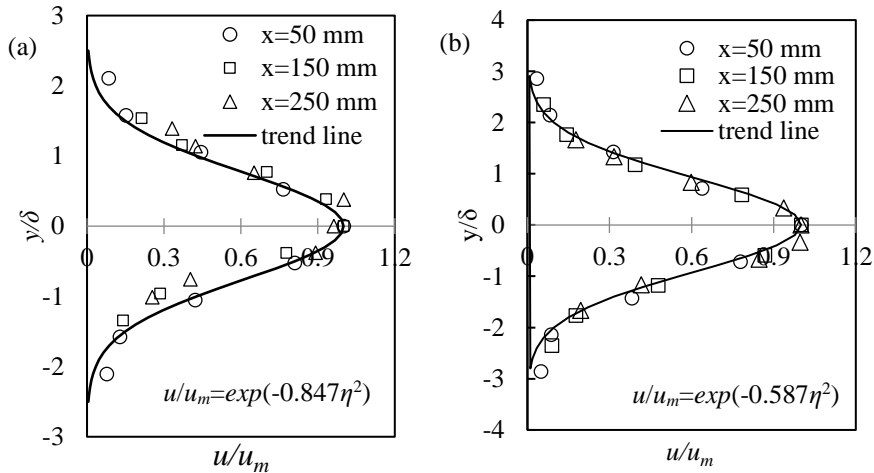


Figure 3.10 Universal profile of velocity for (a) MV 1.2 met and (b) MV 2 met.

Figure 3.10 shows that velocities at different x distances from the mouth opening can be characterized by a universal profile in an exponential function form, corresponding to that of a theoretical free jet. The velocities for MV 1.2 met and MV 2 met show good fitting to the regression equations that are listed in Table 2.2. This further confirms that the fact that the behavior of the exhalation from the manikin's mouth described by the mean peak velocity is quite similar to a steady free jet. Likewise, the velocity and concentration decay of the exhaled air along the centerline are described by powder functions by way of analogy.

Table 3.2 Coefficient of regression equations with 95% confidence bounds.

	MV 1.2 met	MV 2 met
Coefficient n (with 95% confidence bounds)	-0.847(-0.971,-0.724)	-0.587(-0.629,-0.545)
R^2	0.925	0.985

STEP 3

Velocity or concentration along the centerline can be expected to decay with horizontal distance. A power function, similar to a steady jet in form, is assumed by Equation 3.2 and 3.3, respectively.

$$\frac{u_m}{u_0} = K_v \left(\frac{x}{\sqrt{a_0}} \right)^{n_1} \quad (3.2)$$

$$\frac{c_x - c_R}{c_0 - c_R} = K_c \left(\frac{x}{\sqrt{a_0}} \right)^{n_2} \quad (3.3)$$

where K_v and K_c are the characteristic constants for velocity and concentration, respectively, and a_0 is the mouth area. The dimensionless velocity u_m/u_0 is the ratio of the peak velocity along the centerline at horizontal distance x , to the initial velocity, u_0 . The parameters c_x , c_R and c_0 are mean peak concentration values measured at x , in the exhaust of the room and at the mouth, respectively.

Figure 3.11 shows that the velocity decreases with increasing x . The slope of velocity decay, n_1 , is shown in Table 3.3. For $x/a_0^{0.5} < 2$, the velocity is almost constant, corresponding to the “constant velocity core” in the initial section for a steady jet. When $2 < x/a_0^{0.5} < 5$, the initial velocity core is destroyed and the velocity decays with x . But the slopes are -0.1 for 1.2 met cases and around -0.5 for 2 met cases, indicating a more severe damage for lower momentum flow. When $x/a_0^{0.5} > 5$, the velocity decays faster with a slope around -1, basically corresponding to the velocity decay in the main section of a circular free jet. The influence of the ventilation patterns on velocity decay is not significant but the velocity is a little higher with DV 1.2 met than MV 1.2 met.

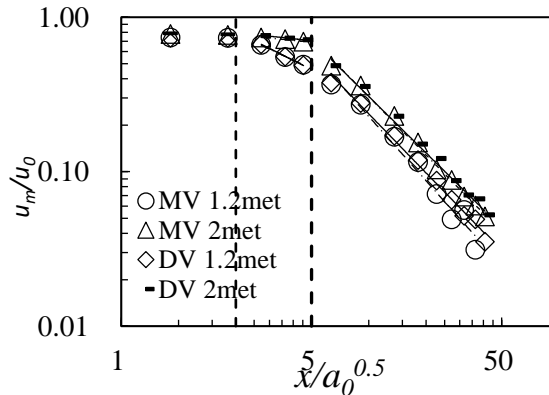


Figure 3.11 Log-log graph of dimensionless velocity versus distance in the centerline for the four cases (solid trend lines are for DV) [a].

Table 3.3 Characteristic constants for velocity decay [a].

Cases	Velocity decay fitting							
	$x/a_0^{0.5} < 2$		$2 < x/a_0^{0.5} < 5$			$x/a_0^{0.5} > 5$		
	K_{v1}	n_1	K_{v2}	n_1	R^2	K_v	n_1	R^2
MV 1.2met	0.74	-0.004	1.17	-0.58	0.996	5.5	-1.38	0.969
MV 2met	0.78	-0.02	0.84	-0.12	0.974	5.46	-1.25	0.994
DV 1.2met	0.71	0.006	1.24	-0.62	0.999	4.41	-1.27	0.992
DV 2met	0.79	-0.02	0.86	-0.13	0.998	5.03	-1.22	0.994

The dimensionless concentration at the centerline with increasing x shows different trend with that of the velocity, as shown in Figure 3.12 and Table 3.4. The concentration decays faster for $x/a_0^{0.5} > 10$ than that for $x/a_0^{0.5} < 10$. The slope of the concentration decay is around -1 for MV cases when $x/a_0^{0.5} > 10$, similar to that of the velocity decay when $x/a_0^{0.5} > 5$. But the concentration decays significantly slower for DV cases than MV cases. The temperature gradients under DV obviously elevate the contaminant concentration in the exhaled flow. That is in line with the measured results in Figure 3.5 and 3.6, implying a relatively stable air condition in room with DV.

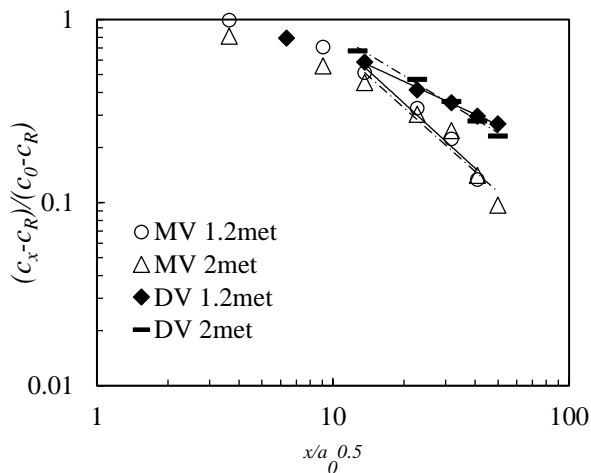
**Figure 3.12** Log-log graph for dimensionless concentration versus distance in the centerline for the four cases [a].

Table 3.4 Characteristic constants for concentration decay [a].

Cases	Concentration decay fitting		
	$x/ao^{0.5}>10$		
	K_c	n_2	R^2
MV 1.2met	11.9	-1.18	0.963
MV 2met	10.4	-1.15	0.928
DV 1.2met	2.74	-0.6	0.996
DV 2met	5.14	-0.78	0.989

3.1.4. CONCLUSIONS IN THIS SECTION

The results in this section show that the airflow patterns influence the dispersion of exhaled flow and the distribution of the exhaled contaminant in the room.

For mixing ventilation, the vertical temperature gradient is almost zero and the exhaled air mixes well with ambient air. While the displacement ventilation yields temperature gradient in vertical direction and creates a clean lower zone and a contaminated upper zone. The exhaled contaminant is stratified at certain height due to the lock-up effect of the vertical temperature gradient with DV, which may cause higher exposure risk to a receptor person than MV. The stratification height is also found to be lowered with higher temperature gradient.

The exhaled velocity from the thermal manikin shows a sinusoidal shape. If it is characterized by the mean peak velocity, it behaves quite similar to a steady free jet. The dimensionless velocity at different x sections can be depicted by a universal profile in an exponential function and the mean peak velocity at the centerline decays with a powder function. The concentration shows different trend with the velocity. The temperature gradient considerably affects the concentration decay and shows an elevated contamination level of exhaled air under DV. Moreover, the influences of the temperature gradient show more significant influence on exhaled flow with lower metabolic rate (1.2 met) than that with higher metabolic rate (2 met).

3.2. PERSONALIZED VENTILATION

3.2.1. INTRODUCTION

Human body releases heat to the environment mainly by: convection, radiation, evaporation and respiration (Fanger, 1967). The convective upward flow generated due to the temperature difference between the human body and the cooler ambient environment is known as the thermal plume (Clark and Edholm, 1985, Liu et al. 2009b). The thermal plume induces natural flow of surrounding air and rises above

the head, creating a thermal boundary layer (TBL) around human body, as shown in Figure 3.13.

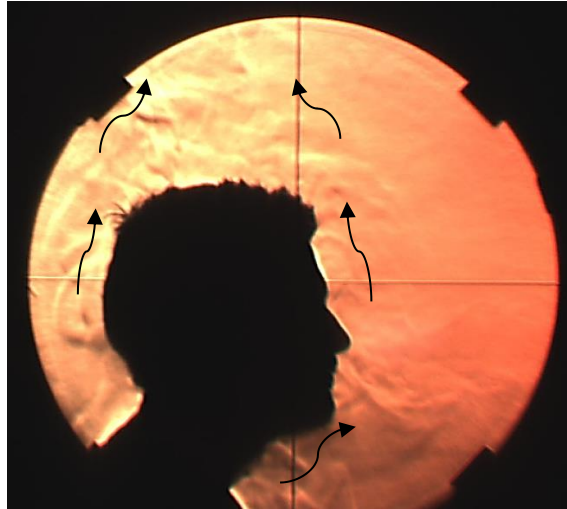


Figure 3.13 Thermal plume generated by a person visualized by schlieren imaging technique.

When the personalized air is supplied to a person, the TBL interacts with the air and may prevent the cold and fresh air being delivered to his/her breathing zone. Bolashikov et al.(2011a) reported that personalized jet at low flow rate could not reach the BZ and indicated a minimum velocity for complete penetration of the TBL is 0.3 m/s. The manikin was without breathing function and turbulent interaction was not considered. This penetration velocity has become a recommendation index for PV system design. Here a further work looks into the problems:

- A thermal manikin with breathing function is used to study if the personalized air enters a person's inhalation or not in this work.
- Interactions of the PV with the TBL are visualized and the inhaled air quality of the BTM is evaluated instead of examining the velocity vector in a steady state.

In this section, the penetration of the PV flow to inhalation will be examined based on above observations. The challenge of PV jet's penetration under low flow rates and the influence of interactions on PV performance will be illustrated.

Air quality index

Tracer gas (N_2O) is added in front of the nozzle with a constant volume, see Table 2.7. An air quality index, ϵ_p , defined as the fraction of PV air in inhaled air is used to

indicate the air quality in the BZ (Khalifa, et al. 2009) or the reduced pollutant exposure level in the BZ due to the application of PV (Gao and Niu 2004).

$$\varepsilon_p = \frac{c_{bz} - c_R}{c_{pv} - c_R} \quad (3.2)$$

where c_{pv} is the N_2O concentration at the nozzle exit, c_R the N_2O concentration in the exhaust, and c_{bz} the N_2O concentration in inhalation or at a point in the BZ.

Description of the nozzle jet

Figure 3.14 presents variations of both velocity and concentration of N_2O along the centerline of the free nozzle jet. The centerline velocity, u_m , and N_2O concentration, c , are normalized with respect to their nozzle exit values, u_0 and c_0 . The normalized velocity and concentration along the centerline basically correspond to each other over a varying flow rate of 1.5~4 l/s expressing that the flow is a fully developed turbulent flow.

The length of clean air core or constant velocity core can be obtained by concentration or velocity measurements or through depictions of the schlieren images. It is found to be 3~4 times the diameter of the nozzle. In the main section of the nozzle jet, the centerline velocity and concentration decays rapidly, serving as a power function, as shown in Figure 3.14.

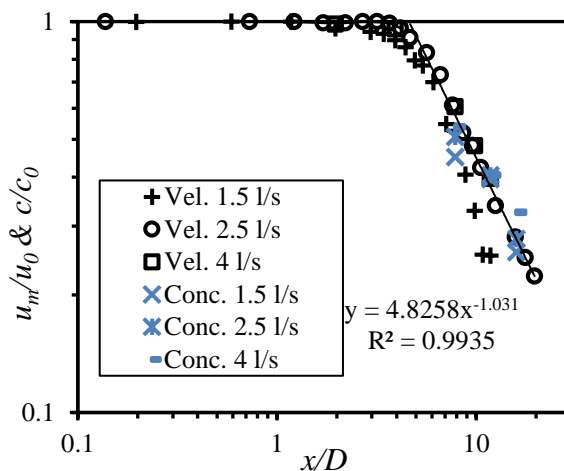


Figure 3.14 Velocity and concentration decay along the jet centerline of free nozzle jet (log-log coordinates).

When the PV jet aims at supplying clean air to the BZ of a person, the front edge of the jet will interact with the TBL and cause drastic mixing of clean air with it, as shown in Figure 3.15.

Apparently, the clean air core is not long enough to reach the inhalation zone of the person as illustrated in Figure 3.15. The entrainment of polluted room air with the development of the nozzle jet as well as its turbulent mixing of the thermal plume causes deterioration of inhaled air quality, which will be evaluated with the use of the index ε_p in the following sections.

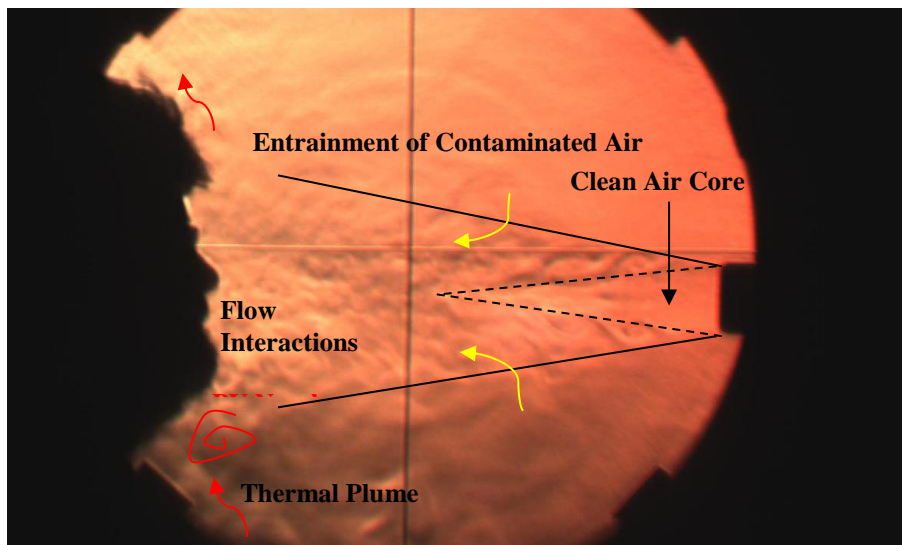
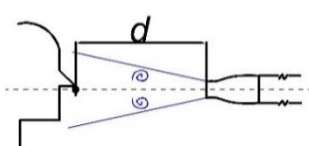


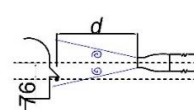
Figure 3.15 Schlieren image of the flow interactions between a male subject and the PV jet (2.5 l/s, $d=40$ cm).

Test cases

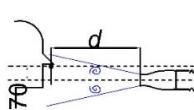
Table 3.5 shows 12 test cases considering different influencing factors on inhaled ε_p : the distances between the manikin and the nozzle ($d=40\sim 81$ cm), the presence of the manikin (with/without thermal manikin facing to the nozzle), the thermal plume layer (isothermal /non-isothermal manikin with identical/higher body temperature than surrounding air), and nozzle positions (cases 8~11). Case 1 is the baseline case.

Table 3.5 Experimental setup for personalized ventilaiton.

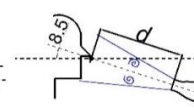
No.	Manikin	d (cm)	Heat output (W)	Relative position
1	Non- isothermal	40	70	
2	Non- isothermal	60	70	
3	Non- isothermal	81	70	
4	No manikin	40	\	
5	No manikin	60	\	
6	No manikin	81	\	
7	Isothermal	60	\	
8	Isothermal	81	\	
9	Non- isothermal	40	70	(a) Nozzle centerline 76 mm above the nose
10	Non- isothermal	40	70	(b) Nozzle centerline 70 mm below the nose
11	Non- isothermal	40	70	(c) 8.5° upward pointing to the nose
12	Non- isothermal	40	70	(d) 7.5° downward pointing to the nose



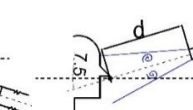
(a)



(b)



(c)



(d)

3.2.2. INTERACTION BETWEEN MANIKIN BODY AND PV FLOW

Penetration velocity

A point, P_0 , with close proximity to the nose is defined in Figure 2.8. And d is the horizontal distance between P_0 and the nozzle, whose center is just pointing to P_0 . Figure 3.16 presents the measured velocity at the nose point P_0 with three conditions: with thermal manikin, with isothermal manikin (cold manikin, no thermal plume) and without manikin. It is obvious that all velocities at the three conditions decrease with increasing distances. The centerline velocity of the nozzle flow is also decreased due to the presence of the manikin for both isothermal and non-isothermal conditions. The blocking effect of the manikin is more significant for lower PV flow rate. When $d=60$ cm, due to the presence of the thermal manikin within the free PV jet, u reduces by about 21% and 84% with 2.5 l/s and 1.5 l/s, respectively. The mean velocity at the nose point for 1.5 l/s with $d=60$ cm is merely 0.047 m/s (RMS=0.087

m/s) which corresponds to the turbulence level in the ventilated room. The minimal velocity at this point may indicate that the PV flow could not penetrate the TBL.

However, the effect of the thermal plume on the velocity decrement is not significant as previous study mentioned (Bolashikov et al. 2011a) when comparing it with the isothermal condition. Here, it is found that the blocking effect of the manikin, instead of the TBL, is the dominant reason for velocity decrement around the manikin.

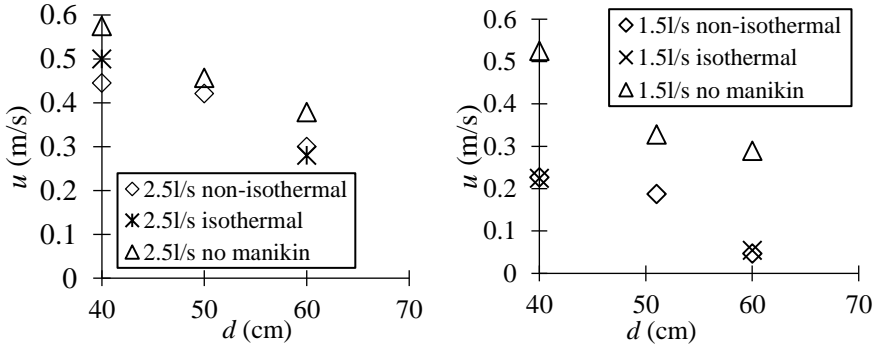


Figure 3.16 Measured average velocity with LDA at the nose point P_0 with PV flow rates of 2.5 l/s and 1.5 l/s [e].

Figure 3.17 indicates that even when the velocity in the BZ is decreased to approximately zero, small fraction of fresh air could still be inhaled by the manikin. Hence, we suggest that the invading velocity from the PV flow should not be used as the only index for judging the penetration degree of the TBL. The influence of the thermal manikin and the TBL on inhaled air quality under PV will be further discussed.

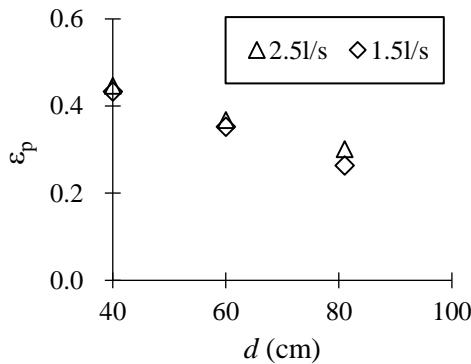


Figure 3.17 Averaged ϵ_p in inhalation [e].

Blocking effect of the manikin

Figure 3.18 presents averaged ε_p in the BZ with cases 1~6 defined in Table 3.5. The increment of ε_p is insignificant with the increment of PV flow rates.

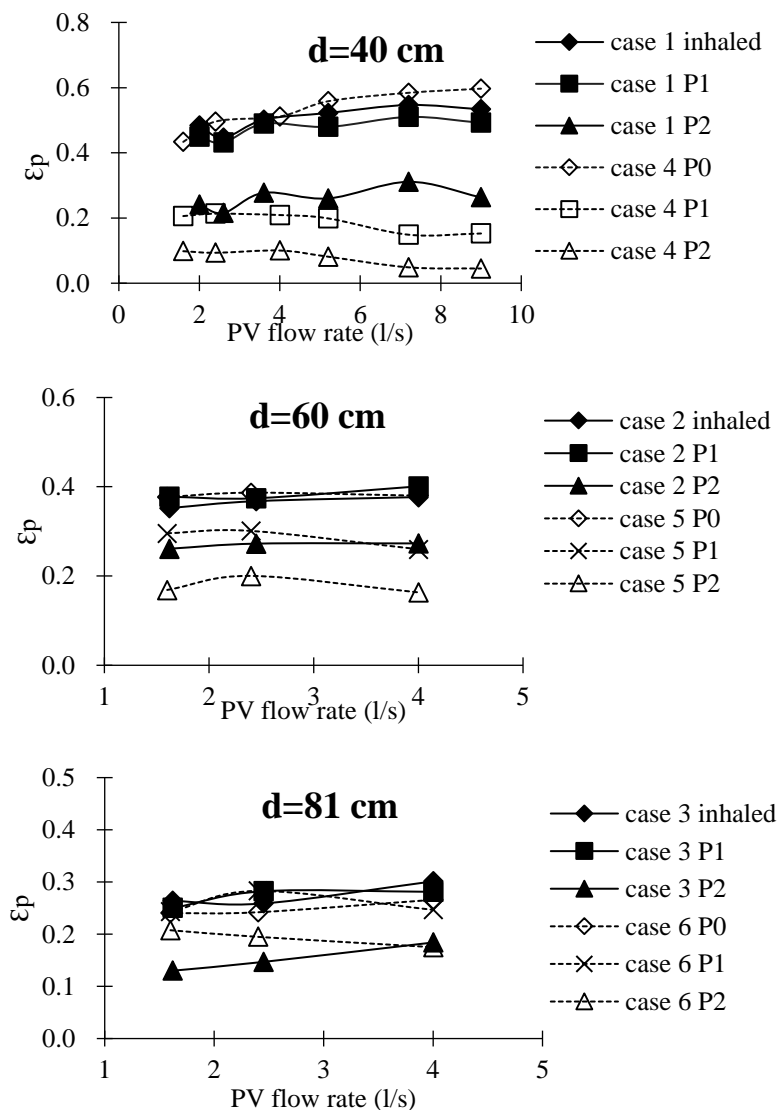


Figure 3.18 ε_p in the BZ with thermal manikin and without manikin. Cases 1~3: non-isothermal manikin, manikin is heated with TBL. Cases 4~6: no manikin, free nozzle jet [e].

It is obvious that the inhaled ϵ_p decreases with increasing d because of entrainment of ambient air with the development of the PV flow. The inhaled ϵ_p is basically comparable to the ϵ_p at P0 of a free jet, indicating close relevance of the inhaled air quality with the air quality at the nose point.

The tendency to a constant ϵ_p at high flow rates indicates that the PV flow is close to fully developed turbulent flow at higher flow rates.

At P1 and P2, ϵ_p is elevated due to the presence of the thermal manikin in the PV flow. The accumulation of the PV air in front of the manikin due to the blocking effect attributes to the elevation of ϵ_p at P1 and P2.

3.2.3. INTERACTION BETWEEN TBL AND PV FLOW

The blocking of the flow's penetration into the TBL should be more significant under low invading velocities. The invading velocity decreases with increasing d . Here, the air quality with non-isothermal and isothermal manikin for $d=60$ cm and 81 cm is respectively compared in Figure 3.19.

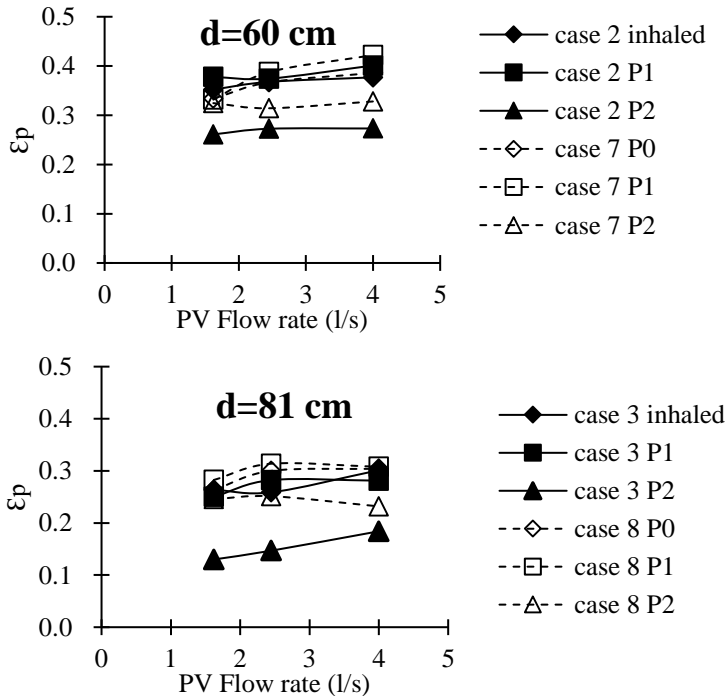


Figure 3.19 ϵ_p in the BZ with non-isothermal and isothermal manikin [e].

However, Figure 3.19 shows that the influence of the TBL on inhaled ε_p is not significant. Meanwhile, ε_p at P2 is reduced due to the intense interaction between the PV flow and the TBL at this region, which can be observed in Figure 3.15.

The increased ε_p at P1 compared to that at P0 can be explained by increased velocity at P1 when the flow passes the sharp jaw point of the manikin.

Effect of interaction directions between the TBL and PV jet

In Figure 3.20, the collisions of the PV flow from different positions with the rising thermal plume are visualized with schlieren imaging technique. An anticlockwise vortex ring can be found at the lower boundary of the nozzle jet due to the interaction between the rising plume and the PV flow. The height of the vortex correspondingly rise when the nozzle height is lifted. The appearance of the vortex indicates highly mixing of the nozzle air with the thermal plume.

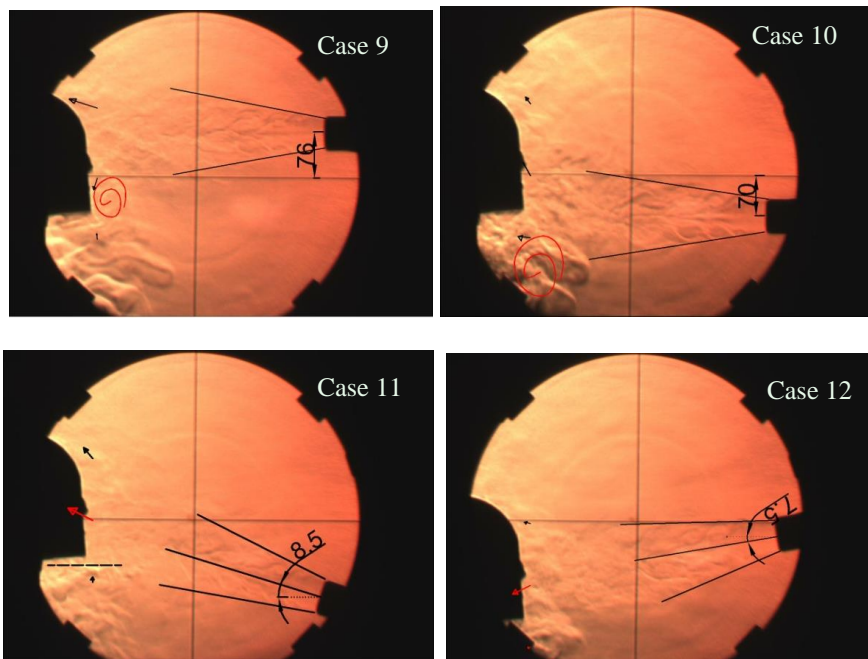


Figure 3.20 Interactions between the TBL and the nozzle with cases 9~12. The measured velocities by LDA at the three points in front of the manikin's face are drawn with vectors with both direction and scale to the real velocity magnitude [e].

Table 3.6 Influence of nozzle position on ε_p [e].

ε_p	Case 9	Case 10	Case 1	Case 11	Case 12
Inhaled	0.35	0.24	0.45	0.36	0.40
P1	0.30	0.42	0.43	0.29	0.50
P2	0.05	0.43	0.22	0.06	0.32

From Table 3.6 it can be seen that the baseline case with the nozzle centerline horizontally pointing to the nose point achieved the highest air quality in inhalation.

It is evident that the deviation of the height of the centerline to the nose height will result in reduced air quality in inhalation. Table 3.6 shows that case 10 has the lowest ε_p in inhalation, indicating the worst inhaled air quality. That is probably because the inhaled air is mostly drawn from the upper boundary of the turbulent nozzle jet as shown in Figure 3.20. Although ε_p at P1 and P2 for case 10 is relatively high, the inhaled ε_p will not be influenced by the higher air quality some distance below the nose. This might be because the majority of air drawn in inhalation is distributed in close proximity to the nose. Although the lower boundary of the nozzle jet also reaches the nose point in case 9, turbulent mixing with the upward plume and enhanced air velocity when the air passes by the jaw result in relatively higher ε_p compared to case 10. In practice, the placement of the PV nozzle should be carefully considered to avoid this condition with the upper boundary of the PV jet lower than the nose height.

The airflow direction of the PV jet also affects the ventilation effectiveness even when the centerline of the flow is exactly pointing to the nose. Table 3.6 shows that ε_p of case 11 is lower than that of case 12. This can be explained by the direction of the PV jet in regard to the thermal plume. In case 11 the velocity component in vertical direction is consistent with the plume direction, while that is opposite in case 12. The downward flow in case 12 suppresses the rising plume which is contaminated and put the fresh air in front of the polluted plume air. On the contrary, more plume air reaches the inhalation zone in case 11.

It can be concluded that the placement of the PV nozzle affects the interaction of the PV flow with the TBL and further influences the ventilation effectiveness of PV.

3.2.4. DISCUSSION AND CONCLUSIONS IN THIS SECTION

The present study indicates that the invading velocity should not be used as the only index to determine the penetration of the PV flow to the BZ. The approach applied in previous studies to evaluate the penetration level of the TBL is based on merely velocity decrement and deflection characteristics of PV flow in the BZ, which is

insufficient to determine the penetration degree. The velocity decrement in close proximity to the manikin is found to be dominated by the blocking effect of the manikin body rather than the TBL. The concern of PV jet's penetration to the thermal plume is therefore not as challenging as expected. According to the inhaled air quality index ε_p , it can be inferred that the TBL is "penetrable" at an invading velocity even lower than 0.177 m/s (1.5 l/s, $d=0.8$ m, $\varepsilon_p=0.35$), which is even lower than the recommended critical value of 0.3 m/s (Bolashikov et al.(2011a)). In practice, lower penetration velocity of clean air is helpful to achieve lower energy consumption to supply decreased amount of fresh air.

The easy penetration feature of the TBL might be partly because the influence of the interactions is mainly distributed at the lower boundary of the PV jet. The thermal plume is therefore weakened at the height of the centerline of the PV flow. Another reason could be the effect of the inhalation process. Figure 3.21 shows the velocity field around the mouth when a person inhales with mouth (Murakami, 2004). Likewise, the air can be inhaled with certain velocity from limited areas around the nose opening when the person performs nose breathing. The driven force generated during inhalation could further destroy the effect of the TBL and cause easy penetration of PV air into inhaled air.

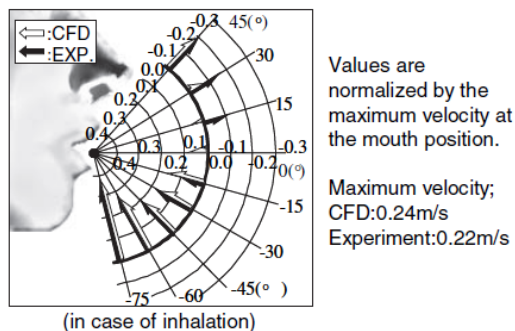


Figure 3.21 Velocity field around the mouth during inhalation (Murakami, 2004).

The airflow interaction between the PV air and the TBL alters the airflow distributions in the BZ and affects the inhaled air quality. This interaction depends on the positioning and direction of the non-uniform invading flow from the nozzle, which should be carefully considered for optimal ventilation design.

Some previous researchers have realized the importance of interaction between thermal plume around human body and personalized air and proposed corresponding PV configurations to enhance the ventilation effectiveness and energy savings. Yang et al. (2009) defined the neutral distance as the one from the PV nozzle where the impact of thermal plume on velocity distribution was observed and found that it

increased from 0.8 m to 1.1 m with the increase of the airflow rate from 4 l/s to 16 l/s for a ceiling mounted PV nozzle. Gao and Niu (2004) placed the PV nozzle just beneath the chin to avoid long distance contamination by ambient air and reported that a minimum flow rate of 0.8 l/s is strong enough to overcome the disturbance of the thermal plume and provide enough clean air to the BZ. Makhoul et al. (2013) proposed the single ceiling PV jet combined with desk fans which were able to control the convective plumes emanating from the human body allowing the personalized air to reach the breathing level more effectively. A reduced energy saving by up to 13% was achieved by this system compared to conventional mixing ventilation systems[e].

The interactions patterns between the supplied air from PV and the TBL should be an important consideration for the improvement of BZ air quality, thermal comfort and energy consumption in optimal ventilation design.

CHAPTER 4. COMPARISONS OF EXHALED BREATH AMONG THE THREE TOOLS

This chapter may serve as an illustration on the usage of tools introduced in Chapter 2.1, e.g. the CSP, the BTM and human subjects. Detailed comparisons of the physiological configurations among the three tools have been made in Table 2.4.

The computer simulated person (CSP) is modeled according to the breathing thermal manikin (BTM). And the BTM is constructed on the basis of human information. A direct comparison between the CSP and the BTM and between the BTM and human subjects will be performed in this chapter to evaluate the accuracy of simulated results of breathing by a computer or a manikin. Meanwhile, special focus is given to the characterization of real human breathing, as data collected on human is the most reliable but at the same time it is short of information.

The CSP and the BTM are applied in case of mixing ventilation and displacement ventilation, respectively. Human subjects are instructed to breathe under mixing ventilation.

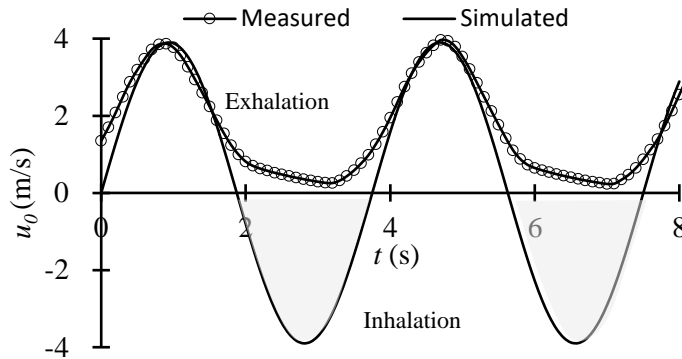
The main findings on real human breathing presented in this chapter are based on Papers [c] and [d].

4.1. CSP VS. BTM

The BTM breathes with an almost sinusoidal shape which can be approximately expressed by the mathematical function in Table 4.1. Villafruela et al. (2013) reported the boundary condition set as a sinusoidal function shows best performance in CFD simulations that are validated by experiment data obtained from manikin. According to Figure 3.4, the peak velocity at the mouth is assumed as 3.9 m/s, excluding the velocity decrement caused by the thermal plume layer and increased exhalation temperature with some distance apart from the mouth. In Figure 4.1, the instantaneous velocity measured by the hot sphere anemometer together with the simulated velocity are plotted. Other details about the computational model, including the full-scale chamber and the CSP, have been discussed in Chapter 2.

Table 4.1 Breathing function of the CSP.

Velocity	CO ₂ mass fraction
$u_0 = 3.9 \sin(1.675t)$	$c_0 = 7.9 \text{ g/kg air}$ if $u_0 > 0$ $c_0 = 0$ if $u_0 \leq 0$

**Figure 4.1** Instantaneous velocity from the mouth of the CSP for 2 breathing cycles.

4.1.1. FLOW FIELD VALIDATION

The non-dimensional temperature distributions along vertical height for MV and DV are shown in Figure 4.2. The numerical temperatures show agreement with experimental values for both ventilation strategies. For the MV case, the dimensionless temperature is approximate to 1, implying well-mixed air condition in the room. However, the temperature at the upper part of L1 seems to be elevated by simulation. As the pole L1 is placed close to the manikin (see Figure 2.5), the enhanced thermal plume above the manikin's head through simulation may cause the temperature increase at this height. Figure 4.2 also indicates a stratified flow in the room for the DV case. For both simulations and measurements, the temperature for DV shows a linear growth with vertical height due to the design of the two radiators (Figure 2.5 and Figure 2.6).

In Figure 4.3, the vertical concentration distribution some distance apart from the person are shown for the simulations and experiments. The concentration profile for the simulations of the DV case indicate good agreements with the measurements, but the MV case has some significant deviations in the upper part of the room compared with the measurements. Obviously, the simulations create an exhaled flow bending more upwards with MV than the experiments, as the maximum concentration appears at a higher location in Figure 4.3. The deviations may be caused by simplification of the whole floor as an inlet, combined with the effect the enhanced thermal plume

around the CSP. Another reason that contributes to the deviations may be because the time-step for the averaged concentration obtained by the measuring instruments is significantly larger than that by CFD simulations.

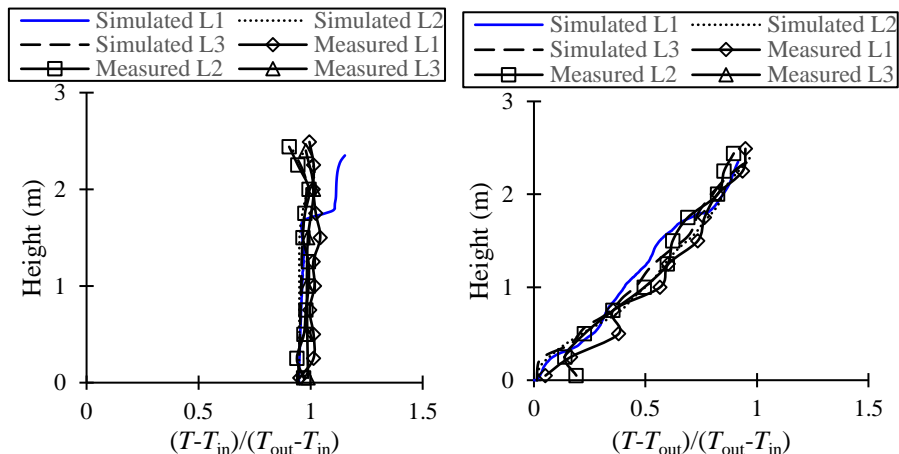


Figure 4.2 Simulated and measured mean temperature at the three vertical poles: L1, L2 and L3, for mixing ventilation and displacement ventilation (T_{out} , the exhausted air temperature and T_{in} , the supplied air temperature).

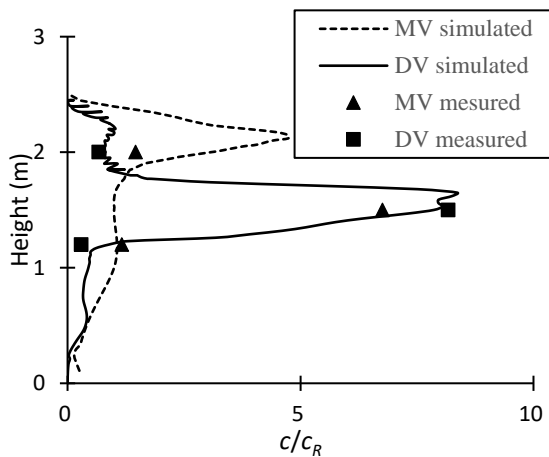


Figure 4.3 Dimensionless concentration along vertical height at a distance of 0.35 m in front of the manikin's face. The concentration c is divided by the exhaust concentration c_R .

4.1.2. EXHALED FLOW VALIDATION

Figures 4.4 and 4.5 compare the dispersion tendency of the simulated tracer gas with smoke experiment.

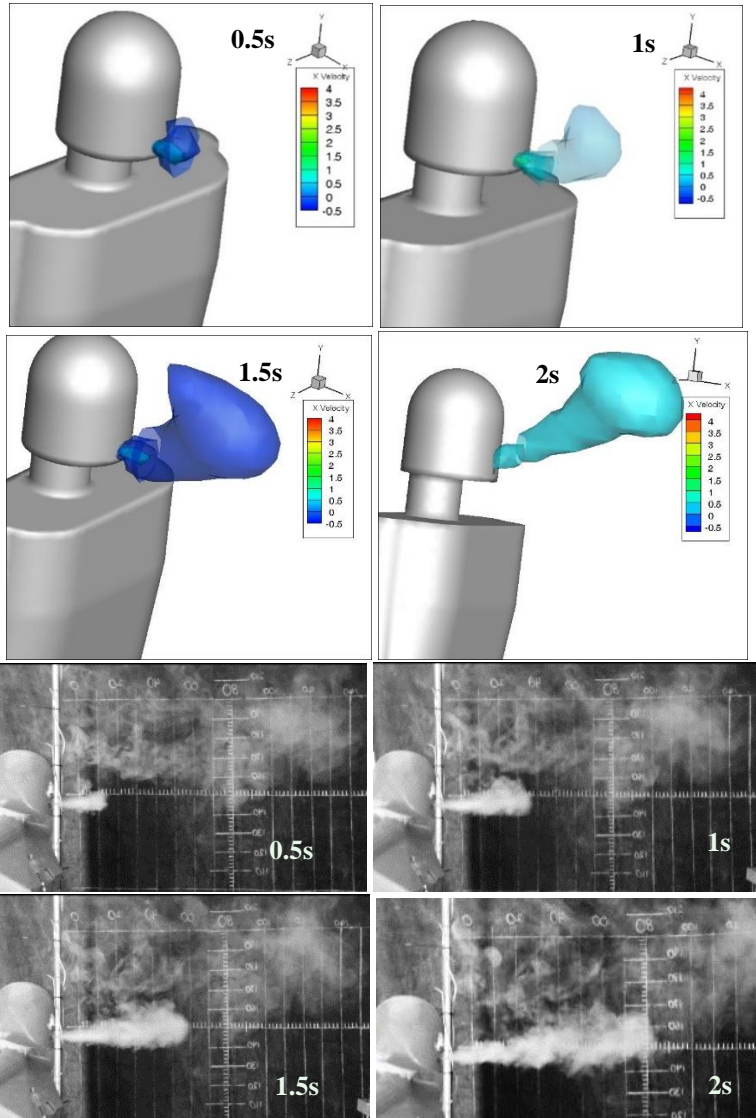


Figure 4.4 Iso-surfaces of CO₂ concentration shaded in velocity module. The simulations are compared with smoke experiments, both of which are conducted under MV within one breathing cycle, corresponding to the time in Figure 4.1. For $t=0.5s$ and $1s$, $c=0.1 c_0$, and for $t=1.5s$ and $2s$, $c=0.05 c_0$. The c_0 is the initial concentration at the mouth and c is the iso-surface concentration.

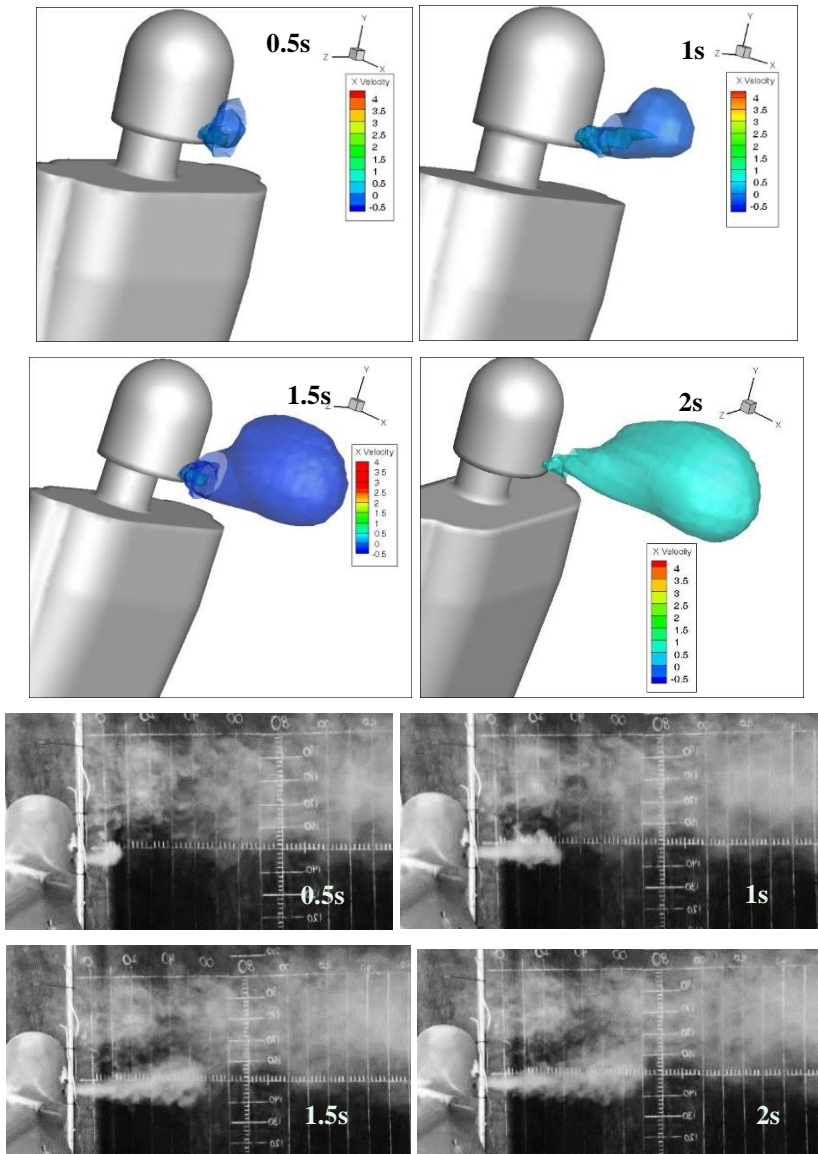


Figure 4.5 Iso-surfaces of CO₂ concentration shaded in velocity module. The simulations are compared with smoke experiments, both of which are conducted under DV within one breathing cycle, corresponding to the time in Figure 4.1. For $t=0.5\text{s}$ and 1s , $c=0.1 c_0$, and for $t=1.5\text{s}$ and 2s , $c=0.05 c_0$. The c_0 is the initial concentration at the mouth and c is the iso-surface concentration.

From both figures (Figures 4.4 and 4.5), it can be seen that the dynamic simulations of the exhaled flow roughly correspond to the experiments by smoke, regarding the flow shape and development process. While the MV case in Figure 4.4 presents a

more upward trend of the exhaled flow by simulations than by experiments. And in Figure 4.5 the simulated exhalation with DV is apparently depressed in vertical development compared to Figure 4.4 due to the presence of temperature gradient.

Besides the qualitative comparisons among the images, further quantitative analysis is performed by using exhaled velocity. Figure 4.6 illustrates the peak velocity decreases immediately when the flow leaves the mouth. The reason for the decrement has been discussed in chapter 3.1.2. However, the simulated decrement close to the mouth is not as significant as the measured one.

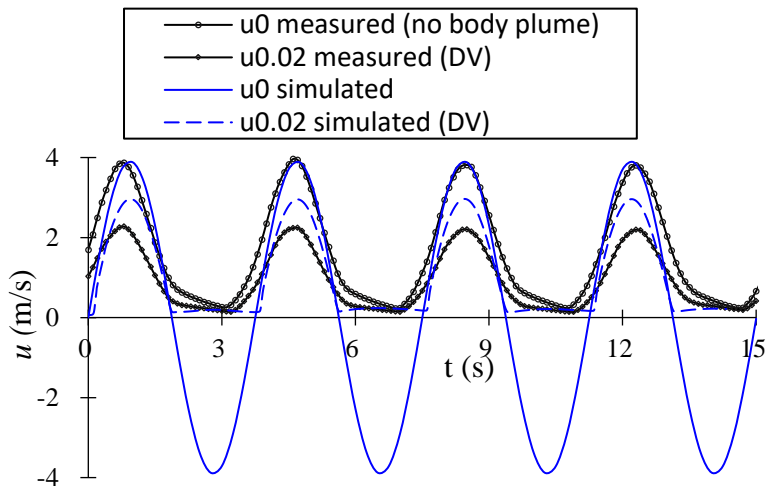


Figure 4.6 Measured and simulated velocity at the mouth opening and with close distance (2 cm) to the mouth opening for the DV case.

The same steps for data processing of exhaled velocity shown in Figure 3.7 are adopted here to illustrate the decay of the centerline velocity. The simulated results combined with the measured results in Figure 3.11 are plotted on a new figure named as Figure 4.7. In Figure 4.7, when $x/a_0^{0.5} > 10$, the simulated velocities with DV is visibly higher than the measurements and is also higher than the simulated ones with MV as well, which stresses the fact that the effect of the temperature gradient on velocity decay may be overestimated by simulations.

The elevated upward flow with MV and the depressed flow with DV from exhalation can be partly due to the enhanced or suppressed development of body plume with the corresponding ventilation pattern, as shown in Figure 4.8. Murakami (2004) reports a peak value of the overhead upward airflow approximately 0.2 m/s. Liu et al. (2009b) reveals that the maximum velocity measured is 0.25 m/s at the location above the top of head with MV and it is merely 0.1 m/s with DV at the same location. In this study, the maximum velocity overhead is found to be around 0.35 m/s for the MV case, implying an enhanced thermal plume with MV by CFD simulations. Liu et al. (2009b)

also reported this problem. Instead, the CFD simulations seem to succeed in predicting the decreased plume velocity with DV, as shown in Figure 4.8.

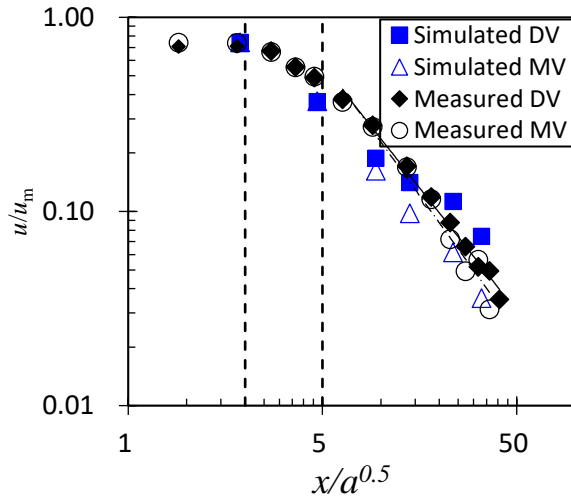


Figure 4.7 Log-log graph of the measured and simulated centerline velocities. The measured velocities correspond to those of Figure 3.11 (MV 1.2 met and DV 1.2 met).

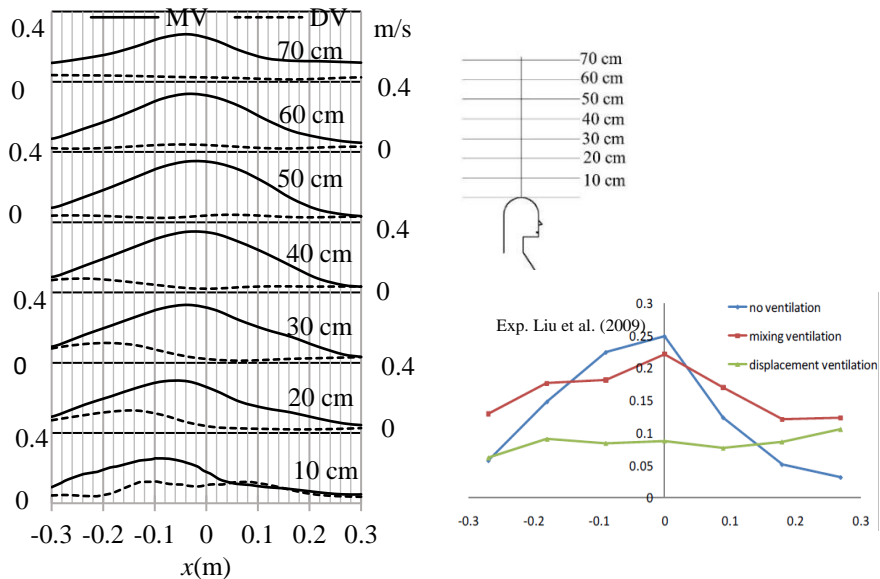


Figure 4.8 Simulated velocity above the CSP's head with MV and DV (left) and measured plume velocity overhead by Liu et al. 2009b (right).

4.1.3. DISCUSSION

To summarize, even though the CFD calculated results roughly agree with measurements, there are still some deviations, in terms of the flow dispersion directions, the exhaled velocity magnitude and the body plume development tendencies, when compare with experiments. There should be a number of possible reasons for the deviations, some of which are discussed in the following.

Boundary conditions directly affect the accuracy of simulated results. Deviations will occur if the boundary conditions are not properly treated. In the present simulations, the ceiling and the floor are prescribed as a whole opening for air supply or return. The plenum above as well as the holes in the ceiling or floor panels are not considered. Meanwhile, the heat release from the CSP is set as a constant and uniform value. During the measurements the manikin's body temperature varies from part to part with a maximum temperature difference of about 2.5 °C. This will to some extent affect the air distribution in the room and around the CSP's body.

Comparing with experiments, we find the main problem of the simulations with CFD is that the buoyancy effect seems to be overestimated with MV, e.g. the exhaled air and the plume overhead. This class of problems can be ascribed to the improper simulations of natural convection. In natural convection, fluid motion is generated due to the density difference in the fluid caused by temperature gradients, namely buoyancy. The stratified flow with DV is also due to the buoyancy forces. So it should be an important consideration in our simulations. To improve the accuracy of simulations for this kind of problem, the following aspects need to be carefully examined in future work.

- For this kind of problem, energy and momentum are strongly coupled. To correctly resolve both the momentum and thermal viscous sublayers, mesh close to the wall should be carefully constructed. The first cell layer is recommended with $y^+ < 1$ by ANSYS FLUENT User's guide (2010).
- For unsteady simulations, the time step size may be determined by the following equation.

$$\tau = \frac{L}{U} \approx \frac{L^2}{\alpha \sqrt{RaPr}} = \frac{L}{\sqrt{\beta g \Delta T}} \quad (4.1)$$

$$t = \tau/4 \quad (4.2)$$

where, t =time step size (s), L =feather size (m), α =thermal diffusivity (m^2/s), Ra =Rayleigh number, Pr =Prandtl number, β =expansivity (K^{-1}), g =gravitational acceleration (m/s^2), ΔT =temperature difference (K).

- Standard pressure discretization may give rise to incorrect velocity near the wall. Other pressure interpolation scheme like Body Force Weighted or PRESTO! can be a possibility to obtain better solutions.

4.2. BTM VS. HUMAN SUBJECTS

Experiments on human subjects are conducted in the same test chamber with identical ventilation and thermal environment as those on the BTM in Chapter 3 in line with MV 1.2 met case. The measuring method on exhaled flow from human subjects is also in line with that on the manikin. The exhaled velocity and CO₂ concentration on the x - y plane are measured by corresponding probes moving with the robot arm to certain measuring points. Figure 2.3 illustrates the measurement on a female subject. The basic information of the human subjects with velocity and concentration measurements is summarized in Table 2.3 (Group 1).

The following sections compare the exhaled flow from the BTM with that from human subjects in terms of velocity profiles, velocity decay and concentration decay along the centerline. The deviations and reasons corresponding to them will be discussed.

4.2.1. PULSATING VELOCITY AND VELOCITY PROFILE

The description of exhaled velocity from human subjects follows the same steps as those in Figure 3.7. One example of the velocity profiles depicted by the mean peak velocity on different x planes are shown in Figure 4.9. It can be seen that both the pulsations of the exhaled velocities and the velocity profiles at different positions of the human subject are different from those of the manikin in Chapter 3.1.3.2.

Pulsating velocity

Under test conditions, the breaths of most human subjects show relatively regular characteristics with respect to breathing frequency and volume. One example is shown in Figure 4.9. However, the breath-to-breath fluctuations are apparently more significant than those of the manikin.

In this chapter, an expression similar to turbulent intensity in form is introduced to indicate the fluctuation degree of peak velocities:

$$I = u_m' / u_m \quad (4.3)$$

u_m is mean peak velocity at centerline, m/s;

u_m' is the standard deviation of peak velocities, m/s.

The I is resulted from the natural fluctuations of human breathing in combination the effect of turbulence of exhalation. The I can be considered as a sort of turbulence intensity only when the breaths from the manikin are considered absolutely identical due to the repeating piston movement of the mechanical lung.

It can be expected that I of human subjects are considerably higher than that of the manikin. The mean I at $x=0.03$ m with 95% confidence intervals is $41 \pm 5\%$ and 1.3% for human subjects and the manikin respectively.

Velocity profiles

The velocity profiles along y section can be depicted by the mean peak velocities $u(x,y)$. Figure 4.9 shows the velocity profiles of one female subject. The maximum velocity at each y section can be considered as the centerline velocity u_m . In Figure 4.9 the centerline has a downward trend. Actually although large variations occur among the individuals, most of the human subjects are reported with downward exhaled flow which may be caused by the asymmetry mouth structure.

In Chapter 3.1.3.2, the exhaled velocity from the manikin is normalized by a universal velocity profile. For human subjects, the velocity profiles slightly differ from the “bell shape”. This is probably because of relative high fluctuations from breath to breath among human breaths. It could also be because the velocity profile in the mouth opening of human subjects are asymmetrical while they are symmetrical from the tube in the manikins.

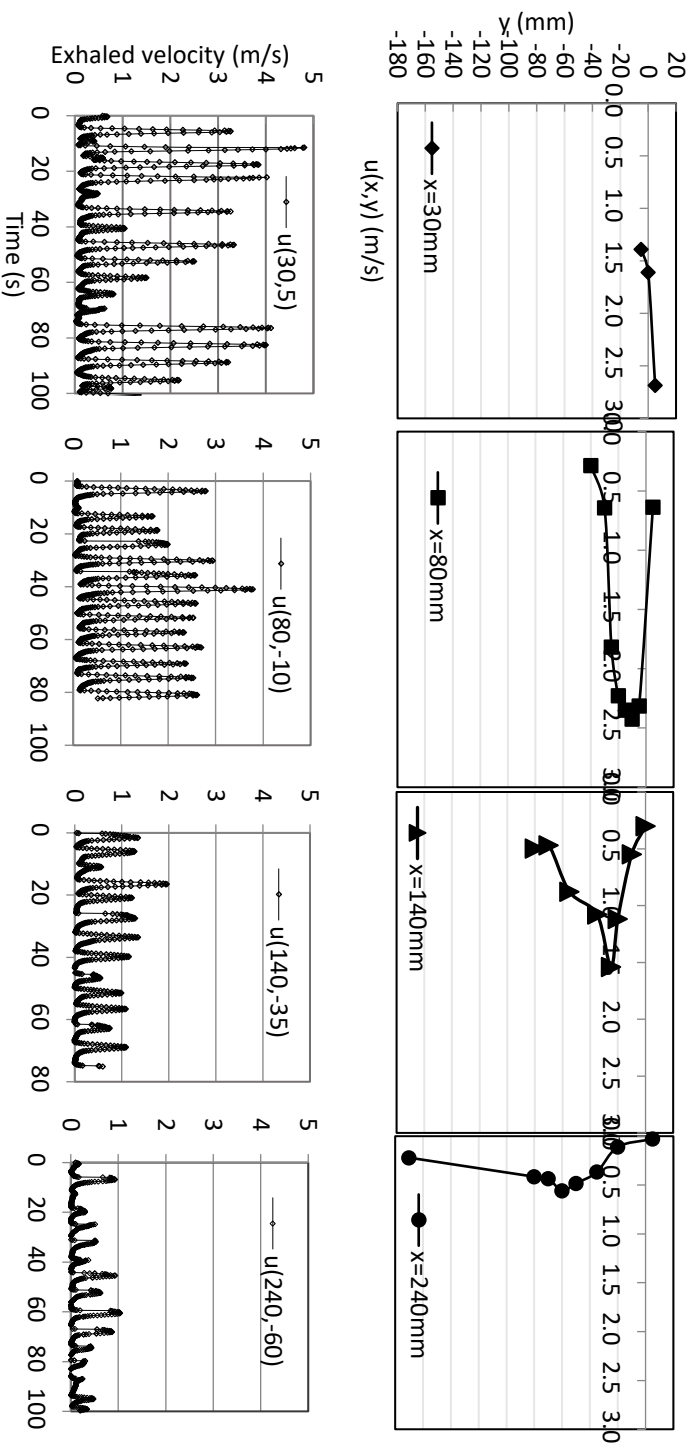


Figure 4.9 Velocity profiles on different x planes and pulsating velocities at the centerline for a female subject without nose clip.

4.2.2. VELOCITY DECAY

Different characteristics of the velocity decay along the centerline between the manikin and human subjects as well as between males and females will be compared in this section. All experiments cover exhalation through the mouth and exhalation only through the nose is not considered here.

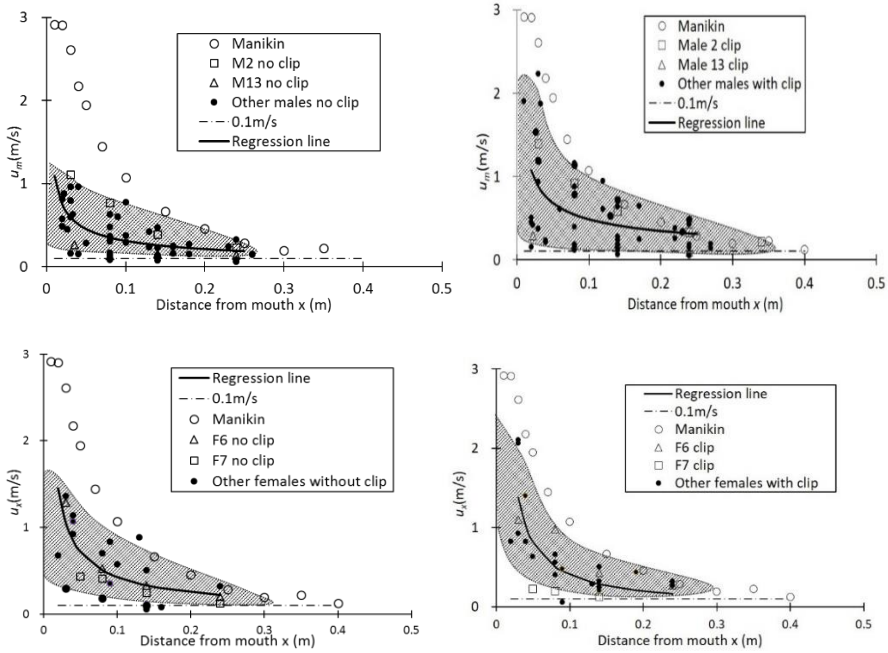


Figure 4.10 Centerline velocities and regression of velocity decay (solid line) of (a) male no clip, (b) male with clip, (c) female no clip and (d) female with clip (with clip-mouth breathing only, no clip-nose in and mouth out) [c].

The centerline velocities extracted from the velocity profiles of each human subject are depicted in Figure 4.10. A dashed line is drawn to cover the scattered velocities, forming a region where the exhaled velocity may locate. A regression equation, assumed as a power function in accordance with that of the manikin, is used to indicate the decay trend of centerline velocities.

$$u_m = ax^b \quad (4.4)$$

The characteristic coefficients a and b , obtained from regression analysis with non-linear least squares algorithm in MATLAB, are listed in Table 4.2.

Table 4.2 Coefficients a and b with 95% confidence intervals [c].

Breathing pattern	<i>a</i>	<i>b</i>
Male nose in and mouth out	0.09 (0.03, 0.14)	-0.55 (-0.74, -0.35)
Male mouth only	0.15 (-0.04, 0.27)	-0.49 (-0.74, -0.24)
Female nose in and mouth out	0.08 (-0.01, 0.16)	-0.76 (-1.12, -0.39)
Female mouth only	0.04 (-0.01, 0.09)	-1.01 (-1.41, -0.62)

Mouth only vs. nose in and mouth out

Two male and two female subjects marked with red symbols are selected to compare the velocity with different breathing patterns. The subject, showing higher exhaled velocity when wearing the nose clip, also shows higher velocity without wearing it. This illustrates relatively unchanged breathing habit for an individual.

The velocity of mouth breathing only is found to be slightly higher than that of nose in and mouth out. This is probably because the use of the nose clip restricts air leak from the nostrils.

Male subjects vs. female subjects

Figure 4.10 illustrates faster velocity decay with female subjects than male, as the characteristic coefficient *b* of male subjects is always higher as shown in Table 4.2. Smaller mouth area and higher breathing frequency in average for female subjects may contribute to the higher initial velocity and more rapid decay with horizontal distance.

Manikin vs. human subjects

A direct comparison of the exhaled velocity in Figure 4.10 shows a higher predicted velocity with the manikin than that with the most majority of human subjects. The breathing frequency and volume of the manikin are set according to an average female, but the manikin’s exhaled velocity shows significant elevation than average human. For the manikin, the respiratory system is simplified as one tube connecting the mouth to the artificial lung. While the respiratory system of human (see Figure 1.1) is so complicated that this simple configuration of the manikin’s respiratory pathway will inevitably cause some deviations. The dominant reason for the elevation of exhaled velocity by the manikin should be the underestimation of the turbulence level of real exhaled flow.

4.2.3. CONCENTRATION DECAY

The concentration of tracer gas (N₂O or CO₂) in centerline of exhaled air is normalized by the following expression:

$$\eta_c = (c_x - c_a) / (c_R - c_a) \quad (4.5)$$

where, c_a is the average concentration of tracer gas in the ambient air in the chamber without a person, ppm; c_R is the average concentration of tracer gas at the exhaust openings of the chamber with a person, ppm; c_x is the average concentration of tracer gas at a horizontal distance of x from the mouth, ppm. For the manikin, $c_a=0$, and η_c can be written as c_x/c_R .

As it is difficult to capture the instantaneous peak concentration because of a relatively long sampling time with present instruments (INNOVA 1303 and 1402), the concentrations defined above are based on average values of the concentration profiles. Owing to the relatively long standing time for a person, less human subjects (2 males and 3 females) than those with velocity measurements are instructed to participate in the tracer gas measurements.

Figure 4.11 shows that the exhaled concentration of the tracer gas from the manikin is also elevated above those from the human subjects, which serves as a further evidence of enhanced turbulence level in human exhaled flow due to the complicated structure of vent pathway.

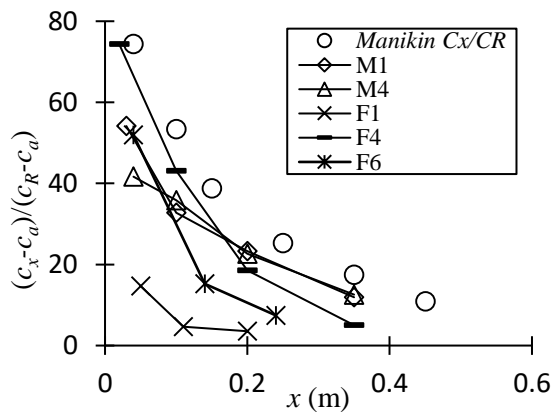


Figure 4.11 Normalized concentration of CO_2 and N_2O in the exhaled air [c].

4.2.4. CONCLUSIONS IN THIS SECTION

Sophisticated manikin can mimic human body shape, body heat and breathing functions to some satisfying degree. However, the exhaled velocity and concentration of contaminant are likely to have an increased level for the manikin, because of the simplified respiratory pathway which results in low diffusion and turbulence levels.

But the elevated breathing of the manikin can to some extent serve as a critical condition for exposure risk assessment.

Due to significant individual differences, the characteristics of actual human breathing is expected to be more complicated and scattered than those of the manikin, including the airflow fluctuations, velocity profiles, exhaled flow directions and decay along the centerline.

Understanding of the characteristics of real human breathing is very important for simulations by using alternative tools, e.g. manikins or CSPs. Chapter 4.3 will provide further characterization of human breathing by using schlieren imaging technique.

4.3. SCHLIEREN IMAGING STUDY ON EXHALED FLOW

4.3.1. INTRODUCTION

Combined with results from human in Chapter 4.2, more new data will be added to the characterization of human breathing. Two aspects: exhaled flow shape and exhaled velocity, will be mainly characterized in this section.

Different human subjects are used in this chapter compared to those in Chapter 4.2. All subjects are of Chinese ethnicity. The basic information of the 18 healthy young adults has been summarized in Table 2.3 (Group 2).

Breathing patterns

All subjects are instructed to breathe with three patterns: (a) nose breathing only, (b) mouth in and nose out and (c) mouth breathing only (wearing a nose clip). A relatively long time of natural breathing (above 10 minutes) is required for each subject with each breathing pattern during tests. And the camera started recording for another 2 minutes without the subjects realizing it.

When a subject is instructed to inhale with nose and exhale with mouth, the air from his or her lung is simultaneously expelled from the nose, which can be observed from the schlieren videos. To characterize the exhaled flow shape and directions, only pattern (a) and (c) are considered.

A subject breathing with mouth only may complain about a dry mouth from time to time. Interruptions of shutting up his or her lips and swallowing saliva during the tests are allowed as a part of his or her breathing pattern.

Postures

The exhaled flow from human subjects whilst standing and lying are investigated. Figure 2.4 shows the placement of a human subject in front of the concave mirror for schlieren experiment. The relative distance between the subject and the mirror is slightly different among subjects, which is calibrated before experiment to exclude the influence of the distance on scales of images.

The subject's head is supported by a height-adjustable holder to avoid head movement whilst standing as in previous tests (Chapter 4.2). When lying flat, the subject is covered with a heavy quilt up to the his or her neck position to block the rising thermal plume from the body and meanwhile mimic the sleeping condition to the most extent.

Propagation velocity and centerline velocity

Two different velocities, u_m and u_p , which are used to describe the exhalation velocity from different aspects, will be compared and discussed in this section.

Flow develops and propagates over time whilst exhaling. The propagation velocity, u_p , is defined by the following expression:

$$u_p = \Delta d / \Delta t \quad (4.6)$$

The propagation distance Δd divided by the corresponding time interval Δt , represents the propagation velocity of the front edge of the exhaled flow. d is derived from the schlieren image along the centerline of the flow as shown in Figure 4.12. The schlieren images are recorded frame by frame with a time interval of 1/15 s.

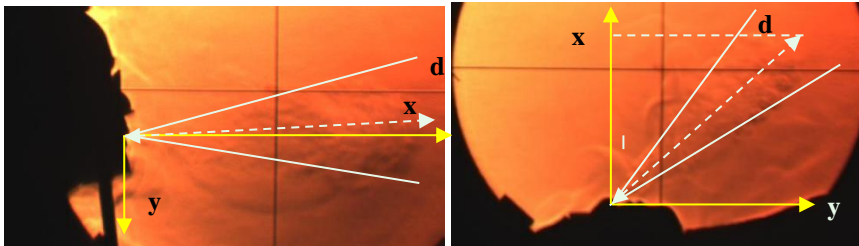


Figure 4.12 Centerline of the exhaled airflow (dashed line) and propagation distance d [d].

The definition and measurements of centerline velocity of human exhaled air, u_m , can be found in Chapter 3.1.3.2. However, the position of the centerline determined here is according to the schlieren images rather than the depicted velocity profiles (e.g. Figure 3.7). Figure 4.12 can serve as an example to determine the centerline of the exhaled flow.

It should be noted that x differs from d and is the horizontal or vertical component of d (depending on postures), see Figure 4.12. Figure 4.12 also shows the coordinate built from the mouth or nose opening with standing and lying postures. The direction of the exhaled flow is determined according to the angle between the centerline and the x axis. The centerline below the x axis is defined as positive.

4.3.2. FLOW SHAPE AND DIRECTION

The schlieren images within a breathing cycle with a time interval of 1/15 s or 2/15 s are stacked together to illustrate the development of the exhaled flow, as shown in Figure 4.13. The breathing cycle is randomly selected from the two-minute recording of about 20~50 breaths dependent on breathing frequency of the subject.

The breathing direction of a mouth or nose is defined by two angles (θ_1 and θ_2) as shown in Figure 4.13. Statistic analysis is performed on the distribution of these breathing angles with SPSS (Statistical Product and Service Solutions).

As no significant differences of these angles are found between males and females, they are joint for our analysis. An approximate normal distribution of the measured angles is found by statistics and the average and confidence intervals are listed in Table 4.3.

Table 4.3 shows that the confidence limit is always small with a maximum of 14° , implying similar breathing angles among subjects. Results also show the breathing direction not varying much between different postures.

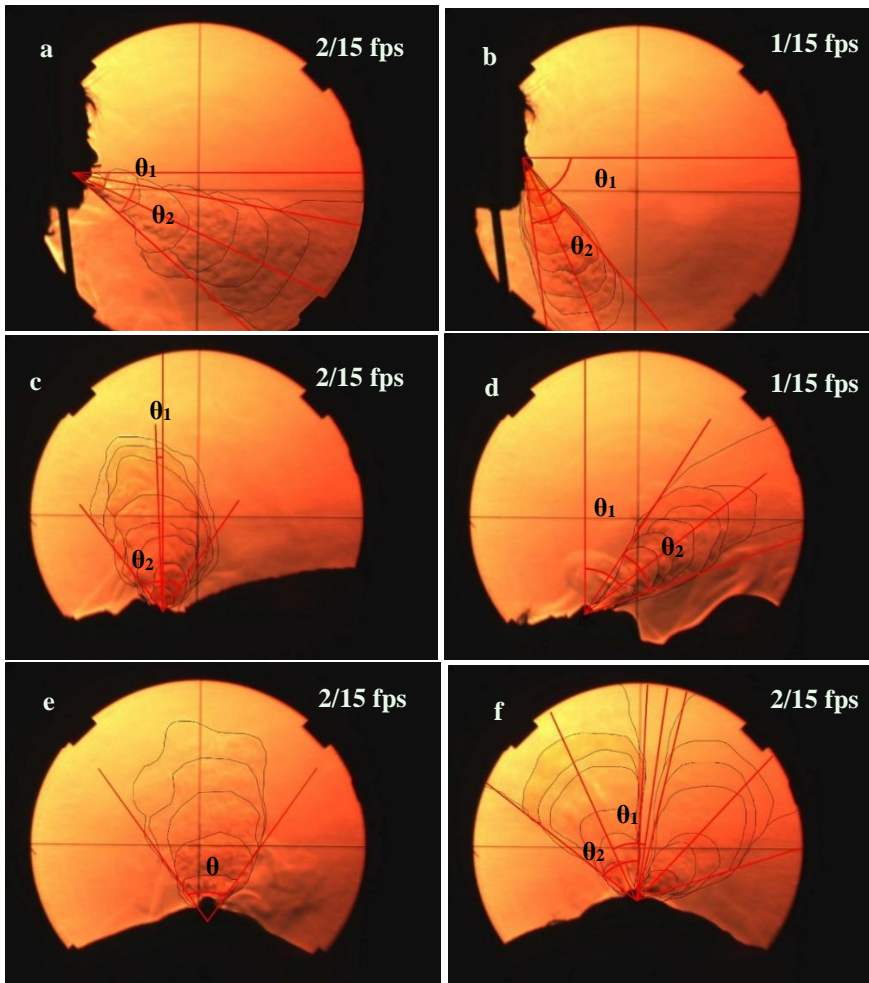


Figure 4.13 Propagation of exhaled flow from the mouth (left) or the nose (right) whilst standing (a, b) and lying (c–f). The development process of exhaled flow is depicted with a time interval of $1/15$ s or $2/15$ s for the three conditions: standing side view (a,b), lying side view (c,d) and lying front view (e,f) [d].

A downward trend of exhaled flow from mouth is found with a positive θ_1 of 14° whilst standing and 9° whilst lying. The downward flow trend for the majority of subjects are also found through velocity measurements in Chapter 4.

Different θ_2 between front and side view indicates an irregular cone shape of the exhaled flow. That is obvious because the mouth or nose opening is not circular.

These angles obtained from human subjects may be helpful to characterize the direction of breathing from CSPs or manikins.

Table 4.3 Average spreading angles of exhaled airflow with 95% confidence limit [d].

View angle	Breathing pattern	This study		Gupta et al. (2010) (sedentary subjects)	
		θ_1	θ_2	θ_1	θ_2
Standing side view	mouth only	$14^\circ \pm 14^\circ$	$36^\circ \pm 6^\circ$	\	30°
	nose only	$57^\circ \pm 6^\circ$	$32^\circ \pm 3^\circ$	$60^\circ \pm 6^\circ$	$23^\circ \pm 14^\circ$
Lying side view	mouth only	$9^\circ \pm 6^\circ$	$44^\circ \pm 7^\circ$	\	\
	nose only	$51^\circ \pm 5^\circ$	$29^\circ \pm 3^\circ$	\	\
Lying front view	mouth only	\	$61^\circ \pm 12^\circ$	\	\
	nose only	$34^\circ \pm 8^\circ$	$43^\circ \pm 6^\circ$	$21^\circ \pm 8^\circ$	$21^\circ \pm 10^\circ$

4.3.3. VELOCITY CHARACTERIZATION

4.3.3.1 Centerline velocity u_m

Initial velocity

The centerline velocity u_m at $x=0.03$ m, which is expressed as $u_{0.03}$, is used to indicate the initial exhaled velocity. Note that $u_{0.03}$ could be lower than real exhaled velocity immediately at the mouth or nose opening, because $u_{0.03}$ might not locate within the constant velocity core similar to that of a free constant jet.

The measured $u_{0.03}$ with range values are given in Table 4.4. The wide spread of these velocities may be due to the wide variation in physiological parameters of our human subjects, e.g. minute volume, breathing frequency and mouth/nose area.

Table 4.4 The $u_{0.03}$ with range values for three breathing patterns [d].

Breathing patterns	Male		Female	
	Standing $u_{0.03}$ (m/s)	Lying $u_{0.03}$ (m/s)	Standing $u_{0.03}$ (m/s)	Lying $u_{0.03}$ (m/s)
Nose only	1.08(0.45–2.00)	1.82(1.00–2.52)	1.63(0.34–2.58)	1.52(0.9–2.27)
Nose in and mouth out	1.22(0.31–2.27)	0.81(0.31–1.55)	1.53(0.36–2.80)	1.35(0.46–2.25)
Mouth only	1.56(0.95–2.03)	1.56(0.67–2.02)	1.64(0.50–2.63)	1.64(0.40–3.22)

Tang et al. (2013) used schlieren imaging technology to determine the nasal and mouth breathing velocities with a maximum of 1.4 m/s and 1.3 m/s, respectively. Apparently, these velocities are underestimated compared to the measured values in Table 4.4.

The application of u_p by Tang et al. (2013) to describe the exhaled velocity may cause this underestimation. The u_p , expressing the propagation velocity of the front edge of the exhaled flow, is essentially different from u_m that is extracted from the peaks of pulsating velocities (Figure 3.7), and should not be used as velocity boundary settings of CFD simulation. The difference between u_p and u_m will be further discussed in the following section.

Velocity decay

The regression equation derived in Chapter 4.2.2 (Equation 4.2) on mouth breathing only is validated here by using different human subjects. Figure 4.14 illustrates that the decay of u_m agrees well with the regression equation.

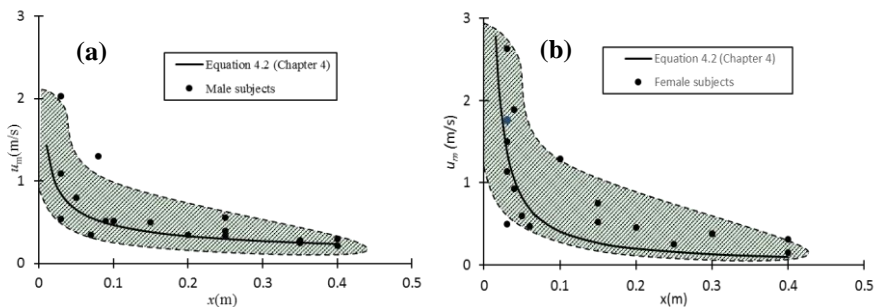


Figure 4.14 Velocity decay along the centerline in the mouth only breathing [d].

4.3.3.2 Propagation velocity u_p

Figure 4.15 shows the propagation distance increasing over time with subjects standing and lying from side view. Due to size limitation of the mirror and dependence on temperature difference for visualization applying shlieren imaging technique, the exhaled flow could penetrate longer distance than observed in Figure 4.15.

Tang et al. (2013) reported a maximum propagation distance for mouth and nose breathing of 0.8 m and 0.6 m, respectively. In Figure 4.15, the observed maximum propagation distance is about 0.4 m. However, it is still difficult to know where the flow could stop. The exhaled air finally mixes with room air in turbulence and the propagation distance should depend on turbulence level of both the exhaled flow and the room air.

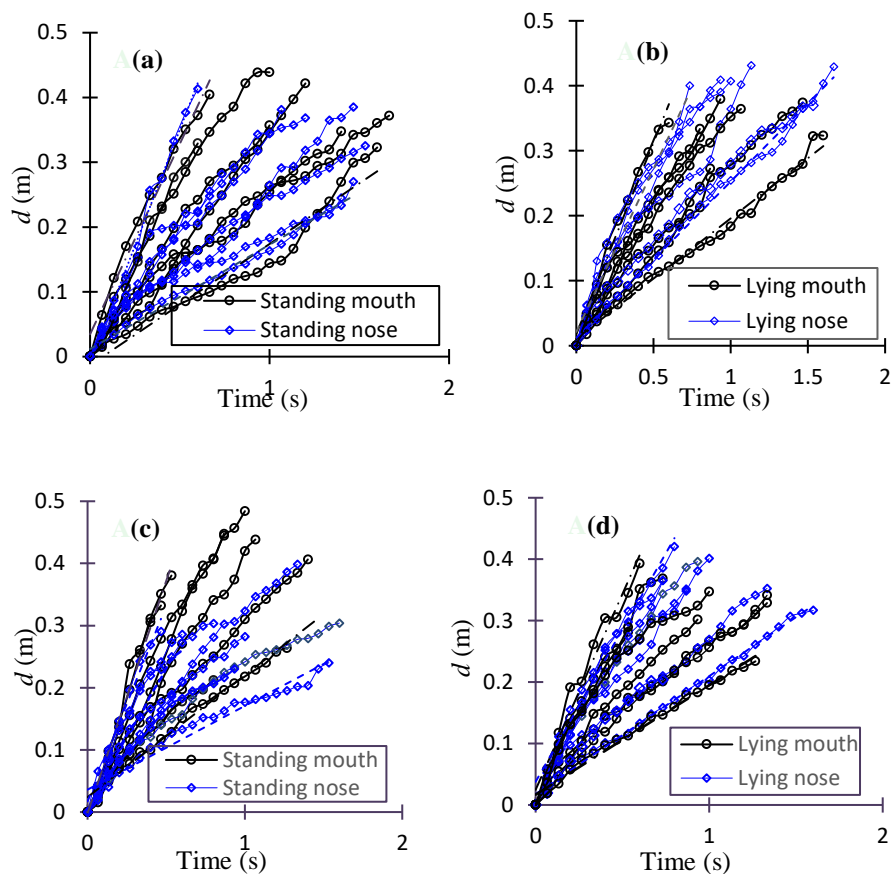


Figure 4.15 Visible propagation distances of mouth only breathing and nose only breathing over time: (a) male, standing posture; (b) male, lying posture; (c) female, standing posture and (d) female, lying posture [d].

From Figure 4.15, it can be seen d increases with time in a roughly linear trend. Linear fitting is hereby performed on curves in Figure 4.15. The slope of the varying distance over time can be recognized as average u_p over observed time according to Equation 4.4. u_p varies among subjects and it is found to be lower than 0.8 m/s in present study, which is significantly lower than averaged $u_{0.03}$ in Table 4.4.

Correlation of u_p with physiological parameters

The propagation velocity would be high when a person breathing with high minute volume (BMV) at a high breathing frequency (BF). This can also be observed from schlieren videos. Gupta et al. (2010) reported that the BMV is linearly related to BSA and an attempt is made here to correlate the u_p obtained from Figure 4.15 with BSA

and BF. No significant correlation between u_p and the separate parameter like BSA or BF, is found. But u_p is found to be basically linear to $BSA \times BF$ as shown in Figure 4.16. A regression equation is assumed by Equation 4.7.

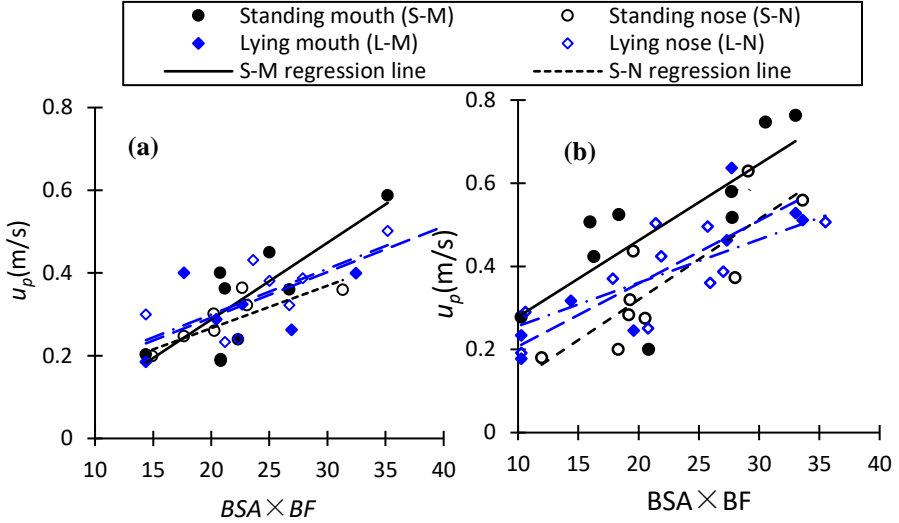


Figure 4.16 Variation of u_p with $BSA \times BF$ of (a) the male subjects and (b) the female subjects [d].

$$u_p \text{ (m/s)} = k \times \text{BSA (m}^2\text{)} \times \text{BF (min}^{-1}\text{)} \quad (4.7)$$

Table 4.6 Regression analysis of u_p obtained by the defined Equation 4.7 [d].

	Male		Female	
	k	Correlation coefficient r	k	Correlation coefficient r
Standing mouth	0.019	0.82	0.018	0.76
Standing nose	0.01	0.74	0.019	0.84
Lying mouth	0.011	0.81	0.015	0.88
Lying nose	0.011	0.71	0.01	0.73

T-test is performed on correlation coefficient, r . The r for all test groups is found to be more than 0.7 for a $p < 0.05$, indicating u_p is basically related to the $BSA \times BF$. The slope k for the linear fitting is listed in Table 4.6. However, due to the limitation of

small numbers of human subjects in present study, more measuring points on larger number of human subjects are needed to validate the reliability of this regression equation.

4.3.3.3 Differences between u_p and u_m

In this study, u_p is found to be always lower than u_m very close to the mouth opening. The u_p of sneezing and coughing reported by Tang et al. (2013) was 4-5 m/s, which was also significantly lower than generally considered values of sneezing and coughing, e.g. sneezing 20-50 m/s, coughing 10 m/s (Chen et al. 2014).

Figure 4.17 shows that the front of airflow in the early stage of an exhalation cycle is similar to a vortex-like airflow. Akhmetov (2009) indicated that it would be a typical condition for a vortex of larger u_m in a fixed point than u_p when the vortex passed this point. This could explain why u_p is always smaller than u_m . To conclude, u_p should not be used as initial exhaled velocity in practice because it may cause underestimation of real exhaled velocity.

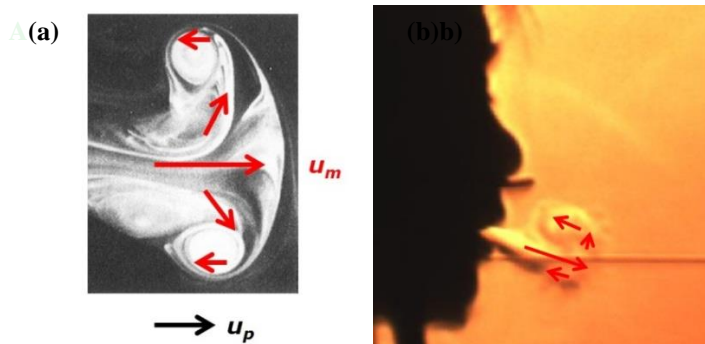


Figure 4.17 Images of (a) a typical vortex flow and (b) airflow from a female subject [d].

4.3.4. CONCLUSIONS IN THIS SECTION

In this section exhaled flow shape and velocity is characterized by using schlieren imaging technique. Accurate information could be provided for CFD boundary settings and configuration of manikins.

The exhaled flow direction from mouth or nose whilst standing and lying is defined by two angles: θ_1 and θ_2 . The two angles are found to have minimal variations between subjects. Hence, the angles observed from schlieren images can be used for breathing geometry description.

Two different velocities, u_p and u_m , are compared and defined for different purposes. The u_m is found to decrease with horizontal distance by power function. The u_p shows strong correlation to physiological parameters, BSA and BF. Due to the limitation of small numbers of human subjects, more measurements are needed to validate the reliability of the correlation. It should be noted that u_p and u_m are two different concepts to describe the dispersion speed of exhaled air. The u_p is obtained by tracing the front edge of exhaled flow, while the u_m is extracted from peaks of velocity pulsation measured at certain points. The u_p is significantly lower than the initial velocity $u_{0.03}$ and cannot be used as the initial exhaled velocity because the u_p may cause underestimation of real exhaled velocity.

CHAPTER 5. CONCLUSIONS AND FUTURE WORK

This chapter presents conclusions and perspectives for future work regarding results obtained in this thesis. Some limitations are also discussed.

Interactions between ventilation with breathing

Room ventilation, body plume and human breathing interacts between each other, causing possible complex dispersion characteristics of exhaled flow and affecting the inhaled air quality for occupants.

The dispersion of exhaled air may act as sources of airborne disease transmission indoor. This study focuses on characterizing the dispersion of exhaled air under different ventilation principles, e.g. mixing ventilation and displacement ventilation. Mixing ventilation, with a vertical temperature gradient of approximate zero, is found to cause exhaled pollutant mixed and diluted by ambient air rapidly. While the exhaled pollutant is stratified at certain height due to the blocking effect of the vertical temperature gradient with displacement ventilation. This blocking effect could cause increased potential exposure risk for a receptor. Centerline velocity and centerline concentration are defined in this thesis to quantify the exhaled flow, and the effect of temperature gradient on velocity decay along the centerline is not as significant as that on concentration decay. The quantification method for exhaled flow from the manikin is also applied on human subjects.

Personalized ventilation (PV) can perform as an effective approach to improve inhaled air quality and reduce contaminant exposure risk for occupants. The present study indicates that even at low invading velocities, small fraction of personalized air can still be inhaled by the person facing to PV nozzle. The lower boundary of the turbulent shear layer of nozzle jet interacts with the rising thermal plume, leading to easier penetration of the jet centerline to the thermal boundary layer around the person. As air is inhaled mainly from the rising thermal plume, the interactions of PV air with the thermal plume in the breathing zone should be carefully considered for optimal ventilation design.

Breathing characterization with three tools

Three tools: the breathing thermal manikin (BTM), computer simulated person (CSP) and human subjects are applied to characterize the exhaled flow. Comparisons are conducted between the CSP and the BTM and between the BTM and human subjects.

The CSP and the chamber where the CSP locates are generated according to the experiments by using the BTM with mixing ventilation and displacement ventilation. The simulations with the CSP can basically agree with experiments with the BTM in terms of the exhaled velocity magnitude, the flow dispersion directions, and the body plume development tendencies. There are also deviations and the possible reasons are briefly discussed. Proper settings with respect to the influencing factors on the accuracy of simulated results, e.g. grid generation, boundary conditions, turbulence models, and discretization schemes, etc., may be helpful to obtain better solutions for this specific kind of problems. Careful considerations and comparisons in every simulation step are needed in future work.

The BTM is used to mimic human breathing by applying similar geometric and respiratory configurations to real people. Real human breathing is more complicated than that of the manikin as expected. The exhaled velocity and concentration of contaminant seem to be elevated by the manikin due to its simplification in respiratory pathway. This may cause increased contaminant exposure risk predicted with the manikin.

Understanding of the characteristics of real human breathing is important for accurate prediction by using manikins or CSPs. The breathing from human subjects whilst standing and lying are further characterized with the aid of schlieren imaging technique in terms of flow direction and propagation velocity. The propagation velocity u_p is compared with the centerline velocity u_m , and is found to be always smaller than u_m . These two velocities should be carefully distinguished for use. The u_m decay can be regressed by a powder function and the u_p can be roughly predicted by human physiological parameters. And u_p should not be considered as the boundary setting of initial exhaled velocity in CFD simulations, because it will cause certain underestimations of the velocity.

CFD has become a promising tool for infection risk assessment. Careful comparisons of the simulations with the measurements are helpful to improve the accuracy of the simulations. More data, especially for real human subjects who provide the most reliable data, will be needed for CFD simulation evaluations.

Limitations

Tracer gas measurements on CO₂ or NO₂ and visualization of exhaled air by means of schlieren technique or oil-based smoke can only present the dispersion of gaseous contaminant or particles with small diameters that have good following feature with exhaled air. Dispersion and deposition characteristics of large droplets are not considered in this thesis.

Another limitation may be caused by using small numbers of human subjects and most of them are Chinese ethnic. Results obtained from human subjects are scattered due

to individual differences. The exhalation from an individual may also vary over time. To exclude the influence of these uncertainties on results when quantifying human breathing, we need to make more attempts on larger number of human subjects to further enhance our understanding on the complexity of human breathing.

Future work

CFD has become a powerful tool to predict exposure risk of contamination from a suspected person. To improve the accuracy of CFD simulations of breathing behaviors, more information should be obtained from real persons. Deviations between simulations and experiment data based on reality should be carefully examined in future work. The influencing factors, such as ventilation pattern, metabolic rate, humidity and turbulence level in the room may add complexity to the prediction of exhaled flow dispersion and their effects should be taken into account in future work.

LITERATURE LIST

- Abramovich, G.N. (1963) *The Theory of Turbulent Jets*, Massachusetts, M.I.T. Press.
- Adams, W.C. (1993) *Measurement of Breathing Rate and Volume in Routinely Performed Daily Activities*, Sacramento, CA, California Environmental Protection Agency.
- Akhmetov, D.G. (2009) *Vortex Rings*, Springer, Verlag Berlin Heidelberg, Berlin.
- ANSYS FLUENT User's guide. Southpointe: ANSYS, Inc.; 2010.
- ASHRAE (2009) *Indoor Environmental Quality*, Atlanta, GA, American Society of Heating, Refrigerating and Air Conditioning Engineers (ASHRAE Handbook of Fundamentals 9.1-9.30).
- Bachy, J.P., Eberhard, A., Baconnier, P., Benchetrit, G. (1986) A program for cycle-by-cycle shape analysis of biological rhythms. Application to respiratory rhythm. *Comput. Meth. Prog. Biomed.*, 23, 297–307.
- Badeau, A., Afshari, A., Goldsmith, T. and Frazer, D. (2002) Preliminary prediction of flow and particle concentration produced from natural human cough dispersion, *Proceedings of the Second Joint EMBS/BMES Conference*, Houston, USA, 23-26.
- Benchetrit, G. (2000) Breathing pattern in humans: diversity and individuality, *Respir. Physiol.*, 122, 123–129.
- Bjørn, E. (1999) Simulation of human respiration with breathing thermal manikin. In: *Proceedings of Third International Meeting on Thermal Manikin Testing*, Stockholm, Sweden, National Institute for Working Life, pp. 78–81.
- Bjørn, E. and Nielsen, P.V. (2002) Dispersal of exhaled air and personal exposure in displacement ventilated room, *Indoor Air*, 12, 147–164.
- Bolashikov, Z., Nagano, H., Melikov, A., Velte, C., Meyer, K.E. (2011a) Airflow characteristics at the breathing zone of a seated person: passive control over the interaction of the free convection flow and locally applied airflow from front for personalized ventilation application. *Proceedings of Roomvent*.
- Brohus, H. (1997) *Personal exposure to contaminant sources in ventilated rooms*, PhD thesis, Aalborg, Denmark, Aalborg University.
- Brohus, H. and Nielsen, P.V. (1996) Personal exposure in displacement ventilated rooms, *Indoor Air*, 6, 157–167.
- Cermak, R., Holsol, J., Meyer, K.E. and Melikov, A.K. (2002) PIV measurements at the breathing zone with personalized ventilation. *Roomvent 2002*, Sept. 8-11: Copenhagen, Denmark.

- Du Bois, D. and Du Bois, E.F. (1989) A formula to estimate the approximate surface area if height and weight be known. 1916, *Nutrition*, 5, 303-311.
- Dye, C., Scheele, S., Dolin, P., Pathania, V. and Raviglione, M.C. (1999) Global burden of tuberculosis: estimated incidence, prevalence, and mortality by country, *JAMA*, 282, 677–686.
- Chao, C.Y.H., Man, M.P., Sze To, G.N. (2008) Transport and removal of expiratory droplets in hospital ward environment, *Aerosol Sci. Technol.* 412, 377–394.
- Chao, C.Y.H., Wan, M.P., Morawska, L., Johnson, G.R., Ristovski, Z.D., Hargreaves, M., Mengersen, K., Corbett, S., Li, Y., Xie, X. and Katoshevski, D. (2009) Characterization of expiration air-jets and droplet size distributions immediately at the mouth opening, *J. Aerosol Sci.*, 40, 122–133.
- Chen, C. and Zhao, B. (2010) Some questions on dispersion of human exhaled droplets in ventilation room: answers from numerical investigation. *Indoor Air*, 20, 95-111
- Clark, R.P. and Edholm, O.G. (1985) *Man and his thermal environment*, London, E. Arnold Publishing Co.
- Eisele, J.H., Wuyam, B., Savourey, G., Etteradossi, J., Bittel, J.H. and Benchetrit, G. (1992) Individuality of breathing patterns during hypoxia and exercise. *J. Appl. Physiol.* 72, 2446-2453.
- Fabian, P., McDevitt, J., DeHaan, W., Fung, R., Cowling, B., Chan, K., Leung, G., Milton, D. (2008) Influenza virus in human exhaled breath: An observational study. *PLoS ONE* 3:e2691.
- Fanger, P.O. (1967) Calculation of thermal comfort: introduction of a basic comfort equation, *ASHRAE Trans.*, 73, III .4.1.
- Fairchild, C.I. and Stamper, J.F. (1987) Particle concentration in exhaled breath. *Am. Ind. Hyg. Assoc. J.* 48, 948-949.
- Gao, N. and Niu, J. (2004) CFD study on micro-environment around human body and personalized ventilation. *Build. Environ.* 39(7),795-805.
- Gao, N., He, Q. and Niu, J. (2012) Numerical study of the lock-up phenomenon of human exhaled droplets under a displacement ventilated room, *Build. Simul.*, 5, 51-60.
- Gold, E. and Nankervis, G.A. (1989) Cytomegalovirus. In: Evans, A. (ed) *Viral Infections of Humans*, New York, Plenum Medical Book Co., 175–176.
- Gupta, J.K., Lin, C. and Chen, Q. (2010) Characterizing exhaled airflow from breathing and talking, *Indoor Air*, 20, 31–39.
- Habchi, C., Ghali, K., Ghaddar, N., Chakroun, W. and Alotaibi, S. (2016) Ceiling personalized ventilation combined with desk fans for reduced direct and indirect

cross-contamination and efficient use of office space. *Energy Convers. Manage.*, 111, 158-173.

- Hayashi, T., Ishizu, Y., Kato, S. and Murakami, S. (2002) CFD analysis on characteristics of contaminated indoor air ventilation and its application in the evaluation of the effects of contaminant inhalation by a human occupant. *Build. Environ.*, 37, 219-230.
- He, G., Yang, X. and Srebric, J. (2005) Removal of contaminants released from room surfaces by displacement and mixing ventilation: modeling and validation, *Indoor Air*, 15, 367–380.
- He, Q., Niu, J., Gao, N., Zhu, T. and Wu, J. (2011) CFD study of exhaled droplet transmission between occupants under different ventilation strategies in a typical office room, *Build. Environ.*, 46, 397–408
- Holmér, I. (2004) Thermal manikin history and applications, *Eur. J. Appl. Physiol.*, 92, 614–618.
- Hoppe, P. (1981) Temperatures of expired air under varying climatic conditions, *Int.J. Biometeorol.*, 25, 127–132.
- Huynh, K.N., Oliver, B.G., Stelzer, S., Rawlinson, W.D., Tovey, E.R. (2008) A new method for sampling and detection of exhaled respiratory virus aerosols. *Clin. Infect. Dis.*, 46, 93–95.
- Hutchinson, J. (1850) Todd's Cyclopaedia of Anatomy and Physiology. Cited by Mead J., 1963. Control of Respiratory frequency. *J. Appl. Physiol.* 15, 325–336.
- Khalifa, H.E., Janos, M.I., and Iii, J.F.D. (2009) Experimental investigation of reduced-mixing personal ventilation jets. *Build. Environ.*, 44(8), 1551-1558.
- Kwon, S.-B., Park, J., Jang, J., Cho, Y., Park, D.-S., Kim, C., Bae, G.N. and Jang, A. (2012) Study on the initial velocity distribution of exhaled air from coughing and speaking. *Chemosphere*, 87, 1260–1264.
- Lai, A.C.K. Cheng, Y.C. (2007) Study of expiratory droplet dispersion and transport using a new Eulerian modeling approach, *Atmos. Environ.* 41, 7473–7484.
- Liu, L., Nielsen, P.V., Li, Y., Jensen, R.L., Litewnicki, M. and Zajac, J. (2009b) The Thermal plume above a human body exposed to different air distribution strategies, In: *Proceedings of 9th Int. Conf. Healthy Buildings*, September 13-17, 2009, Syracuse, NY, USA
- Liu, L, Li, Y, Nielsen, P.V., Wei, J. and Jensen, R.L.(2016) Short-range airborne transmission of expiratory droplets between two people *Indoor Air*, DOI: 10.1111/ina.12314
- Madsen, T. L. (1999) Development of a Breathing Thermal Manikin, *Proceedings of the Third International Meeting on Thermal Manikin Testing*, 3IMM, National Institute for Working Life, Stockholm.

- Makhoul, A., Ghali, K. and Ghaddar, N. (2013) Desk fans for the control of the convection flow around occupants using ceiling mounted personalized ventilation. *Build. Environ.*, 59, 336–348.
- Marr, D., Khan, T., Glauser, M., Higuchi, H. and Zhang, J. (2005) On particle image velocimetry (PIV) measurements in the breathing zone of a thermal breathing manikin, *ASHRAE Trans.*, 111, Part 2, 299-306.
- Melikov, A.K. (2004) Personalized ventilation. *Indoor Air*, 14 (Suppl. 7), 157-167.
- Melikov, A.K. (2015) Human body micro-environment: the benefits of controlling airflow interaction, *Build. Environ.*, 91, 70–77.
- McCluskey, R., Sandin, R. and Greene, J. (1996) Detection of airborne cytomegalovirus in hospital rooms of immune compromised patients, *J. Virol. Methods*, 56, 115–118.
- Morawska, L., Johnson, G.R., Ristovski, Z., Hargreaves, M., Mengersen, K., Chao, C.Y.H., Li, Y. and Katoshevski, D. (2009) Size distribution and sites of origins of droplets expelled from the human respiratory tract during expiratory activities, *J. Aerosol Sci.*, 40, 256–269.
- Mui, K.W., Wong, L.T, Wu, C.L. and Lai, A.C.K. (2009) Numerical modeling of exhaled droplet nuclei dispersion and mixing in indoor environments, *J. Hazard. Mater.*, 167, 736-744.
- Murakami, S. (2004) Analysis and design of micro-climate around the human body with respiration by CFD, *Indoor Air*, 14, 144-156.
- Nielsen, P.V. (1995) Lecture notes on mixing ventilation. Dept. of Building Technology and Structural Engineering, Aalborg University.
- Nielsen, P.V. (2004) Computational fluid dynamics and room air movement. *Indoor Air*, 14 (Suppl 7), 134–143.
- Nielsen, P.V., Jensen, R.L., Litewnicki, M. and Zajas, J. (2009) Experiments on the microenvironment and breathing of a person in isothermal and stratified surroundings, In: *Proceedings of 9th Int. Conf. Healthy Buildings*, Syracuse, NY, USA.
- Nielsen, P.V., Olmedo, I., Ruiz de Adana, M., Grzelecki, P. and Jensen, R.L. (2012) Airborne cross-infection risk between two people standing in surroundings with vertical temperature gradient, *HVAC & R. Research*, 18, 552-561.
- Olmedo, I., Nielsen, P.V., Ruiz de Adana, M., Jensen, R.L. and Grzelecki, P. (2012) Distribution of exhaled contaminants and personal exposure in a room using three different air distribution strategies, *Indoor Air*, 22, 64-76.
- Papineni, R.S. and Rosenthal, F.S. (1997) The size distribution of droplets in the exhaled breath of healthy human subjects, *J. Aerosol Med.*, 10, 105–116.

- Priban, I.P. (1963) An analysis of some short-term patterns of breathing in man at rest. *J. Physiol. London*, 166, 425–434.
- Priban, I.P. and Fincham, W.F. (1965) Self-adaptive control and the respiratory system. *Nature*, 208, 339–343.
- Qian, H., Li, Y., Nielsen, P.V., Hylgaard, C.E., Wong, T.W. and Chwang, A.T.Y. (2006) Dispersion of exhaled droplet nuclei in a two-bed hospital ward with three different ventilation systems, *Indoor Air*, 16, 111–128.
- Raven, P., Johnson, G., Mason, K., Losos, J. and Singer, S. (2007) The capture of oxygen: *Respiration. Biology* (8 ed. ed.). McGraw-Hill Science/Engineering/Math.
- Shrivastav, A., Shah, H. A., Shrivastav, G. and Santwani, P. M. (2013). Utility of acid fast staining and re-aspiration in tubercular lymphadenopathy - 3 year study at tertiary centre. *IEEE International Workshop on Analysis and Modeling of Faces and Gestures (Vol.3, pp.181-186)*. IEEE.
- Stampe, O. B. (1982) *Glent ventilation*. Publisher, Hvidovre : Glent & Co, Edition 2 (in Danish).
- Stelzer-Braid, S., Oliver, B.G., Blazey, A.J., Argent, E., Newsome, T.P., Rawlinson, W.D. and Tovey, E. R. (2009) Exhalation of respiratory viruses by breathing, coughing, and talking, *J. Med. Virol.*, 81, 1674–1679.
- Srebrica J, Vukovica V, Heb G, et al. CFD boundary conditions for contaminant dispersion, heat Transactionsfer and airflow simulations around human occupants in indoor environments. *Building and Environment*, 2008,43(3):294–303
- Tanabe, S., Zhang, H., Arens, E. A., Madsen, T. L., and Bauman, F. S. (1994). Evaluating thermal environments by using a thermal manikin with controlled skin surface temperature. *ASHRAE Trans.*, 100(1), 39-48.
- Tang, J.W., Nicolle, A.D.G., Pantelic, J., Jiang, M., Sekhr, C., Cheong, D.K.W., and Tham, K.W. (2011) Qualitative Real-Time Schlieren and Shadowgraph Imaging of Human Exhaled Airflows: An Aid to Aerosol Infection Control, *PLoS One* 6 e21392.
- Tang, J.W., Nicolle, A.D., Klettner, C.A., Pantelic, J., Wang, L., Bin Suhaimi, A., Tan, A.Y.L., Ong, G.W.X., Su, R., Sekhar, C., Cheong, D.D.W. and Tham, K.W. (2013) Airflow Dynamics of Human Jets: Sneezing and Breathing - Potential Sources of Infectious Aerosols, *PLoS One* 8 e59970.
- Wei, J., and Li, Y. (2016). Airborne spread of infectious agents in the indoor environment. *Ajic American Journal of Infection Control*, 44(9), S102-S108.
- West, J. B. (1994). *Respiratory physiology-- the essentials*. Baltimore: Williams & Wilkins.

- Wikipedia (2014) http://en.wikipedia.org/wiki/Respiratory_system (accessed 05.08.2014)
- World Health Organization (2010).
<http://www.searo.who.int/timorleste/areas/h1n1/en/> (accessed 08.08.2017)
- Xia, Y.Z., Niu, J.L., Zhao, R.Y. and Burnett. J. (2000) Effects of turbulent air on human thermal sensations in a warm isothermal environment. *Indoor Air*, 10, 289-296.
- Xie, X., Li, Y., Chwang, A. T. Y., Ho, P. L. , Seto, W. H. (2007) How far droplets can move in indoor environments - revisiting the Wells evaporation - falling curve, *Indoor Air*, 17, 211–225.
- Yang, B., Melikov, A. and Sekhar, C. (2009) Performance evaluation of ceiling mounted personalized ventilation system. *ASHRAE Trans.*, 115 (2), 395-406.
- Yang, B., Sekhar, C. and Melikov, A.K. (2010) Energy analysis of the personalized ventilation system in hot and humid climates. *Energy Build.*, 42(5), 699-707.
- Zhang, C., Heiselberg, P.K., Pomianowski, M., Tao, Y. and Jensen, R.L. (2015) Experimental study of diffuse ceiling ventilation coupled with a thermally activated building construction in an office room. *Energy Build.*, 105, 60-70.

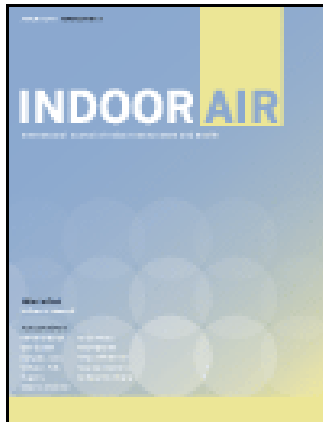
APPENDIX A.

INFLUENCE OF AIR STABILITY AND METABOLIC RATES ON EXHALED FLOW

The paper presented in Appendix A is published in Indoor Air, Volume 25, Issue 2, Pages 198-209, 2015.

doi:10.1111/ina.12135

<http://onlinelibrary.wiley.com/doi/10.1111/ina.12135/pdf>



Influence of air stability and metabolic rate on exhaled flow

Abstract The characteristics of contaminant transport and dispersion of exhaled flow from a manikin are thoroughly studied in this article with respect to the influence of two important factors: air stability conditions and metabolic rates. Four cases with the combinations of stable and neutral conditions as well as lower (1.2 met) and higher (2 met) metabolic rates for a breathing thermal manikin are employed. The exhaled contaminant is simulated by smoke and N₂O to visualize and measure the contaminant distribution both around and in front of the manikin. The results show that the microenvironment around the manikin body can be affected by different air distribution patterns and metabolic heating. Under stable conditions, the exhaled contaminant from mouth or nose is locked and stratified at certain heights, causing potentially high contaminant exposure to others. In addition, velocity profiles of the pulsating exhaled flow, which are normalized by mean peak velocities, present similar shapes to a steady jet. The outlet velocity close to the mouth shows decrement with both exhalation temperature and body plume. The velocity decay and concentration decay also show significant dependence on air stability and metabolic level.

**C. Xu¹, P. V. Nielsen², G. Gong¹,
R. L. Jensen², L. Liu²**

¹College of Civil Engineering, Hunan University, Changsha, China, ²Department of Civil Engineering, Aalborg University, Aalborg, Denmark

Key words: Air stability; Metabolic rate; Exhalation; Near-human microenvironment; Body plume; Manikin.

G. Gong
College of Civil Engineering
Hunan University
Changsha 410082, China
Tel.: +86 13973123865
Fax: +86 88823082
e-mail: gcgong@hnu.edu.cn

Received for review 9 October 2013. Accepted for publication 24 May 2014.

Practical Implications

Results obtained from experimental studies in this investigation reveal the influence of air stability and metabolic rates on human-exhaled flow. The concept of air stability can be applied to demonstrate the 'lock-up phenomenon' of the exhaled air under displacement ventilation. The detailed analysis of these two influencing factors on transport and dispersion of exhaled air may be helpful to (i) the selection of appropriate ventilation system to minimize airborne infection risk in indoor environment; and (ii) the accurate specification of metabolic levels for manikins or computer-simulated persons.

Nomenclature

a_0	area of manikin's mouth (m ²)	n_2	characteristic concentration exponent
A	maximum flow rate of exhalation (l/s)	\dot{q}	instantaneous exhaled flow rate (l/s)
BF	breathing frequency (min ⁻¹)	RMV	respiratory minute volume (l/min)
c_0	mean peak concentration at the manikin's mouth (ppm)	T_a	ambient air temperature (°C)
c_R	concentration at the exhaust openings (ppm)	T_b	body surface temperature (°C)
c_x	mean peak concentration at a horizontal distance of x from mouth (ppm)	T_{exh}	exhaled air temperature (°C)
h_c	convective heat transfer coefficient [W/(m ² ·K)]	t	time (s)
h_r	radiative heat transfer coefficient [W/(m ² ·K)]	TV	tidal volume (l)
K_c	characteristic constant for concentration decay	$u(x, y)$	mean peak velocity at (x, y) (m/s)
K_v	characteristic constant for velocity decay	$\dot{u}(x, y)$	instantaneous exhaled velocity at (x, y) (m/s)
n_1	characteristic velocity exponent	u_0	outlet velocity close to manikin's mouth (m/s)
		u_x	mean peak velocity along the centerline at a horizontal distance of x from mouth (m/s)
		x	horizontal distance (m)
		y	vertical distance (m)
		ω	frequency (s ⁻¹)

Introduction

Human respiratory behavior and the near-human microenvironment have drawn more attention from researchers in recent years. Many experimental (Bjørn and Nielsen, 2002; Brohus, 1997; Brohus and Nielsen, 1996; Gupta et al., 2010; Nielsen et al., 2008, 2009, 2012; Olmedo et al., 2012; Qian et al., 2006, 2008) and numerical (Chen and Zhao, 2010; Gao and Niu, 2004, 2005; Hayashi et al., 2002; He et al., 2011; Liu and Li, 2012; Liu et al., 2009; Murakami, 2004; Villafruela et al., 2013; Zhu et al., 2005) investigations have been carried out to study the characteristics of exhaled flow dispersion and the region near the body from which inhalation air is drawn.

Many infectious respiratory diseases, such as tuberculosis, human avian influenza, SARS, and flu can be transmitted directly through air or droplets. It is therefore vital to know exactly how the exhaled flow from a person disperses for the purpose of reducing the infection risk to the susceptible persons who share the indoor environment. However, the human breathing process is complicated, affected by multiple factors, which can be mainly summarized in these broad terms: a person's metabolic rate and activity; ventilation strategy (Chung and Hsu, 2001; Gao et al., 2008; Olmedo et al., 2012; Qian et al., 2006); ambient air temperature and humidity (McCutchan and Taylor, 1951; Holmer, 1984); and the local temperature gradient, air velocity and turbulence around the person. Two of these factors: temperature gradients and metabolic rates are studied in the current investigation, keeping constant all other factors which influence the exhalation characteristics.

With the growing use of displacement ventilation (DV) to manage ventilation and thermal comfort in public buildings, the influence of temperature gradients on human respiratory flow, contaminant distribution, jets from diffusers and even development of heat plume have gradually attracted more attention. Many investigations have identified the 'lock-up phenomenon,' in which exhaled contaminants are maintained at high concentration in the breathing zone when there occur certain temperature gradients in the occupied zone. This phenomenon challenges the earlier thinking that DV provides higher ventilation effectiveness and therefore achieves a protective benefit in comparison with conventional mixing ventilation (MV). Bjørn and Nielsen (2002) found the exhaled contaminant to be stratified at breathing zone height with a vertical temperature gradient of $0.5^{\circ}\text{C}/\text{m}$. Qian et al. (2006) observed thermal stratification locking of the exhaled droplet nuclei in a hospital ward with DV and reported that the exhaled flow could penetrate long distances. Gao et al. (2008, 2012) described similar locking observations by means of CFD simulation of human-exhaled droplets. Nielsen et al. (2012) and Olmedo

et al. (2012) revealed correlations among ventilation strategies, exhaled flow trajectories and personal contaminant exposure. In addition to breathing, emanations from sneezing (Seepana and Lai, 2012), jets from diffusers (Jacobsen and Nielsen, 1992; Nielsen, 2000), and heat plumes from different kinds of heat sources (Kofoed and Nielsen, 1990; Liu et al., 2009) are found to be significantly affected by certain temperature gradients. Theoretically, the locking phenomenon in rooms has a parallel in the influence of atmospheric stability on contaminant dispersion outdoors, which can be classified in terms of the temperature lapse rate (Turner, 1970). Gong et al. (2010) pointed out that the concept of air stability was not only applicable in the atmosphere but also in indoor spaces because the accumulation or lockup of contaminants could be reasonably explained under stable conditions. Several attempts have been made in this study to reveal the dependence of the transport and dispersion of exhaled air on air stability.

Another objective of this article is to study the influence on exhalation flow and associated contaminant transport and dispersion between relatively low and high metabolic rates which vary over a wide range, depending on the activity, posture, person, and physical conditions. As increasing information on human respiration and microenvironment around human body has been provided by use of thermal manikins or computer-simulated persons, sufficient consideration of the metabolic rate and activity level for these human-like models is needed.

Accordingly, four cases are studied in a two by two matrix, investigating how airflow and contaminant transport and dispersion from human exhalation are influenced by the combined effects of metabolic level and room temperature structure.

Experimental facilities and method

Test room

All measurements were conducted in a full-scale room with dimensions of 3.0 m (long) \times 2.3 m (wide) \times 2.5 m (high) as illustrated in Figure 1. The walls of the room are well-insulated and can be considered to be adiabatic. The test room is equipped with whole floor and whole ceiling ventilation to achieve uniform and calm environment. Cold and fresh air is continuously supplied from the right side of the room with a temperature of 17°C . The ventilation system can be alternated between MV and DV by opening A1 and A2 or B1 and B2, respectively, see Figure 1a.

It can be expected that vertically distributed temperature is primarily uniform with MV. Stable stratification (Gong et al., 2010), with temperature increasing with height, should be obtained by DV. To create a relatively linear temperature gradient, two radiators (R1

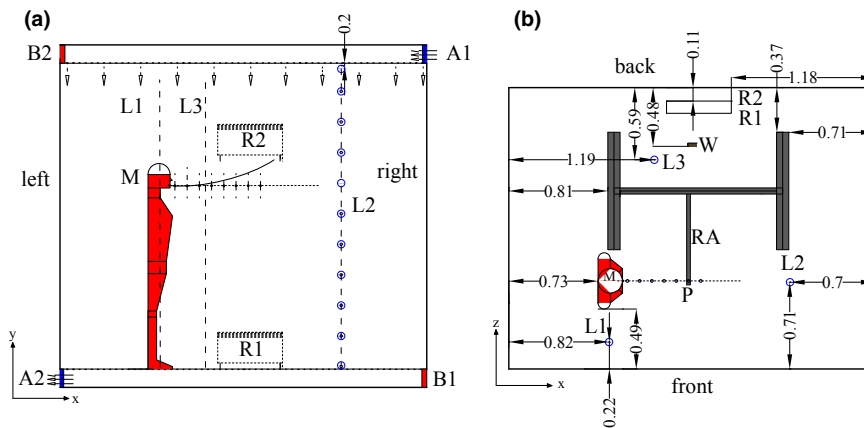


Fig. 1 (a) Front view of the chamber, with two radiators (R1 and R2) positioned at different heights, vertically distributed thermocouples on pole L2 and the combinations of supply and exhaust openings to realize mixing ventilation (A1, A2) and displacement ventilation (B1, B2). (b) Top view showing the locations of manikin (M), robot and robot arm (RA) with probes (P), three poles with thermocouples (L1, L2 and L3), two radiators (R2 and R1), and webcam (W). Dimensions are indicated in units of meters

350 W and R2 40 W) are placed in different vertical heights, as shown in Figure 1. The room attains a uniform dT/dy value. At least 4 h of ventilation was employed to stabilize the room temperature before the measurements. The heating and breathing for the manikin were operated simultaneously for more than 4 h. Thus, all experiments can be considered to be under steady-state conditions.

Measurement facilities

Two kinds of type K thermocouples are used with different functions. The thick ones are equally distributed on three poles (L1, L2 and L3) to record the temperature gradients. L1 and L2 each have eleven thermocouples and L3 has six. Thin thermocouples with much smaller volume and faster response are placed in the mouth and the nostril and on the body surface. All thermocouples were calibrated before the experiments to attain an accuracy of $\pm 0.1^\circ\text{C}$.

The exhalation from the mouth or nose is visualized by means of oil-based smoke to simulate the release of droplet nuclei from a real person. The SAFEX fog generator was applied (Dantec Dynamics A/S type F2010; Tonsbakken, Skovlunde, Denmark), to generate fine oil fog, with a mean droplet size of about $1\ \mu\text{m}$. Smoke visualization was performed upon two breathing modes: (i) inhaling through the mouth and exhaling through the nose; and (ii) inhaling through the nose and exhaling through the mouth. But for the convenience of measurements, only mode (ii) with a relatively horizontal exhalation was applied to attain velocity and concentration distribution in the exhaled air from the mouth.

Nitrous oxide (N_2O) with a density close to CO_2 is commonly used as a tracer gas to simulate exhaled contaminants by means of adding approximately 4% N_2O by volume to the exhaled flow (Bjørn and

Nielsen, 1996; Olmedo et al., 2012; Qian et al., 2006). The volume flow rates of N_2O were set at 0.35 l/min for 1.2 met and 0.60 l/min for 2 met, calculated according to the metabolic rates of the manikin. Multipoint sampler and doser (INNOVA 1303) and photoacoustic field gas monitor (INNOVA 1412) were used to measure the concentrations of N_2O with an accuracy of $\pm 1\%$.

Exhalation velocities were measured with Dantec 54R50 hot sphere anemometer, calibrated horizontally in a wind tunnel and then placed in the transient exhaled flow in the same way. The measured velocity can vary from 0 to 5 m/s. Utilizing a Prema 5017 precision multimeter and a computer, the velocity was recorded at a frequency of 10 Hz.

One robot arm (RA) installed on a robot stand was remotely controlled by a robot controller outside, moving with a maximum horizontal distance of 1060 mm and a vertical distance of 1240 mm, so the whole x and y plane in front of the manikin could be scanned. The precision of each step was $\pm 0.1\ \text{mm}$. The probes (P) for measuring temperature, velocity, and tracer gas can be installed on the RA and move with it to different positions.

Breathing thermal manikin with the metabolic rate of 1.2 met and 2 met

One breathing thermal manikin without clothes (1.68 m height and $1.44\ \text{m}^2$ body surface area) was utilized throughout the experimental studies to simulate an average-sized female. The mouth opening has a semi-ellipsoid shape, and the area is about $120\ \text{mm}^2$. The nose consists of two cylindrical nostrils with a diameter of 12 mm. More details about the thermal manikin can be found in Bjørn (1999). The air is exhaled through the mouth and inhaled through the nostrils during these measurements. And the exhaled

flow from both the nose and the mouth are visualized by the smoke.

According to Fanger’s (1967) heat balance equation for the human body given a certain metabolic rate, four major contributions to heat loss should be considered when calculating a manikin’s heat output with two metabolic levels. First, as the evaporation of sweat cannot be realized by an aluminum-shelled manikin, the contribution of latent heat loss is neglected, despite some deviation from reality. Second, the latent and dry heat release from respiration is converted to control the exhaled temperature at a given value (around 33°C), close to the temperature of real persons’ exhalation from the mouth in the presence of 22°C ambient air (Hoppe, 1981). Two other parts of heat loss are through radiation and convection from the body surface, which affect the strength of the body’s thermal plume directly. Many experimental and numerical investigations have been carried out to calculate the radiation, convection, and even evaporation heat transfer coefficients for human bodies with different postures, such as sitting or standing (Brohus, 1997; de Dear et al., 1997; Gao and Niu, 2005; Homma and Yakiyama, 1988; Murakami et al., 2000; Stampe, 1982; Sørensen and Voigt, 2003). For this study, the metabolic rates of 1.2 met and 2 met are applied and translated to 70 W/m² and 115 W/m², respectively, in accordance with ASHRAE (2009) for an average adult. The radiative and convective heat releases for the standing manikin are based on the literature cited above, see Tables 1 and 2.

It can be seen from Tables 1 and 2 that the heat flux and heat transfer coefficients applied to the manikin in this study agree well with previous results. The parameter $h_c = 2.38 (T_b - T_a)^{0.25}$ is calculated according to the measured body temperature (T_b) and the ambient air temperature (T_a) under MV to validate the settings of heat flux (Fanger, 1970). The calculated h_c in this study is in good agreement with de Dear et al. (1997) and Murakami et al. (2000), as shown in Table 2. However, a human with the metabolic rate of 2 met should be walking at an average speed of 3.2 km/h in line with ASHRAE (2009). Nevertheless,

Table 1 Radiative heat transfer coefficient h_r and heat flux for a standing person in stagnant air

Research	Method	h_r^a [W/(m ² ·K)]	Heat flux (W/m ²)	Percentage of metabolic heat
de Dear et al. (1997)	Experiment	4.5	–	–
ASHRAE (1993)	Standard	4.7	–	–
Murakami et al. (2000) 1.7 met	CFD	–	24.3	38.1
Stampe (1982) 1 met	Experiment	–	22.5	35.3
Stampe (1982) 2 met	Experiment	–	36.9	28.9
This study 1.2 met (70 W/m ²)	–	–	23.8	34.0
This study 2 met (115 W/m ²)	–	–	34.5	30.0

^aEquation for h_r refers to ASHRAE (1993).

Table 2 Convective heat transfer coefficient h_c and heat flux for a standing person in stagnant air

Research	Method	h_c^a [W/(m ² ·K)]	Heat flux (W/m ²)	Percentage of metabolic heat
de Dear et al. (1997)	Experiment	3.4	–	–
Brohus (1997)	Experiment	6.1	–	–
Murakami et al. (2000) 1.7 met	CFD	4.3	24.3	29.0
Stampe (1982) 1 met	Experiment	–	23.8	37.3
Stampe (1982) 2 met	Experiment	–	40.6	31.9
This study 1.2 met (70 W/m ²)	–	3.7	24.5	35.0
This study 2 met (115 W/m ²)	–	4.0	35.7	31.0

^aConvective heat transfer coefficient h_c is calculated by equation given by Fanger (1970).

as the manikin used in this experiment is not movable in the study room, the metabolic rate of 2 met can be expressed as a person standing still but metabolizing more rapidly than normal or the transient state shortly after a person stops walking. The manikin was built with a simplified structure (Bjørn, 1999) and heat output from the body can be recognized as the sum of heat from the internal heating wires (1.2 met corresponds to 30 W and 2 met corresponds to 67 W), heat release from two small fans inside the body shell (30 W) and heat losses from an exhalation pipe when it passes through the manikin’s inner body. Finally, breathing functions corresponding to given metabolic rates for the four cases combined with air stability are summarized in Table 3.

Results and discussion

Temperature gradients in room and concentration distributions

Gong et al. (2010) suggested that the air stability in rooms be roughly classified into three types: stable, neutral, and unstable in terms of the directions of temperature gradients. But because of the effect of buoyancy, the unstable thermal condition with negative temperature gradient is rarely found, in which the air becomes unstable and easily mixed. Only neutral (zero gradient) and stable conditions (positive gradient) are discussed here. Temperature profiles are illustrated in Figure 2.

Figure 2 demonstrates that the experiments attained almost uniform thermal conditions in the room at different positions (L1, L2 and L3), but with temperatures at L1, adjacent to the thermal manikin, a little higher. No significant temperature differences are found between Case 1 in Figure 2a and Case 2 in Figure 2b, indicating essentially identical thermal conditions for the fully mixed air. On the other hand, Case 3 and Case 4 give different dT/dy values of about 1.5°C/m and 1.8°C/m, respectively, as the manikin operated at 2 met releases more heat, which causes the steeper slope shown in Figure 2d.

Figure 3 shows the trajectory of the exhalation from the mouth and nose for all four cases. It can be

Table 3 Breathing functions for the thermal breathing manikin with 1.2 met and 2 met metabolic rates under MV and DV

Case No.	Ventilation	Metabolic rate			Breathing frequency BF (min ⁻¹)	Minute volume RMV (l/min)	Mean body temp. <i>T_b</i> (°C)	Exhaled temp. <i>T_{exh}</i> (°C)	Ambient air temp. ^b <i>T_a</i> (°C)	ACR (h ⁻¹)
		ASHRAE (2009)		Heat output ^a (W)						
		(met)	(W/m ²)							
1	MV	1.2	70	69.6	15.5	8.8	27.6	32.5	22	7.5
2	MV	2	115	101	19	15.2	30.4	33.7	22	
3	DV	1.2	70	69.6	15.5	8.8	26.3	33	21.1	10
4	DV	2	115	101	19	15.2	29.4	33.5	22.2	

ACR, air change rate; DV, displacement ventilation; MV, mixing ventilation.
^aHeat output in this table is the total heat release through radiation and convection.
^bAmbient air temperature is the average temperature at the manikin's mouth height (1.5 m).

expected that the exhaled flow would penetrate a longer distance with a higher metabolic rate because of the higher frequency and volume of breathing. The trajectories of exhaled non-isothermal periodic flow also have a tendency of bending upward. Significant differences between stable and neutral thermal conditions can be observed in Figure 3. The flow from nostrils with an angle of 45° below the horizontal plane moves upward at the end and is diluted quickly in neutral conditions, so the smoke in Figure 3a2,b2 presents a 'right-angle' shape. But for Figure 3c2,d2, the smoke is blocked at the manikin's chest height because the stable air has a tendency to resist vertical movement (Gong et al., 2010; Turner, 1970). Air stability has similar impact on the exhaled flow from the mouth, yielding a stratification height above the head. How-

ever, Figure 3d gives a bit lower stratified layer compared with Figure 3c. It can be explained by the larger temperature gradient for the DV 2 met case. The dependence of stratification height on the magnitude of temperature gradient has been observed by Bjørn and Nielsen (1996, 2002) as well as by Gao et al. (2012) through experiment and simulation, respectively. Actually, the air is more stable with a higher dT/dy and therefore has an increased capacity to resist vertical movement. The vertical temperature gradient also seems to slow the plume rise around the manikin (Liu et al., 2009).

The mean concentration of N₂O surrounding the manikin is examined in detail, as presented in Figure 4. Earlier studies (Hayashi et al., 2002; Murakami, 2004; Zhu et al., 2005) have shown that the

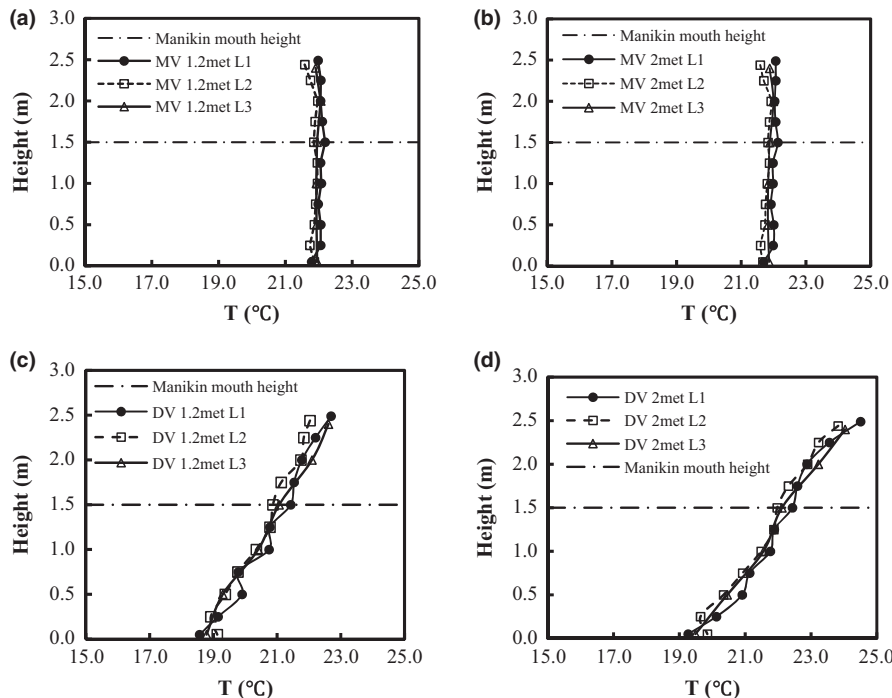


Fig. 2 Vertical temperature gradients in the room of the four cases: (a) mixing ventilation (MV) 1.2 met, (b) MV 2 met, (c) displacement ventilation (DV) 1.2 met, and (d) DV 2 met

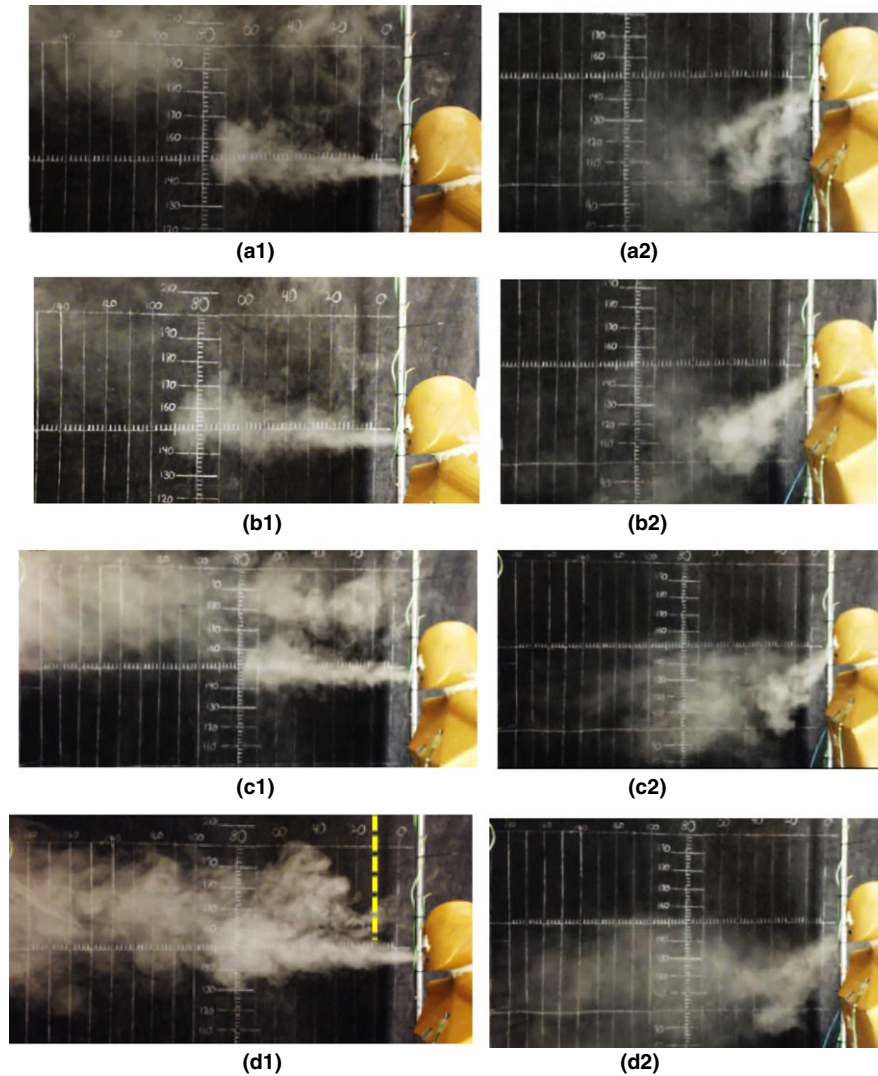


Fig. 3 Smoke visualization of the exhaled flow from the manikin's mouth (a1, b1, c1 and d1) and nose (a2, b2, c2 and d2) with two metabolic rates and two air stability types: (a1) and (a2) mixing ventilation (MV) 1.2 met, (b1) and (b2) MV 2 met, (c1) and (c2) displacement ventilation (DV) 1.2 met, (d1) and (d2) DV 2 met

inhalation region is mainly around human body and the highest percentage is from the front part of the body. Two significant characteristics of the concentration c/c_R in dimensionless form can be observed in Figure 4. One is that the concentration at different height under DV is lower than MV, when comparing results at the same metabolic level. This can be explained by the clean zone created by DV. At chest and thigh height, the DV yields approximately zero c/c_R . As the inhaled air is drawn upward from the lower zone by the rising air stream caused by metabolic heating (Hayashi et al., 2002; Murakami, 2004; Zhu et al., 2005), the person inhales air from the lower part of the body in DV, protecting him or her from rebreathing the exhaled contaminant. Another characteristic is that the inhaled concentration for 2 met is significantly lower than with 1.2 met. It seems reasonable that higher strength of metabolic heating at 2 met results in more entrainment of ambient air and

higher velocity in the boundary layer around the body (Liu et al., 2009). It can also be addressed by comparing Figure 3c1 with d1. On the right side of the dashed line in Figure 3d1, the air is relatively clean under the effect of a stronger body plume and higher velocity in the main flow for 2 met. Different characteristics of the tracer gas distribution around the manikin body for the four cases indicate that air distribution patterns in the room and the metabolic levels influence the microenvironment in the vicinity of the manikin body.

Figure 5 describes a different trend sampled along a line segment 0.35 m in front of the manikin. At chest height and at 2 m, the exposure levels are similar with those around the manikin in Figure 4. However, at the breathing height of 1.5 m, owing to the influence of the stable air conditions, the contaminant exposure for DV 1.2 met with $c/c_R \approx 8$ is considerably higher than for the MV 1.2 met case, for which $c/c_R \approx 4.7$. Olmedo

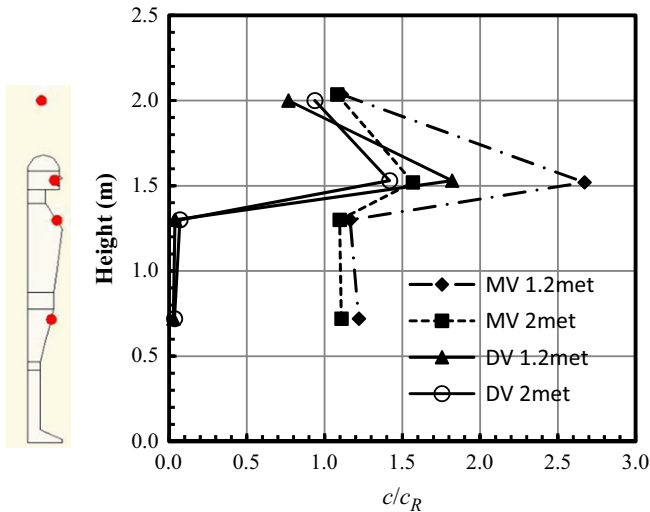


Fig. 4 Concentration measurements around the manikin at different heights: thigh, chest, nose, and above head

et al. (2012) and Qian et al. (2006) have stated that the DV is not suitable for hospital ventilation because a receptor person facing the source may suffer elevated cross-infection risk. For the manikin with a higher metabolic rate (2 met), the concentrations are comparable for DV and MV, despite the different air stabilities. This finding indicates that the effect of air stability is more significant for lower activity level due to lower momentum flow.

Velocity profiles of pulsating flow

A manikin connected to artificial ‘lungs’ can produce a pulsating sinusoidal breathing (Bjørn, 1999), corresponding approximately with human respiration (Gupta et al., 2010). One breathing cycle changing with time for MV 1.2 met case is presented in Figure 6.

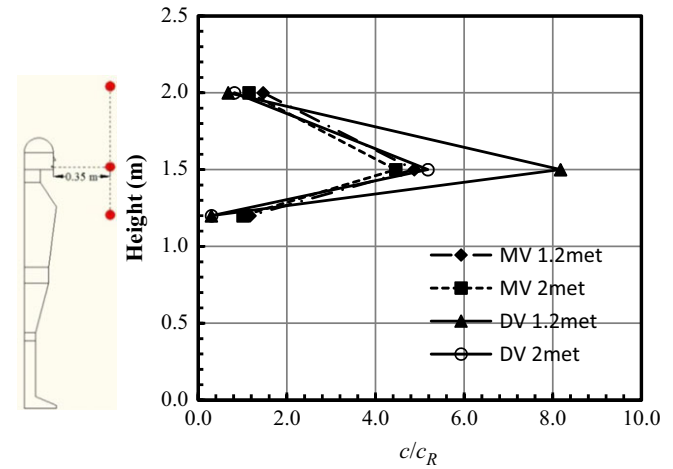


Fig. 5 Concentration measurements at a distance of 0.35 m in front of the manikin’s face at the heights of chest, mouth, and above head

The turbulent pulsating flow develops both in width and length by entraining and mixing the ambient air when the manikin exhales (Figure 6a–d). During inhalation, the exhaled air continues to move up and disperse in vortex rings (Figure 6e,f). In stable air, the dispersion of exhaled air is slowed and blocked in a stratified layer. (Results not shown).

A two-dimensional coordinate system is built from the manikin’s mouth center, as shown in Figure 6f. The hot sphere anemometer moving with the robot arm along the x and y axes measures the pulsating velocity $\dot{u}(x, y)$. Examples of the measured instantaneous velocity at different positions are illustrated in Figure 7. Only the peak values are extracted and averaged for analysis. As Nielsen et al. (2009, 2012) and Olmedo et al. (2012) have reported, the pulsating exhalation flow described by mean peak velocities $u(x, y)$ has similar behavior as a steady-state jet. This

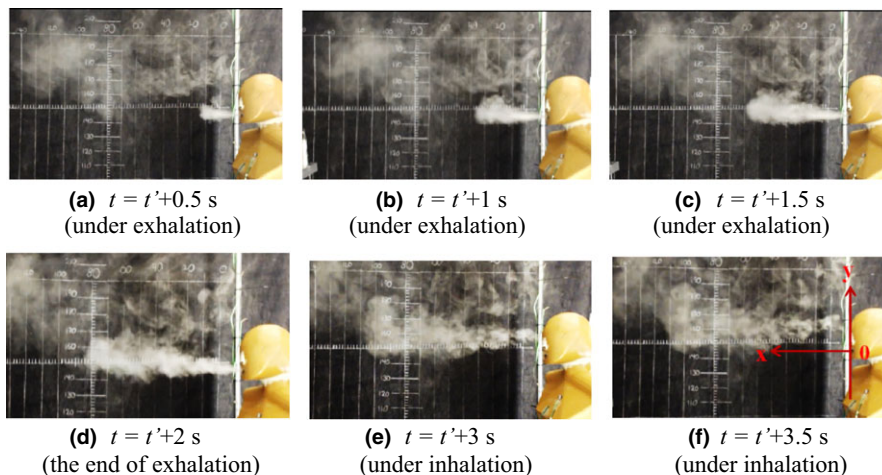


Fig. 6 One respiration cycle (3.9 s) starting from the beginning of exhalation ($t' = 0$) with mouth exhalation and nose inhalation for Case 1 (mixing ventilation 1.2 met)

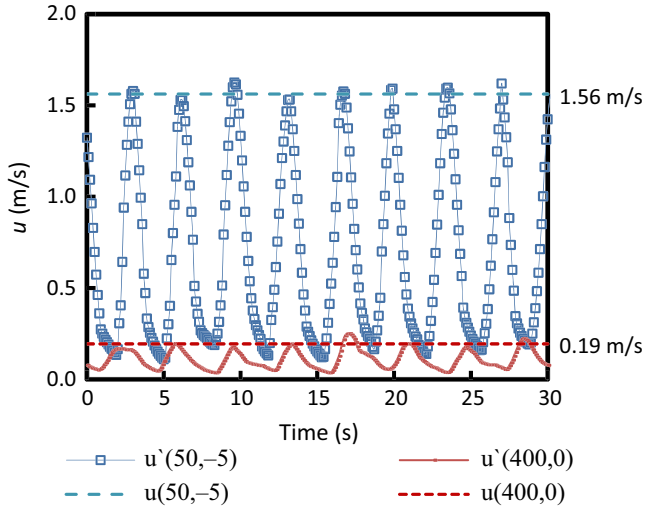


Fig. 7 Pulsating velocity $\dot{u}(x, y)$ measured by the hot sphere anemometer every 100 ms for displacement ventilation 1.2 met case. The coordinate scale is in units of mm

principle is further validated by the velocity profiles depicted in Figure 8. Downstream of the exhalation, the peaks gradually disappear, hidden in turbulence (Nielsen et al., 2009). For 1.2 met and 2 met, the critical distance for flow dissipation is about 400 mm and 500 mm, respectively.

The instantaneous peak velocity profiles at different x distances show similarity with the steady-free jet as shown in Figure 8. An influence of air stability is also observed, with slightly higher velocity in stable air, probably because of the restriction of turbulent entrainment from ambient air under stable conditions (Liu et al., 2009; Nielsen et al., 2009; Olmedo et al., 2012). Furthermore, the centerline with maximum velocity (u_x) can be easily determined through the velocity profiles, which is basically horizontal even though the profiles do not show a symmetrical shape to the centerline but rather exhibit an upward tendency.

Outlet velocity close to the mouth

The outlet velocity from the manikin's mouth can be obtained by means of measurement at the nearest distance to the mouth (here 10 mm is applied) or calculated from the integral expression assuming that respiration is sinusoidal with respect to time. (See Figure 7). Both of these methods are employed and compared with obtain the outlet velocity. However, it was observed during measurements that the outlet velocity varies with different thermal conditions, such as isothermal or non-isothermal exhalation and manikin body, air stability, etc. Only the velocity measured under isothermal condition is applied as the scale velocity, u_0 . This means that the person has the same breathing frequency (BF) and minute volume (RMV)

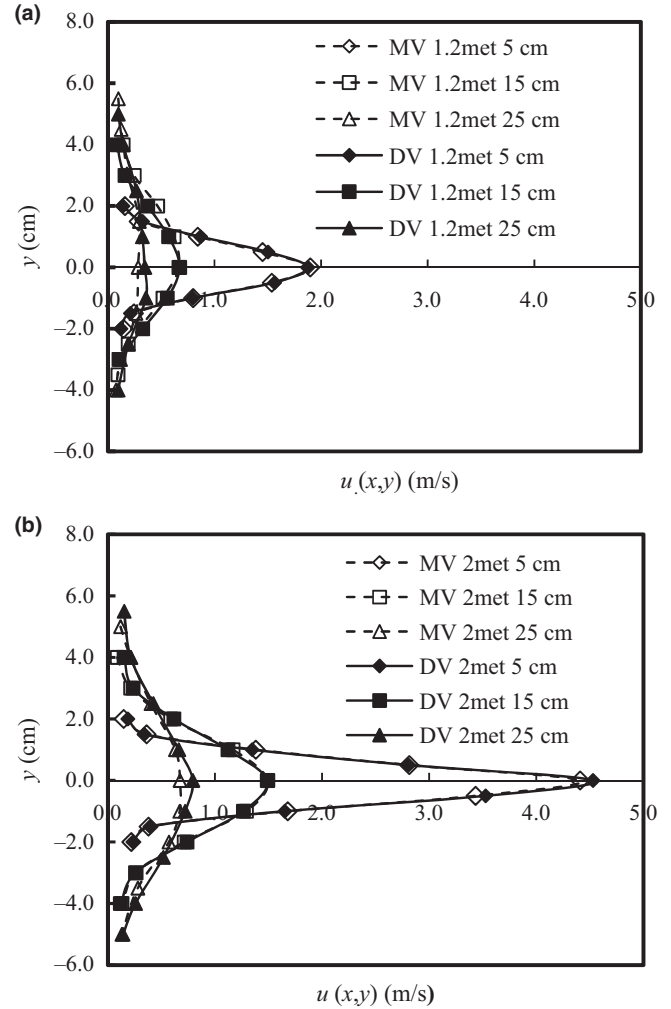


Fig. 8 Velocity profiles of exhalation from the mouth for (a) 1.2 met and (b) 2 met

as a real case for 1.2 or 2 met, but has no body or breathing heating. The equation to calculate u_0 is based on the isothermal condition. It is noticeable that u_0 is the mean peak velocity. Another assumption is made that the velocity is uniformly distributed across the mouth area. The measuring point (10 mm) is assumed to lie within the constant velocity core, similar to the steady-free jet. The u_0 value is calculated according to these equations:

$$\dot{q} = A \sin(\omega t) \quad (1)$$

where

$$\omega = \frac{\pi \cdot \text{BF}}{30} \quad (2)$$

Here, \dot{q} is the instantaneous flow rate (l/s) and A is the maximum flow rate (l/s), which equals u_0 (m/s) multiplied by the area of mouth a_0 (m²). The frequency ω can be obtained from the breathing frequency BF (min⁻¹). Tidal volume TV = RMV/BF (l) is obtained by integrating the flow rate over time, as expressed by

Equation 3.

$$TV = \frac{RMV}{BF} = \int_0^{\frac{30}{BF}} \dot{q} dt = \int_0^{\frac{30}{BF}} A \sin(\omega t) dt = A \cdot \frac{60}{\pi \cdot BF} \quad (3)$$

$$u_0 = \frac{A}{a_0 \cdot 10^3} \quad (4)$$

Substituting the parameter values from Table 3 into Equations 1–4 gives u_0 of 3.90 m/s and 6.57 m/s for 1.2 met case and 2 met case without heating, respectively. The measured u_0 is 3.94 m/s for 1.2 met case under non-heated isothermal condition. As the calculated value agrees well with the measurement, the calculated u_0 for the 2 met case under non-heated isothermal condition is assumed to apply, as this value of 6.57 m/s exceeds the anemometer’s measuring range.

The manikin’s exhalation velocity at the centerline for MV 1.2 met is compared among three thermal conditions: (i) isothermal manikin and isothermal breathing (non-heated manikin); (ii) body-heated manikin; and (iii) manikin operated at 1.2 met (full heated manikin). Results are shown in Figure 9. The outlet velocity decreases by adding heat load to the body and then to breathing step by step. The measured exhaled velocity for the manikin operated at 2 met is 4.94 m/s, significantly lower than 6.57 m/s at isothermal condition. The results indicate that both the exhalation temperature and the body plume affect the initial velocity from the mouth.

Hayashi et al. (2002) has pointed out that the inhalation region is greatly affected by the rising air stream generated by metabolic heating. This effect can be seen in Figure 10a. However, it can also be observed

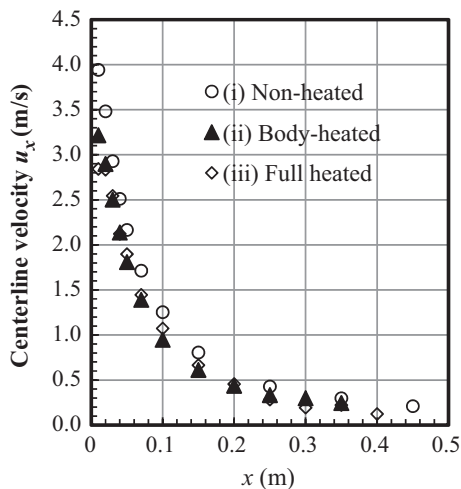


Fig. 9 Velocity at the centerline for (i) non-heated manikin; (ii) body-heated manikin; and (iii) full heated manikin (Case 1). The measurements are conducted under mixing ventilation. The BF and RMV correspond to Case 1

that the stream rising from the lower part heated by human body not only influences inhalation but also enters the exhalation flow moving up along the manikin’s jaw, as illustrated in Figure 10b. During inhalation, the manikin inspires by nose from the thermal boundary layer. During exhalation, the flow should first break through the thermal plume layer. The momentum is partly consumed when the exhaled flow tries to penetrate the rising stream. It explains why the initial velocity is lowered with higher body temperature. Gao et al. (2012) and Liu et al. (2009) also showed that the temperature gradient may influence the strength of the body plume and further inhibit the exhaled air as it penetrates the plume. The reason why the exhalation temperature also influences the initial velocity is probably because entrainment is not perpendicular to the momentum flow due to buoyancy and may resist it somehow. See Figure 6 and velocity vectors of real respiration reported by Murakami (2004). Overall, the detailed flow patterns are complicated and should be further validated.

Exhaled velocity and concentration decay

Nielsen et al. (2009, 2012) and Olmedo et al. (2012) have found that the dimensionless velocity or concentration in the centerline is inversely proportional to the dimensionless distance using peak values for people’s exhalation, like the steady-free jet. Thus similar expressions of velocity and concentration decay are given in the following equations:

$$\frac{u_x}{u_0} = K_v \left(\frac{x}{\sqrt{a_0}} \right)^{n_1} \quad (5)$$

$$\frac{c_x - c_R}{c_0 - c_R} = K_c \left(\frac{x}{\sqrt{a_0}} \right)^{n_2} \quad (6)$$

Here, K_v and K_c are the characteristic constants for velocity and concentration, respectively, and a_0 is the mouth area. The dimensionless velocity u_x/u_0 is the

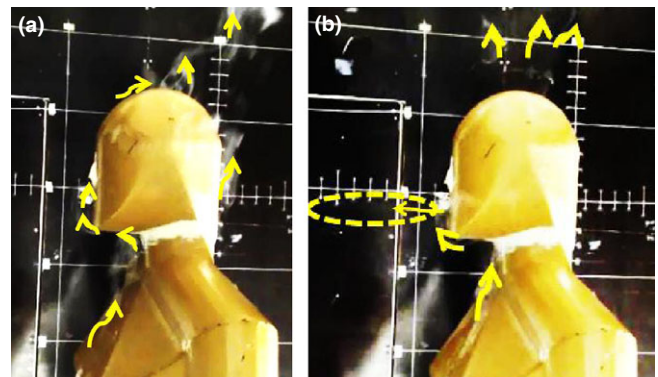


Fig. 10 Body plume visualized by chemical smoke during (a) inhalation and (b) exhalation for Case 1

Table 4 Characteristic constants for velocity and concentration decay

Cases	Velocity decay fitting						Concentration decay fitting					
	$x/a_0^{0.5} < 2$		$2 < x/a_0^{0.5} < 5$			$x/a_0^{0.5} > 5$			$x/a_0^{0.5} > 10$			
	K_{v1}	n_1	K_{v2}	n_1	R^2	K_v	n_1	R^2	K_c	n_2	R^2	
MV 1.2 met	0.74	-0.004	1.17	-0.58	0.996	5.5	-1.38	0.969	11.9	-1.18	0.963	
MV 2 met	0.78	-0.02	0.84	-0.12	0.974	5.46	-1.25	0.994	10.4	-1.15	0.928	
DV 1.2 met	0.71	0.006	1.24	-0.62	0.999	4.41	-1.27	0.992	2.74	-0.6	0.996	
DV 2 met	0.79	-0.02	0.86	-0.13	0.998	5.03	-1.22	0.994	5.14	-0.78	0.989	
Isothermal ^a	0.98	-0.18	1.35	-0.59	0.996	3.77	-1.14	0.997	-	-	-	

DV, displacement ventilation; MV, mixing ventilation

^aIsothermal condition here is for MV 1.2 met case with identical body and exhalation temperature with the surrounding air.

ratio of u_x , the peak velocity along the centerline at horizontal distance x , to u_0 , the scale velocity obtained under isothermal condition. The parameters c_x , c_R , and c_0 are peak concentration values measured at x , in the exhaust of the room and at the mouth, respectively. Because of the restriction of sampling and analysis time, the peak concentration c_x uses the average of peak values measured for a relatively long time (more than half an hour) in comparison with u_x for a few seconds at one measuring point. The constants and exponents obtained through measurements are listed in Table 4 for all four cases.

The depiction of velocity and concentration decay in log-log form is helpful to evaluate the results. Figure 11 shows the variations of slopes with distance. The velocity from the semi-ellipsoid mouth for all four cases has a slope of slightly below zero for $x/a_0^{0.5} < 2$, which can be recognized as the ‘constant velocity core’ similar to a free jet. However, the slope changes to about -0.6 for the manikin at 1.2 met and to about -0.12 for the manikin at 2 met when $2 < x/a_0^{0.5} < 5$. It can be concluded that the ‘constant velocity core’ has been destroyed to different extents with the impact being more severe at 1.2 met. Moreover, for longer distance with $x/a_0^{0.5} > 5$, the slopes change rapidly to

about -1.25 including the isothermal condition, which is unique with the former two parts and slightly corresponds to the jet from circular openings with a slope of -1.0 (Nielsen et al., 2009).

Figure 12 shows different trends than Figure 11. The influence of air stability on velocity is not as significant as on concentration. Figures 8 and 11 have shown the velocity under DV is a little higher in comparison with MV. Figure 12 shows that the measured concentration under stable conditions is obviously elevated above the values obtained in neutral air conditions. From Table 4, the same conclusions can be inferred by comparing n_1 and n_2 under different air stability conditions ($x/a_0^{0.5} > 5$), where the characteristic exponents for DV are always larger than for MV, indicating slower decay in the thermally stratified case.

To summarize, as the concentration and velocity are not measured by the same instruments, errors resulting from measurements may influence the obtained results. But the similarity of concentration at the same air stability condition in Figure 12 can be explained by previous observations of stratified contaminant layer in Figure 3, which may result in the sampled contaminants not only being obtained from the exhaled flow but also partly from the blocking layer.

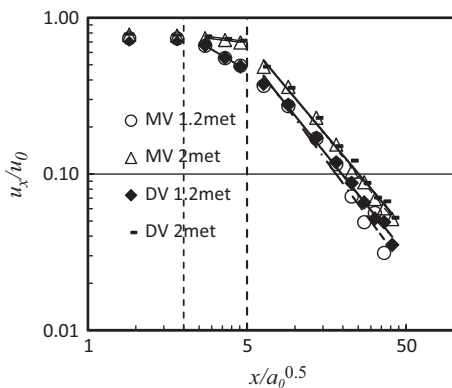


Fig. 11 Log-log graph of dimensionless velocity vs. distance in the centerline for the four cases (solid trend lines are for displacement ventilation)

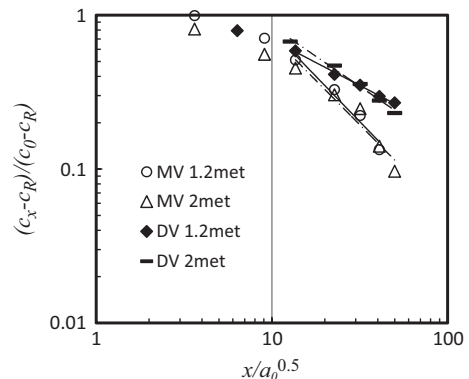


Fig. 12 Log-log graph for dimensionless concentration vs. distance in the centerline for the four cases

Conclusions

Two air stability conditions combined with two metabolic rates of a standing manikin have been investigated. Standard metabolic rates of 1.2 met and 2 met are applied for the manikin with different breathing functions. The exhaled flow from the mouth can penetrate longer distance at higher metabolic level with larger initial momentum. The results show air stability not only influences people's breathing at lower activity but also at relatively higher levels.

The exhaled contaminant becomes stratified at different heights in stable air because of different exhalation angles and temperature gradients. For mouth exhalation, it is locked above the manikin's head while for nose exhalation it is at chest height. The stratification height decreases with increasing dT/dy . Displacement ventilation yields a clean lower zone in the room but also brings stable thermal stratifications at certain heights, which may resist the vertical movement of contaminant. As some researchers have suggested, DV may not be suitable for occasions with contaminant sources, such as hospitals or clinics, because the contaminant or droplet nuclei will not be readily diluted under stable air conditions, which may cause an elevated cross-infection risk for a receptor person facing the source.

When measuring the pulsating exhalation flow, the velocity profiles and decay show similar shapes to those of a steady jet normalized by its peak velocity. The outlet velocity under isothermal condition is measured and calculated for further analysis. The body plume and breathing temperature affect the outlet velocity close to the mouth and reduce it when the exhaled flow

penetrates the thermal boundary layer. Different characteristics of the tracer gas distribution around the manikin body for the four cases also indicate that the near-human microenvironment is closely related to air distribution patterns in the room and the metabolic levels of the body.

The air stability affects the decay of concentration and velocity in different ways. The velocity at a lower activity level is more significantly affected, whereas the concentration is considerably higher in stable air in comparison with in neutral air for both lower and higher metabolic levels.

In conclusion, this study has investigated the 'lock-up phenomenon' from the perspective of air stability in room, namely temperature gradients. Human exhalation presents different characteristics influenced by this phenomenon with different metabolic rates. Sufficient consideration of air stability pattern in rooms as well as metabolic level of the human body is needed when studying human respiration and the near-human microenvironment.

Acknowledgements

This project is financially supported by China Scholarship Council (CSC), Hunan Provincial Innovation Foundation for Postgraduate (CX2012B131), International S&T Cooperation Program of China (ISTCP) (2010DFB63830), Important Science Program of Hunan Province of China (2010FJ1013), and National Natural Science Foundation of China (51378186).

References

- Adams, W.C. (1993) *Measurement of Breathing Rate and Volume in Routinely Performed Daily Activities*, Sacramento, CA, California Environmental Protection Agency.
- ASHRAE (1993) *Physiological Principles and Thermal Comfort* (ASHRAE Handbook of Fundamentals 8.1–8.29), Atlanta, GA, American Society of Heating, Refrigerating and Air Conditioning Engineers.
- ASHRAE (2009) *Indoor Environmental Quality* (ASHRAE Handbook of Fundamentals 9.1–9.30), Atlanta, GA, American Society of Heating, Refrigerating and Air Conditioning Engineers.
- Björn, E. (1999) Simulation of human respiration with breathing thermal manikin. In: *Proceedings of Third International Meeting on Thermal Manikin Testing*, Stockholm, Sweden, National Institute for Working Life, 78–81.
- Björn, E. and Nielsen, P.V. (1996) Passive smoking in a displacement ventilated room. In: *Proceedings of Indoor Air '96, 7th International Conference on Air Quality and Climate*, Nagoya, Japan, Vol. 1, 887–892.
- Björn, E. and Nielsen, P.V. (2002) Dispersal of exhaled air and personal exposure in displacement ventilated room, *Indoor Air*, **12**, 147–164.
- Brohus, H. (1997) *Personal exposure to contaminant sources in ventilated rooms*, PhD thesis, Aalborg, Denmark, Aalborg University.
- Brohus, H. and Nielsen, P.V. (1996) Personal exposure in displacement ventilated rooms, *Indoor Air*, **6**, 157–167.
- Chen, C. and Zhao, B. (2010) Some questions on dispersion of human exhaled droplets in ventilation room: answers from numerical investigation, *Indoor Air*, **20**, 95–111.
- Chung, K.C. and Hsu, S.P. (2001) Effect of ventilation pattern on room air and contaminant distribution, *Build. Environ.*, **36**, 989–998.
- de Dear, R.J., Arens, E., Hui, Z. and Oguro, M. (1997) Convective and radiative heat transfer coefficient for individual human body segments, *Int. J. Biometeorol.*, **40**, 141–156.
- Fanger, P.O. (1967) Calculation of thermal comfort: introduction of a basic comfort equation, *ASHRAE Trans.*, **73**, III.4.1.
- Fanger, P.O. (1970) *Thermal Comfort-Analysis and Applications in Environmental Engineering*, Copenhagen, Danish Technical Press.
- Gao, N. and Niu, J. (2004) CFD study on micro-environment around human body and personalized ventilation, *Build. Environ.*, **39**, 795–805.
- Gao, N. and Niu, J. (2005) CFD study of the thermal environment around a human body: a review, *Indoor Built Environ.*, **14**, 5–16.
- Gao, N., Niu, J. and Morawska, L. (2008) Distribution of respiratory droplets in enclosed environments under different

- distribution methods, *Build. Simul.*, **1**, 326–335.
- Gao, N., He, Q. and Niu, J. (2012) Numerical study of the lock-up phenomenon of human exhaled droplets under a displacement ventilated room, *Build. Simul.*, **5**, 51–60.
- Gong, G., Han, B., Luo, H., Xu, C. and Li, K. (2010) Research on the air stability of limited space, *Int. J. Green Energy*, **7**, 43–64.
- Gupta, J.K., Lin, C. and Chen, Q. (2010) Characterizing exhaled airflow from breathing and talking, *Indoor Air*, **20**, 31–39.
- Hayashi, T., Ishizu, Y., Kato, S. and Murakami, S. (2002) CFD analysis on characteristics of contaminated indoor air ventilation and its application in the evaluation of the effects of contaminant inhalation by a human occupant, *Build. Environ.*, **37**, 219–230.
- He, Q., Niu, J., Gao, N., Zhu, T. and Wu, J. (2011) CFD study of exhaled droplet transmission between occupants under different ventilation strategies in a typical office room, *Build. Environ.*, **46**, 397–408.
- Holmer, I. (1984) Required clothing insulation (IREQ) as an analytical index of cold stress, *ASHRAE Trans.*, **90**, 1116–1128.
- Homma, H. and Yakiyama, M. (1988) Examination of free convection around occupant's body caused by its metabolic heat, *ASHRAE Trans.*, **94**, 104–124.
- Hoppe, P. (1981) Temperatures of expired air under varying climatic conditions, *Int. J. Biometeorol.*, **25**, 127–132.
- Jacobsen, T.V. and Nielsen, P.V. (1992) Velocity and temperature distribution in flow from an inlet device in rooms with displacement ventilation. In: *ROOM-VENT '92, Third International Conference on Air Distribution in Rooms*, Aalborg, Denmark.
- Kofoed, P. and Nielsen, P.V. (1990) Thermal Plumes in Ventilated Rooms: measurements in stratified surroundings and analysis by use of an extrapolation method. In: *ROOMVENT '90, International Conference on Engineering Aero- and Thermodynamics of Ventilated Rooms*, Oslo.
- Liu, L. and Li, Y. (2012) Simulation of interpersonal transport of expiratory droplets and droplet nuclei between two standing manikins. In: *Proceedings of the 10th International conference, Healthy Buildings*, Vol. 3, Brisbane, Qld, Australia, 2465–2470.
- Liu, L., Nielsen, P.V., Li, Y., Jensen, R.L., Litewnicki, M. and Zajas, J. (2009) The Thermal plume above a human body exposed to different air distribution strategies. In: *Proceedings of 9th Int. Conf. Healthy Buildings*, Syracuse, NY, USA, Paper ID: 605.
- McCutchan, J.W. and Taylor, C.L. (1951) Respiratory heat exchange with varying temperature and humidity of inspired air, *J. Appl. Physiol.*, **4**, 121–135.
- Murakami, S. (2004) Analysis and design of micro-climate around the human body with respiration by CFD, *Indoor Air*, **14**, 144–156.
- Murakami, S., Kato, S. and Zeng, J. (2000) Combined simulation of airflow, radiation and moisture transport for heat release from a human body, *Build. Environ.*, **35**, 489–500.
- Nielsen, P.V. (2000) Velocity distribution in a room ventilated by displacement ventilation and wall-mounted air terminal devices, *Energ. Buildings*, **31**, 179–187.
- Nielsen, P.V., Buus, M., Winther, F.V. and Thilageswaran, M. (2008) Contaminant flow in the microenvironment between people under different ventilation conditions, *ASHRAE Trans.*, **114**, 632–638.
- Nielsen, P.V., Jensen, R.L., Litewnicki, M. and Zajas, J. (2009) Experiments on the microenvironment and breathing of a person in isothermal and stratified surroundings. In: *Proceedings of 9th Int. Conf. Healthy Buildings*, Syracuse, NY, USA, Paper ID: 374.
- Nielsen, P.V., Olmedo, I., Ruiz de Adana, M., Grzelecki, P. and Jensen, R.L. (2012) Airborne cross-infection risk between two people standing in surroundings with vertical temperature gradient, *HVAC&R Res.*, **18**, 552–561.
- Olmedo, I., Nielsen, P.V., Ruiz de Adana, M., Jensen, R.L. and Grzelecki, P. (2012) Distribution of exhaled contaminants and personal exposure in a room using three different air distribution strategies, *Indoor Air*, **22**, 64–76.
- Qian, H., Li, Y., Nielsen, P.V., Hyldgård, C.E., Wong, T.W. and Chwang, A.T.Y. (2006) Dispersion of exhaled droplet nuclei in a two-bed hospital ward with three different ventilation systems, *Indoor Air*, **16**, 111–128.
- Qian, H., Li, Y., Nielsen, P.V. and Hyldgård, C.E. (2008) Dispersion of exhalation pollutants in a two-bed hospital ward with a downward ventilation system, *Build. Environ.*, **43**, 344–354.
- Seepana, S. and Lai, A.C.K. (2012) Experimental and numerical investigation of interpersonal exposure of sneezing in a full-scale chamber, *Aerosol Sci. Technol.*, **46**, 485–493.
- Sørensen, D.N. and Voigt, L.K. (2003) Modeling flow and heat transfer around a seated human body by computational dynamics, *Build. Environ.*, **38**, 753–762.
- Stampe, O.B. (1982) *Glent Ventilation*, 2nd edn, Hvidovre, Glent & Co (in Danish).
- Turner, D.B. (1970) *Workbook of atmospheric dispersion estimates*. Office of Air Program Pub. No. AP-26, Environmental Protection Agency, USA.
- Villafruela, J.M., Olmedo, I., Adana, M.R., Méndez, C. and Nielsen, P.V. (2013) CFD analysis of the human exhalation flow using different boundary conditions and ventilation strategies, *Build. Environ.*, **62**, 191–200.
- Zhu, S., Kato, S., Murakami, S. and Hayashi, T. (2005) Study on inhalation region by means of CFD analysis and experiment, *Build. Environ.*, **40**, 1329–1336.

APPENDIX B.

EFFECT OF AIR STABILITY ON THE DISPERSAL OF EXHALED CONTAMINANT IN ROOMS

The paper presented in Appendix B is published in Proceedings of SET 2013 : 12th International Conference on Sustainable Energy Technologies, The Hong Kong Polytechnic University, 2013.8.27-2013.8.29.



Effect of Air Stability on the Dispersal of Exhaled Contaminant in Rooms

Chunwen Xu^{1,*}, Guangcai Gong¹, Peter V. Nielsen², Li Liu², Rasmus L. Jensen² and Hangxin Li¹

¹College of Civil Engineering, Hunan University, Changsha 410082, China

²Department of Civil Engineering, Aalborg University, Aalborg 9000, Denmark

*Corresponding email: xcw@hnu.edu.cn

ABSTRACT

Experiments are conducted in a full-scale chamber equipped with whole floor and whole ceiling supply or exhaust to form approximately zero and larger temperature gradients corresponding to unstable and stable air conditions. It can be observed that the air with smoke exhaled from a life-sized thermal manikin is locked and stratified at certain heights at stable condition while it mixes well with the ambient air and is diluted quickly through upper openings when the air is relatively unstable. The concentration of contaminant simulated by tracer gas (N₂O) is measured both around and 0.35m from the manikin, indicating that the person who exhales the contaminant may not be polluted by himself because of the protective effect of the thermal boundary layer around the body, especially in stable condition with two concentration zones and clean air drawn from the inlets. However, other persons facing the respiration some distance away may suffer higher contaminant exposure if the air in room is quite stable and contaminant from the mouth can penetrate a longer horizontal distance. In addition, the air stability slightly changes the velocity profiles, giving higher velocity decay and more turbulent mixing with surrounding air at unstable air condition.

KEYWORDS: *air stability, contaminant, exhalation, full-scale experiment*

1 INTRODUCTION

Air stability which exists in indoor environment similarly with the atmosphere impacts the vertical and horizontal diffusion of exhaled contaminant in rooms. Atmospheric stability is commonly evoked in many dispersion studies as the single parameter used to define the turbulent state of the atmosphere or to describe the dispersion capabilities of the atmosphere [1]. Pasquill and Gifford mainly classified the atmospheric stability into six types designated as A (highly unstable or convective), B (moderately unstable), C (slightly unstable), D (neutral), E (moderately stable), and F (extremely stable). Later Turner further improved the six indices leading to general use of stability indices 1-6 corresponding to A-F and these are widely used in plume models [2]. The concept of indoor air stability based on the theory of atmospheric stability is proposed and is briefly classified into three indices

according to the temperature lapse rate in rooms, that is stable, neutral and unstable [3].

With the increasing implementation of displacement ventilation as comfort ventilation in indoor environment, more and more phenomena of air stability are observed because of the significant temperature gradients compared with almost zero temperature gradients under mixing ventilation. Bjorn and Nielsen [6] discovered that air exhaled through the mouth can lock in a thermally stratified layer, if the vertical temperature gradient in breathing zone height is sufficiently large. Nielsen and Liu et al. [4,5] also found that the exhalation from a manikin was almost “locked” through smoke visualization and the velocity decay was slower at thermal stratified surroundings. By comparing different ventilation strategies such as no ventilation, mixing ventilation, downward ventilation and displacement ventilation, Qian et al. [7] and Olmedo et al. [8] both indicated the exhaled jet penetrated a short distance and is diluted quickly by ventilated air under mixing and downward ventilation but can penetrate a long distance for displacement ventilation. Olmedo et al. [8] and Nielsen et al. [9] also pointed out that the upward trend of the warmer exhaled flow from people was significant for mixing and no ventilation while it was inhibited somehow for displacement ventilation and the flow turned out to be more horizontal. However, these studies mainly focus on comparing the characteristics of different ventilation strategies, neglecting the nature of these phenomena was caused by air stability. In fact for stable condition leading to difficult upward or downward motion of the air parcel or contaminant, the temperature lapse rate of indoor air γ ($\gamma = -\partial T / \partial z$) is negative, which corresponds to the temperature gradient in displacement ventilation. As the highly unstable type with positive γ is rarely found in indoor environment due to the effect of buoyancy mixing the air well from warmer lower zone to colder upper zone, the condition with approximate zero γ which is classified as neutral in atmosphere field can be recognized as unstable in room.

Since the stable condition which may cause contaminant “blocking” at certain height, high concentration exposure to individuals and more risk of cross infection[7,8], it should be paid more attention to, particularly on occasions with contaminant source or diseases like in hospitals. On the other hand this blocking phenomenon can be utilized to find the best positions of exhausts. The objective of this study is to further validate the effect of air stability on the dispersal of exhaled contaminant in rooms as human beings can act as contaminant sources in indoor environment by exhaling carbon dioxide, and sometimes even infectious bacteria or viruses and to give a thorough examine of the different characteristics of the effect of stable and unstable room air on contaminant dispersion.

2 METHODS

2.1 Test room

Experiments are conducted in a full-scale room (3m×2.3m×2.5m) with whole floor and whole ceiling ventilation. Different temperature lapse rates namely different ventilation strategies can be obtained by supplying cold air through floor or ceiling from the right side and exhausting the air through ceiling or floor from the left side.

Fig.1 illustrates the displacement ventilation (DV) with cold air supplied from the bottom of the room and being heated by the heat sources (the manikin and radiator). Both the ceiling and floor are double-skinned with cavities of 15cm high. The walls of the test room are well insulated. Likewise, if the cold air from the left side enters the ceiling cavity firstly and leaves the room through the floor cavities, opposite to which Fig.1 shows, the mixing ventilation (MV) condition can be realized. Small holes with a diameter of 1cm and 5cm's distance between each other distribute equally both on the inner floor and the inner ceiling, ensuring the flow in the room is uniform. The air change rate is applied with 8h^{-1} and 10h^{-1} for mixing ventilation and displacement ventilation respectively. The velocity caused by ventilation is measured by distributing the anemometer in different positions in the room before the start of exhalation velocity measurements. It is found that the speed is always lower than 0.03m/s and that can be ignored considering the influence of it on the exhalation.

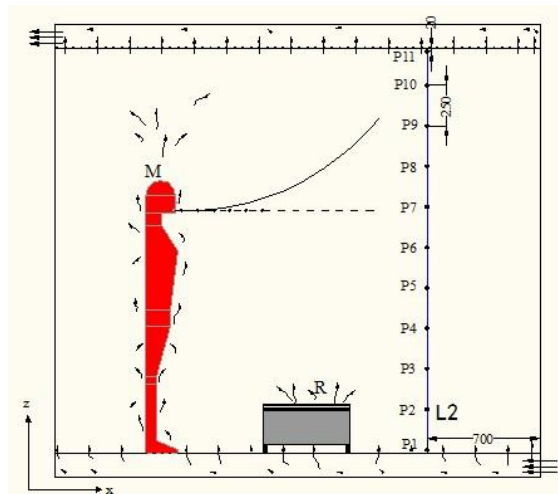


Fig.1 Sketch of the displacement ventilation with thermal manikin(M), radiator(R) and vertically distributed thermocouples(L2)

2.2 Instruments and measuring method

The air temperature is measured by type K thermocouples at different positions with three poles L1, L2 and L3 respectively on the right side of the manikin, in front of the manikin and in the center of the room. For both L1 and L2, eleven thermocouples are distributed equally in the vertical line with an average distance of 250mm between two thermocouples and only 5 thermocouples for L3. Four thermocouples are separately pasted on the manikin's head, chest, stomach and leg with silicon paste to measure the temperature of the body. Velocity of the exhalation is tested by Dantec 54R50 hot sphere anemometer. N_2O is used as the tracer gas and is measured by INNOVA 1303 Multipoint Sampler and Doser and INNOVA 1412 photoacoustic field gas-monitor. Six plastic tubes are connected to the sampler channels with three pasted on the manikin's chest, hips and one in nostril. The concentration of the exhaust air is measured by one of the six tubes and the other

one is put in the lab to ensure the safety level of the working person. One of the tube is bounded with the hot sphere anemometer and is put on a movable robot arm in front of the manikin to measure the cocentration and velocity at different positions. The robot arm controlled by the robot controller from the outside of the room can move both at X and Y direction with a precision of 0.1mm. After more than 3 hours' ventilaiton and thermal manikin's breathing the steady state is achieved.

2.3 Thermal manikin

One breathing thermal manikin is used to simulate the breathing and body plume of an average-sized woman. Detailed size and body shape can be found in literature [10]. The manikin inhales through nose and exhales through a semi-ellipsoid mouth and the breathing is a sinusoidal flow produced by a mechanical lung where the breathing frequency and volume flow can be set. The velocity from the mouth is measured and recorded and only the peaks velocities are used for analysis. The peak velocity u_0 at 0.02m away from the mouth is tested under isothermal condition and it is 4.53m/s. Table 1 shows the basic setup of the manikin. Four transformers are used in the experiments to change and get the accurate power supply for two radiators, mankin's body heating wires and the heating pipe for exhalation. In order to get linear temperature gradients for displacement ventilation, two radiator at different vertical height are applied with 350w heat realse from the taller one and only 30W for the lower one. The larger heat load in displacement ventilaiton leads to higher temperature in the room and higher temperature of the exhaled air because the exhaled air temperature is affected by the ambiant air as illustrated by P.Hoppe[11].

Table 1. Manikin's breathing function and heat sources in the room

Ventilation	A/C Ratio [h ⁻¹]	Radiator or heat output [W]	Exhalation temperature [°C]	Manikin heat output [W]	Body temperature [°C]	Breathing frequency [min ⁻¹]	Minute volume [l/min]	Volume flow rate of N ₂ O [l/min]
DV	8	380	34.4	96	29.4	16	17.6	0.35
MV	10	0	32	99	28.7			

3 RESULTS AND DISCUSSION

3.1 Temperature lapse rates and smoke visulazition

Temperatures in different positions at the same vertical height is uniform with nearly the same trends for L1, L2 and L3, as shown in Fig.2. It can also be seen from Fig.2 that environmental temperature lapse rate γ is about zero with mixing ventilation and is around -1.5°C/m with displacement ventilation which is a quite stable condition . But for DV L2 the temperature from 1.5m to 2m is higher than the surrounding air maybe because L2 is placed facing the manikin and the exhaled flow can penetrate longer distance at stable condition and reach L2.

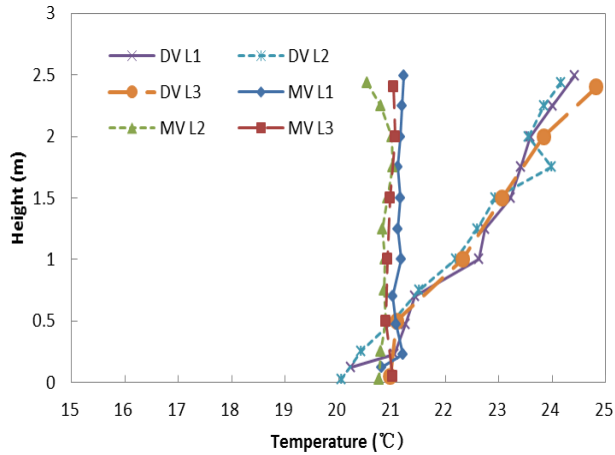


Fig.2 Vertical temperature gradients under mixing ventilation (MV) and displacement ventilation (DV) at different positions in the room

Smoke generated by SRFEX F2010 fog generator is added to the manikin's exhalation and then the preheated smoke with air is exhaled through the mouth at a certain speed. For the stable condition, shown in Fig.3(a), the smoke can penetrate a longer distance and the vertical motion of the smoke is inhibited, causing a more horizontal flow. While the unstable environment makes the smoke mix well with the surrounding air and bend significantly upwards due to higher exhalation temperature compared with the surrounding air, shown in Fig.3(b). Another significant difference between the two conditions is that for stable room air there is stratified smoke layer above the manikin's head where the smoke accumulates and is affected by the temperature gradient, making it difficult to move both up and down. These phenomena are also observed by Liu et al. [4,5], Bjorn and Nielsen [6], Qian et al. [7], Olmedo et al. [8]. In addition, a two-zone model can be predicted for stable condition [6].

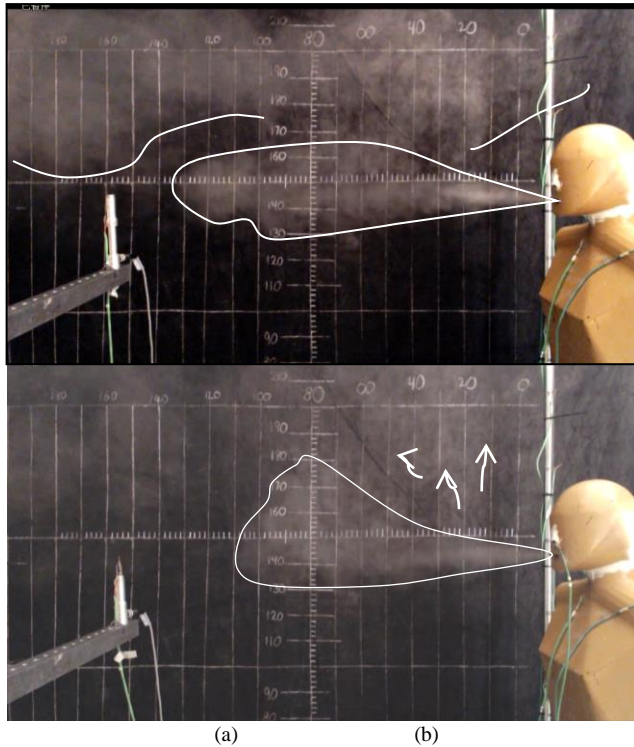


Fig.3 Exhaled flow at stable condition (a) and unstable condition (b)

3.2 Velocity and concentration decay

The velocity and concentration decay are calculated by the following equations:

$$\frac{u_x}{u_0} = K_{\text{exp}} \left(\frac{x}{\sqrt{a}} \right) \quad (1)$$

$$\frac{c_x - c_R}{c_{0.04} - c_R} = K_c \left(\frac{x}{\sqrt{a}} \right)^{n2} \quad (2)$$

Where, u_x , u_0 , K_{exp} and a are the peak velocity of the x horizontal distance from the mouth, peak velocity from the mouth, characteristic constant of velocity decay and the area of manikin's mouth (123mm^2). C_x is the averaged concentration values measured at a horizontal distance of x from mouth, C_R the concentration at exhaust and $C_{0.04}$ concentration 0.04m from the mouth. For Equation (1) the velocities are all peak velocity but as the tracer gas sampler and analyzer is not fast enough to capture the peaks as the anemometer does, only averaged concentrations are applied for Equation (2).

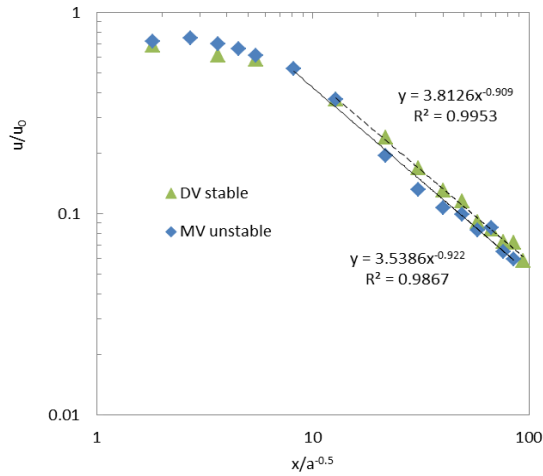


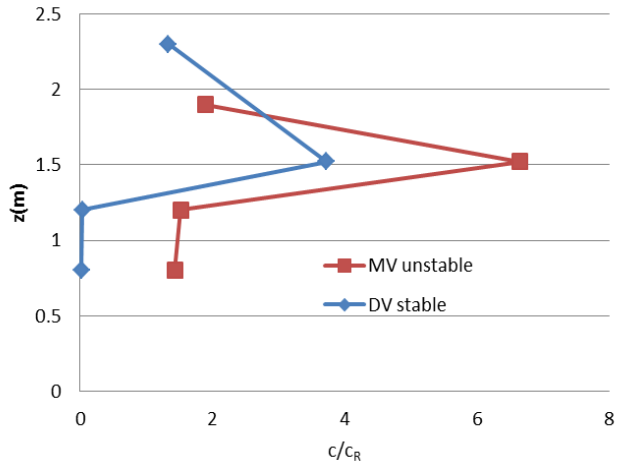
Fig.4 Velocity decay of stable and unstable conditions in the centerline of the exhalation

For the first few points close to the manikin’s mouth, the velocity decreases slowly and the velocity of unstable condition is slightly higher than stable condition due to higher exhalation and body temperature in DV. However, the velocity decays faster for unstable condition compared with the stable with the dashed line always higher than the solid line, shown in Fig.4. The reason for the difference of velocity decay is probably caused by the inhibited turbulence entrainment of the exhaled flow for stable condition. And since the flow can rapidly mix with the ambient air and diffuse upwards for unstable condition after it goes out from the manikin’s mouth, the momentum of the flow dissipates quickly and decreases faster. Similarly, the concentration for stable is significantly higher which can be concluded both from Table 2 and Fig.3. The tracer gas mixes well with the room air and velocity decreases more quickly for unstable with higher K_c .

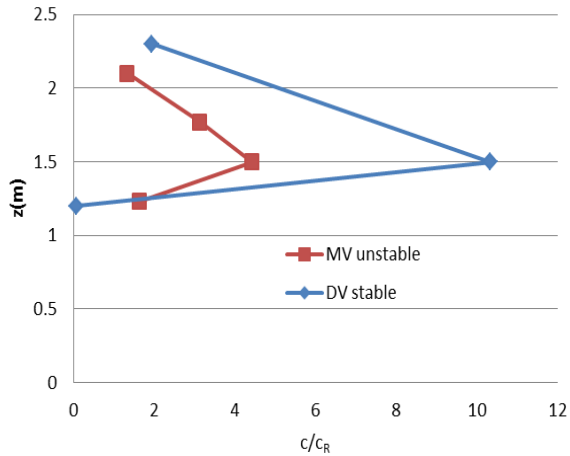
Table 1. Cosntants of the velcotiy and concentration decay

	K_{exh}	$n1$	K_c	$n2$
Stable	3.8126	-0.909	5.0369	-0.889
Unstable	3.5386	-0.922	14.138	-1.423

3.3 Concentration of N2O in different positions



(a)



(b)

Fig.5 concentration of N₂O close to the manikin at hip, chest, nose and above head (a) and 0.35m from the manikin at 1.2m, 1.5m and above head

Tracer gas N₂O which has the same molecular weight with CO₂ is added to the manikin's exhalation by inserting a pipe from the gas tank to the manikin's mouth. As it is expected before, under displacement ventilation which is a typical stable condition the concentration of pollutant is much higher than that under unstable because the stability blocks turbulent development of the pulsating jet and entrains less ambient clean air to the exhalation.

DV creates a cleaner zone at the lower part of the room. Because of the body plume, cleaner air from the floor is entrained and heated to move up, giving a lower contaminant exposure of inhalation from the nose, as shown in Fig. 5(a). The exposure of inhalation is lower for DV than that of MV not only because of the

cleaner air entrained from the lower and cleaner zone but also due to the ventilation pattern with fresh air supplied from the floor.

Concentration for stable is over two times higher than unstable at some distance from the manikin because the concentration decreases much slower than unstable. At 1.2m height, The concentration is close to zero for stable as it's located at the cleaner zone created by DV. This can also be seen from Fig.5(b).

4 CONCLUSIONS

For stable air condition, the upward trend of pulsating exhalation from a person is relatively weak because the stable air blocks the upward movement of the flow, and the flow can penetrate a longer distance. It can be observed that the air with smoke exhaled from a life-sized thermal manikin is locked and stratified at certain heights at stable condition while it mixes well with the ambient air and is diluted quickly through upper openings when the air is relatively unstable.

The concentration of contaminant simulated by tracer gas (N_2O) is measured both around and 0.35m from the manikin, indicating that the person who exhales the contaminant may not be polluted by himself because of the protective effect of the thermal boundary layer around the body, especially in stable condition with two concentration zones and clean air drawn from the inlets. However, other persons facing the respiration some distance away may suffer higher contaminant exposure if the air in room is quite stable. In addition, the air stability changes the velocity profiles, giving higher velocity decay and more turbulent mixing with surrounding air at unstable air condition.

ACKNOWLEDGMENT

The project is partly financially supported by China Scholarship Council (CSC), Hunan Provincial Innovation Foundation for Postgraduate (CX2012B131), National Special Program of International Cooperation and Exchange (No.2010DFB83650) and Important Science Program of Hunan Province of China (No. 2010FJ1013).

REFERENCES

- [1] Manju Mohan and T.A. Siddiqui. Analysis of various schemes for the estimation of atmospheric stability classification. *Atmospheric Environment* 32(1998): 3775-3781.
- [2] Turner, D. B. (1970) Workbook of atmospheric dispersion estimates. Oice of Air Program Pub. No. AP-26, Environmental Protection Agency, USA.
- [3] Gong Guangcai, Han Bing, Luo Hongfeng, Chunwen Xu, Kongqing Li. Research on the Air Stability of Limited Space. *International Journal of Green Energy*, 7(2010):43-64.
- [4] Peter V. Nielsen, Rasmus L. Jensen, Michal Litewnicki and Jan Zajac. Experiments on the microenvironment and breathing of a person in isothermal and stratified surroundings. *Healthy Buildings 2009: 9th International Conference & Exhibition, Syracuse, NY USA. 2009.*
- [5] Li Liu, Yuguo Li, Peter V. Nielsen, Rasmus L. Jensen, Michal Litewnicki and Jan Zajac. An Experimental Study of Human Exhalation during Breathing and Coughing in a Mixing Ventilated Room. *Healthy Buildings 2009 : 9th International Conference & Exhibition, September 13-17, 2009, Syracuse, NY USA. 2009.*
- [6] E. Bjorn and P. V. Nielsen. Dispersal of exhaled air and personal exposure in displacement ventilated rooms. *Indoor Air*, 12(2002): 147-164.
- [7] H. Qian, Y. Li, P. V. Nielsen, C.E. Hyldgaard, T. W. Wong, A.T.Y. Chwang. Dispersion of exhaled droplet nuclei in a two-bed hospital ward with three different ventilation systems. *Indoor Air* 16(2006): 111-128.

- [8] I. Olmedo, P.V. Nielsen, M. Ruiz de Adana, R.L. Jensen, P. Grzelecki. Distribution of exhaled contaminants and personal exposure in a room using different air distribution strategies. *Indoor Air*, 22(2011):64-76.
- [9] Peter V. Nielsen , F. V. Winther , M. Buus , M. Thilageswaran. contaminant flow in the microenvironment between people under different ventilation conditions. *ASHRAE Transactions*, 114(2008):632-640.
- [10] E. Bjorn. Simulation of human respiration with breathing thermal manikin. *Proceedings of Third International Meeting on Thermal Manikin Testing*, Stockholm, Sweden, National Institute for Working Life, 78–81.
- [11] P.Hoppe. Temperatures of Expired Air under Varying Climatic Conditions. *Int.J.Biometeor*, 25(1981): 127-132.

APPENDIX C.

MEASURING THE EXHALED BREATH OF A MANIKIN AND HUMAN SUBJECTS

The paper presented in Appendix C is published in Indoor Air, Volume 25, Issue 2, Pages 188-197, 2015.

doi:10.1111/ina.12129

<http://onlinelibrary.wiley.com/doi/10.1111/ina.12129/pdf>



Measuring the exhaled breath of a manikin and human subjects

Abstract Due to scarcity of accurate information and available data of actual human breathing, this investigation focuses on characterizing the breathing dynamic process based on the measurement of healthy human subjects. The similarities and differences between one breathing thermal manikin and the human subjects, including geometry and breathing functions, were thoroughly studied. As expected, actual human breathing is more complicated than that of the manikin in terms of airflow fluctuations, individual differences, and exhaled flow directions. The simplification of manikin mouth structure could result in overestimated exhaled velocity and contaminant concentration. Furthermore, actual human breathing appears to be relatively stable and reproducible for an individual person in several conditions and is also accompanied by some uncertainties simultaneously. The averaged values are used to analyze the overall characteristics of actual human breathing. There are different characteristics of the exhaled breath between male and female subjects with or without wearing a nose clip. The experimental results obtained from the measurement of human subjects may be helpful for manikin specification or validation and accuracy assessment of CFD simulations.

**C. Xu¹, P. V. Nielsen², G. Gong¹,
L. Liu², R. L. Jensen²**

¹College of Civil Engineering, Hunan University, Changsha, China, ²Department of Civil Engineering, Aalborg University, Aalborg, Denmark

Key words: Breathing; Manikin; Human subjects; Constant temperature anemometer; Mean peak velocity; CFD.

G. Gong
College of Civil Engineering
Hunan University, Changsha
410082, China
Tel.: +86 13973123865
Fax: +86 88823082
e-mail: gcgong@hnu.edu.cn

Received for review 12 January 2014. Accepted for publication 6 May 2014

Practical implications

A number of studies relevant to human breathing have been performed upon manikins or computer-simulated persons, but few relevant data have been provided to validate the accuracy of the predicted results. The aim of this investigation was to fill the gap by measuring the actual breathing of human subjects. The reliability of manikin experiment or CFD simulation of mouth breathing can be evaluated by the experimental data provided in this paper, and the results may be helpful in improving our current understanding of actual human breathing.

Introduction

Human respiratory activities can act as sources of infectious disease transmission. The World Lung Foundation has reported over four million deaths each year caused by acute respiratory infections (ARIs), including pneumonia, influenza, and respiratory syncytial virus (RSV), which are mainly transmitted through airborne droplets. Earlier studies (Duguid, 1946; Xie et al., 2007; Morawska et al., 2009; Chao et al., 2009; Redrow et al., 2011) have thoroughly studied coughing and sneezing that are generally considered of higher infectious risk, while some influenza viruses have been found present in human breathing (Fabian et al., 2008; Milton et al., 2013; Stelzer-Braid et al., 2009). Papineni and Rosenthal (1997) even found higher concentration of droplets ($>1 \mu\text{m}$) from mouth breathing than coughing in one test subject. Based on disease control and health consideration, accurate prediction of

human breathing with high flow volume and frequency in human life should be also of concern.

To substitute human respiration in an indoor environment, various types of thermal manikins and computer-simulated persons (CSPs) have been developed and used. As a powerful tool for indoor climate research, some otherwise hazardous methods or techniques to humans become possible by using these breathing thermal manikins. These methods include gas or particle tracing methods, smoke visualization as well as phase Doppler anemometry (Spitzer et al., 2010). The manikins are used to explore the role of human respiratory behavior in the spreading of infectious disease between occupants (Bjørn and Nielsen, 2002; Brohus and Nielsen, 1996; Nielsen et al., 2007, 2008, 2010; Olmedo et al., 2012, 2013; Qian et al., 2006, 2008). Breathing thermal manikins also contribute to the validation of the computational fluid dynamics predictions as well as the design and

optimization of indoor environment. Admittedly, some well-designed and sophisticated manikins (Bjørn, 1999; Bjørn and Nielsen, 2002; Melikov and Kaczmarczyk, 2007) can represent human breathing and the thermo-physiological properties to some satisfying degree, but the difference in results between these human-like models and actual human beings remains a question. Compared with the substantial information on manikin or CSP breathing, only a few published studies have provided accurate information about actual human breathing (Gupta et al., 2010; Tang et al. 2013). This investigation will specify the dispersion of mouth exhaled breath by measuring human subjects and explore the characteristics of human breathing.

CFD simulations were set to utilize available physiological parameters obtained from human subjects as input for boundary settings, and most of these simulations had further simplifications of these parameters to save computing time or cost. For example, the complicated mouth structure was replaced by a circular opening with comparable areas in some studies or the periodic breathing was substituted by constant velocity or flow rate. However, the dispersion of exhaled airflow and the propagation of a contaminant may be sensitive to these changes or simplifications (Nielsen, 2004). Additionally, even though the input of physiological parameters is kept consistent with those of humans, simulations could result in an inaccurate outcome. Thus, comparisons with actual human data are needed. But no relevant literature has reported the discrepancies between the predicted data derived from the manikins or CSPs and reality. Hence, this investigation explores the similarity and differences of human breathing between a standard manikin and human subjects and focuses on characterizing human breathing to provide experimental data for CFD validation or model improvement.

Methods and design

Manikin vs. human subjects

The investigation uses a breathing thermal manikin made with a simple geometrical shape in accordance

with a life-sized woman. This manikin was developed by Aalborg University and was designed to be similar to another average-sized manikin with the accurate geometrical likeness of a real person (Bjørn, 1999). This series of manikins have been widely used in earlier studies to investigate characteristics of human breathing and evaluate indoor air environment (Bjørn and Nielsen, 2002; Brohus and Nielsen, 1996; Melikov and Kaczmarczyk, 2007; Nielsen et al., 2007, 2008, 2010; Olmedo et al., 2012, 2013; Qian et al., 2006, 2008). The nose of the manikin consists of two circular nostrils with a diameter of 12 mm (according to Grymer et al., 1991), 45° below the horizontal plane and an intervening angle of 30° between the vertical planes. The mouth opening (about 120 mm²) is semi-ellipsoid shaped and directly connected to an artificial lung by a tube (inner diameter 10 mm), as shown in Figure 1. The sizes of opening areas and spreading angles all fall within the equation limits reported by Gupta et al. (2010) by measuring on human subjects who were smoking and exhaling smoke. This manikin also complies with the important characteristics and requirements for a breathing thermal manikin as proposed by Melikov (2004), which can be recognized as a ‘standard’ manikin in the present studies.

To be as realistic as an average human subject, the manikin was placed at a metabolic level of 1.2met in line with ASHRAE (2009) and Adams (1993) – 70W/m², breathing at a respiratory frequency of 15.5 min⁻¹ and a minute volume of 8.8 l/min. The breathing function of the manikin was realized by an artificial lung, presenting a sinusoidal airflow shape and corresponding approximately with human respiration (Gupta et al., 2010). The component of CO₂ in exhalation was simulated by use of nitrous oxide (N₂O) with 4% by volume. As the exhaled air from the manikin was not saturated with water vapor, the temperature of exhalation by using ambient air mixed with N₂O should be corrected. The mean exhalation temperature was set as 34°C when the ambient temperature was 20°C (Bjørn, 1999; Hoppe, 1981).

Douglas et al. (1983) found varying respiratory frequency (RF) between nasal and mouth breathing. If it is proved to be true, the RF for the manikin should be

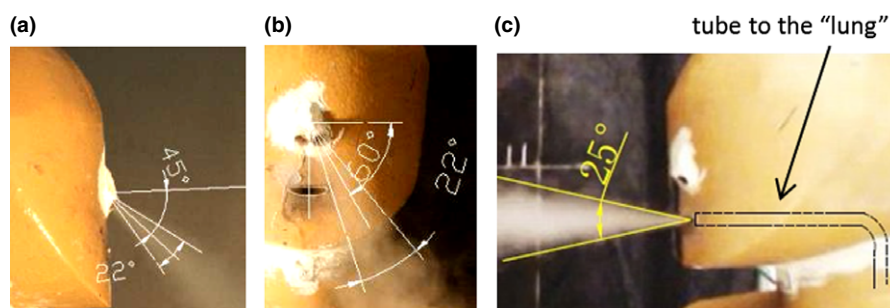


Fig. 1 Visualization of nasal (a, b) and mouth (c) exhalation from the manikin

adjusted according to different breathing routes. Human volunteers (young adults, 20 males and 11 females) went through two sets of tests (standing relaxed and walking at a normal speed) to count the RF, respectively, during four breathing patterns: (i) free breathing, (ii) inhaling through nose and exhaling through mouth, (iii) nasal breathing, and (iv) mouth breathing. The last three patterns are usually applied to a breathing manikin for experimental purposes. But no significant differences were found among the four breathing routes because different organs were used. This finding was in alignment with Gupta et al. (2010). Also, the mean RF of all four patterns for standing and walking subjects, respectively, corresponded well with the RF offered by Adams (1993) at 1.2met and 2met. Relevant figures can be found under Supporting Information.

The velocity and concentration in the exhaled air of the manikin and the human subjects were measured. Human subjects were required to breathe in two modes: (a) inhaling through nose and exhaling through mouth and (b) mouth breathing only. A nose clip was attached when only mouth breathing was allowed. The breathing manikin used only mode (a). Table 1 lists the numbers of volunteers involved in different experiments. Table 2 gives the basic information of the subjects for velocity measurements. Systematic differences might occur between ethnic and geographical groups, but the obtained results from both Chinese and European subjects were combined for analysis.

Measurement facilities and procedures

The measurements were conducted in a 3.0 × 2.3 × 2.5 m chamber, equipped with complete ceiling and complete floor ventilation. Cold air (17 ± 1°C) was supplied from the ceiling and exhausted through the floor. The air change rate was set at 7.5/h. Temperature measurements were made at three positions (poles L1, L2, and L3) at eleven heights, and the ambient air temperature was almost constant at about 22°C when performing experiments on the manikin or real persons. Figure 2a shows the experimental domain with locations of the manikin or persons and the robot used to carry the measuring probes. A holder with a height-adjustable bar is used to support the head of a human subject in case of any movement during

Table 1 Numbers of volunteers for different experiments

Types	Male	Female
RF (standing and walking)	20	11
Velocity		
(a) Nose in and mouth out	15	8
(b) Mouth only	15	8
CO ₂ concentration		
(a) Nose in and mouth out	2	3

Table 2 Mean and range values of the subjects involved in velocity measurement

	Male	Female
Age	26 (23–35)	27 (21–33)
Chinese subject no.	9	6
European subject no.	6	2
Weight (kg)	71.8 (52.9–95.0)	53.3 (46.0–70.4)
Height (cm)	175.9 (160.0–186.0)	164.8 (158.0–171.0)
BSA (m ²) (Du Bois and Du Bois, 1989)	1.87 (1.57–2.20)	1.56 (1.44–1.82)
MV ^a (l/min) (Gupta et al., 2010)	9.78 (8.21–11.48)	7.22 (6.67–8.45)

BSA, body surface area.

^aMV is the minute volume with sitting posture and nose breathing (Gupta et al., 2010).

measurements, as presented in Figure 2b. A coordinate system is defined from the center of the mouth (Figure 2b). Probes for measuring temperature, velocity, and concentration can be installed on the robot arm and move along the two directions in the axis *x* and *y*.

The exhaled temperature along the *x* axis was measured first, followed by velocity and concentration measurements. The temperature was used for the reference of anemometer calibration (Dantec 54N50 hot-sphere anemometer, constant-temperature type, developed by DANTEC Dynamics A/S). The measured velocity may be influenced by surplus temperature and humidity in the exhaled air. Figure 3 illustrates the temperature changes with *x* by using a thin thermocouple. When *x* = 0, it means the thermocouple was put in the mouth of the manikin or the human subject, not touching the inner surfaces of the mouth cavity. Over 2 min of mouth breathing was required for human subjects, and the breathing temperature fluctuations changing with time were recorded. Figure 3 shows one example (Male No. 12). The peak temperatures were extracted and then averaged for analysis. The ambient air was kept around 22°C with a measured maximum temperature difference of 0.5°C between each measurement. The exhaled temperature varied from 32 to 36°C among individuals and decreased rapidly with increasing *x*. The temperature decay of human subjects was faster than that of the manikin due to readily mixing with cold ambient air. At *x* ≈ 3 cm, from which the velocity measurement took place, the exhaled temperature of subjects dropped to merely 24–26°C, and the influence of temperature was ignored as the density difference between the exhaled air (24°C) and the calibration air (22°C) was negligible. Likewise, due to the complicated fluctuations and decay of humidity (maximum RH of about 80% at *x* ≈ 3 cm, tested by HygroDat 100), the influence of humid air was not considered in this work, although a velocity error of 1–5% might occur for a constant-temperature anemometer due to the influence of humidity (Larsen and Busch, 1980).

The anemometer was calibrated in a jet-wind tunnel, horizontally positioned, in the presence of 22°C ambient

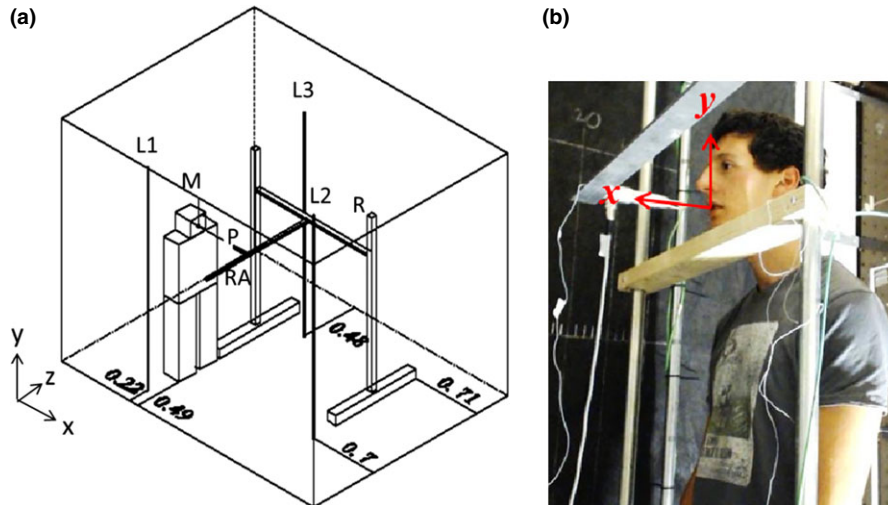


Fig. 2 (a) Configuration for the test chamber with a manikin or a person (M), three poles (L1, L2, and L3) carrying thermocouples at 11 different heights, robot (R), and robot arm (RA) with probes (P). (b) Velocity measurement of one male subject without nose clip. Dimensions are indicated in units of meters

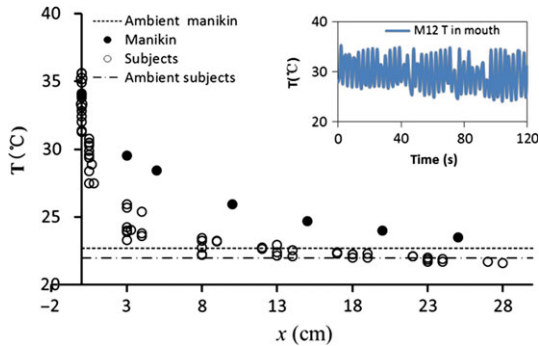


Fig. 3 Exhaled temperatures changing with x distance. ($x = 0$ accounts for the temperature measured in a subject's mouth)

air. The instantaneous velocity range of the anemometer was from 0.05 to 5 m/s, with Omni directional direction sensitivity and a working temperature range of 18–35°C. Jensen et al. (2007) have tested the dynamic properties of the hot-sphere anemometer in a highly transient sine flow, and the anemometer responded well to transient fluctuations. Human exhalation is highly transient, and it is measured by a constant-temperature anemometer. The measurements, control, display, and analysis were performed with a Prema precision multimeter (10 Hz) and the LabVIEW software package.

The direction of velocity cannot be detected by using a constant-temperature anemometer. But compared with other techniques for velocity measurement, such as the PIV or LDA, the application of the thermistor sensor is safe for human experimentation and convenient to operate. Actually, a number of studies have reported the implementation of the constant-temperature type anemometer for measuring expiratory parameters (Araujo et al., 2004; Ferreira et al., 2001;

Kandaswamy et al., 2002; Silva et al., 2002). To diminish the influence of the sensor dimensions, only one anemometer was used. Four distances, $x \approx 3$ cm, $x = 8$ cm, $x = 14$ cm, and $x = 24$ cm, were selected to obtain the velocity profiles on these four vertical sections along y direction.

The N_2O which has the same molecular weight with CO_2 was used for manikin experiment as a tracer gas to mimic the content of CO_2 in human exhalation. The volume fraction of N_2O in the exhaled air of the manikin was set as 4%. And no extra gases were added to human experiments as CO_2 is a natural tracer gas indoors. Multipoint sampler and doser (INNOVA 1303) and photoacoustic field gas monitor (INNOVA 1412) with an accuracy of $\pm 1\%$ were applied. Four horizontal measuring points were located in front of a person.

Results

Pulsating breathing velocity

Figure 4a and b illustrate the breathing velocity profile of the manikin and a male subject, respectively. As the velocity directions cannot be acquired by the hot-sphere anemometer, the measured instantaneous velocity magnitude should never be negative. During the inhalation process, the velocity was still above zero. The remaining velocity after the exhalation process within one breathing cycle was probably caused by the inhaled airflow through the nostrils (no clip) or the mouth (clip on), combined with the impact of constantly rising thermal plume adjacent to the body. In addition, in the vicinity of the manikin body, the plume resulted in a maximum velocity of 0.2 m/s. Extrapolating from the evidence mentioned previously, the

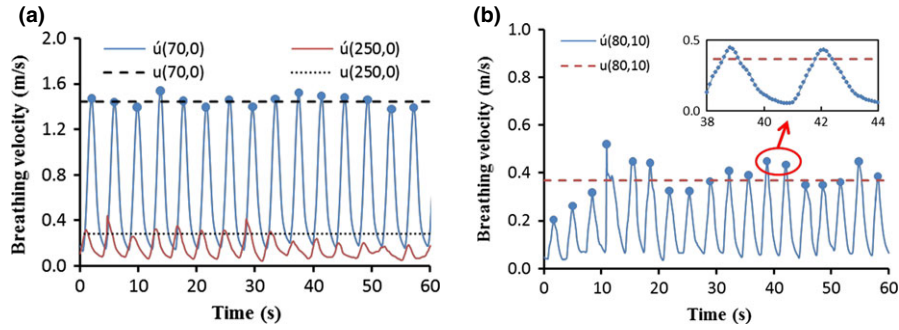


Fig. 4 Comparison of breathing velocity for (a) the manikin and (b) for a person

remaining velocity should decrease when moving the probe away from the human body, which is confirmed by Figure 4a.

The breathing velocity profiles of the manikin and the human subjects had similar shapes but different RF and magnitudes. Under relaxed conditions, the breaths of human subjects are likely to become relatively regular and repeating as is the case for the manikin, see Figure 4. Priban and Fincham (1965) also demonstrated that the breathing profiles of human subjects are very regular with respect to the frequency and volume. Two peaks are extracted from the velocity profile and they can, to some extent, be identified as sinusoidal in shape (Figure 4b). Thereby, the sinusoidal flow generated by the artificial lung can represent human breathing to some decent degree. But the natural differences between each breath for human subjects cannot be simulated by the artificial lung.

Despite large individual differences and relatively unstable features of human breathing, the peak velocity of each exhaled breath could be acquired by the anemometer. And the mean peak value $u(x,y)$ at the coordinate point (x,y) is used to depict velocity profile in sections, as shown in Figure 5.

Velocity profiles and centerline of exhaled flow

The direction of the exhaled flow is governed by the direction of human exhalation, which can be found by measuring the velocity profiles in front of the person. The velocity profile along the y direction can be

obtained from the mean peak velocity $u(x,y)$ measured in section x , as shown in Figure 5. The velocity profiles of the exhaled flow from the manikin were normalized by mean peak velocities, and they presented similar shapes as a turbulent circular jet (Abramovich, 1963). This similarity was also reported by Nielsen et al. (2009) and Olmedo et al. (2012). The velocity centerline should have the maximum velocity in each vertical section, expressed as u_m , which was almost horizontal for the manikin even though the exhalation was non-isothermal. For persons, the heads were placed horizontally on the wooden bar during measurements. However, none of those velocity centerlines was perfectly horizontal, indicating either a slight upward or a downward trend (Figures 5b,c and 6).

Human exhalation tends to be complex as it is affected by multiple factors. Clark and Edholm

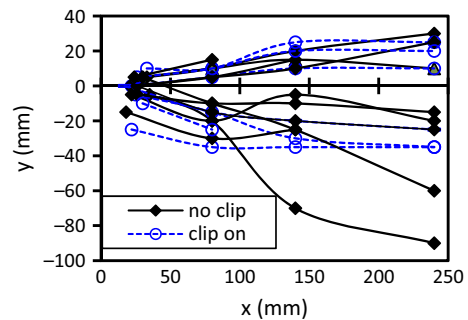


Fig. 6 Positions of the velocity centerline (with and without clip)

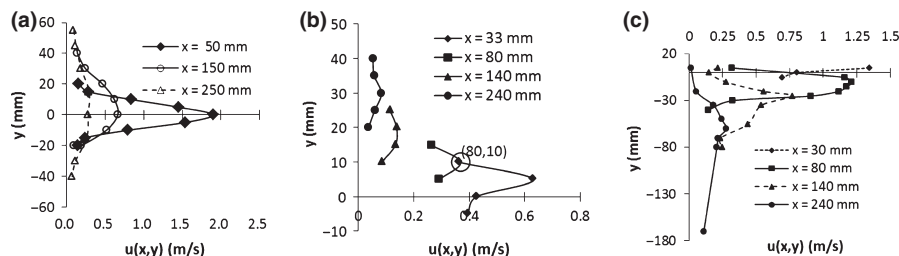


Fig. 5 Velocity profiles in different sections for: (a) the manikin, (b) one male subject (without clip), and (c) one female subject (without clip)

(1985) observed an upward development of the exhaled flow from living persons by means of Schlieren photography. Gupta et al. (2010) reported relatively downward spreading angles by visualizing the exhaled flow from people’s smoking. It is difficult to connect human mouth exhalation with a certain direction because besides the depending factors such as exhaled temperature and momentum, ambient air temperature or boundary streams around body, the dispersion of human exhaled flow may be influenced by mouth shapes, teeth locations and angles at which the head placed. Large variations occurred among the individuals. Even for the same subject, the positions of the centerline would vary with breathing patterns. It was also found that the motion of lips or teeth could change the initial angle of exhalation. Nevertheless, mouth exhalation can be considered basically horizontal in applications, because the scattered centerlines still distribute around the horizontal line with fluctuations up or down for only few centimeters, as illustrated in Figure 6.

Tang et al. (2013) visualized human exhalation by means of the Schlieren photography technique and observed the maximum propagation distance of 0.8 m, which was considerably higher than predictions in this investigation. Beyond 0.3 m downstream of exhalation from mouth, velocity peaks of a large percentage of subjects disappeared, hidden in turbulence. But it is possible for the exhaled flow to propagate a bit farther due to the inertia force and the concentration difference. The Schlieren photography technique may also overestimate the distance through observation because

the temperature difference remains at longer distances between exhaled and ambient air (Tang et al., 2013).

Velocity and concentration decay

This section focuses on exploring different characteristics of the dispersion and spread of exhaled flow between manikin and real persons as well as between males and females. Figure 7 shows the centerline velocity u_m and the decay of centerline velocity. The velocity decay of two male and two female subjects were, respectively, marked with different symbols to highlight the differences of velocity magnitudes, which indicated a relatively unchanged breathing habit for an individual over a period of time. This finding further confirmed the fact that one particular breathing pattern appears to be a relatively stable characteristic of an adult individual, being reproducible in several conditions, as addressed by Benchetrit (2000).

A direct comparison of the exhaled velocity between the manikin and the human subjects shows a lower exhaled velocity of the vast majority of the human subjects than that of the manikin. The scattered points are covered by a dashed line, forming a region in which the exhaled velocities from persons may locate, as shown in Figure 7. If the velocity in the exhaled flow is smaller than 0.1 m/s, it is probably caused by turbulence rather than breathing, because the velocity distribution in the chamber has been tested to be of a maximum value around 0.1 m/s. The solid regression line was drawn based on the hypothesis that the centerline velocity decays with distance, in the form of a power

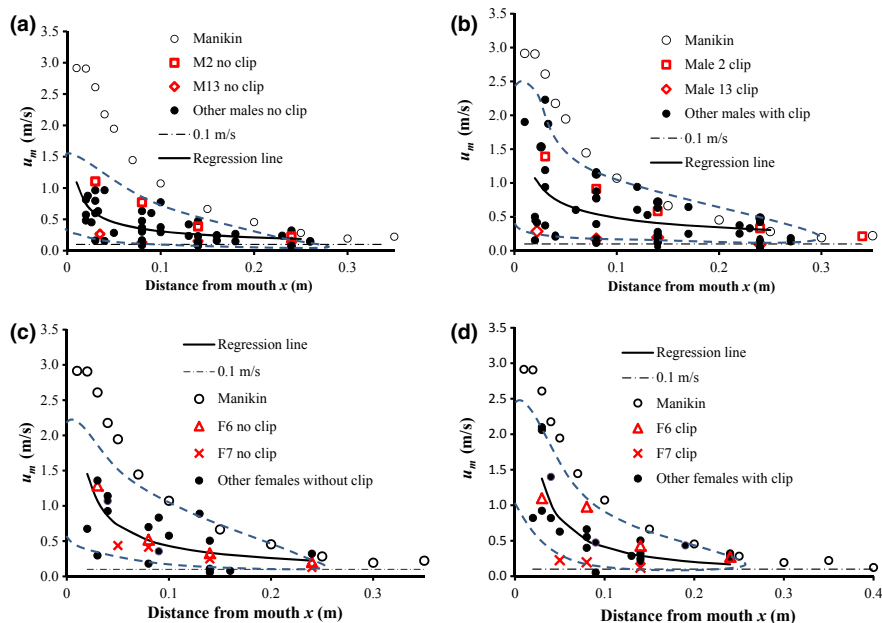


Fig. 7 Magnitudes of velocities along the centerline and regression of the velocity decay (solid line) for: (a) male nose in and mouth out, (b) male mouth breathing only, (c) female nose in and mouth out, and (d) female mouth breathing only

Table 3 Coefficient a and b and corresponding confidence intervals with 95% bounds

Type	a and confidence intervals	b and confidence intervals
Male nose in and mouth out	0.09 (0.03, 0.14)	-0.55 (-0.74, -0.35)
Male mouth only	0.15 (-0.04, 0.27)	-0.49 (-0.74, -0.24)
Female nose in and mouth out	0.08 (-0.01, 0.16)	-0.76 (-1.12, -0.39)
Female mouth only	0.04 (-0.01, 0.09)	-1.01 (-1.41, -0.62)

function, assumed as $u_m = ax^b$. Similar expression has been validated by manikin experiments (Nielsen et al., 2009; Olmedo et al., 2012). The regression equation was fitted by nonlinear least squares algorithm. Table 3 shows the coefficients of a and b with 95% confidence bounds. A smaller b indicates a faster decay. The exhaled velocity region and the regression line of female subjects seem to be steeper than those of male subjects. For female subjects, the mean velocity from the mouth was initially higher, but it decreased rapidly with increasing distance, indicating a short distance and a rapid breath. In comparison, the exhaled breath of male subjects presented a long and lasting characteristic, as the initial velocity was lower than that of females, but the flow could penetrate a longer distance. The larger initial velocity of female subjects can be explained by higher RF and smaller mouth opening areas despite lower breathing volume compared with male subjects. The flow rate of exhaled air may slightly increase owing to wearing the nose clip, which blocks the air leakage from the nose during exhalation process. Compared with Figure 7a, for male subjects the velocity distributions become more scattered when the nose clip is used, with some points close to the manikin level, as shown in Figure 7b. For female subjects, the velocities are also slightly increased with the nose clip attached, see Figure 7d,c. However, even when the total exhaled breath was through the mouth, the majority of the human subjects exhaled at an apparently low speed.

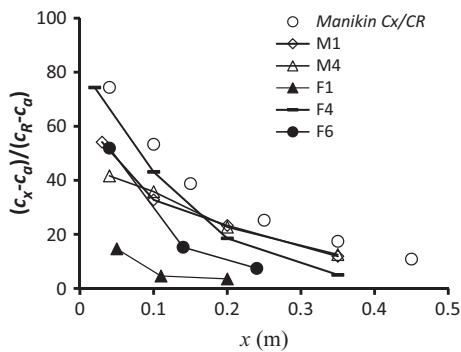


Fig. 8 Relative concentration of CO₂ and N₂O in the exhaled air. c_a is concentration in the ambient air in the chamber without a person, c_R is concentration at the exhaust openings of the chamber, and c_x is concentration at a horizontal distance of x from the mouth. c_a , c_R and c_x are the mean peak concentrations in the exhaled air at the locations defined earlier and are indicated in unit of ppm

The respiratory parameters of the manikin were set according to the values for an average adult (ASHRAE, 2009 and Adams, 1993). Consequently, the manikin breathing was expected to simulate the average level of human subjects, but it appears to overestimate human breathing. Figure 8 shows the relative concentration of CO₂ from human subjects and the relative concentration of N₂O from the manikin, respectively. The exhaled concentration of the tracer gas from the manikin was obviously elevated above those from the human subjects. This was not surprising by comparing the breathing passage of the manikin with that of a person. For the manikin between the mouth and the ‘lung’, the breathing passage is simplified as a circular tube (Figure 1c). But for a person, after the air leaves the lungs through the bronchi and trachea, it needs to successively pass through the larynx, pharynx, and oral cavity, touching surfaces of the tongue, teeth and lips, and eventually reach the terminal. The respiratory system of human being is so complicated that the flow from the mouth will obtain a high diffusion and reduced velocity level like advanced diffusers in the ventilation area. Thereby, more delicate design of the mouth structure will be needed to make manikin breathing more realistically.

Discussion

Initial velocity close to the mouth and variation in the breathing flow

There are a number of studies on simulations of human respiratory which consider exhaled flow rate or velocity as a standard sinusoidal curve (Hyun and Kleinstreuer, 2001; Gao and Niu, 2004, 2006; Gupta et al., 2011), like manikin breathing. Variations in the breathing flow were commonly neglected due to the lack of information on actual human breathing. Most of the CFD simulations treated the breathing boundary conditions as a varying flow rate or velocity without clearly indicating the turbulence features, or as flow with low turbulence intensity (Gao and Niu, 2004; nose with $I = 0.5\%$). However, it seems impossible to quantify the turbulence intensity for human breathing, because the turbulence is clearly accompanied by uncertain breath-to-breath fluctuations despite not only appearing randomly (Figure 4b). An expression of u'_m/u_m , similar to turbulent intensity in form was introduced to investigate the fluctuation range of the peak velocities. The u'_m is the standard deviation of the peak velocities and u_m is the mean peak value at velocity centerline. This u'_m/u_m ratio accounts for the spreading of peak velocities. On the other hand, the ratio for the manikin could be considered as turbulence intensity if the influence of breath-to-breath fluctuations resulting from the manikin itself can be ignored owing to the identical piston driven movements (Figure 4a). It can be expected that u'_m/u_m of the manikin should be much lower than

Table 4 Mean peak velocity and the fluctuation ratio with 95% confidence intervals at the first measuring point (0.03 ± 0.01 m)

	Persons		Manikin	
	u_m (m/s)	u'_m/u_m	u_m (m/s)	u'_m/u_m
Male nose in and mouth out	0.58 ± 0.15	$41 \pm 5\%$	2.44 ± 0.03	1.3%
Male mouth only	0.81 ± 0.40			
Female nose in and mouth out	1.03 ± 0.56			
Female mouth only	1.03 ± 0.51			

that of a person. Furthermore, the ratio should grow with increasing x , which increased from about 1 to 35% from merely $x = 0.01$ m to $x = 0.4$ m for the manikin. This finding indicated that the influence of room air turbulence became more evident in the downstream of the flow.

Table 4 shows the mean peak velocity and the ratio of u'_m to u_m , respectively, for the human subjects and the manikin, at the first measuring point with a distance of about 0.03 m from the mouth opening. The maximum velocity measured close to the mouth may be useful for CFD validation and boundary specifications. The u_m of the human subjects in Table 3 is the mean value of mean maximum velocity at around 0.03 m for all male and female subjects, with confidence bounds of 95%. The u'_m/u_m for human subjects is the mean fluctuation ratio obtained from each measurement with a level of confidence of approximately 95%. Owing to the complexity of human respiratory system as well as the relatively unstable breath-to-breath variations, the apparent turbulence level of the human respiration should be much larger than that of the manikin. The rapid temperature, velocity, and concentration decay of the exhaled breath from the majority of human subjects, resulting from easy entrainment and mixing with the ambient air, confirmed this fact.

Uncertainty and regularity of human breathing

The results of human respiratory are expected to be scattered among individuals, see Figure 7, because the measurements were conducted on real people with significant individual differences. Differences were also observed among repeated measurements for the same human subject. Quantifying human respiration should certainly work with these uncertainties, which are usually averaged by repeated measurements (applied three times in this paper) and by a large number of human subjects. Even though the results are scattered among human subjects, some relatively evident conclusions can be drawn from the average values, for example, the differences of exhaled velocity between males and females as well as between the manikin and the human subjects (Figures 7 and 8). Figure 7 also indicates a relatively stable and reproducible characteristic

of an individual in terms of exhalation velocity and decay, which corresponds with the observations of Benchetrit (2000). These regularities provide some possibilities to quantify human breathing and more attempts should be made to improve our understandings of the complexity and uncertainty of actual human breathing.

Limitations

The u_m illustrated in Figure 7 is the mean maximum velocity along centerline which appears to be covered by that of the manikin. However, in some cases, the instantaneous velocity can exceed the manikin level with respect to fluctuations and uncertainties. Hence, if the breathing and metabolic heating of a manikin is specified according to the data collected from human adults, such as ASHRAE, 2009 and Adams (1993), the infection risk estimated by the manikin may be recognized as a critical condition or the top boundary (Figures 7 and 8). But if a manikin is required to simulate an average level of human breathing, a more delicate design of the breathing system is needed, and the results obtained in this investigation are recommended to validate the improvement. The current study provides results for when the subjects are standing still. The movement or natural sway of the body may result in more complicated breathing patterns. Additionally, the constant-temperature type anemometer can only measure the magnitude of the velocity. If the velocity vectors are needed for further illustration, a PIV system may be helpful, which has been implemented by some researchers on human subjects (Chao et al., 2009; Kwon et al., 2012).

Conclusions

As there are very few estimates of human breathing and little comparative data available for verifying the reliability of manikin experiment or CFD predictions, this investigation focuses on characterizing the breathing process of human subjects. The similarities and differences between a standard manikin and over twenty human subjects have been comprehensively studied from the perspective of geometry and breathing functions. The results show that the manikin can simulate human breathing to some satisfying degree in terms of the respiratory frequency, minute volume, and airflow pattern. However, the exhaled velocity and concentration of contaminant are likely to have an increased level because of the simplified mouth structure, low diffusion, and low turbulence levels. The characteristics of actual human breathing is expected to be more complicated and scattered than those of the manikin, including the airflow fluctuations, individual differences, and exhaled flow directions. This investigation

provides the average values obtained from a number of subjects. Overall, our present level of understanding of the characteristics of actual human breathing should be further advanced, and this work only provides a small step forward.

Acknowledgements

The authors gratefully acknowledge the contributions of all the volunteers involved in this experiment. This study is funded by China Scholarship Council (CSC), Hunan Provincial Innovation Foundation for Post-graduate (CX2012B131), National Special Program of International Cooperation and Exchange (No. 2010DFB63830) and National Natural Science Foundation of China (Grant No. 51378186).

References

- Abramovich, G.N. (1963) *The Theory of Turbulent Jets*, Massachusetts, M.I.T. Press.
- Adams, W.C. (1993) *Measurement of Breathing Rate and Volume in Routinely Performed Daily Activities*, Sacramento, CA, California Environmental Protection Agency.
- Araujo, G.A.L., Freire, R.C.S., Silva, J.F., Oliveira, A. and Jaguaribe, E.F. (2004) Breathing flow measurement with constant temperature hot-wire anemometer for forced oscillation technique. In: Petri, D. (ed.) *Proceedings of the 21st IEEE, Instrumentation and Measurement Technology Conference*, Vol. 1, 730–733.
- ASHRAE (2009) *Indoor Environmental Quality*, Atlanta, GA, American Society of Heating, Refrigerating and Air Conditioning Engineers (ASHRAE Handbook of Fundamentals 9.1-9.30).
- Benchetrit, G. (2000) Breathing pattern in humans: diversity and individuality, *Respir. Physiol.*, **122**, 123–129.
- Bjørn, E. (1999) Simulation of human respiration with breathing thermal manikin, In: Nilsson, H.O and Holmér, I. (eds) *Proceedings of Third International Meeting on Thermal Manikin Testing*, Stockholm, Sweden, National Institute for Working Life, 78–81.
- Bjørn, E. and Nielsen, P.V. (2002) Dispersal of exhaled air and personal exposure in displacement ventilated room, *Indoor Air*, **12**, 147–164.
- Brohus, H. and Nielsen, P.V. (1996) Personal exposure in displacement ventilated rooms, *Indoor Air*, **6**, 157–167.
- Chao, C.Y.H., Wan, M.P., Morawska, L., Johnson, G.R., Ristovski, Z.D., Hargreaves, M., Mengersen, K., Corbett, S., Li, Y., Xie, X. and Katoshevski, D. (2009) Characterization of expiration air jets and droplet size distributions immediately at the mouth opening, *J. Aerosol Sci.*, **40**, 122–133.
- Clark, R.P. and Edholm, O.G. (1985) *Man and His Thermal Environment*, London, Hodder Arnold.
- Douglas, N.J., White, D.P., Weil, J.V. and Zwillich, C.W. (1983) Effect of breathing route on ventilation and ventilatory drive, *Respir. Physiol.*, **51**, 209–218.
- Du Bois, D. and Du Bois, E.F. (1989) A formula to estimate the approximate surface area if height and weight be known. 1916, *Nutrition*, **5**, 303–311.
- Duguid, J.P. (1946) The size and the duration of air-carriage of respiratory droplets and droplet-nuclei, *J. Hyg.*, **44**, 471–479.
- Fabian, P., McDevitt, J.J., DeHaan, W.H., Fung, R.O., Cowling, B.J., Chan, K.H., Leung, G.H. and Milton, D.K. (2008) Influenza virus in human exhaled breath: an observational study, *PLoS ONE*, **3**, e2691.
- Ferreira, R.P.C., Freire, R.C.S., Deep, G.S., Rocha Neto, J.S. and Oliveria, A. (2001) Hot-wire anemometer with temperature compensation using only one sensor, *IEEE Trans. Instrum. Meas.*, **50**, 954–958.
- Gao, N. and Niu, J. (2004) CFD study on micro-environment around human body and personalized ventilation, *Build. Environ.*, **39**, 795–805.
- Gao, N. and Niu, J. (2006) Transient CFD simulation of the respiration process and inter-person exposure assessment, *Build. Environ.*, **41**, 1214–1222.
- Grymer, L.F., Hilberg, O., Pedersen, O.F. and Rasmussen, T.R. (1991) Acoustic rhinometry: values from adults with subjective normal nasal patency, *Rhinology*, **29**, 35–47.
- Gupta, J.K., Lin, C.-H. and Chen, Q. (2010) Characterizing exhaled airflow from breathing and talking, *Indoor Air*, **20**, 31–39.
- Gupta, J.K., Lin, C.-H. and Chen, Q. (2011) Transport of expiratory droplets in an aircraft cabin, *Indoor Air*, **21**, 3–11.
- Hoppe, P. (1981) Temperatures of expired air under varying climatic conditions, *Int. J. Biometeorol.*, **25**, 127–132.
- Hyun, S. and Kleinstreuer, C. (2001) Numerical simulation of mixed convection heat and mass transfer in a human inhalation test chamber, *Int. J. Heat Mass Transf.*, **44**, 2247–2260.
- Jensen, R.J., Kalyanova, O. and Hyldgård, C.E. (2007) On the use of hot-sphere anemometer in a highly transient flow in a double-skin façade. In: Seppänen, O. and Säteri, J. (eds) *Proceedings of Roomvent 2007*, Finland, Helsinki, 246.
- Kandaswamy, A., Kumar, C.S. and Kiran, T.V. (2002) A virtual instrument for measurement of expiratory parameters. *IEEE Instrumentation and Measurement Technology Conference*, Anchorage, AK, USA.
- Kwon, S.-B., Park, J., Jang, J., Cho, Y., Park, D.-S., Kim, C., Bae, G.-N. and Jang, A. (2012) Study on the initial velocity distribution of exhaled air from coughing and speaking, *Chemosphere*, **87**, 1260–1264.
- Larsen, S.E. and Busch, N.E. (1980) On the humidity sensitivity of hot-wire measurements, *DISA Inf.*, **25**, 4–5.
- Melikov, A. (2004) Breathing thermal manikins for indoor environmental assessment: important characteristics and requirements, *Eur. J. Appl. Physiol.*, **92**, 710–713.
- Melikov, A. and Kaczmarczyk, J. (2007) Measurement and prediction of indoor air quality using a breathing thermal manikin, *Indoor Air*, **17**, 50–59.
- Milton, D.K., Fabian, M.P., Cowling, B.J., Grantham, M.L. and McDevitt, J.J. (2013) Influenza virus aerosols in human

Supporting Information

Additional Supporting Information may be found in the online version of this article:

Figure S1. RF at standing conditions for (a) male subjects and (b) female subjects with four breathing patterns: nose only, nose in, and mouth out (corresponding to manikin breathing), mouth only, and normal breathing.

Figure S2. RF at walking conditions for (a) male subjects and (b) female subjects with four breathing patterns: nose only, nose in, and mouth out (corresponding to manikin breathing), mouth only, and normal breathing.

Figure S3. Variations of RF of males with height at (a) standing and (b) walking conditions.

- exhaled breath: particle size, culturability, and effect of surgical masks, *PLoS Pathog.*, **9**, e1003205.
- Morawska, L., Johnson, G.R., Ristovski, Z., Hargreaves, M., Mengersen, K., Chao, C.Y.H., Li, Y. and Katoshevski, D. (2009) Size distribution and sites of origins of droplets expelled from the human respiratory tract during expiratory activities, *J. Aerosol Sci.*, **40**, 256–269.
- Nielsen, P.V. (2004) Computational fluid dynamics and room air movement, *Indoor Air*, **14**, 134–143.
- Nielsen, P.V., Jiang, H. and Polak, M. (2007) Bed with integrated personalized ventilation for minimizing cross infection. *Roomvent 2007, 10th International Conference on Air Distribution in Rooms*, Helsinki.
- Nielsen, P.V., Winther, F.V., Buus, M. and Thilageswaran, M. (2008) Contaminant flow in the microenvironment between people under different ventilation conditions, *ASHRAE Trans.*, **114**, 632–640.
- Nielsen, P.V., Jensen, R.L., Litewnicki, M. and Zajas, J. (2009) Experiments on the microenvironment and breathing of a person in isothermal and stratified surroundings. In: Bogucz, E.A. (ed.) *Proceedings of 9th International Conference on Healthy Buildings*, Syracuse, NY, USA, Paper ID:374.
- Nielsen, P.V., Li, Y., Buus, M. and Winther, F.V. (2010) Risk of cross-infection in a hospital ward with downward ventilation, *Build. Environ.*, **45**, 2008–2014.
- Olmedo, I., Nielsen, P.V., Ruiz de Adana, M., Jensen, R.L. and Grzelecki, P. (2012) Distribution of exhaled contaminants and personal exposure in a room using three different air distribution strategies, *Indoor Air*, **22**, 64–76.
- Olmedo, I., Nielsen, P.V., Ruiz de Adana, M. and Jensen, R.L. (2013) The risk of airborne cross-infection in a room with vertical low-velocity ventilation, *Indoor Air*, **23**, 62–73.
- Papineni, R.S. and Rosenthal, F.S. (1997) The size distribution of droplets in the exhaled breath of healthy human subjects, *J. Aerosol Med.*, **10**, 105–116.
- Priban, I.P. and Fincham, W.F. (1965) Self-adaptive control and the respiratory system, *Nature*, **208**, 339–343.
- Qian, H., Li, Y., Nielsen, P.V., Hyldgård, C.E., Wong, T.W. and Chwang, A.T.Y. (2006) Dispersion of exhaled droplet nuclei in a two-bed hospital ward with three different ventilation systems, *Indoor Air*, **16**, 111–128.
- Qian, H., Li, Y., Nielsen, P.V. and Hyldgård, C.E. (2008) Dispersion of exhalation pollutants in a two-bed hospital ward with a downward ventilation system, *Indoor Air*, **43**, 344–354.
- Redrow, J., Mao, S., Celik, I., Posada, J.A. and Feng, Z.G. (2011) Modeling the evaporation and dispersion of airborne sputum droplets expelled from a human cough, *Build. Environ.*, **46**, 2042–2051.
- Silva, I.S.S., Frcirc, R.C.S., da Silva, J.F., Naviner, J.F., Soura, F.R. and Catunda, S.Y.C. (2002) Architectures of anemometer using the electric equivalence principle. *IEEE Instrumentation and Measurement Technology Conference*, Anchorage, AK, USA.
- Spitzer, I.M., Marr, D.R. and Glauser, M.N. (2010) Impact of manikin motion on particle transport in the breathing zone, *J. Aerosol Sci.*, **41**, 373–383.
- Stelzer-Braid, S., Oliver, B.G., Blazey, A.J., Argent, E., Newsome, T.P., Rawlinson, W.D. and Tovey, E.R. (2009) Exhalation of respiratory viruses by breathing, coughing, and talking, *J. Med. Virol.*, **81**, 1674–1679.
- Tang, J.W., Nicolle, A.D., Klettner, C.A., Pantelic, J., Wang, L., Suhaimi, A.B., Tan, A.Y.L., Ong, G.W.X., Su, R., Sekhar, C., Cheong, D.D.W., and Tham, K.W., et al. (2013) Airflow dynamics of human jets: sneezing and breathing - potential sources of infectious aerosols, *PLoS ONE*, **8**, e59970.
- Xie, X., Li, Y., Chwang, A.T., Ho, P.L. and Seto, W.H. (2007) How far droplets can move in indoor environments—revisiting the Wells evaporation-falling curve, *Indoor Air*, **17**, 211–225.

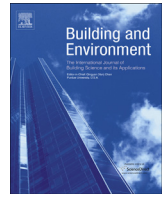
APPENDIX D.

HUMAN EXHALATION CHARACTERIZATION WITH THE AID OF SCHLIEREN IMAGING TECHNIQUE

The paper presented in Appendix D is published in Building and Environment, Volume 112, Pages 190-199, 2017.

<https://doi.org/10.1016/j.buildenv.2016.11.032>





Human exhalation characterization with the aid of schlieren imaging technique



Chunwen Xu ^{a,b,*}, Peter V. Nielsen ^b, Li Liu ^b, Rasmus L. Jensen ^b, Guangcai Gong ^c

^a College of Pipeline and Civil Engineering, China University of Petroleum, Qingdao 266580, China

^b Department of Civil Engineering, Aalborg University, Aalborg 9000, Denmark

^c College of Civil Engineering, Hunan University, Changsha 410082, China

ARTICLE INFO

Article history:

Received 26 September 2016

Received in revised form

17 November 2016

Accepted 18 November 2016

Available online 19 November 2016

Keywords:

Disease transmission

Schlieren photography

Exhaled airflow

Propagation velocity

Airflow interaction

ABSTRACT

The purpose of this paper is to determine the dispersion and distribution characteristics of exhaled airflow for accurate prediction of disease transmission. The development of airflow dynamics of human exhalation was characterized using nonhazardous schlieren photography technique, providing a visualization and quantification of turbulent exhaled airflow from 18 healthy human subjects whilst standing and lying. The flow shape of each breathing pattern was characterized by two angles and averaged values of 18 subjects. Two exhaled air velocities, u_m and u_p , were measured and compared. The mean peak centerline velocity, u_m was found to decay correspondingly with increasing horizontal distance x in a form of power function. The mean propagation velocity, u_p was found to correlate with physiological parameters of human subjects. This was always lower than u_m at the mouth/nose opening, due to a vortex like airflow in front of a single exhalation cycle. When examining the talking and breathing process between two persons, the potential infectious risk was found to depend on their breathing patterns and spatial distribution of their exhaled air. Our study when combined with information on generation and distributions of pathogens could provide a prediction method and control strategy to minimize infection risk between persons in indoor environments.

© 2016 Elsevier Ltd. All rights reserved.

1. Introduction

Airborne infection has always been a worldwide concern for medical profession and building management professions. Many diseases including tuberculosis, influenza, measles, anthrax and meningitis could be transmitted via air in indoor environments [1]. The outbreaks of severe acute respiratory syndrome (SARS) in 2003 and H1N1 flu in 2009 have further increased concerns about the life-threatening transmission of aerosol infection [2].

Airborne diseases are spread when droplets of pathogens are expelled into the air during human exhalation [3,4]. To control and reduce the contamination risk of these infectious aerosols, many studies have been focusing on characterizing the dynamics of exhaled airflow and behaviors of aerosol containing droplets in indoor environments [5–40]. These studies on exhaled airflow behaviors are the first step to understand the potential of airborne

transmission and could provide a way to predict and control disease infection. In previous studies, detailed information on exhaled airflow dispersion as an indicator of potential airborne disease transmission have been investigated using three types of objects: human volunteers [11–18], breathing thermal manikins [19–27] and computer simulated persons (CSPs) [28–40]. Although studies based on breathing behaviors of manikins or CSPs can provide relatively comprehensive prediction of airflow patterns and infection prone zones, there could be errors with the use of these two techniques for prediction of real breathing conditions without a proper understanding of breathing characteristics of actual human subjects [13,16].

There has been little information on airflow dynamics of human exhalation. Chen and Zhao [37] reported that the initial exhaled velocity could greatly influence the dispersion of droplets in the range of 0.1 μm –200 μm in terms of trajectories and distances. To predict the evaporation, dispersion and transportation of respiratory droplets in indoor environment using Computational Fluid Dynamics (CFD), boundary conditions such as expelled airflow velocity are necessary [14]. Different techniques have been used to estimate exhaled velocities during different expiration behaviors

* Corresponding author. College of Pipeline and Civil Engineering, China University of Petroleum, Qingdao, 266580, China.

E-mail address: cxu@upc.edu.cn (C. Xu).

such as coughing, sneezing and breathing. Various results have been reported with different methods of study, providing little data in previous literature. Some studies [30,37] used approximate values of exhaled velocities produced during different respiratory activities (e.g. normal breathing 1 m/s, talking 5 m/s, coughing 10 m/s, and sneezing 20–50 m/s). Chao et al. [12] applied the particle image velocimetry (PIV) technique for measuring expelled velocities during coughing (11.7 m/s) and speaking (3.9 m/s). Tang et al. [16] used schlieren imaging technology to determine the maximum nasal and mouth breathing velocities of 1.4 m/s and 1.3 m/s, respectively. The maximum expiration air velocities for coughing and sneezing was found to be 4–5 m/s. Gupta et al. [13] developed a source modelling of air flow rate, flow direction and area of mouth/nose opening using human subjects for boundary settings for CFD simulations. Xu et al. [17] pointed out that even though the boundary settings complied with real human breathing characteristics, there could still be differences in the exhaled airflow of a complicated manikin than real persons. Similar problems could also occur in CSPs. The preclusion of using hazardous lasers, toxic tracer gases or particles on human subjects, which can otherwise be applied to the manikins, has so far limited research investigations and very little information on real breathing airflow has been provided. One method of studying real human exhaled airflow without the aid of hazardous techniques or materials is the use of schlieren photography [2,15,16].

Schlieren photography technique has been widely used in visualizing the flow of fluids of varying density, such as a gas jet [41], water jet [42] or flame jet [43]. Tang et al. [15,16] expanded this technique to quantify human exhaled airflow in order to assess their contamination potentials. Some other methods have been used in previous studies to achieve similar purpose, like the particle imaging velocimetry (PIV) [12,14] and using smoker subjects to visualize their breaths [13]. Schlieren imaging relies only on density differences to refract the light beam to visualize an airflow [44]. Human exhaled flow differs from the surrounding air in density, especially when air is immediately expelled from the mouth or nose [17,45]. No invasive or potentially irritant tracers are needed, so human volunteers are quite safe [2,15,16]. The implementation of schlieren imaging technique on human volunteers can further enhance our understanding of the behavior of real human respiration and the potential contamination risk of these breathing activities. The accuracy for the prediction of the transmission behavior could be further improved by using other additional techniques, such as CFD or breathing manikins, to provide a powerful tool for evaluating the infection risk of respiratory pathogens.

Infection risk assessment is very useful in understanding the transmission dynamics of infectious diseases and in predicting the risk of these diseases to the public, while a number of factors could also influence the transmission process and outcome [46], such as dispersion and distribution of airborne pathogens, ventilation strategies, droplet sizes, air turbulence etc.. These factors have contributed to the complexity of these exposure and risk assessment of infectious pathogens on human beings. The Wells–Riley model has been one of the most extensively used models for quantitative infection risk assessment of respiratory infectious diseases in indoor premises [47]. However, the Wells–Riley model assumes a uniform airborne pathogen distribution at a steady-state condition, which could yield errors in the assessment.

In our study, the respiratory activities between two human subjects were visualized using schlieren photography technique. The spatial variation and unsteady distribution of exhaled contaminants in the microenvironment between two persons are illustrated.

The goal of this present study is to characterize the dispersion of

human exhaled airflow by schlieren technique and provide accurate information in three aspects: flow shape, exhaled velocity and interactions of exhalations between two persons. This investigation could provide accurate information on boundary conditions of human breathing for CFD simulation and could be helpful to validate the accuracy of risk prediction of airborne disease transmission.

2. Methods and design

2.1. Schlieren experimental set-up

The schlieren imaging technique was used to visualize the real-time breathing process of human subjects. The temperature differences between the exhaled air (32–36 °C at the mouth or nose opening) [17] and the laboratory environment controlled at around 23 °C, would lead to a refraction of the light ray when passing through the media of different densities. The different components of exhaled air that have different densities to the room air would contribute to the refraction of light for our experimental investigation.

The schematic of the schlieren experimental setup is shown in Fig. 1. A standard schlieren structure with a beam splitter was constructed, consisting of a spherical concave mirror of astronomical telescope quality (0.61 m diameter and 7 m focal length) and a high-speed camera (Chameleon CMLN-13S2C, resolution of 1296 by 964 pixels). The breathing images were captured by a camera with a speed of 15 frames per second (fps) for a lasting of 2 min for each breathing pattern and these were downloaded to a laptop. The software, PointGrey FlyCap 2, installed on the laptop was used to control the high-speed camera remotely and download the shadowgraph images.

2.2. Characterization of breathing behavior of human subjects

The breathing characteristics of human subjects whilst standing and lying were investigated in this study. Fig. 2 shows the placement of a human subject in front of a concave mirror. The relative distance between the subject and the mirror would affect the size of these images. The reduced scale of these images were thence calibrated for every subject and every breathing pattern. In normal standing conditions, these human subjects were asked to stand approximately 0.5 m in front of and to one side of the mirror. A height-adjustable holder was used to support the subject's head in case of any movement during the experiment. A special bed with adjustable height was placed first in parallel and then perpendicular to the mirror, forming respectively a side and front view of a lying person to the observer as shown in Fig. 2. A soft cushion and a pillow were placed on the bed and a heavy quilt was used to cover the subject up to the neck position to block the thermal plume arising from the body and mimic the sleeping condition of a normal person to the most extent. The subject was asked to lie on the bed quietly for about 10 min before the experiment.

The basic information of 18 healthy young adults participated in the experiment is given in Table 1. All participants were of Chinese ethnicity. Three breathing modes were tested for both standing and lying postures: (a) nose breathing only; (b) inhaling through the nose and exhaling through the mouth and (c) mouth breathing only. These subjects were instructed to breathe naturally for a relatively long time (above 10 min) with each breathing pattern. However, these subjects constantly complained about their dry mouth due to saliva evaporation during their mouth only breathing with a nose clip restricting breathing from their nose. Interruption by shutting up their lips and saliva swallowing were permitted as a part of their breathing pattern. The camera recorded each breathing

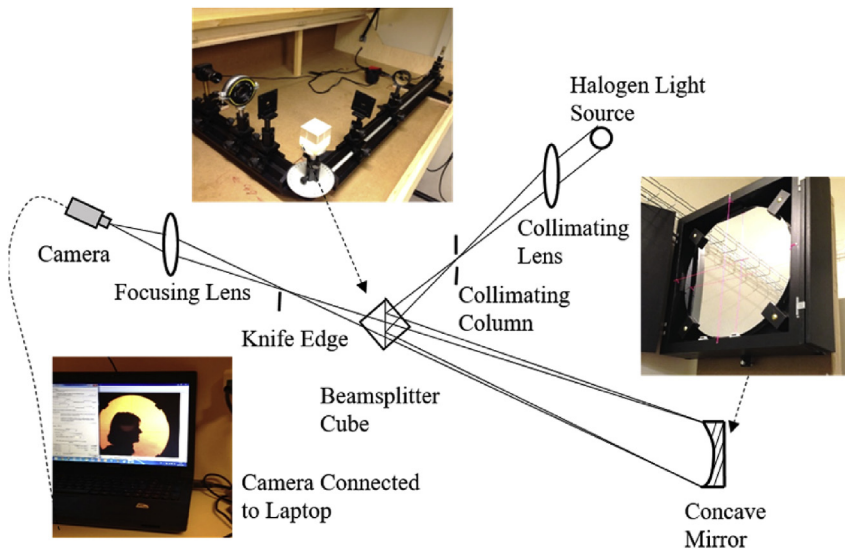


Fig. 1. Schematics of schlieren setup.

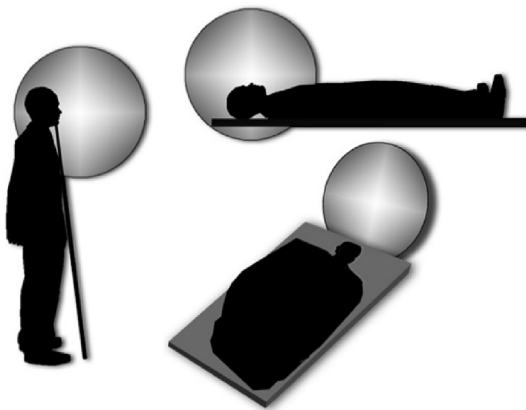


Fig. 2. A schematic diagram of the placement of a human subject in front of a mirror whilst standing and lying.

process for about 2 min without the subject realizing the beginning of the recording. When a subject was instructed to inhale through the nose and exhale through the mouth; the air from his or her lung was actually expelled from the nose and mouth simultaneously (see Appendix A), as the nasal and oral cavities are connected and air leaks into these cavities even when a person is not intended to exhale with his/her nose.

Supplementary video related to this article can be found at <http://dx.doi.org/10.1016/j.buildenv.2016.11.032>.

Table 1
Description details of subjects participated in the experiment.

	Male	Female
Subject no.	8	10
Age	29 (22–33)	28 (26–29)
Weight (kg)	69.7 (62.0–75.1)	52.9 (47.2–64.1)
Height (m)	1.74 (1.64–1.81)	1.63 (1.55–1.72)
BSA ^a (m ²)	1.83 (1.73–1.92)	1.55 (1.49–1.71)

^a BSA, body surface area.

2.3. Velocity measurement

2.3.1. Centerline velocity

In this study, a hot sphere anemometer (Dantec 54N50, DANTEC Dynamics A/S) with an accuracy of ± 0.01 m/s was placed near the mouth or nose opening to measure the initial velocity at a frequency of 10 Hz. The anemometer was calibrated in a standard jet-wind tunnel positioned in both horizontal and vertical directions, in the presence of 22 °C conditioned air.

The influence of exhaled air temperature and humidity on measurements was ignored in this work, which has been explained in Ref. [17]. A coordinate was built from the mouth/nose opening. For mouth breathing, the anemometer was horizontally placed in front of the mouth at a distance of about 0.03 m. When the person performed nose breathing, the anemometer was vertically placed approximately 0.03 m down to the nostrils. The variation in the position of the anemometer was adjusted by the movement of a robot arm and according with the schlieren photography to ensure that the probe would be exactly positioned within the exhaled airflow and close to the center of the airflow.

The determination of the centerline of the airflow is shown in Fig. 3. For mouth only breathing in standing posture, the velocity decays along the centerline. The mean peak air velocity at the centerline of the airflow was defined as u_m . In this study, the u_m at the nearest measuring points from the mouth/nose opening (around 0.03 m) was expressed as $u_{0.03}$ and was used to indicate the initial velocity of exhalation.

2.3.2. Propagation velocity

The visible propagation distance d was derived from schlieren images frame by frame along the centerline of exhaled flow. The propagation velocity, u_p , was expressed as $\Delta d / \Delta t$, in which Δt is the time interval. Note that d differs from x and x is the horizontal component of d , see Fig. 3.

3. Results and discussion

3.1. Flow shape characterization

3.1.1. Thermal plume around human body

The movement of body plume and exhaled air can be clearly

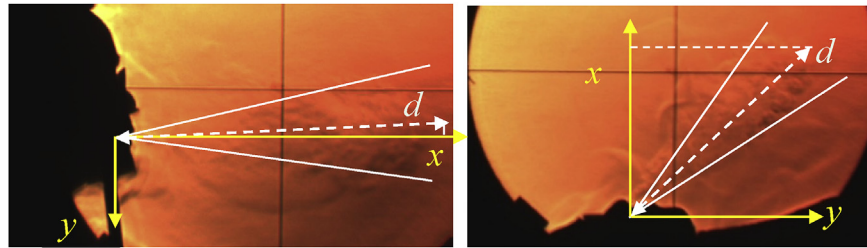


Fig. 3. Centerline of the exhaled airflow (dashed line) and propagation distance d .

observed with the aid of schlieren photography technique. For a standing person, the thermal plume would arise along the body height and continue to develop above the person's head. The plume velocity was measured using a hot-sphere anemometer placed along different vertical heights above the subject's head. The maximum velocity measured was approximate 0.23 m/s.

Murakami [28] and Melikov [48] indicated that the majority of inhaled air for a standing still person would be directly from the limited area below the nose (nose breathing) or the mouth (mouth breathing) and in the front part of the body. The rising thermal plume can be inferred to contribute to the inhaled air to a large extent for a standing person. Whilst the upward stream around the body collides with the expelled air, causing possible velocity decrement immediately at the mouth/nose opening when the exhaled plume enters the thermal boundary layer of the body [26,29].

A curved flow affected by the rising thermal plume, especially at low initial exhaled velocities was observed. For a person lying on his or her back, the plume would rise vertically from the exposed part of the body (i.e. head, face and neck) without the heavy quilt covering and then mix with the exhaled air. Comparing the airflow during the standing posture to the air movement with a person lying flat; the upward thermal stream could somehow accelerate the vertical movement of the exhaled airflow instead of blocking it. This was due to the identical dispersal direction of these flows.

3.1.2. Flow direction and development

Schlieren images within one breathing cycle for each subject were extracted from a series of high contrast images captured by the camera within a recording time of around 2 min. The extraction was conducted randomly among the 20–50 breaths (depending on breathing frequency) for each breathing pattern and each subject. These 2-D images were stacked together with a time interval of 1/15 s or 2/15 s to illustrate the development of exhaled flow within one breathing cycle as shown in Fig. 4. The boundaries of these exhaled flows were connected, forming a region that the exhalation could affect.

From Fig. 4, the expelled airflow was shown to be turbulent full of vortex rings and the periodic exhaled flow was shown to have similar characteristics with a constant jet in terms of flow shape. The width and length of the airflow was shown to grow with increasing distance from the origin by mixing with the surrounding air. Therefore, the velocity and concentration of exhaled contaminants could also be reduced by the development of the exhaled flow. There are obvious individual differences in the exhaled airflows in terms of flow shapes, propagation distances and dispersal directions.

The angles would be needed to define the breathing direction of a nose or mouth as shown in the side or front view in Fig. 4. These angles did not vary much among our human subjects. The measured breathing angles of male and female subjects were combined for our analysis. These breathing angles were measured

in each breathing pattern and have an approximately normal distribution verified by statistics (Statistical Product and Service Solutions, SPSS). Table 2 shows the average of these measured angles with a confidence limit of 95% and the confidence interval for the means was always tight with a maximum of 14°.

The direction of θ_1 for the side view condition was defined in Fig. 4(a–d). This was positive when the centerline of the airflow was below the x axis as shown in Fig. 4(a and b) or to the right of the x axis (Fig. 4(c and d)). Otherwise, θ_1 would be negative, which means the exhaled airflow would have an upward dispersal trend. For nose breathing, the averaged downward angle between nostrils and horizontal line was about 57°, and this corresponds with Gupta et al.'s average of 60° [13]. For mouth only breathing, most measurements were found with a downward flow trend with an averaged θ_1 of about 14°, even though in most conditions of the airflow in the mouth breathing was considered horizontal [12–14,19–24,28–35]. This might be due to the longitudinal asymmetry of the mouth cavity structure.

From Table 2, the θ_1 and θ_2 of the mouth only and nasal only breathing that were obtained from the side view did not vary much between different postures. As expected, the exhaled airflow from the nose or mouth was not a regular cone because the spreading angles of θ_2 that were observed respectively from the side and in front of the body are considerably different. The θ_2 is significantly wider in the front view than the side view in the lying posture. The value is also bigger than that obtained by Gupta et al. [13].

3.2. Velocity characterization

3.2.1. Initial exhaled velocity

Fig. 5 shows typical centerline velocity variations over time during moth only breathing of a subject. Because the hot sphere anemometer can only measure the velocity magnitude without direction, the measurements are always positive. Fig. 5 shows the repeated breaths of one male subject with a breathing frequency of about 10 min⁻¹ and variations of amplitudes of exhaled velocities over time. The peak value of each breath was extracted and then averaged for the definition of the mean peak velocity, u_m . The ratio, u_m'/u_m , of the standard deviation of amplitudes to the mean value was used to indicate the fluctuation degree of a person's breathing [17]. In this work, the $u_{0.03}'/u_{0.03}$ was at $x = 0.03$ m with a variation of merely 9% to about 160%, meaning that some people was breathing regularly and some did not. The irregularity of the breathing could further increase the turbulence degree of the exhaled air. This $u_{0.03}$ should be lower than the real initial velocity that was obtained from the immediate mouth/nose opening; as there could be velocity decay with increasing distance from the origin when the measured point did not fall within the constant velocity core [17].

The $u_{0.03}$ for the male and female subjects and their range values are given in Table 3. One main reason for the wide spread of measured velocities could be due to the wide variation in our

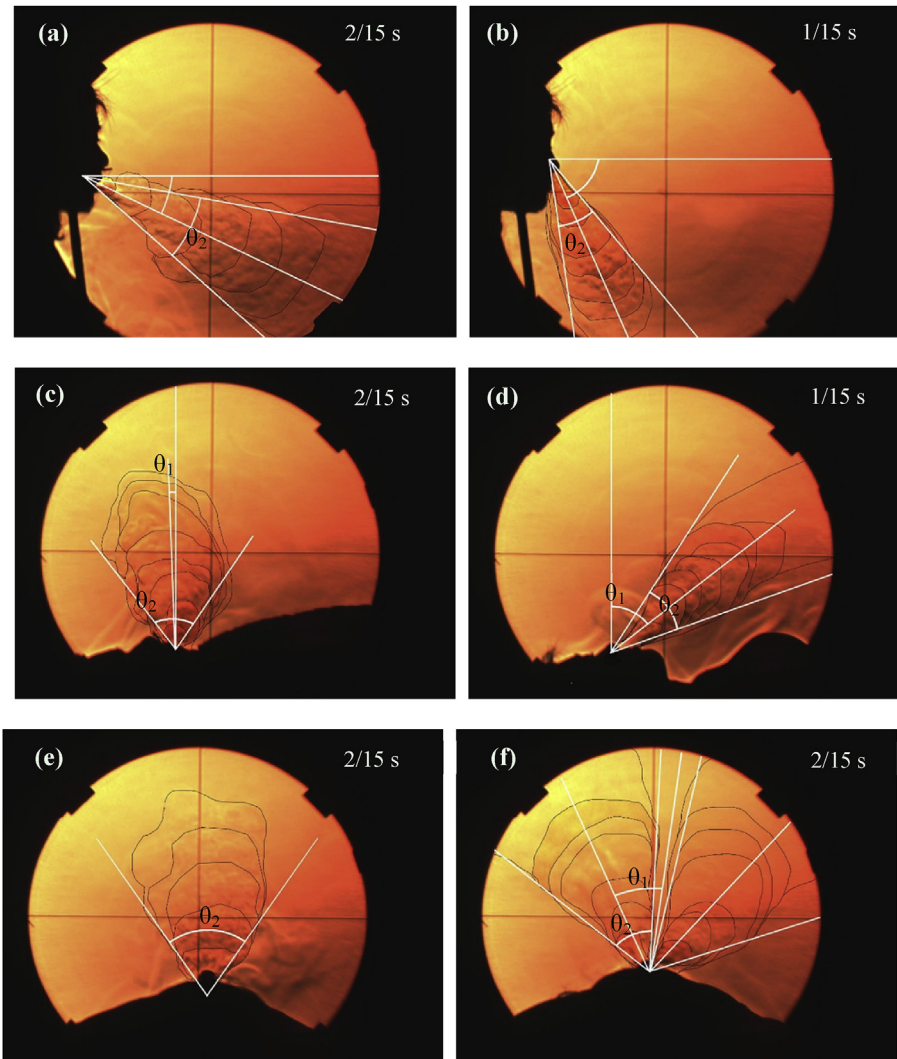


Fig. 4. Propagation of exhaled flow from the mouth only (left) or nose only breathing (right) whilst standing (a, b) and lying (c–f) viewing from the subject's side (a–d) and front (e, f) with a time interval of 1/15 s or 2/15 s.

Table 2

Average spreading angles of exhaled airflow with 95% confidence limit.

View angle	Breathing route	This study		Gupta et al. [13] ^a	
		θ_1	θ_2	θ_1	θ_2
Standing side view	Mouth only	$14^\circ \pm 14^\circ$	$36^\circ \pm 6^\circ$	\	30°
	Nose only	$57^\circ \pm 6^\circ$	$32^\circ \pm 3^\circ$	$60^\circ \pm 6^\circ$	$23^\circ \pm 14^\circ$
Lying side view	Mouth only	$9^\circ \pm 6^\circ$	$44^\circ \pm 7^\circ$	\	\
	Nose only	$51^\circ \pm 5^\circ$	$29^\circ \pm 3^\circ$	\	\
Lying front view	Mouth only	\	$61^\circ \pm 12^\circ$	\	\
	Nose only	$34^\circ \pm 8^\circ$	$43^\circ \pm 6^\circ$	$21^\circ \pm 8^\circ$	$21^\circ \pm 10^\circ$

^a These angles were measured by Gupta et al. [13]; both male and female volunteers were sedentary rather than in lying or standing position.

human subjects used in the current study. The physiological parameters of a person: exhaled minute volume (MV, the volume of exhaled air from a person's lungs per minute), breathing frequency (BF) and mouth/nose shape and area could contribute to the variation; and these could be different from person to person. In spite of smaller MV, the initial velocities of female subjects were shown to be higher than those of male subjects mainly due to higher RF and smaller mouth/nose opening [13,17]. The air leakages from the nose could result in relatively lower mean initial velocity from the

mouth when people inhale with their nose and exhaled with their mouth as shown in Table 3. Human postures could also affect the breathing by influencing the activity of abdominal muscle [13], but no significant relationship between postures and breathing velocities was found in our present study.

The mean value of $u_{0.03}$ was found to be even higher than the maximum breathing velocity measured from nose/mouth opening obtained by Tang et al. [16] by schlieren photography. The main reason of the deviation lies in different methods used to evaluate

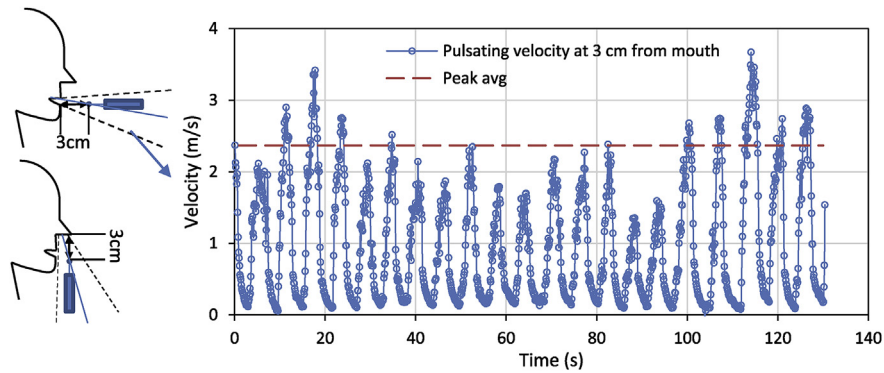


Fig. 5. Pulsating velocity measured during a subject's mouth only breathing. The mean peak velocity (red dashed line) is defined as u_m . (For interpretation of the references to colour in this figure legend, the reader is referred to the web version of this article.)

Table 3
The $u_{0.03}$ with range values for three breathing patterns.

Breathing patterns	Male		Female	
	Standing $u_{0.03}$ (m/s)	Lying $u_{0.03}$ (m/s)	Standing $u_{0.03}$ (m/s)	Lying $u_{0.03}$ (m/s)
Nose only	1.08 (0.45–2.00)	1.82 (1.00–2.52)	1.63 (0.34–2.58)	1.52 (0.9–2.27)
Nose in and mouth out	1.22 (0.31–2.27)	0.81 (0.31–1.55)	1.53 (0.36–2.80)	1.35 (0.46–2.25)
Mouth only	1.56 (0.95–2.03)	1.56 (0.67–2.02)	1.64 (0.50–2.63)	1.64 (0.40–3.22)

the exhaled velocity. Our study employed the mean peak velocity as depicted in Fig. 5, while Tang et al. [16] used the visible propagation distance divided by the propagation time as shown in Fig. 4. The latter method describes the propagation speed of the exhalation flow measured at the leading front edge of the flow within certain time interval rather than the initial pulsating flow generated by a person. This could also be the reason why velocities of sneezing and coughing reported by Tang et al. (4–5 m/s) [16] are significantly lower than the generally recognized velocities of sneezing and coughing (e.g. sneezing 20–50 m/s, coughing 10 m/s) [18]. The maximum propagation velocity obtained by quantification given by schlieren images should not be considered as the exhaled velocity as this might cause underestimation for boundary setting of CFD simulation. The propagation velocity of the exhaled airflow will be further discussed in Section 3.2.3.

3.2.2. Centerline peak velocity decay

Our previous study [17] found that u_m decayed with x in the form of a power function, as defined by Equation (1).

$$u_m = ax^b \tag{1}$$

The mean peak air velocity of female subjects' breathing from the mouth was found initially higher than that of male subjects; but the air velocity of females' breathing decayed more rapidly than the males' along the centerline [17]. In our work, different human subjects were used in the present study compared to the previous study to validate the applicability of the regression equation.

Fig. 6 shows that the u_m of mouth only breathing corresponds well with the regression equation reported [17]. The dashed line forms a region where scattered points of exhaled velocities could be located. As shown in Fig. 6, although the exhaled air velocity, u_m at $x = 0.4$ m for most human subjects was reduced to below 0.1 m/s; this was equivalent to the turbulence level of room air, and the exact maximum propagation distance of the exhaled flow would be difficult to determine. The regression equation would suggest a measurable u_m could continue well beyond the region where experimental data were collected, but this is likely to be an artifact

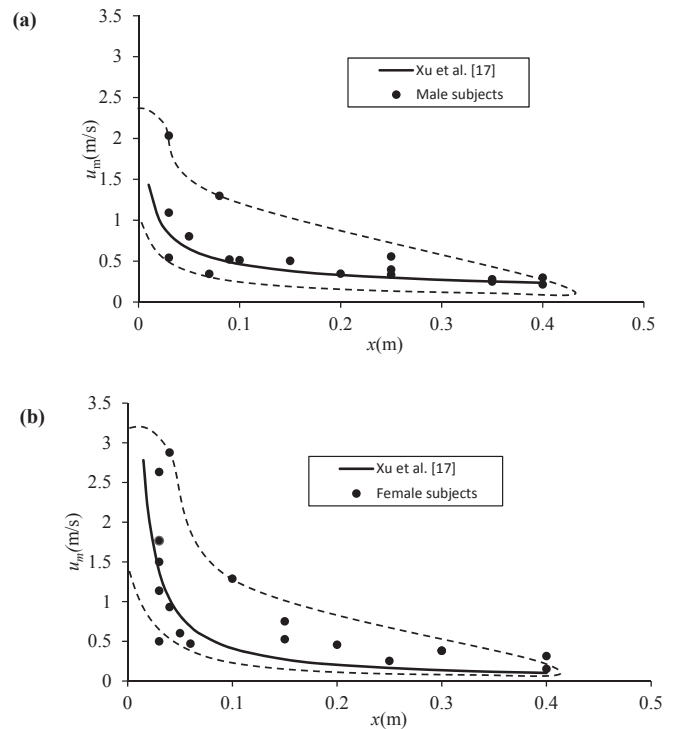


Fig. 6. Velocity decay along the centerline in the mouth only breathing for (a) male subjects and (b) female subjects.

of the fitted curve. Although Tang et al. [16] reported the observed maximum propagation distance of mouth only breathing and nose only breathing was 0.8 m and 0.6 m, respectively; it is still difficult to know exactly where the exhaled airflow should stop; if it stops, it must be dependent on the surrounding turbulence level of the airflow in the room.

Similar decay trends of CO₂ in the exhaled air were also found,

indicating a reduced exposure level of contamination to the receptor with increasing distance apart. Chen and Zhao [14] reported that the exhaled droplets with a diameter smaller than 10 μm could travel to some distance along in a room. The long-distance transportation of small droplets could largely dependent on turbulence level and air distribution in the room [49–54].

3.2.3. Propagation velocity

The propagation images obtained from side view, as shown in Fig. 4(a–d), were extracted and analyzed. The observed propagation distance was dependent on the temperature difference between the exhaled air and ambient air. However, to recognize the maximum propagation distance in this work is difficult due to the size limitation of the mirror and the resolution limitation. Hence, d was derived merely within the viewable area of the camera and the distinguishable propagation boundaries. This could result in some underestimation of the maximum propagation distance. Fig. 7 shows the visible propagation distance, which was increased correspondingly with time. The recognized maximum propagation distance was around 0.4 m, corresponding to the velocity decay distance shown in Fig. 6. Many equations were tested for the fitted curve but the linear one was found to perform the best (the R-square always above 0.97). The slope of the connected line of the propagation distance over time, that is the slope of the linear fitting equation, would be recognized as the averaged propagation velocity u_p within the observed time. Fig. 7 shows that u_p could vary among subjects and was always below 0.8 m/s; which was significantly lower than the measured $u_{0.03}$ given in Table 3.

Our determination of u_p was by the observable dissemination distance measured at the front end of the exhaled airflow within

the viewable area given by the camera. The maximum length of the airflow propagation could be even longer than the concave mirror boundary and could not be clearly visible. Despite the limitation of the schlieren imaging technique, the propagation velocity was still useful and valid for the prediction of exhaled flow dispersion speed [16]. These two velocities, u_m and u_p , should be clearly distinguished for use. The u_m was derived from certain measurement points along the centerline of the airflow, while the u_p was obtained by tracing the airflow movement to the leading front edge of the image of the exhaled air. From Fig. 7, u_p for our male subjects and female subjects in standing posture and with mouth only breathing, varied from 0.2 m/s to 0.6 m/s and from 0.3 m/s to 0.8 m/s, respectively, which is significantly lower than the u_m measured near the mouth opening (about 0.03 m). Even for the maximum u_p derived close to the mouth/nose opening [16], u_p was still lower than the mean peak velocity $u_{0.03}$ listed in Table 3. Fig. 8 shows that the front of a single exhalation cycle was similar to a vortex like airflow or to a puff. The peak exhaled air velocity u_m in a point close to the mouth was measured when the vortex airflow passed this point, and this was typically larger than the propagation velocity of the same vortex. This would be the typical situation for a vortex as illustrated by Akhmetov [55].

The u_p would be high when a person exhaled with high MV at a high BF. The u_p should be correlated to MV and BF. Robinson [56] and Gupta et al. [13] reported a linear relationship between MV and the body surface area (BSA). Regression analysis was performed to obtain the correlation between the u_p and the $\text{BSA} \times \text{BF}$. Fig. 9 shows that the u_p would be increased with an increase in $\text{BSA} \times \text{BF}$ for both genders. Fig. 9 also shows that the u_p was basically linear in relation to the $\text{BSA} \times \text{BF}$. A linear regression equation

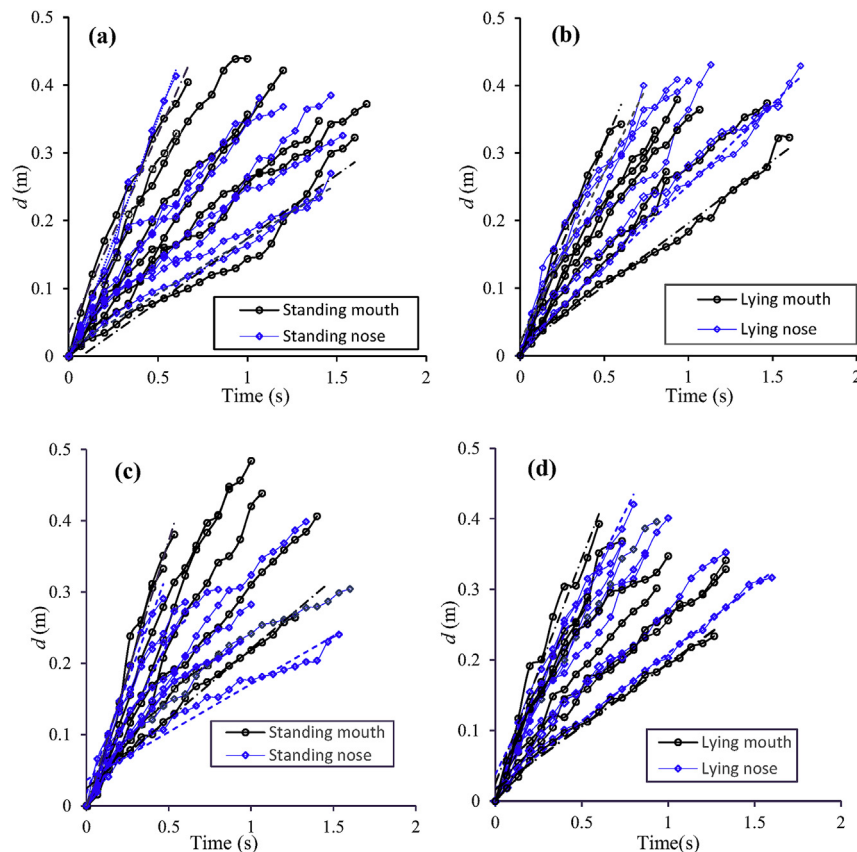


Fig. 7. Visible propagation distances of mouth only breathing and nose only breathing over time: (a) male, standing posture; (b) male, lying posture; (c) female, standing posture and (d) female, lying posture.

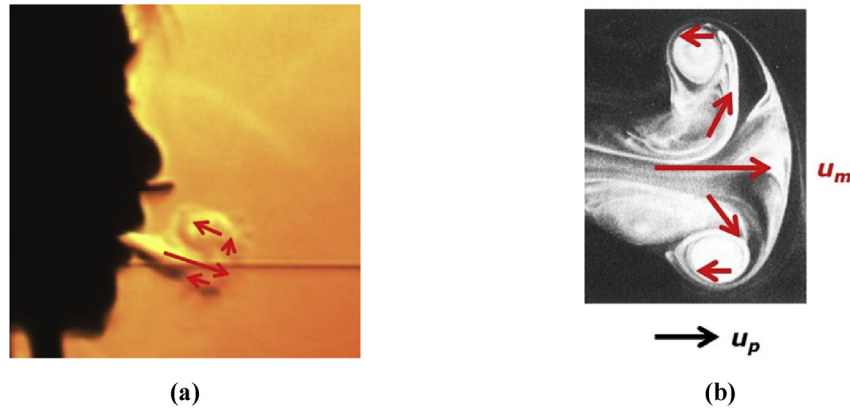


Fig. 8. Image of an exhalation airflow produced by a female subject (a) and details of the airflow in a vortex (b). The front of a single exhalation is typically corresponding to a vortex like flow and the peak velocity in the vortex is larger than the propagation velocity of the vortex.

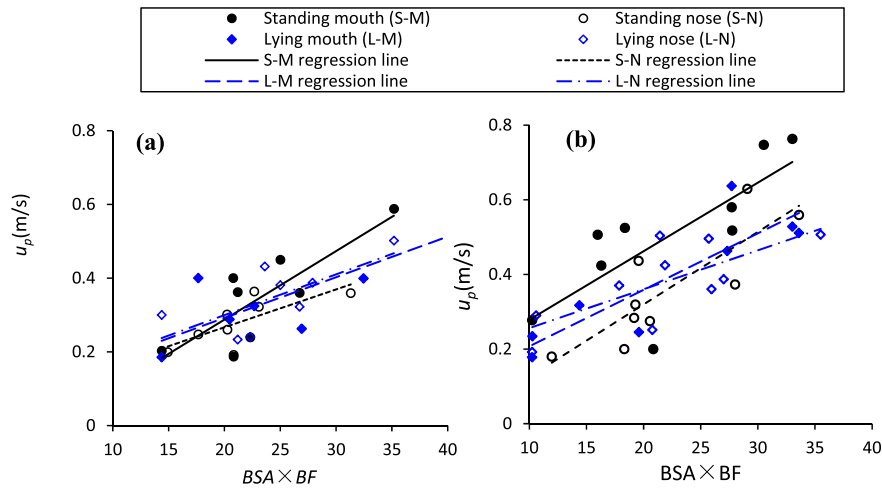


Fig. 9. Variation of u_p with $BSA \times BF$ of (a) the male subjects and (b) the female subjects.

was assumed as given by Equation (2). Table 4 gives the regression analysis results of the slope k , the correlation coefficient r and the t -test for r . The r for all test groups was found to be more than 0.7 for a $p < 0.05$, which shows that the u_p is linearly related to the $BSA \times BF$. However, due to the small number of points, the equation should be further validated by more measurements.

$$u_p \text{ (m/s)} = k \times BSA \text{ (m}^2\text{)} \times BF \text{ (min}^{-1}\text{)} \quad (2)$$

3.3. Infection prone zones between two persons

As respiratory infection cases are often transmitted due to obvious proximity relationship to the index case, to enable further understanding of the exposure risk of contamination between two persons, the exhaled flows generated by talking and breathing between two subjects were visualized and captured by the high speed camera.

The dispersion of the visualized exhaled flow would be recognized as an indicator of infection transmission especially for droplets smaller than $1 \mu\text{m}$ with good air following performance. As

Table 4
Regression analysis of u_p obtained by the defined Equation (1).

	Postures and breathing patterns	k	Correlation coefficient r	t -test	
				$t_r = \frac{r-0}{\sqrt{\frac{1-r^2}{n-2}}}$	$t_{0.025}$
Male	Standing mouth	0.019	0.82	3.52	2.45
	Standing nose	0.010	0.74	2.67	2.45
	Lying mouth	0.011	0.81	3.09	2.57
	Lying nose	0.011	0.71	2.45	2.45
Female	Standing mouth	0.018	0.76	3.06	2.36
	Standing nose	0.019	0.84	4.11	2.36
	Lying mouth	0.015	0.88	4.49	2.45
	Lying nose	0.010	0.73	3.00	2.31

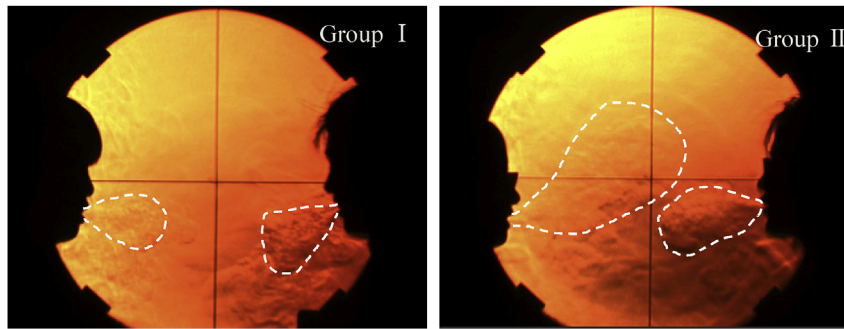


Fig. 10. Two pairs of female subjects performing mouth breathing.

airflow patterns could vary between subjects, flow interactions between two different pairs of female subjects (Group I - 0.34 m apart and Group II - 0.41 m apart) were studied, as illustrated in Fig. 10. These subjects were situated on the edge of the concave mirror. Their head positions were not fixed as in previous tests. Corresponding real-time video clips are shown in Appendix B.

Supplementary video related to this article can be found at <http://dx.doi.org/10.1016/j.buildenv.2016.11.032>.

During a free conversation, the exhaled airflows from two pairs of subjects was shown to be relatively short compared to mouth or nose only breathing. Air flows expelled from both nose and mouth during talking were observed and flow directions from the mouth varied due to the content of the conversation. Most of the time, expiration airflows from opposite subjects would remain separate and were brought up by a constantly rising thermal plume around their bodies (with a thickness of approximate 10 cm), although occasionally the flow was shown to interact with the receptor's thermal plume layer and interfered with the breathing zone. Mouth breathing (nose in and mouth out) was shown to have a higher potential to transmit diseases to receptor subject as the flow generated by mouth breathing could spread over a longer distance as compared with talking and are more horizontally directed than nose breathing.

For Group I, the female subject on the right hand side was shown to perform a downward mouth exhalation and the flow was shown to enter the breathing zone of opposite person. While for Group II, the upward flow from the person on the right side, was shown to directly bend up over the head of the opposite person without interacting with the breathing zone, demonstrating the potential of mouth-breathing to transmit infection, which could vary among individuals and also dependent on relative frequencies in an unsteady state.

From our analysis of the infectious prone zone between two persons using schlieren technique, the exposure level and hence the infectious risk posed by respiratory pathogens were not at a steady condition and always expected to have spatial variation. The spatial distribution of airborne pathogens would govern the exposure level of the receptor person. However, no existing models could predict the complicated disease transmission process and the infectious risk accurately by simply considering the spatial variation alone.

CFD would be a very promising tool to overcome existing shortcomings of current risk evaluation models and would provide useful information for infection control. Full understanding of respiratory characteristics of real human subjects could play an important role for accurate prediction using CFD simulation. More work should be done to enhance our understanding of flow dynamics of human breathing.

4. Conclusions

How airborne pathogens disperse and distribute in the room air could govern the exposure levels of susceptible persons to infectious diseases. Accurate prediction of airborne disease transmission and characterization of infection prone zones can aid infection control. This work characterized the exhaled airflow behaviors of human subjects and provided accurate boundary conditions for CFD simulations of human breathing or by using manikins. The main conclusions of this study are summarized as follows:

- The expelled air could interact with the constantly rising body plume from human subjects in different ways whilst standing or lying. The spreading angles of the exhaled plume was shown to have minimal variations between human subjects. The θ_1 and θ_2 of mouth and nasal breathing measured from side view were consistent in different postures with little variation. The measured mean angles obtained in our study could be used to describe the average level of the physical geometry of human breathing.
- The u_p and u_m could be used to describe the breathing velocity from different aspects. The u_p would be significantly lower than the measured initial velocity $u_{0.03}$. However, u_p would not be useful as velocity boundary condition for CFD settings as it could cause underestimation of the exhaled velocity. The u_m would decay with increasing horizontal distance along the centerline and the decay could be predicted by a power function. The mean u_p within the observed region was found to be correlated to human physiological parameters. Although the maximum propagation distance of exhaled airflow by measuring u_m or u_p would be difficult to determine, as the exhaled airflow over 0.4 m would interact with turbulent room air. We suggest more measurements with human subjects to validate the prediction method for the u_m and u_p .
- The interaction of exhaled airflows with opposite (facing) subjects could vary between subjects and breathing patterns, implying possible complexity in prediction of infectious risk exposure of human occupants in close proximity in room air. The information on spatial distribution of airborne pathogens in the microenvironment between two persons is particularly important for identifying and implementing infection control strategies.

Acknowledgement

This project was financially supported by the Fundamental Research Funds for the Central Universities (2014010588, 15C02041A), National Natural Science Foundation of China

(51378186), International S&T Cooperation Program of China (ISTCP) (2010DFB63830) and National Sci-Tech Support Plan (2015BAJ03B00). The authors thank Professor Chuck Yu for his language editing and his helpful comments particularly in the revision of the conclusion section.

References

- [1] J.S. West, S.D. Atkins, J. Emberlin, B.D.L. Fitt, PCR to predict risk of airborne disease, *Trends Microbiol.* 16 (2008) 380–387.
- [2] J.W. Tang, Investigating the airborne transmission pathway - different approaches with the same objectives, *Indoor Air* 25 (2015) 119–124.
- [3] L. Morawska, Droplet fate in indoor environments, or can we prevent the spread of infection? *Indoor Air* 16 (2006) 335–347.
- [4] J.W. Tang, C.X. Gao, B.J. Cowling, G.C. Koh, D. Chu, C. Heilbronn, B. Lloyd, J. Pantelic, A.D. Nicolle, C.A. Klettner, J.S.M. Peiris, C. Sekhar, D.K.W. Cheong, K.W. Tham, E.S.C. Koay, W. Tsui, A. Kwong, K. Chan, Y. Li, Absence of detectable influenza RNA transmitted via aerosol during various human respiratory activities—experiments from Singapore and Hong Kong, *Plos One* 9 (2014) e107338–e107338.
- [5] F.B. Wurie, S.D. Lawn, H. Booth, P. Sonnenberg, A.C. Hayward, Bioaerosol production by patients with tuberculosis during normal tidal breathing: implications for transmission risk, *Thorax* 71 (2016) 549–554.
- [6] X. Xie, Y. Li, A.T.Y. Chwang, P.L. Ho, W.H.W. Seto, How far droplets can move in indoor environments - revisiting the Wells evaporation–falling curve, *Indoor Air* 17 (2007) 211–225.
- [7] J.W. Tang, C.J. Noakes, P.V. Nielsen, I. Eames, A. Nicolle, Y. Li, G.S. Settles, Observing and quantifying airflows in the infection control of aerosol- and airborne-transmitted diseases: an overview of approaches, *J. Hosp. Infect.* 77 (2011) 213–222.
- [8] S.W. Zhu, J. Srebric, J.D. Spengler, P. Demokritou, An advanced numerical model for the assessment of airborne transmission of influenza in bus microenvironments, *Build. Environ.* 47 (2012) 67–75.
- [9] M. King, C.J. Noakes, P.A. Sleight, M.A. Camargo-Valero, Bioaerosol deposition in single and two-bed hospital rooms: a numerical and experimental study, *Build. Environ.* 59 (2013) 436–447.
- [10] I. Goldasteh, Y.L. Tian, G. Ahmadi, A.R. Ferro, Human induced flow field and resultant particle resuspension and transport during gait cycle, *Build. Environ.* 77 (2014) 101–109.
- [11] R.S. Papineni, F.S. Rosenthal, The size distribution of droplets in the exhaled breath of healthy human subjects, *J. Aerosol Med.* 10 (1997) 105–116.
- [12] C.Y.H. Chao, M.P. Wan, L. Morawska, G.R. Johnson, Z.D. Ristovski, M. Hargreaves, K. Mengersen, S. Corbett, Y. Li, X. Xie, D. Katoshevski, Characterization of expiration air jets and droplet size distributions immediately at the mouth opening, *J. Aerosol Sci.* 40 (2009) 122–133.
- [13] J.K. Gupta, C.-H. Lin, Q. Chen, Characterizing exhaled airflow from breathing and talking, *Indoor Air* 20 (2010) 31–39.
- [14] S.-B. Kwon, J. Park, J. Jang, Y. Cho, D.-S. Park, C. Kim, G.N. Bae, A. Jang, Study on the initial velocity distribution of exhaled air from coughing and speaking, *Chemosphere* 87 (2012) 1260–1264.
- [15] J.W. Tang, A.D.G. Nicolle, J. Pantelic, M. Jiang, C. Sekhr, D.K.W. Cheong, K.W. Tham, Qualitative Real-Time Schlieren and Shadowgraph Imaging of human exhaled airflows: an aid to aerosol infection control, *PLoS One* 6 (2011) e21392.
- [16] J.W. Tang, A.D. Nicolle, C.A. Klettner, J. Pantelic, L. Wang, A. Bin Suhaimi, A.Y.L. Tan, G.W.X. Ong, R. Su, C. Sekhar, D.D.W. Cheong, K.W. Tham, airflow dynamics of human jets: sneezing and breathing - potential sources of infectious aerosols, *PLoS One* 8 (2013) e59970.
- [17] C. Xu, P.V. Nielsen, G. Gong, L. Liu, R.L. Jensen, Measuring the exhaled breath of a manikin and human subjects, *Indoor Air* 25 (2015) 188–197.
- [18] C. Chen, C. Lin, Z. Jiang, Q. Chen, Simplified models for exhaled airflow from a cough with the mouth covered, *Indoor Air* 24 (2014) 580–591.
- [19] E. Bjørn, P.V. Nielsen, Dispersal of exhaled air and personal exposure in displacement ventilated rooms, *Indoor Air* 12 (2002) 147–164.
- [20] H. Qian, Y. Li, P.V. Nielsen, C.E. Hyltdgaard, T.W. Wong, a T.Y. Chwang, Dispersion of exhaled droplet nuclei in a two-bed hospital ward with three different ventilation systems, *Indoor Air* 16 (2006) 111–128.
- [21] I. Olmedo, P.V. Nielsen, M. Ruiz de Adana, R.L. Jensen, P. Grzelecki, Distribution of exhaled contaminants and personal exposure in a room using three different air distribution strategies, *Indoor Air* 22 (2012) 64–76.
- [22] I. Olmedo, P.V. Nielsen, M.R. de Adana, R.L. Jensen, The risk of airborne cross-infection in a room with vertical low-velocity ventilation, *Indoor Air* 23 (2013) 62–73.
- [23] X. Li, K. Inthavong, J. Tu, Numerical investigation of micron particle inhalation by standing thermal manikins in horizontal airflows, *Indoor Built Environ.* 15 (2014) 299–304.
- [24] D. Licina, A. Melikov, J. Pantelic, C. Sekhar, K.W. Tham, Human convection flow in spaces with and without ventilation: personal exposure to floor-released particles and cough-released droplets, *Indoor Air* 25 (2014) 952–958.
- [25] C. Yang, X. Yang, B. Zhao, The ventilation needed to control thermal plume and particle dispersion from manikins in a unidirectional ventilated protective isolation room, *Build. Simul.* 8 (2015) 1–15.
- [26] C. Xu, P.V. Nielsen, G. Gong, R.L. Jensen, L. Liu, Influence of air stability and metabolic rate on exhaled flow, *Indoor Air* 25 (2015) 198–209.
- [27] L. Feng, S. Yao, H. Sun, N. Jiang, J. Liu, TR-PIV measurement of exhaled flow using a breathing thermal manikin, *Build. Environ.* 94 (2015) 683–693.
- [28] S. Murakami, Analysis and design of micro-climate around the human body with respiration by CFD, *Indoor Air* 14 (Suppl.7) (2004) 144–156.
- [29] N.P. Gao, CFD study of the thermal environment around a human body: a review, *Indoor Built Environ.* 14 (2005) 5–16.
- [30] N.P. Gao, J.L. Niu, Modeling particle dispersion and deposition in indoor environments, *Atmos. Environ.* 41 (2007) 3862–3876.
- [31] Q. He, J. Niu, N. Gao, T. Zhu, J. Wu, CFD study of exhaled droplet transmission between occupants under different ventilation strategies in a typical office room, *Build. Environ.* 46 (2011) 397–408.
- [32] J.K. Gupta, C.-H. Lin, Q. Chen, Risk assessment of airborne infectious diseases in aircraft cabins, *Indoor Air* 22 (2012) 388–395.
- [33] J.M. Villafrauela, I. Olmedo, M. Ruiz de Adana, C. Méndez, P.V. Nielsen, CFD analysis of the human exhalation flow using different boundary conditions and ventilation strategies, *Build. Environ.* 62 (2013) 191–200.
- [34] C. Chen, C.H. Lin, Z. Long, Q. Chen, Predicting transient particle transport in enclosed environments with the combined computational fluid dynamics and Markov chain method, *Indoor Air* 24 (2014) 81–92.
- [35] J.M. Villafrauela, I. Olmedo, J.F.S. José, Influence of human breathing modes on airborne cross infection risk, *Build. Environ.* 106 (2016) 340–351.
- [36] J. Hang, Y. Li, R. Jin, The influence of human walking on the flow and airborne transmission in a six-bed isolation room: tracer gas simulation, *Build. Environ.* 77 (2014) 119–134.
- [37] C. Chen, B. Zhao, Some questions on dispersion of human exhaled droplets in ventilation room: answers from numerical investigation, *Indoor Air* 20 (2010) 95–111.
- [38] S. Zhai, Z. Li, B. Zhao, State-space analysis of influencing factors on airborne particle concentration in aircraft cabins, *Build. Environ.* 74 (2014) 13–21.
- [39] J. Hang, Y. Li, W.H. Ching, J. Wei, R. Jin, L. Liu, X. Xie, Potential airborne transmission between two isolation cubicles through a shared anteroom, *Build. Environ.* 89 (2015) 264–278.
- [40] S. Mazumdar, Z. Long, Q. Chen, A coupled computational fluid dynamics and analytical model to simulate airborne contaminant transmission in cabins, *Indoor Built Environ.* 23 (7) (2014) 946–954.
- [41] C.C. Ting, C.C. Chen, Detection of gas leakage using microcolor schlieren technique, *Meas. J. Int. Meas. Confed.* 46 (2013) 2467–2472.
- [42] T. Rothenfluh, M.J. Schuler, P.R. Von Rohr, Penetration length studies of supercritical water jets submerged in a subcritical water environment using a novel optical Schlieren method, *J. Supercrit. Fluids* 57 (2011) 175–182.
- [43] Y. Wang, Y. Zhang, Simultaneous high speed schlieren and direct imaging of ignition process with digitally enhanced visualisation, *Energy Procedia* 66 (2015) 241–244.
- [44] A. Braeuer, Chapter 4-Shadowgraph and schlieren techniques, *Supercrit. Fluid Sci. Technol.* 7 (2015) 283–312.
- [45] P. Höppe, Temperatures of expired air under varying climatic conditions, *Int. J. Biometeorol.* 25 (2) (1981) 127–132.
- [46] G.N. Sze To, C.Y.H. Chao, Review and comparison between the Wells-Riley and dose-response approaches to risk assessment of infectious respiratory diseases, *Indoor Air* 20 (2010) 2–16.
- [47] W.F. Wells, Airborne Contagion and Air Hygiene. An Ecological Study of Droplet Infections, Harvard University Press, Cambridge, MA., 1955.
- [48] A.K. Melikov, Human body micro-environment: the benefits of controlling airflow interaction, *Build. Environ.* 91 (2015) 70–77.
- [49] C.A. Gilkeson, M.A. Camargo-Valero, L.E. Pickin, C.J. Noakes, Measurement of ventilation and airborne infection risk in large naturally ventilated hospital wards, *Build. Environ.* 65 (2013) 35–48.
- [50] J. Fiser, M. Jicha, Impact of air distribution system on quality of ventilation in small aircraft cabin, *Build. Environ.* 69 (2013) 171–182.
- [51] C. Habchi, K. Ghali, N. Ghaddar, A. Shihadeh, Chair fan-enhanced displacement ventilation for high IAQ: effects on particle inhalation and stratification height, *Build. Environ.* 84 (2015) 68–79.
- [52] H.C. Yu, K.W. Mui, L.T. Wong, H.S. Chu, Ventilation of general hospital wards for mitigating infection risks of three kinds of viruses including middle east respiratory syndrome coronavirus, *Indoor Built Environ.* (2016), <http://dx.doi.org/10.1177/1420326X16667177> (accepted).
- [53] A. Kokkonen, M. Hyytinen, R. Holopainen, K. Salmi, P. Pasanen, Performance testing of engineering controls of airborne infection isolation rooms by tracer gas techniques, *Indoor Built Environ.* 23 (7) (2014) 994–1001.
- [54] Q. Zhou, H. Qian, L. Liu, Numerical investigation of airborne infection in naturally ventilated hospital wards with central-corridor type, *Indoor Built Environ.* (2016), <http://dx.doi.org/10.1177/1420326X16667177> (accepted).
- [55] D.G. Akhmetov, Vortex Rings, Springer, Verlag Berlin Heidelberg, Berlin, 2009.
- [56] S. Robinson, Experimental studies of physical fitness in relation to age, *Eur. J. Appl. Physiol.* 10 (1938) 251–323.

APPENDIX E.

IMPACTS OF AIRFLOW INTERACTIONS WITH THERMAL BOUNDARY LAYER ON PERFORMANCE OF PERSONALIZED VENTILATION

The paper presented in Appendix D is submitted to Building and Environment

Ref. No. BAE-D-18-00024



Impacts of airflow interactions with thermal boundary layer on performance of personalized ventilation

Chunwen Xu^{a,b,*}, Peter V. Nielsen^b, Li Liu^{b,c}, Rasmus L. Jensen^b,
Guangcai Gong^d

^a College of Pipeline and Civil Engineering, China University of Petroleum, Qingdao 266580, China

^b Department of Civil Engineering, Aalborg University, Aalborg 9000, Denmark

^c School of Environmental and Municipal Engineering, Xi'an University of Architecture and Technology, Xi'an 710055, China

^d College of Civil Engineering, Hunan University, Changsha 410082, China

*Corresponding author. Tel.: +86 18661723972; fax: +86

053286980022

E-mail address: cxu@upc.edu.cn (C. Xu)

Abstract

The flow interactions between the personalized air and the thermal boundary layer (TBL) may play an important role to the inhaled air quality and energy efficiency performance of a personalized ventilation (PV) system. This paper aims to investigate these interactions and their impacts on the performance of a PV system. Schlieren imaging technique, Laser Doppler Anemometry (LDA) and tracer gas measurements are employed to identify the airflow patterns in the breathing zone (BZ) and the effect of the interactions on ventilation effectiveness. Although it has always been considered that it is difficult for a PV jet of low flow rate to penetrate the TBL, it is found in this study that the TBL is penetrable even at invading velocities lower than the normally recognized value of 0.3 m/s. The advantage of the reduced blockage effect allows for a more effective delivery of fresh air to the BZ. It is also shown that the airflow

interactions alter the airflow distributions in the BZ and affect the inhaled air quality. This interaction depends on the positioning and direction of the non-uniform invading flow from the nozzle, which should be carefully considered for optimal ventilation design to enhance the effectiveness of ventilation at relatively low energy consumptions.

Keywords: thermal boundary layer; personalized ventilation; penetration; ventilation effectiveness; inhaled air quality; energy efficient

1. Introduction

Personalized ventilation (PV) is a promising air distribution approach to deliver clean air directly to occupants' breathing zone (BZ), improving inhaled air quality, reducing contaminant exposure risk [1-4]. Individual control of personalized air supply may increase the occupant satisfaction. The PV systems can also reduce energy consumption and achieve the same BZ air quality as obtained with conventional ventilation systems such as mixing or displacement ventilation systems [5-10].

The design intent of a PV system is to achieve effective localization thermal comfort and indoor air quality (IAQ) at minimal energy cost. The usage of PV system will permit to confine the conditioned air just around each occupant separately thus allowing for considerable energy saving. Yang et al. [5] reported 5% energy saving of a ceiling PV when compared to a mixing ventilation system that maintains almost equal thermal comfort and fresh air supply. Makhoul et al. [9] found that the ceiling PV system of Yang et al. [5] assisted with desk-mounted fans for reducing the convection thermal plume around the occupant induced considerable energy savings of 13% compared to mixing ventilation for equivalent thermal comfort and IAQ in terms of CO₂ in a space. Habchi et al. [10] optimized the ceiling PV combined with desk fans and achieved enhanced IAQ at significant decrease in the energy consumption. Greater efficiency in the ventilation systems and reduced fresh air supply lead to energy and cost savings of the ventilation facilities. However, it has always been a concern that personalized airflow may not be able to penetrate the free thermal boundary layer (TBL) around human body at low invading velocities

or flow rates [1,13]. The constantly rising TBL, caused by temperature difference between the human body surface and cooler surrounding air, may deflect the low-velocity personalized jet upwards and prevent it delivering clean air to the BZ. This possible problem of PV could be against the previously mentioned advantages, resulting in low efficiency and potential high energy cost maintaining of the required BZ air quality by the increasing the PV flow rate. On the other hand, compared with substantial information on PV system configurations and placement options [4-8,11-13], little is known about the nature of the flow interactions between the personalized air and the TBL[14-19], which are essential to IAQ, thermal comfort and energy consumption of the ventilation system. Bolashikov et al. [14] indicated a minimum velocity needed for complete penetration is 0.3 m/s for flow directly against face. An airflow of 6 l/s supplied from the front was reported to be able to penetrate the TBL, while personalized jet at the lower flow rate could not reach the BZ [15]. Licina et al. [16] investigated how surrounding airflow patterns (assisting, opposing or transverse to TBL) in the occupied spaces affect the development of the TBL and found that uniform horizontal flow disturbs the TBL at the BZ even at 0.175 m/s. These studies investigated the airflow interactions only in terms of mean velocity profiles in the BZ by using PIV system and did not focus on how the flow interactions affect the inhaled air quality. The manikin in their study was also not state-to-art as its inhalation was not considered. While due to the disturbance that invading flow exerts over the TBL, the flow in the BZ can be highly turbulent and it is hard to estimate the penetration extent by merely velocity measurements and meanwhile without considering the breathing process.

The interaction is affected by numerous factors: strength of the TBL, metabolic rate and activities of the person, PV flow rate, direction, temperature and turbulence intensity, etc. In practice, two ways are normally suggested to enhance the penetration [3,9,10,15]: (a) to increase the PV flow rate and (b) to decrease the strength the TBL at the BZ. The first way may cause increased energy consumption and eye irritation or draught risk for occupants. The second way can be realized by blocking the development of the body plume with barriers or decreasing the temperature gradients between the body surface and the surrounding air. Melikov [1] indicated that

the highest ventilation efficiency of PV is obtainable when the clean personalized air penetrates the TBL with minimum entrainment of polluted room air. The interaction of the personalized flow with the thermal plume around human body is therefore an important consideration for the performance of PV system. However, little information has been provided by previous literatures to understand how the interaction between these flows influences the performance of a PV system.

The objective of this paper is twofold: (1) to elucidate the possible challenge associated with the use of low supply flow by the PV system that may have difficulty penetrating the TBL; (2) to investigate the impacts of the interactions between the TBL and the PV flow on the performance of the PV system. Experiments are conducted in a full-scale room equipped with diffuse ceiling ventilation. Schlieren imaging technique is employed for this study to characterize the turbulent flow interactions, complemented with velocity measurement by LDA, which will provide both qualitative and quantitative information for the TBL and PV flow investigations. The inhaled air quality is evaluated by an index derived from ventilation effectiveness by means of measuring the BZ concentration of tracer gas. Findings of this study contribute to the knowledge of how the PV jet interacts with human TBL and the improvement of efficiency of personalized ventilation.

2. Methods and design

2.1 Experimental set-up

Measurements were performed in a full-scale chamber equipped with diffuse ceiling ventilation. It is divided by the diffuse ceiling into two zones: the plenum (4.8 m×3.3 m×0.35 m) and the working zone (4.8 m×3.3 m×2.4 m). The facade of the chamber is constructed by highly insulated wooden structures with a thickness of 0.33 m. The heat transmission coefficient for the double glazing windows is measured as 0.71 W/(m²·K).

A desk and a sedentary thermal manikin (TM) were placed in the working zone to simulate a typical work place. Fig. 1 shows the vertical section view of the test chamber. The cement-bounded wood wool panels, penetrable to air, with a thickness of 0.035m, are constructed as the diffuse ceiling to separate the two different functional zones and distribute air uniformly. The general ventilation

air is supplied through an upper opening, enters the plenum for circulation and then goes through the ceiling-mounted diffuse panels into the working zone. The exhaust is located in the lower corner of the facade with a diameter of 0.16 m. It is connected to an orifice plate and a frequency variable fan. The volume of the general ventilated air is controlled by a valve mounted on the exhaust duct and measured by a micro manometer connected to the orifice plate. Similar setup was also applied to the PV supply ducting, as shown in Fig. 1. The fan, creating a pressure difference between the chamber and the outside, produces driving force of the air circulation. The circulated air is exhausted through the building exhaust ducting. Six vertical columns, containing 7 thermocouples (type K, accuracy ± 0.15 °C) and 6 anemometers (Dantec 54N10, accuracy ± 0.01 m/s) for each, placed along the axes of the chamber were used to measure the air temperature and velocity distributions in both vertical and horizontal directions. It is found that the temperature gradients along vertical height are negligible under mixing ventilation induced from the diffuse ceiling. The temperature is basically uniform in the working space, which is slightly higher close to the TM. The velocity generated by the general ventilation system in the test chamber is below 0.06 m/s, except for higher measured value in the vicinity of the diffuse ceiling of around 0.13 m/s. Relevant description of the test chamber with diffuse ceiling and test probes can be found elsewhere [20,21].

The personalized ventilation nozzle was designed to have a nozzle diameter of 50.8 mm and a tube diameter of 83.0 mm, with a length 160 mm, which is slightly different from the dimensions in literature [13]. The nozzle was aligned with the manikin, with the nose tip 0.4 ~ 0.8 m away from the nozzle exit. Fresh air from outdoor was supplied through PV ducting to the manikin's BZ. The PV flow rate were measured and adjusted, with a minimum value of 1.5 l/s, which is lower than the amount of clean air recommended per person by ANSI/ASHRAE Standard 62.1-2004 [22]. However, a lower flow rate would present a more challenging condition for the PV jet to penetrate the TBL. Due to the flow acceleration in the convergent nozzle, and with the aids of two honeycomb flow straighteners placed in the upstream of the nozzle, the measured turbulence intensity at the nozzle exit was considerably low, with a maximum value of 5% for 1.5 l/s.

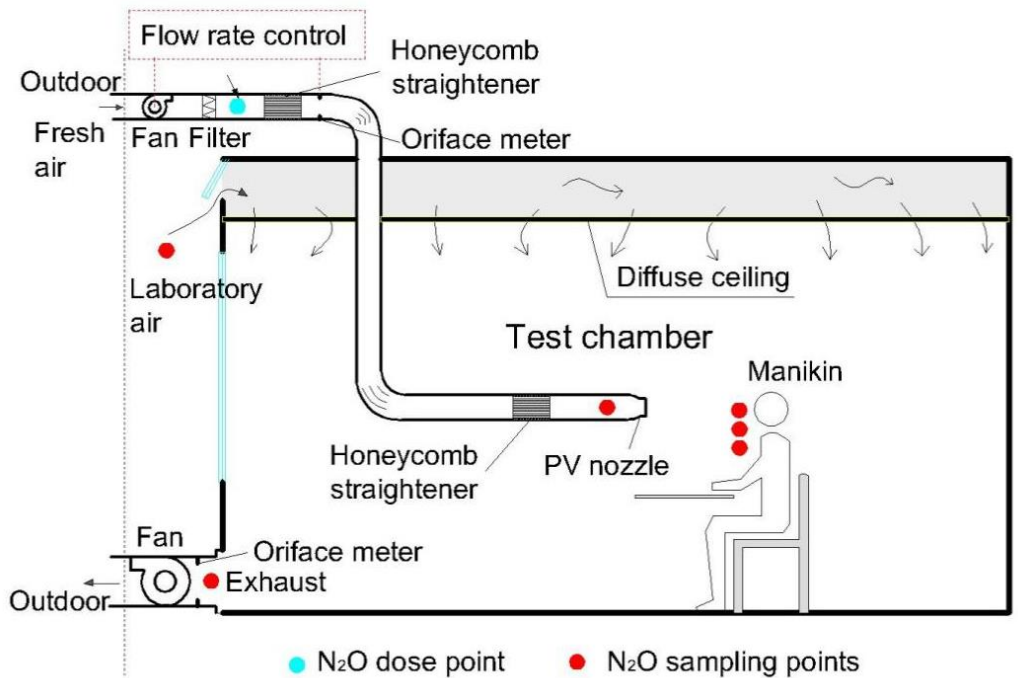
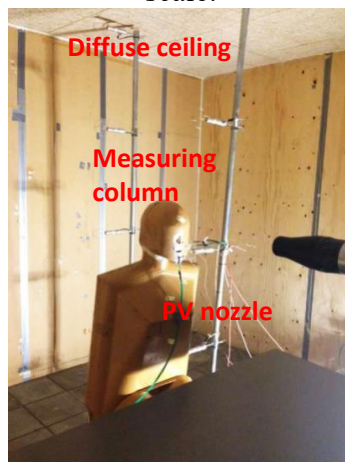


Fig. 1. Experimental set-up of the test chamber. The drawing is not to scale.



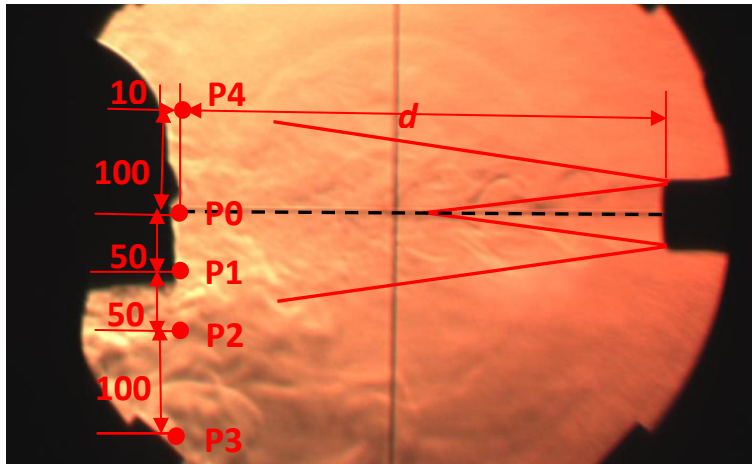


Fig.2 Relative position between the nozzle and the manikin. The centerline of the nozzle is pointing to the nose point P0 which is 10 mm away from the face. Velocities at P0~P4 are measured by the LDA. Tracer gas concentration, c , was measured at P0~P2 for test cases without manikin and for cases with manikin the c is measured in the tube connected to the artificial lung and at P1 and P2. Units of the drawings are in millimeter.

The TM represents 1.68 m tall female as shown in Fig. 2. The manikin was nude and assigned seated upright in a wooden chair. During the measurements, the manikin was placed 0.12 m away from the front table edge. The heat flux of the manikin body was controlled to a desired set point at a metabolic rate of 1.2 met, corresponding to a sedentary female for light office work [23]. The latent heat release was neglected and the detailed calculation process of the total heat input for the manikin with a metabolic rate of 1.2 met can be found in Xu et al. [24,25]. The manikin's skin temperature was measured at an average value of 30.1 °C and the average plume velocity near the face was measured as 0.18 m/s in calm indoor environment. To test the inhaled air quality, the manikin was attached to an artificial lung to perform nose breathing (breathing frequency 10 min⁻¹, minute volume 6 l/min, exhalation disabled).

2.2 Measuring facilities and design

The real-time schlieren technique was applied in this study to visualize the dynamic development process of the nozzle jet and the turbulent interactions between it and the rising thermal plume. The

structure of the optical system was in consistent with the one used in literature [26]. The underlying principle of shadowgraph imaging relies on light passing through air of different temperatures, which have differing refractive indices. Cooler nozzle jet and warmer thermal plume around the body than the ambient air produce light refractions and would be visible in the camera. One example of the PV nozzle supplying air to a male subject is given in Fig. 3.

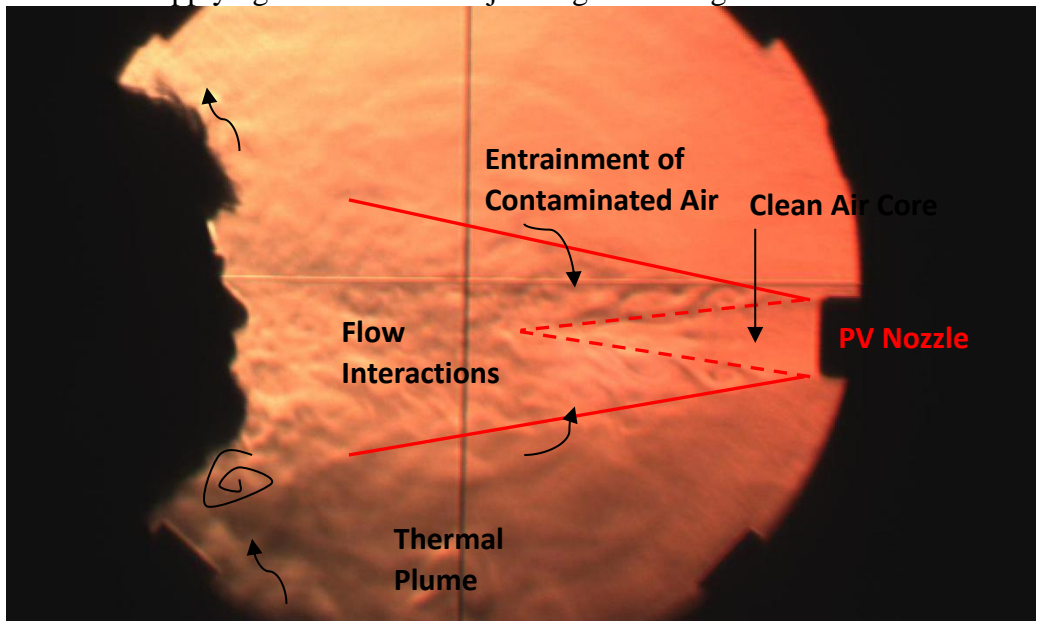


Fig. 3. Schlieren image of the flow interactions between a male subject and the PV jet. A real-time video can be found in the supporting information.

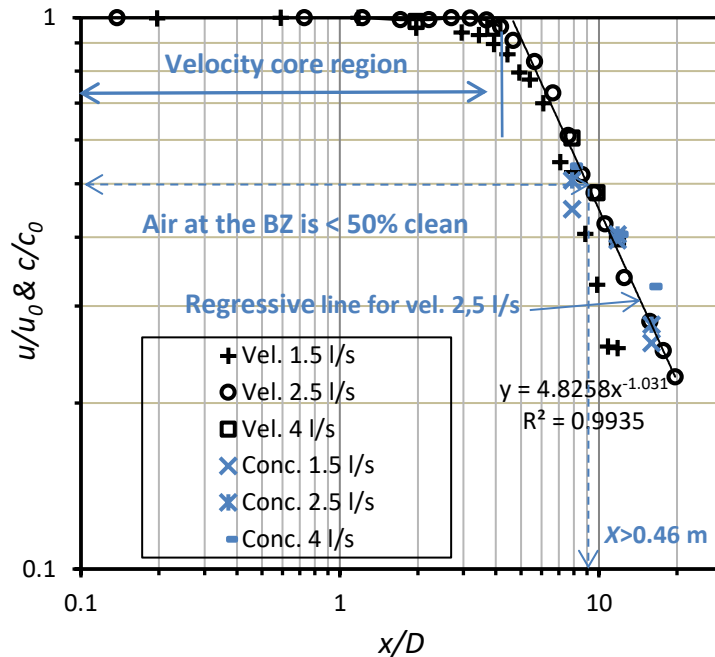


Fig. 4. Velocity and concentration decay along the jet centerline for free nozzle jet (log-log coordinates).

Fig. 3 shows the PV jet aims at supplying clean air to the BZ of a person. However, with the development of the nozzle jet, polluted air from the surroundings is entrained in form of vortex rings in the turbulent shear layer. As a result, the clean air core shrinks and gradually disappears after a length, l . Here the clean air core is not long enough to reach the inhalation zone of the person as illustrated in Fig. 3. The front end of the jet interacts with the TBL and causes drastic mixing of clean air with it. As depicted in Fig. 3 the length of the clean air core is 3~4 times the diameter of the nozzle, D , over a flow rate ranging from 1.5 l/s to 4 l/s, which corresponds well with that of a free jet [27] as well as the length of constant velocity core determined in Fig. 4. The centerline velocity, u , and concentration, c , are normalized with respect to their nozzle exit values, u_0 and c_0 . Fig.4 presents the decay of centerline velocity and concentration for the free nozzle jet, which serves as a powder function. The decay profile of u and c basically corresponds with each other with a more rapid velocity decay for 1.5 l/s.

A laser, placed in the BZ at 10 mm away from the nose tip along a

vertical transverse line near the manikin's face, was used to measure the velocity components of u_x (mean velocity along the x axis) and u_y (mean velocity along the y axis), providing quantitative analysis of the flow interactions within the TBL. The mean resultant velocity, u_b , within the two-dimensional BZ plane is given as:

$$u_b = \sqrt{u_x^2 + u_y^2} \quad (1)$$

The general ventilation supplies 60.2 l/s of air, corresponding to 5.4 ACR. Nitrogen Oxide (N₂O) was used as tracer gas in this study, which was dosed to the PV supply air by a constant volume ratio of 4%. Concentration measurements were taken in the manikin's nose, along a vertical line within the manikin's BZ (5 cm and 10 cm down away from the manikin's nose, with a horizontal distance of 10 mm to the manikin's nose tip, see Figure 2), in the PV nozzle (before exit) and the chamber exhaust, as shown in Fig. 1. Multipoint sampler and doser (INNOVA 1303) and photoacoustic field gas monitor (INNOVA 1412) were used to measure the concentrations of N₂O. The temperature of each segment of the manikin was recorded, as was the temperature of the nozzle jet, the chamber, the ceiling supply air, and the exhaust air. Temperature was measured using thin type K thermocouples

The index related to ventilation effectiveness has been widely used to assess the performance of a ventilation system [12]:

$$\varepsilon_v = \frac{c_{pv} - c_e}{c_{pv} - c_{bz}} \quad (2)$$

in which c_{pv} is the N₂O concentration at the nozzle exit, c_e is N₂O concentration in the exhaust, and c_{bz} is the N₂O concentration in the inhalation or at a point in the BZ. In order to assess the percentage of clean air inhaled with PV, an air quality index, ε_{pv} , related to ε_v , was employed by normalizing the N₂O concentration in inhalation or the BZ with respect to that in PV, which can be expressed by [13]:

$$\varepsilon_{pv} = \frac{c_{bz} - c_e}{c_{pv} - c_e} = 1 - \frac{1}{\varepsilon_v} \quad (3)$$

This index also indicates the mixing degree of personalized ventilation with room air at the BZ [28]. We note that $\varepsilon_{pv}=0$ for fully mixed conditions and $\varepsilon_{pv}=1$ when the air as clean as the PV is present at the BZ. ε_{pv} was also used to present the ability of the PV's

penetration of the TBL around the body. ε_{pv} should be lowered with the presence of the TBL and may reach zero even when the thermal plume isolates the person from clean air [14]. The tracer gas concentrations, c_e and c_{pv} are found to be relatively stable during experiments, so they are considered to be constants or each measurement. The uncertainty of ε_{pv} is expressed by the deviations of c_{bz} , regarding the intense interactions between the PV flow and the TBL in the BZ.

Table 1 lists the three test series investigated in this study, which compares the impacts of the interactions of the TBL with PV and the presence of TM as an obstacle on the effectiveness of PV. The effects of the PV flow rates (≥ 1.5 l/s), the relative horizontal distances (40 cm~100 cm) and the placements of the nozzle were also discussed.

Table 1 Setup of three experimental series.

	Thermal Manikin or Non-isothermal Manikin (TM)	Isothermal Manikin (ISOM)	No Manikin (NM)
Manikin heat output	70 W	0	\
Avg. body surface temp.	30.1 °C	24.2 °C	\
Ventilation conditions	PV temp. 22.6~23.2°C; Room air temp. 24.3°C; Room surface temp. 24.1°C; Room air velocity 0.01~0.13 m/s		

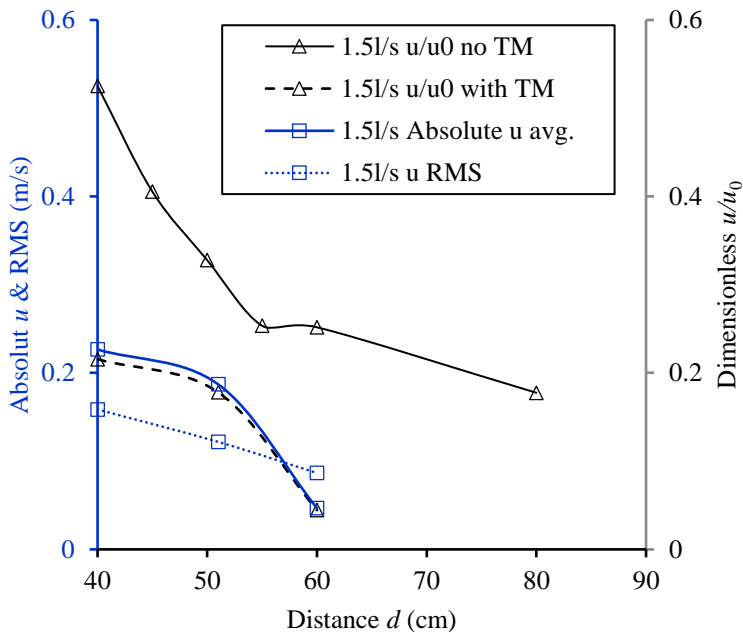
3. Results and discussion

3.1 Penetration velocity

For two different PV flow rates of 1.5 l/s and 2.5 l/s, corresponding to average exit velocities of 1.05 m/s and 1.63 m/s, respectively, it can be seen in Fig. 5 that the centerline velocity approaching the manikin's nose decreases significantly with the presence of the TM than without manikin. The received velocity in the BZ, u_b , 10 mm from the manikin's nose, decreases with longer nozzle-exit-to-target distance, d . For 2.5 l/s, the centerline velocity, u , at a $d=100$ cm drops nearly by half (from 0.363 m/s to 0.186 m/s), which implies the PV jet may still penetrate the TBL even at relative long facing distances. However, for 1.5 l/s at $d=60$ cm, u is reduced from 0.265 m/s to merely 0.047 m/s, approaching the turbulence level of the calm room air. It seems the invading velocity is too low to penetrate the TBL. This basically coincides with the critical value of penetration

recommended by Bolashikov et al. for a minimum of 0.3 m/s. A schlieren image video (Appendix Video S2) that records the dynamic process of flow interactions for 1.5 l/s shows that the PV jet collides with the constantly rising plume around body at the mouth height and induces an anticlockwise vortex ring in this area. The jet is then lifted by the upward plume and mostly moves above the manikin's head. Previous studies [14,15] reported that the velocity decrement to nearly zero and the upward velocity deflection could serve as the proof that the PV flow failed to penetrate of the TBL.

However, it seems unreasonable if compare the velocity decrement in the BZ between the non-isothermal manikin case (TM) and the isothermal manikin case (ISOM). The TBL around the manikin may not be the dominate reason for the velocity decrement. Table 2 shows that u for ISOM case near the nose point (10 mm from the nose tip) is also reduced to merely 0.063 m/s, even without the interference of the thermal plume around the manikin body. It is evident that the influence of the thermal plume on the velocity decrement in the BZ is insignificant.



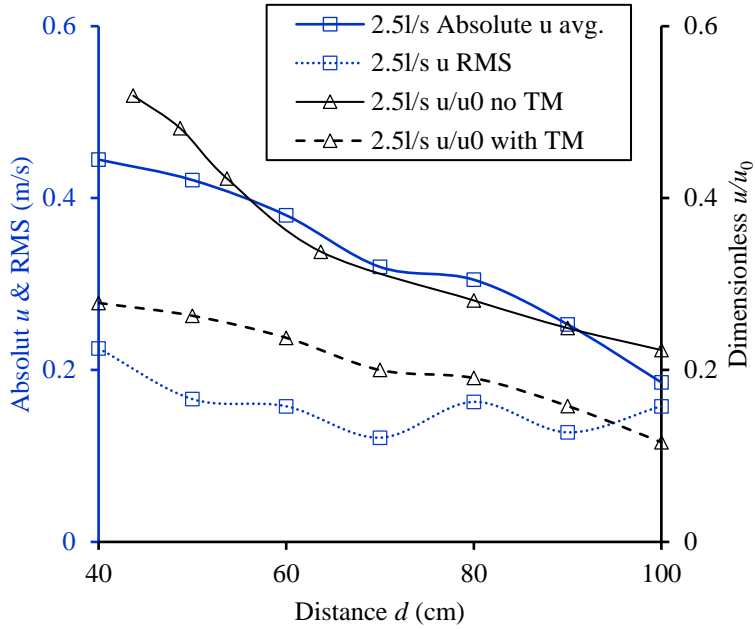


Fig. 5. Absolute velocity at the manikin's nose point with different relative distances between the thermal manikin (TM) and the PV nozzle.

Table 2 Velocity measurement by LDA in the BZ for 1.5 l/s at $d=0.6$ m

Vertical Height (Fig. 2)		TM (Non-isothermal Manikin)		ISOM (Isothermal Manikin)	
		u_x	u_y	u_x	u_y
Above 10 cm (P4)	Avg (m/s)	0.112	0.097	0.181	0.220
	RMS (m/s)	0.103	0.085	0.120	0.155
	Turb (%)	91.6	86.8	66.2	70.5
Nose point (P0)	Avg (m/s)	0.047	0.002	0.054	0.032
	RMS (m/s)	0.087	0.080	0.116	0.09
	Turb (%)	185.4	4088.4	213.1	281.3
Down 10 cm (P2)	Avg (m/s)	0.082	0.048	0.056	0.024
	RMS (m/s)	0.138	0.107	0.103	0.096
	Turb (%)	168.6	222.5	185.6	409.1
Down 20 cm (P3)	Avg (m/s)	0.053	0.181	0.117	-0.005
	RMS (m/s)	0.054	0.184	0.188	0.065
	Turb (%)	101.8	101.9	160.6	1190.7

The velocity decrement can be attributed to the momentum loss as the PV airflow approaches the manikin's body that is present as an obstacle in the flow. Yang et al. [29] reported that blockage effect of an unheated manikin on downward personalized airflow distribution was able to reduce the centerline velocity to about 85% at 0.2 m right above the manikin's head. Fig. 6 further verifies this result, as no significant difference of the u_b is found over varying PV flow rates (1.5 l/s~5 l/s) at both P0 (nose point) and P1 (chin point) between the TM and ISOM. The PV jet decelerates as it approaches the stagnation point at the nose. While it accelerates, in contrast, as it passes by the sharp chin point from P1.

We therefore note that the judgment of penetration by merely velocity measurement could be insufficient, which should be complemented by the concentration measurement to show whether the PV air enters inhalation. Fig. 7 illustrates the decay of inhaled ε_{pv} with increasing d . For 1.5 l/s at $d=0.6\sim 0.8$ m, the ε_{pv} is very low but still over 0.25, corresponding to a ventilation effectiveness of 1.3, which means that a small fraction of clean air can still be inhaled even at a low invading velocity ($d=0.8$ m, $u=0.177$ m/s), probably attributable to the turbulent circulation and mixing of clean air with polluted plume air at the BZ, as illustrated in Video S2. The effect of interactions with the thermal plume on the PV performance will be further discussed in section 3.3. To summarize, the TBL is proved to be penetrable by clean air from PV even at an invading velocity below 0.3 m/s in this study. From Table 2 and Fig.6 it can be seen that both the manikin body and the TBL affect the velocity distribution patterns in the BZ.

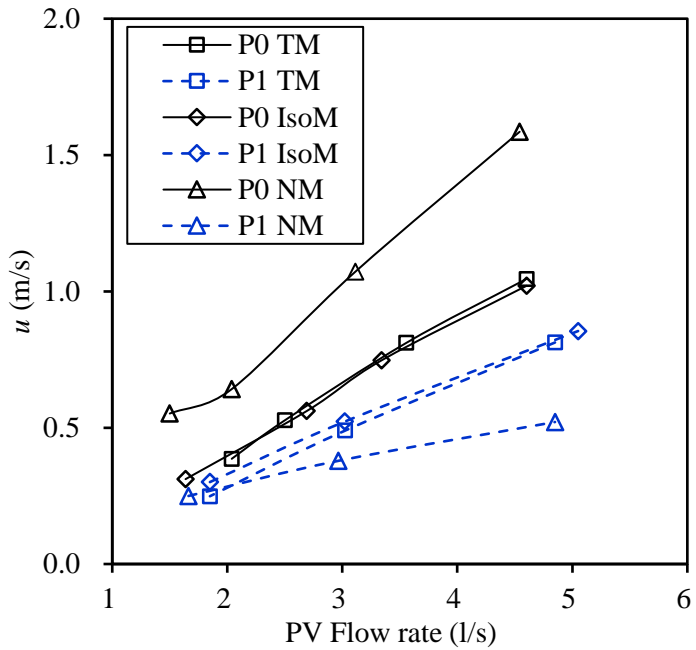


Fig. 6. Measured average velocity u at the nose point (P0) and 5cm down (P1) for the three conditions (TM, ISOM and NM) with a relative distance of 40 cm.

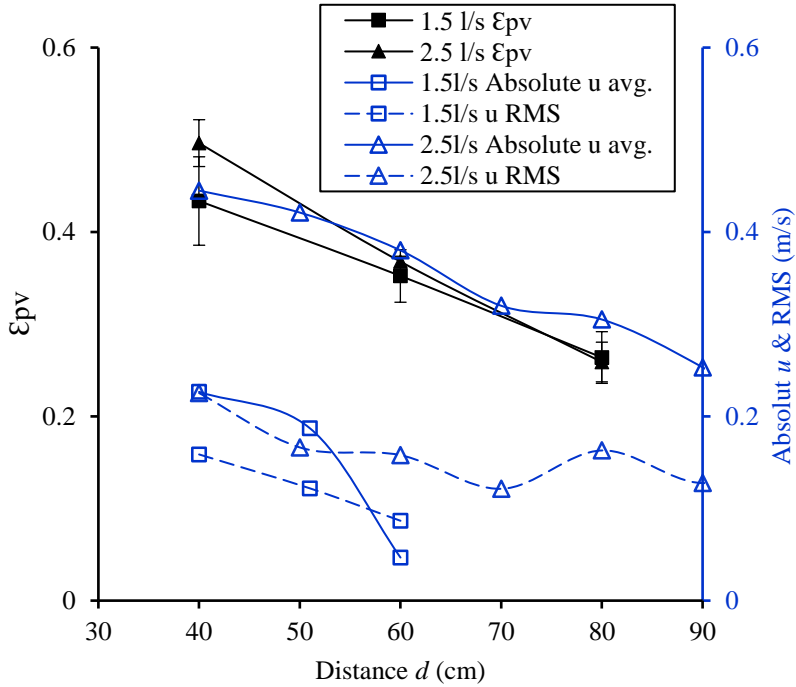


Fig. 7. Inhaled ϵ_{pv} for the TM with different nozzle-exit-to-target distances.

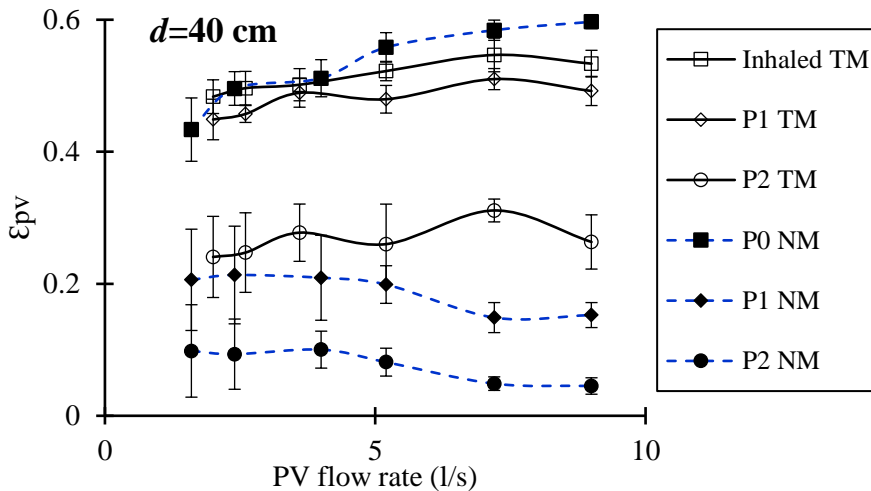
3.2 Effect of thermal manikin

Fig. 8 compares the measured ϵ_{pv} for the TM and without manikin (NM) along a vertical line 10 mm from the manikin's nose for $d=40$, 60 and 81 cm, respectively. It can be seen that the presence of the TM modifies the PV airflow distributions in the BZ. At low clean air supply (≤ 5 l/s), the conventional single nozzle PV system can achieve a BZ ventilation effectiveness of merely 2. As expected, the increased clean flow results in improved BZ air quality, albeit not in proportion to the increased clean flow.

When there is no manikin in the downstream of the PV jet, the concentration profile along y -axis (vertical direction) presents a "bell shape" with the maximum value in the centerline and deteriorating air quality till the jet's boundary layer due to the entrainment of polluted ambient air. Here also, ϵ_{pv} decreases with longer y down from the nozzle centerline. For the $d=40$ and 60 cm cases, the dashed lines in Fig.8 show clear stratification for $y=0$, 5 and 10 cm, respectively. While the ϵ_{pv} is all quite low for the three y distances for $d=81$ cm

case over a limited range between 0.2~0.3, as the “bell cap” of the concentration profile is becoming flat with the increasing d . For $d=40$ cm, ε_{pv} is merely around 0.1 at $y=10$ cm. This is probably because the location of this sampling point is close to the jet’s shear boundary.

With the presence of the TM, the ε_{pv} at $y=5$ cm is significantly advanced, which is even higher than the inhaled ε_{pv} for the $d=60$ cm case. This can be explained by the enhanced u_b when the jet bypasses the manikin’s chin due to the blocking effect. The ε_{pv} at $y=10$ cm is also increased for $d=40$ and 60 cm cases. The results indicate that the manikin changes the original directions of the nozzle flow and accumulates it in the vicinity of manikin’s BZ, and the inhaled air quality is not improved but slightly lowered because of the effect of the polluted thermal plume air.



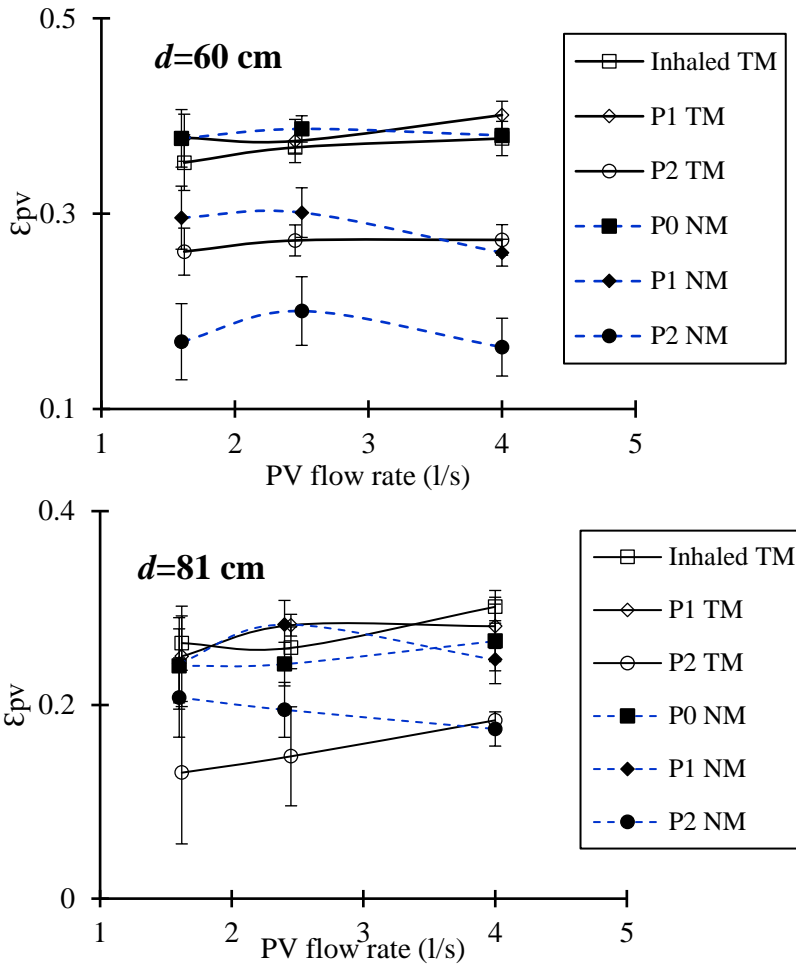


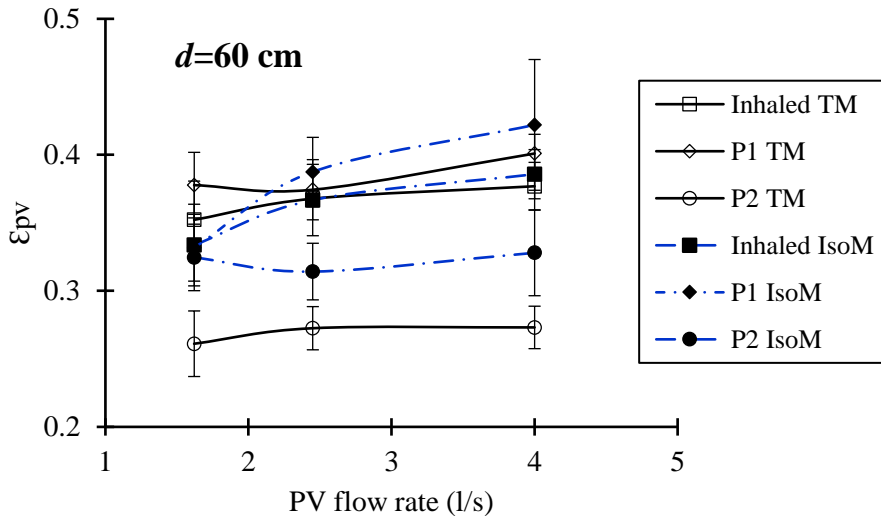
Fig. 8. Effect of the presence of TM on ϵ_{pv} .

3.3 Effect of thermal plume

Fig. 9 shows measurements of the flow both when the manikin is isothermal (ISOM) and when the manikin has a thermal boundary layer (TM). The Fig.9 shows the effect of thermal plume for $d=60$ and 81 cm, respectively. It can be seen that the most significant effect of the thermal plume on the ϵ_{pv} is at $y=10$ cm, the neck height, which is lowered when there is thermal plume interacting with the PV jet. But the lowered ϵ_{pv} at this height did not affect the inhaled air quality significantly. The difference between the inhaled ϵ_{pv} for the two cases is small. The increased ϵ_{pv} at both $y=5$ and 10 cm for ISOM compared with NM (Fig. 7) also indicates the clean air distribution can be

considerably influenced by the presence of the manikin.

Although the manikin, placed farther away from the nozzle exit and given lower clean flow rates, exhibits certainly lower values of ε_{pv} in the BZ, a small fraction of the amount of clean air can still break through the resistance of the TBL and reaches the BZ. This is partly because the upward thermal plume interacts with the transverse PV jet in the BZ and leads to turbulent circulation and mixing of clean air with contaminated room air, which will be drawn by the manikin's inhalation afterwards. Another reason for the penetration is probably relying on the weakened body surface temperature owing to the draught from the cooler PV jet. Measurements show that the increasing PV flow (1.5 l/s ~ 4 l/s) decreases the surface temperature around the head and the chest by 2~3 °C. Melikov and Zhou [30] also reported that a horizontal isothermal airflow from behind with a mean velocity of 0.1 m/s and a turbulence intensity of 10% was able to decrease the air temperature near the skin surface by 4 °C and to increase the local heat flux by 22%. The decreased body surface temperature would therefore weaken the strength of the thermal plume and present a less challenging condition for the PV jet's penetration of the thermal plume. The reduced challenge leads to potential energy savings of the ventilation facilities.



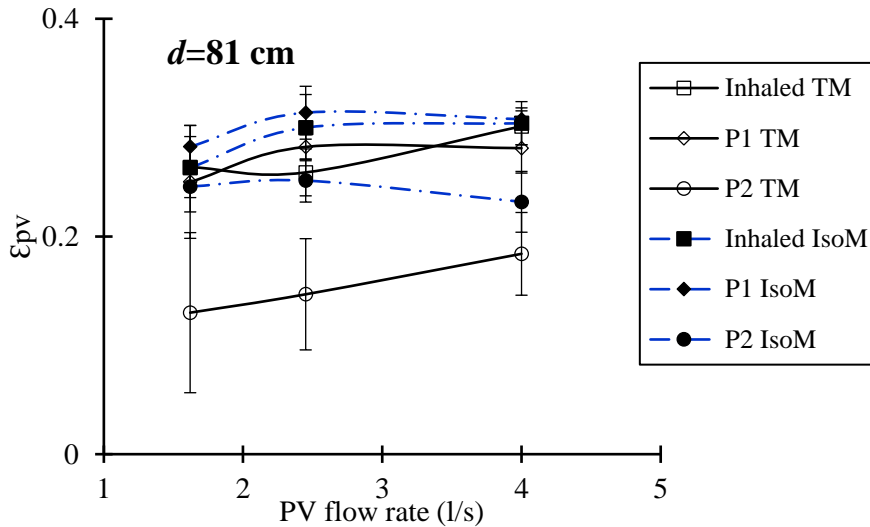


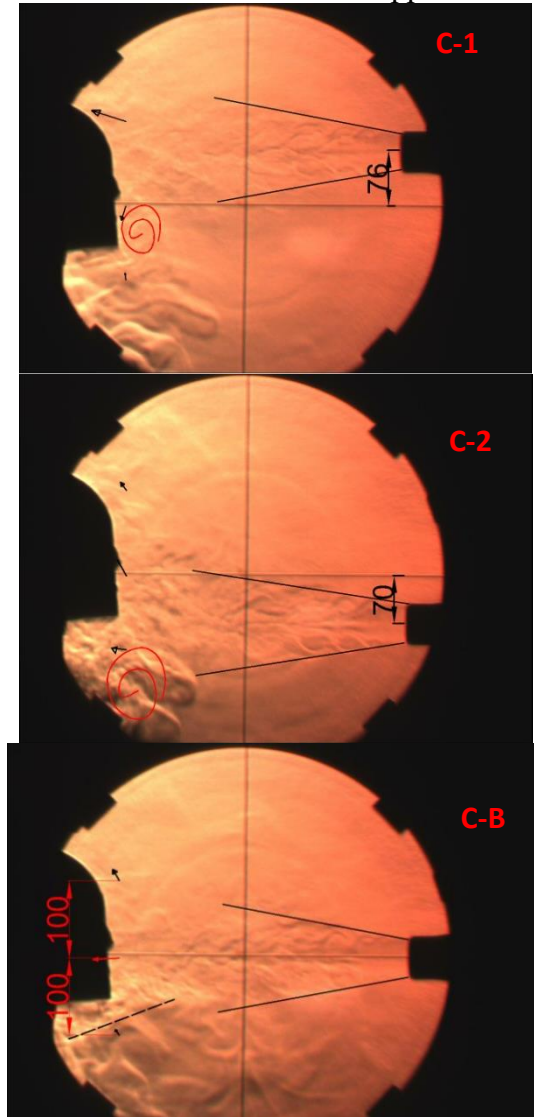
Fig. 9. Effect of the manikin's thermal plume on ϵ_{pv} .

3.4 Effect of placement of nozzle

The amount of inhaled clean air from the PV has shown dependence on the design of the nozzle and its positioning in regard to the occupant and the direction of the personalized airflow [12]. The air terminal devices of PV systems should also allow adjustments of directions according to the occupants' preference. The Fig. 10 and Fig.11 show the effect of the nozzle's positioning and direction on the BZ air interactions and the air quality. The nozzle horizontally aligned to the manikin's nose was used as the baseline case (C-B). Two different heights: 76 mm above (C-1) and 70 mm below (C-2) the nose height with the nozzle horizontally placed, and two different angles: 8.5° upwards (C-3) and 7.5° downwards (C-4) pointing to the manikin's nose were compared for analysis, as shown in Fig. 10. The relative distance between the nozzle exit and the nose front is maintained at 40 cm for all the preceding five cases. So is the PV flow rate with an identical value of 2.5 l/s. Schlieren video clips (S3-S7) recording the five different airflow interaction processes may be found in the supporting information.

The velocity vectors measured by LDA at three vertical heights (10 cm above the nose, the nose front, and 10 cm below the nose) are scaled and plotted on the Fig. 10. As seen in Fig. 10 the velocity distributions in the BZ are changed by the positions and angles in which the nozzle is placed. The schlieren images also show different

airflow interaction characteristics among the five cases, in terms of different conflicting heights and directions with the TBL as well as vortex ring sizes and the locations where it appears.



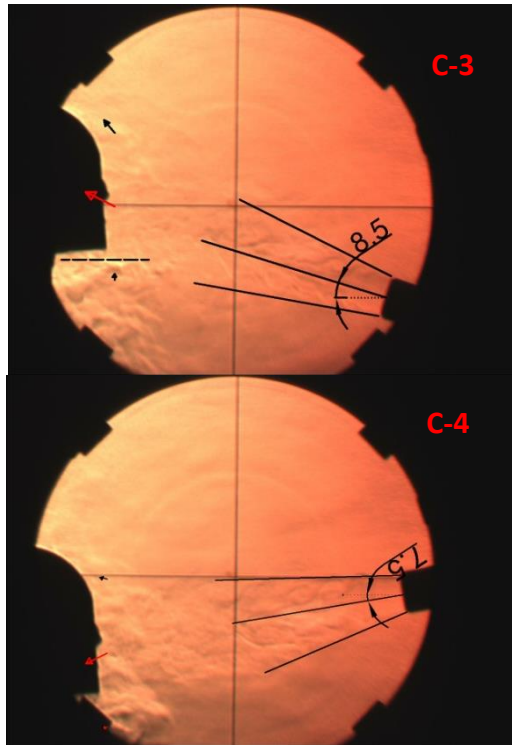


Fig. 10. Schlieren images of the interaction between the TBL and the nozzle placed in different positions.

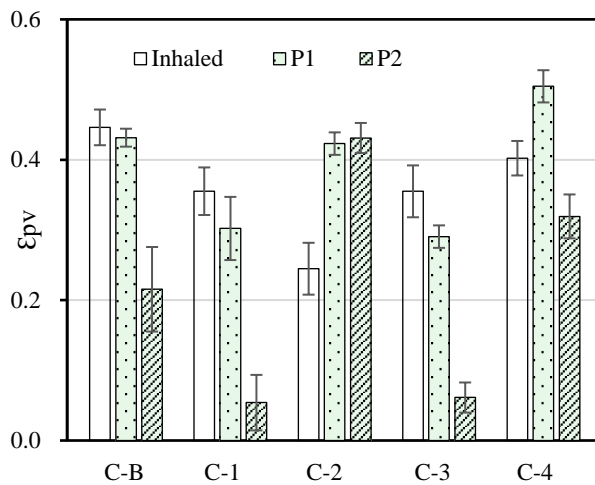


Fig. 11. ϵ_{pv} for different nozzle positions (2.5 l/s, $d=40$ cm).

In the base line case, the interaction between the PV jet and the TBL for the manikin is similar to that for a real person (Fig. 3). The vortex ring occurs both at the jaw height due to the competing turbulent airflows from transverse and vertical directions. As for the ε_{pv} , it is considerably lowered when the nozzle is horizontally placed higher or lower than the nose height, decreasing from 0.45 to 0.35 and 0.24, respectively. For test series C-1 and C-2, the anticlockwise vortex ring respectively appears at mouth height and the chest height, where the lower boundary of the nozzle jet collides with the rising body stream. The vortex at the chest height is larger in size than the one at the mouth height. Actually, the inhaled air for C-1 is mainly drawn from the eddy flow, while for C-2 the inhaled air is from the upper boundary of the nozzle jet mixed with the thermal plume turning up around the jet column from the left and right sides rising from the lower part of the body. The directions of the nozzle jet in regard to the thermal plume also have significant impacts on the ventilation effectiveness of the PV. When the nozzle inclines upward pointing to manikin's nose (Fig. 10 C-3), the upward direction of the velocity component along axis y is consistent with that of the body plume, so the confliction between these flows is not as intensive as that in the base line case. The thermal plume in this case (C-3) remains upward and is not strongly disturbed by the PV flow. The inhaled air is hence drawn from the rising mixture of the personalized air as well as the thermal plume, causing lower ε_{pv} than that in C-B. On the contrary, ventilation enhancement in the BZ can be found in C-4 with downward supply air. This is probably because the downward cold flow restrains the upward development of the warmer thermal plume and results in higher percentage of clean air in the BZ compared to C-3. The results indicate that the transverse and downward flow (pointing to the manikin's nose) in this condition performs better than flow from other directions.

3.5 Energy saving potential of PV

Previous studies [5,9,10] have indicated the advantages of PV compared with conventional mixing ventilation (MV) resulting in considerable energy saving. The usage of PV allows a higher macroclimate temperature in the room while maintaining the acceptable thermal comfort and air quality simultaneously, owing to the personalized air creates a relatively clean and comfortable

microenvironment around the occupant. In addition, the distance between occupants may also be properly reduced, resulting in more efficient space use, as the PV has been observed with the ability to prevent contamination and disease transmission between occupants [10]. These preceding characteristics of the PV could lead up to a high energy saving potential comparing to the conventional MV systems where the temperature and freshness of air of the whole room should be maintained to achieve the equivalent thermal comfort and air quality.

This study applies a conventional PV system coupled with the diffuse ceiling ventilation (DCV). Ventilation effectiveness of the DCV is comparable to conventional MV in spite of slight indications of displacement effect. The real operating performance of the DCV has been tested in a classroom [31] and it shows a complete mixing of CO₂ with room air within the occupied zone, implying a ventilation effectiveness of around 1. It can be inferred that even though the total volume of supplied air from the ceiling diffuser is increased to a considerable amount, the ventilation effectiveness will not be significantly improved but keep around 1. This is the key feature of the MV system which has almost homogeneous air everywhere in the room. However, the ventilation effectiveness could be significantly improved by using PV coupled with MV because fresh air is directly delivered to the occupant's BZ by the PV without circulating in the whole room. In this study, a small portion the DCV air of about 4~10% used as personalized air (PV of 2.5~6 l/s divided by DCV of 60.2 l/s) can achieve of ϵ_v of around 2. Proper combinations of PV-MV may therefore result in higher energy savings than a PV or MV system alone [9,10,32,33] as the integrated system can be able to provide the best compromise between comfort and air quality.

This study indicates that a small fraction of clean air can still be inhaled even at a low invading velocities. The PV is able to provide an improved inhaled air quality with less amount of fresh air and create relatively clean microenvironment around the occupant. The localized airflow dynamics directly affect the performance of a PV system and should be carefully considered for optimal design. Some previous researchers have realized the importance of interaction between thermal plume around human body and personalized air and proposed corresponding PV configurations to enhance the ventilation

effectiveness and energy savings. Yang et al. [29] defined the neutral distance as the one from the PV nozzle where the impact of thermal plume on velocity distribution was observed and found that it increased from 0.8 m to 1.1 m with the increase of the airflow rate from 4 l/s to 16 l/s for a ceiling mounted PV nozzle. Gao and Niu [28,35] placed the PV nozzle just beneath the chin to avoid long distance contamination by ambient air and reported that a minimum flow rate of 0.8 l/s is strong enough to overcome the disturbance of the thermal plume and provide enough clean air to the BZ. Makhoul et al. [9] proposed the single ceiling PV jet combined with desk fans which were able to control the convective plumes emanating from the human body allowing the personalized air to reach the breathing level more effectively. A reduced energy saving by up to 13% was achieved by this system compared to conventional mixing ventilation systems. The interactions patterns between the supplied air from PV and the TBL should be an important consideration for the improvement of BZ air quality, thermal comfort and energy consumption in optimal ventilation design.

4. Conclusions

This study found that the velocity decrement in close proximity to the manikin is dominated by the blocking effect of the manikin body rather than the thermal plume. The concern of PV jet's penetration of the thermal plume seems not as challenging as expected and should not be considered as a critical factor for PV system design. In practice, lower penetration velocity of clean air may be helpful to achieve lower energy consumption to supply decreased outdoor clean air.

However, the interaction between the PV flow and the TBL cannot be neglected even when the penetration of clean air is achieved, because of its significant impacts on the BZ air distributions. The presence of the manikin in combination with the effect of the interaction modifies the airflow patterns in the BZ in terms of velocity and clean air concentration distributions. This airflow interaction also depends on the direction and the magnitude of the non-uniform invading flow from the nozzle. Different placement of the nozzle, aligned with the manikin with different vertical heights or angles, alters the interaction characteristics in the BZ and leads to inhaled air quality variations. These findings imply that the airflow dynamics in the localized area around the occupant plays an important role in the performance of a PV system and should be carefully considered in

order to reduce personal exposure to ambient pollutants, thermal discomfort and energy consumption. .

Acknowledgements

This project is financially supported by Natural Science Foundation of Shandong Province (ZR2016RL18), the Fundamental Research Funds for the Central Universities (2014010588, 15CX02041A), National Key Research and Development Program of China (2017YFC0702700), National Natural Science Foundation of China (51378415), and National Sci-Tech Support Plan (2015BAJ03B00).

Supporting Information/ Appendices

Additional supporting information may be found in the online version of this article:

Video S1: One male subject facing to the nozzle with PV flow rate of 2.5 l/s and $d=0.4$ m.

Video S2: Interaction between the TBL and the supplied air from the nozzle at 1.5 l/s and $d=0.6$ m.

Video S3: Test series C-B, and C-1~4 (Fig. 10).

References:

- [1] Melikov AK. Personalized ventilation. *Indoor Air* 2004;14 Suppl. 7:157-67.
- [2] Assaad DA, Habchi C, Ghali K, Ghaddar N. Effectiveness of intermittent personalized ventilation in protecting occupant from indoor particles. *Build Environ* 2018;128:22–32.
- [3] Bolashikov Z, Melikov AK, Spilak M, Nastase I, Meslem A. Improved inhaled air quality at reduced ventilation rate by control of airflow interaction at the breathing zone with lobed jets. *HVAC&R Res* 2013;20 (2):238-50
- [4] Bolashikov Z, Melikov AK, Spilak M. Experimental investigation on reduced exposure to pollutants indoors by applying wearable personalized ventilation. *HVAC&R Res* 2013;19 (4):385-99.
- [5] Yang B, Sekhar C, Melikov AK. Energy analysis of the personalized ventilation system in hot and humid climates. *Energy Build* 2010;42(5):699-707.
- [6] Schiavon S, Melikov AK. Energy-saving strategies with personalized ventilation in cold climates. *Energy Build*

2009;41(5): 543-50.

- [7] Niu JL. Potential IAQ and energy benefits achievable with personalized air supply, *Healthy Building 2003*, Singapore, 7-11 Dec 2003
- [8] Lyubenova V, Holsoe J, Melikov A. Potential energy savings with personalized ventilation coupled with passive chilled beams. In *Proc. of Roomvent 2011*, Trondheim, paper 226.
- [9] Makhoul A, Ghali K, Ghaddar N. Desk fans for the control of the convection flow around occupants using ceiling mounted personalized ventilation. *Build Environ* 2013;59:336–48.
- [10] Habchi C, Ghali K, Ghaddar N, Chakroun W, Alotaibi S. Ceiling personalized ventilation combined with desk fans for reduced direct and indirect cross-contamination and efficient use of office space. *Energy Convers Manage* 2016;111:158-73.
- [11] Cermak R, Melikov AK, Forejt L. Performance of personalized ventilation in conjunction with mixing and displacement ventilation. *HVAC&R Res* 2006;12(2):295-311.
- [12] Melikov AK, Cermak R, Mayer M. Personalized ventilation: Evaluation of different air terminal devices. *Energy Build* 2002;34:829-36.
- [13] Khalifa HE, Janos MI, Iii JFD. Experimental investigation of reduced-mixing personal ventilation jets. *Build Environ* 2009;44(8):1551-8.
- [14] Bolashikov ZD, Nikolaev L, Melikov AK, Kaczmarczyk J, Fanger PO. Personalized ventilation: air terminal devices with high efficiency. In *Proceedings of Healthy Buildings 2003*. Singapore: Healthy Buildings 2003. 2003. p. 850-5.
- [15] Bolashikov ZD, Nagano H, Melikov AK, Velte CM, Meyer KE. Airflow Characteristics at the Breathing Zone of a Seated Person: Passive Control over the Interaction of the Free Convection Flow and Locally Applied Airflow from Front for Personalized Ventilation Application. In *Roomvent 2011*. 2011.
- [16] Licina D, Melikov AK, Sekhar C, Tham KW. Human convective boundary layer and its interaction with room ventilation flow. *Indoor Air* 2015;25(1):21-35
- [17] Licina D, Melikov A, Sekhar C, Tham KW. Transport of Gaseous Pollutants by Convective Boundary Layer around a Human Body, *Science and Technology for the Built Environment*, 2015;21

(8):1175-86.

- [18] Licina D, Melikov A, Pantelic J, Sekhar C, Tham KW. Human convection flow in spaces with and without ventilation: Personal exposure to floor released particles and cough released droplets, *Indoor Air* 2015; 25(6):672-82.
- [19] Melikov AK, Cermak R, Kovar O, Forejt L. Impact of airflow interaction on inhaled air quality and transport of contaminants in rooms with personalized and total volume ventilation, *Proceedings of Healthy Buildings 2003, Singapore*, 7-1 National University of Singapore, Department of Building, vol. 2, pp. 592-7.
- [20] Zhang C, Heiselberg PK, Pomianowski M, Tao Y, Jensen RL. Experimental study of diffuse ceiling ventilation coupled with a thermally activated building construction in an office room. *Energy Build* 2015;105:60-70.
- [21] Yu T, Heiselberg P, Lei B, Zhang C, Pomianowski M, Jensen RL. Experimental study on the dynamic performance of a novel system combining natural ventilation with diffuse ceiling inlet and tabs. *Appl Energy* 2016;169:218-29.
- [22] ANSI/ASHRAE Standard 62.1-2004. Ventilation for acceptable indoor air quality; 2004.
- [23] ASHRAE Handbook of Fundamentals. Indoor Environmental Quality. Atlanta, GA, USA: American Society of Heating, Refrigerating and Air Conditioning Engineers, Inc.; 2009.
- [24] Xu C, Nielsen PV, Gong G, Jensen RL, Liu L. Influence of air stability and metabolic rate on exhaled flow. *Indoor Air* 2015;25(2):198–209.
- [25] Xu C, Nielsen P V, Gong G, Liu L, Jensen RL. Measuring the exhaled breath of a manikin and human subjects. *Indoor Air* 2015;25(2):188–97.
- [26] Xu C, Nielsen PV, Liu L, Jensen RL, Gong G. Human exhalation characterization with the aid of schlieren imaging technique. *Build Environ*,2016;112:190-9.
- [27] Abramovich GN, Schindel L. The theory of turbulent jets. Cambridge, MA: MIT Press; 1963.
- [28] Gao N, Niu J. CFD study on micro-environment around human body and personalized ventilation. *Build Environ* 2004;39(7):795-805.

- [29] Yang B, Melikov AK, Sekhar C. Performance evaluation of ceiling mounted personalized ventilation system. *ASHRAE Trans* 2009;115(2):395-406.
- [30] Melikov AK, Zhou G. Air movement at the neck of the human body. *Proceedings of Indoor Air '96*, 1996, Nagoya, Japan, 1, 209-14.
- [31] Kristensen MH, Jensen JS, Heiselberg PK. Field study evaluation of diffuse ceiling ventilation in classroom during real operating conditions. *Energy Build* 2017;138, 26-34.
- [32] Assaad DA, Ghali K, Ghaddar N, Habchi C. Mixing ventilation coupled with personalized sinusoidal ventilation: optimal frequency and flow rate for acceptable air quality. *Energy Build* 2017;154:569–80.
- [33] Dalewski M, Melikov AK, Vesely M. Performance of ductless personalized ventilation in conjunction with displacement ventilation: physical environment and human response. *Build Environ* 2014;81(7):354-64.
- [34] Zuo H, Niu J, Chan DWT. Experimental study of facial air supply method for the reduction of pollutant exposure, *Indoor Air 2002 - The Ninth International Conference on Indoor Air Quality and Climate*, Monterey, California, June 30 - July 5, 2002, pp.1090-5
- [35] Niu J, Gao N, Ma P, Zuo H. Experimental study on a chair-based personalized ventilation system. *Build Environ* 2007;42(2):913-25.

ISSN (online): 2446-1636
ISBN (online): 978-87-7210-129-3

AALBORG UNIVERSITY PRESS